Institut für Wasserbau · Universität Stuttgart

Mitteilungen

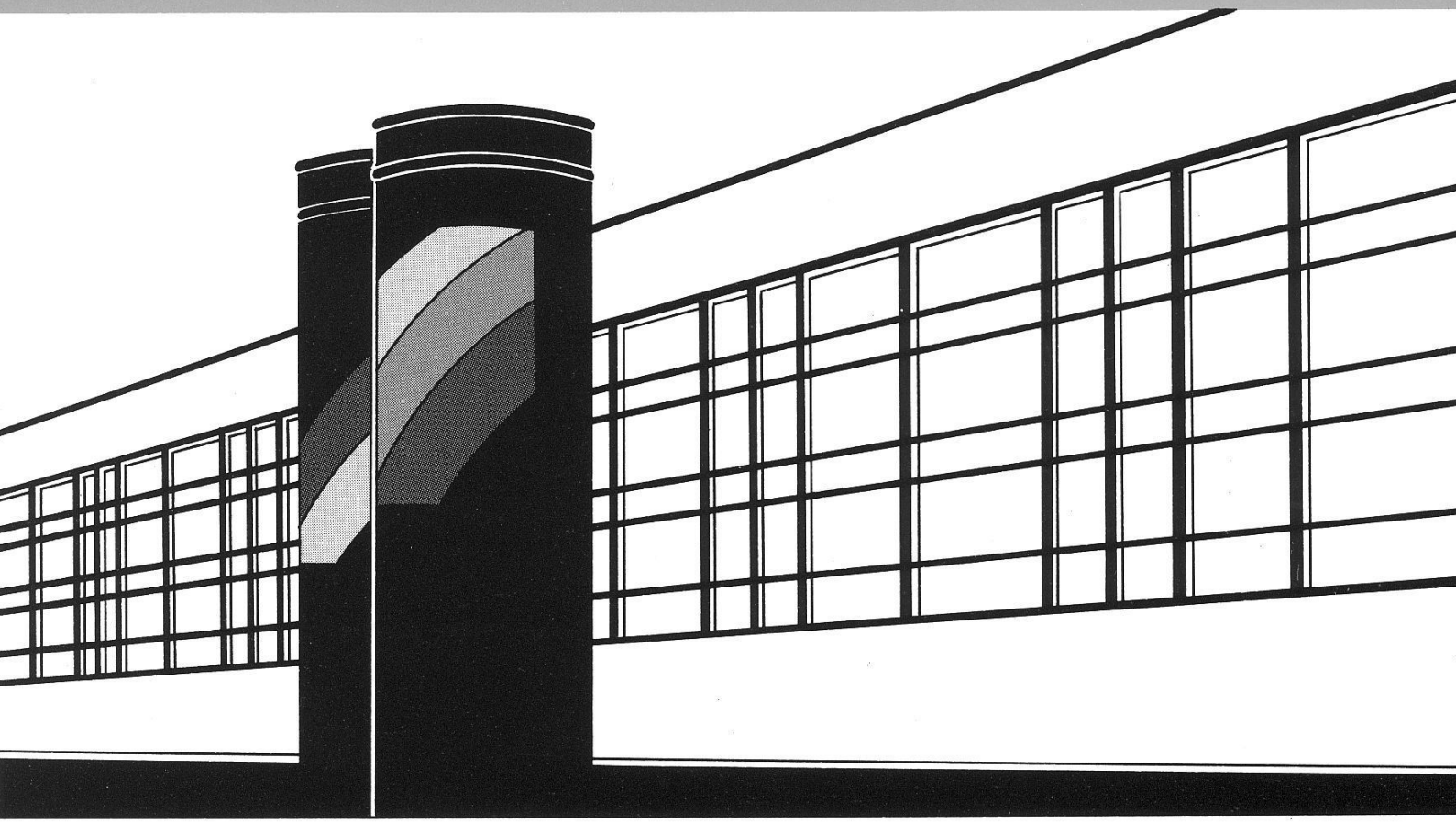

Heft 209

Anna Kuhlmann

Influence of soil structure and root water uptake on flow in the unsaturated zone

Influence of soil structure and root water uptake on flow in the unsaturated zone

Von der Fakultät Bau- und Umweltingenieurwissenschaften der Universität Stuttgart zur Erlangung der Würde eines Doktor-Ingenieurs (Dr.-Ing.) genehmigte Abhandlung

Vorgelegt von

Anna Kuhlmann

aus Freiburg

Hauptberichter:	Prof. Dr. rer. nat. Insa Neuweiler
Mitberichter:	Prof. Dr. Ing. Rainer Helmig
	Prof. Dr. Ir. S.E.A.T.M. van der Zee

Tag der mündlichen Prüfung: 14. November 2011

Institut für Wasserbau
der Universität Stuttgart
2012

Heft 209

Influence of soil structure and root water uptake on flow in the unsaturated zone

von
Dr.-Ing.
Anna Kuhlmann

Eigenverlag des Instituts für Wasserbau
der Universität Stuttgart
2012

D93 Influence of soil structure and root water uptake on flow in the unsaturated zone

Bibliografische Information der Deutschen Nationalbibliothek
Die Deutsche Nationalbibliothek verzeichnet diese Publikation in der Deutschen Nationalbibliografie; detaillierte bibliografische Daten sind im Internet über http://www.d-nb.de abrufbar

Anna Kuhlmann:
Influence of soil structure and root water uptake on flow in the unsaturated zone / von Anna Kuhlmann. Institut für Wasserbau, Universität Stuttgart. - Stuttgart: Inst. für Wasserbau, 2012

(Mitteilungen / Institut für Wasserbau, Universität Stuttgart: H. 209).
Zugl.: Stuttgart, Univ., Diss., 2012
ISBN 978-3-942036-13-9
NE: Institut für Wasserbau <Stuttgart>: Mitteilungen

Herausgegeben 2012 vom Eigenverlag des Instituts für Wasserbau

Druck: Document Center S. Kästl, Ostfildern

Acknowledgment

This work was carried out within the International Research Training Group NUPUS (http://www.nupus.uni-stuttgart.de) funded by the German Research Foundation DFG (GRK 1398) and the Netherlands Organisation for Scientic Research NWO (DN 81-754). I also acknowledge funding by the Institute for Modelling Hydraulic and Environmental Systems Stuttgart and the Institute of Fluid Mechanics and Environmental Physics in Civil Engineering Hannover.

First of all, I would like to thank my supervisor Prof. Dr. rer. nat. Insa Neuweiler for guiding me during these years. I benefited greatly from her expertise and her way of conveying the knowledge. I appreciate the explanations, discussions, corrections ... and the friendly relationship. I also thank Prof. Dr.-Ing. Rainer Helmig for his advice and his positive and motivating nature. It was a pleasure to work at his institute. I am also very grateful for the supervision of Prof. Dr. Ir. Sjoerd van der Zee. His great knowledge, the discussions and the five-month stay in Wageningen were a valuable part of my education. I appreciate the continuous interest in my work and the improvements to the manuscripts. I also thank Prof. Dr. Ir. Toon Leijnse for the helpful discussions in Wageningen and at the NUPUS meetings.

Moreover, I would like to thank all colleagues from the IWS Stuttgart, the ISU Hannover and Wageningen University for a great working environment, I am grateful for the joyful time, the help i received and the friends i have made there. Special thanks to the Verfügungsgebäude-Team, Milos Vasin, Veronica Heiß, Li Yang and Wolfgang Nowak, Katherina Baber, the NUPUS Team, especially Florian Doster, Irina Komarova, Anozie Ebigbo and Jochen Fritz, Philipp Leube, Jonas Koch, Alexandros Papafotiou, Melanie Darcis, Klaus Mosthaf, Karin Erbertseder, Andreas Lauser, Bernd Flemisch, Holger Class, Prudence Lawday, Maria Costa, David Werner, Michelle Hartnick, Theresa Betz, Nikolai Otto, Jing Li, Philipp Guthke, Claus Haslauer, Jan Tecklenburg, Thomas Graf, Daniel Erdal, Jos van Dam, Klaas Metselaar, and the Cluster help, Martin Hecht at HLRS Stuttgart and Paul Cochrane and Andreas Gerdes at RRZN Hannover.

Finally, i would like to thank my friends from Stuttgart, Heidelberg and home, Lena, Anja, Heike, Didi, Re, Eva M., Caro, Eva V., Eva D., Barbara, and, in particular, my boyfriend Fabio and my family for their love and support.

Contents

List of Figures

List of Tables

Notation

The following table shows the significant symbols used in this work. Local notations are explained in the text.

Symbol	Definition	Dimension
Greek Letters:		
Ω	control volume	[m^2]
α	Van-Genuchten parameter	[1/m]
δ	e-folding depth of root density	[m]
η_i	set of all neighboring nodes of node i	[-]
γ	surface tension	[J/m^2]
Γ	control volume boundary	[m]
λ	mobility	[(m s)/kg]
μ	dynamic fluid viscosity	[kg/(m s)]
ϕ	porosity	[-]
ϕ_t	variable $\phi_t = \exp(\alpha\psi)$	[-]
ψ	pressure head	[m]
Ψ	total potential	[J/m^3]
ρ	fluid density	[kg/m^3]
ρ_U	correlation function of random field U	[-]
σ_U^2	variance of random field U	[U^2]
τ	transpiration demand	[m/s]
τ_A	amplitude of transpiration cycles	[m/s]
Θ	water content	[-]
Θ_r	residual water content	[-]
Θ_s	maximum water content	[-]
Latin Letters:		
b_u	scaling factor	[-]
B_i	box for node i	[-]
∂B_i	boundary of box B_i	[-]
c	normalized total concentration in domain	[-]

C_U	covariance function of random field U	[U^2]
CV_U	coefficient of variation of random field U	[-]
d	characteristic grain size diameter	[m]
d_r	root density distribution	[1/m]
dA	area element	[m]
dV	volume element	[m^2]
E_i	set of elements connected to node i	[-]
F	loghydraulic conductivity $F = \ln(K_s)$	[-]
f	fluctuation of loghydraulic conductivity or zero-mean loghydraulic conductivity	[-]
f_{c2},f_{c3}	scaling factor	[-]
f_d	frequency of infiltration/root water uptake cycles	[-]
$f_{d,c}$	critical frequency of infiltration/root water uptake cycles	[-]
f_F	stress-response function (Feddes-function)	[-]
$\mathbf{g}$	vector of gravitational acceleration $(0, 0, -\mathrm{g})^T$	[m/s^2]
g	(scalar) gravitational acceleration	[m/s^2]
h_1 -h_4	critical pressure head values in Feddes-function	[m]
H	domain height	[m]
i, j	node of the finite element mesh	[-]
I_U	integral scale of the random field U	[m]
$\mathbf{j}$	*Darcy* flux, volume flux per cross-sectional area	[m/s]
k_r	relative permeability	[-]
$\mathbf{k}$	tensor of permeability	[m^2]
$\mathbf{k_s}$	tensor of (intrinsic) permeability	[m^2]
$\mathbf{K}$	tensor of hydraulic conductivity	[m/s]
$\mathbf{K_s}$	tensor of saturated hydraulic conductivity	[m/s]
$K_{s,g}$	geometric mean of saturated hydraulic conductivity	[m/s]
$M_{ij}^{(lump)}$	(lumped) mass matrix	[-]
n	Van - Genuchten parameter	[-]
$\mathbf{n}$	unit normal vector	[-]
nb_{unstr}	number of unstressed nodes	[-]
N_i	Ansatz function for node i	[-]
M_2,M_3	root water uptake strategy	[-]
p	pressure	[Pa]
p_a	air pressure	[Pa]
p_c	capillary pressure	[Pa]
p_{non}	pressure of the non-wetting phase	[Pa]
p_u	probability density function	[-]
p_{wet}	pressure of the wetting phase	[Pa]
p_w	soil water pressure	[Pa]
q	infiltration rate at top boundary	[m/s]
q_A	amplitude of infiltration cycles	[m/s]
q_l	local net infiltration rate $q - T_z$	[m/s]

q_n	net infiltration rate $q - \tau$	[m/s]
R	sinks due to water extraction by roots	[1/s]
$R_1 - R_4$	root water uptake parametrizations	[1/s]
R_p	local potential root water uptake rate	[1/s]
R_a	local actual root water uptake rate	[1/s]
ΔR_{loss}	global deficit of uptake rate	[1/s]
S	saturation	[-]
S_e	effective saturation	[-]
t	time	[s]
t_1-t_3	characteristic time scales	[s]
t_{DS}	timescale for formation of dry spots	[s]
t_{RC}	time for recovery of dry spots	[s]
T_{pot}	global potential root water uptake	[m^2/s]
T_{act}	global actual root water uptake	[m^2/s]
T_z	potential root water uptake up to location z ($T_z = \int_z^H R_p dz$)	[m/s]
u	unknown quantity	[-]
U	random field	[U]
$\langle U \rangle$	mean of random field	[U]
W_i	weighting function for node i	[-]
$\mathbf{x}$	position vector	[m]
x	horizontal position	[m]
z	vertical position	[m]

Subscripts:

U	random field (f, α, ψ or S)
R_1, R_2	uptake strategy
0	characteristic quantity
p	pressure
g	gravity

Superscripts:

0	zeroth order
1	first order
$'$	fluctuations of random field
r	reference soil

Abstract

The unsaturated zone is the part of the soil between the aquifer and the atmosphere. Unsaturated flow processes are highly dynamic and control e.g. the growth of plants or groundwater recharge. Environmental problems such as the agricultural use of arid regions and groundwater contamination call for sustainable solutions, which can only be achieved with model predictions. To improve model quality, a sound understanding of unsaturated flow processes and the used model approaches is necessary.

The present work is intended to contribute to the understanding of modeling unsaturated flow with focus on the influence of water extraction by plant roots (root water uptake) and soil structure. The model for root water uptake, in the following called standard or basic approach, is determined by atmospheric demand, distribution of roots in the soil and soil water status. Soil properties are described by autocorrelated random fields with layered structure (1D) and multi-Gaussian or non multi-Gaussian distribution (2D).

For steady state flow in layered media, a semi-analytical first-order second-moment solution for mean and variance of pressure head is presented. Flow in 2D heterogeneous media is analyzed using numerical simulations where steady state and dynamic scenarios with one or several drying-rewetting phases are carried out.

Results show that only under very wet conditions, the mean pressure head in the differently structured fields is well predicted by the analytical solutions while variances of pressure head are overestimated if the variance of the loghydraulic conductivity is large.

Under drier conditions, root water uptake and soil structure have combined effects on unsaturated flow, which are not observed if one of these two factors is neglected, and which cannot be predicted by first-order second-moment effective models. In particular, distinct regions with pressure head values at the wilting point, where root water uptake is zero (local wilting), occur in lenses of coarse material. Furthermore, root water uptake affects the variance of pressure head and saturation during drying and rewetting phases in comparison to an equally dry state where root water uptake is not accounted for. Other effects introduced by root water uptake arise from a decreasing local net infiltration rate with depth, caused by the continuous extraction of water by roots within the root-zone. With decreasing local net infiltration rate, which leads to drier states, the impact of soil structure increases. For water flow, this leads e.g. to a depth dependency of the width of the infiltration front during rewetting. For solute transport, earlier arrival, smaller tailing and less impact of the considered structures of soil properties are observed due to root water uptake, when scenarios with and without root water uptake, which have the same groundwater recharge rate, are compared.

To test modeling approaches for root water uptake, alternative uptake strategies that allow for compensation of stressed (uptake-reduced) locations by enhanced uptake at other, more favorable locations are considered. These strategies affect the distribution of pressure head and saturation, leading to smaller variances in the root-zone and attenuated local wilting, but do not prevent local wilting.

The difficulty to evaluate the effect of local wilting as realistic physical phenomenon or unrealistic model artifact, the fact that the trend of the impact of root water uptake on the variability of flow depends on the uptake strategy and the lack of knowledge of how roots really extract water in heterogeneous soils emphasize the need for a deeper understanding of root functioning at smaller scales before macroscopic models for root water uptake can be used for reliable predictions of flow in heterogeneous media.

Zusammenfassung

Die ungesättigte Zone ist der Bereich des Bodens zwischen Grundwasserleiter und Atmosphäre. Strömungsprozesse in der ungesättigten Zone spielen u.a. eine tragende Rolle für das Wachstum von Pflanzen, die Grundwasserneubildung oder den Eintrag von Wasser in die Atmosphäre. Nachhaltige Lösungsstrategien für umweltpolitische Fragestellungen wie z.B. die agrikulturelle Nutzung von ariden Gebieten oder die Verschmutzung von Grundwasserressourcen werden mit Hilfe von Modellvorhersagen entwickelt. Um die Genauigkeit der Vorhersagen zu verbessern, ist ein fundiertes Verständnis von Strömungsprozessen in der ungesättigten Zone und der verwendeten Modelle notwendig.

Die vorliegende Arbeit soll zur Verbesserung dieses Verständnisses beitragen. Im folgenden wird die Modellierung von Strömungs- und Transportprozessen in der ungesättigten Zone behandelt. Der Schwerpunkt liegt hierbei auf dem Zusammenwirken des Einflusses der Wasseraufnahme von Wurzeln und der Bodenstruktur. Für die Modellierung der Wasseraufnahme von Wurzeln werden vereinfachte, makroskalige Modelle verwendet. Die Wasseraufnamerate ist, im hier als 'Standard-Modell' bezeichneten Ansatz, vom atmosphärischen Bedarf, der Verteilung von Wurzeln und dem vorhandenen Wasser im Boden bestimmt. Die Bodenparameter werden durch autokorrelierte Zufallsfelder mit geschichteter Struktur (1D-Felder) und multi-Gaußschen oder nicht-multi-Gaußschen 2D-Feldern beschrieben.

Für die Strömung in geschichteten Medien werden semi-analytische (first-order second-moment) Lösungen vorgestellt. Die Strömung in 2D heterogenen Strukturen wird mittels numerischer Simulationen untersucht, wobei sowohl stationäre Randbedingungen als auch zeitlich veränderliche Randbedingungen mit einem oder mehreren Trocknungs-Bewässerungszyklen angelegt werden.

Die Ergebnisse zeigen, dass der Mittelwert des Drucks in den unterschiedlichen Strukturen, mit den gewählten Parametern, nur unter sehr nassen Bedingungen gut von den analytischen Lösungen wiedergegeben wird. Die Varianz des Drucks wird hingegen überschätzt, sobald die Varianz der logarithmischen hydraulischen Leitfähigkeit zu groß wird.

Unter trockeneren Bedingungen nehmen Wasseraufnahme von Wurzeln und Bodenstruktur gemeinsam Einfluss auf Strömungsprozesse in der ungesättigten Zone, was zu Effekten führt, die unter Vernachlässigung einer der beiden Faktoren nicht beobachtet werden und die von effektiven Modellen, welche auf first-order second-moment Lösungen beruhen, nicht vorhergesagt werden. Ein Beispiel dafür ist das Auftreten von extrem trockenen Stellen in aus grobem Material bestehenden Linsen, an denen der Wasserdruck Werte am Welkpunkt erreicht und die Wasseraufnahme von Wurzeln null ist (lokales Welken). Desweiteren beeinflusst die Wasseraufname von Wurzeln, im Vergleich zu gleich trockenen Zuständen bei denen Wurzelaufnahme nicht berücksichtigt wird, die Varianz von Druck

und Sättigung während Trocknungs- und Bewässerungsphasen. Weitere Effekte, die unter Miteinbeziehung der Wasseraufnahme von Wurzeln beobachtet werden, entstehen hauptsächlich aufgrund der kontinuierlichen Entnahme von Bodenwasser durch Wurzeln, was zu einer abnehmenden lokalen Netto-Infiltrationsrate mit steigender Tiefe führt, wodurch die Struktur mit steigender Tiefe an Einfluss gewinnt. Dies wirkt sich auf den zeitlichen Verlauf der Varianz von Druck und Sättigung und den Transport von Schadstoff aus. Die einzelnen Punkte werden im folgenden ausführlicher behandelt.

Lokales Welken

Aus grobem Material bestehende Linsen haben unter trockenen Bedingungen eine geringe hydraulische Durchlässigkeit, wodurch es zum Aufstau von Wasser oberhalb der Linsen kommt. Die maximale Wasserdruckhöhe auf der Linse ist aufgrund des lateralen Druckausgleichs von den Druckwerten in der Umgebung bestimmt, welche wiederum aus der angelegten Flussrandbedingung an der Oberfläche des Gebiets resultieren. Die Flussrate von Regenwasser ins Innere der Linsen ist deshalb begrenzt. Falls lokal mehr Wasser von Wurzeln aufgenommen wird, als von außen in Linsen aus grobem Material nachfliesst, verringert die Wasseraufnahme von Wurzeln kontinuierlich den Wasserdruck in diesen, innerhalb der Wurzelzone situierten, Linsen bis der Welkpunkt, an dem die Wasserwurzelaufnahme null ist, erreicht wird. Linsen aus grobem Material können somit aufgrund der begrenzten Nachlieferung von Regenwasser ins Innere der Linsen austrocknen. Die trockenen Stellen sind von relativ nassem Material umgeben. Da der Welkpunkt bei einer Druckhöhe von $-150\,\mathrm{m}$ liegt, werden Mittelwert und Varianz der Druckhöhe beim Auftreten solcher Stellen erheblich beeinflusst. Der Mittelwert sinkt ab, die Varianz zeigt extrem hohe Werte auf. Das kritische Merkmal der Bodenstruktur, welches zum Auftreten lokal verwelkter Stellen führt, ist das Vorhandensein von Linsen aus grobem Material, deren Länge die typische Längenskala, über die Wasser von Wurzeln gezogen werden kann, übertrifft. Diese Eigenschaft der Struktur ist nicht notwendigerweise in der Korrelationslänge des heterogenen Parameterfeldes beinhaltet. Die räumliche (zwei-Punkt) bivariate Kopula hingegen spiegelt die Längenskala der Strukturen für die einzelnen Parameterbereiche wieder. Die Ausbildung von lokal ausgetrockneten Stellen könnte somit mithilfe der räumlichen zwei-Punkt bivariaten Kopula vorhergesagt werden.

Eine Zeitskala für die Ausbildung solcher Stellen während Trocknungsphasen kann mittels einer charakteristischen Zeitskala für Wasserwurzelaufnahme abgeschätzt werden. Der Zeitraum innerhalb derer eine Linse während Bewässerungsphasen wiederaufgefüllt wird, wird von der verwendeten charakteristischen Zeitskala für gravitationsbestimmte Strömung erheblich unterschätzt. Bei periodischen Trocknungs-Bewässerungszyklen lässt sich eine kritische Frequenz, unterhalb derer ausgetrocknete Stellen auftreten, ableiten. Da in tieferen Bodenschichten, aufgrund einer verspäteten Ankunft der Infiltrationsfront, Trocknungs- und Bewässerungsphasen nicht voneinander getrennt werden können, gilt diese Abschätzung nur für nah an der Oberfläche gelegene Schichten.

Das Auftreten lokal verwelkter Stellen hat unter Verwendung des Standard-Modells für Wurzelaufnahme eine Verringerung der global von Planzen aufgenommenen Wassermenge zur Folge, so dass der atmosphärische Bedarf an Wasser nicht gedeckt werden kann. Die Simulationsergebnisse zeigen, dass die lokale aktuelle Wasseraufnahme während Trocknungsphasen verringert ist. Auch wenn der Ernteertrag, der mit der globalen (über das Gebiet integrierten) aktuellen Wasseraufnahme verbunden ist, in den durchgeführten Test-Szenarien kaum betroffen ist, kann man sich jedoch darauf basierend, Szenarien vorstellen in denen das Auftreten lokal verwelkter Stellen den jährlichen Ernteertrag massgeblich reduziert. Dies könnte z.B. der Fall sein, wenn Wurzeln mit tieferer Reichweite, Bodenstrukturen mit großen Linsen, die aus gröberem Material bestehen oder Szenarien mit extrem ausgedehnten Trocknungsphasen miteinbezogen würden.

Experimentelle Studien besagen, dass Pflanzen eine reduzierte Aufnahmerate aufgrund von auftretendem Stress an oberen Bodenschichten durch erhöhte Aufnahme in unteren Schichten kompensieren können, so dass die globale aktuelle Aufnahme dem atmosphärischen Bedarf gegenüber kein Defizit aufweist. Auf der Annahme basierend, dass Pflanzen sowohl lokal auftretenden Stress an bestimmten Stellen ausgleichen können, wird das Standard-Modell für Wasserwurzelaufnahme (Strategie 1) mit alternativen Modellen verglichen, die Kompensationsmechanismen beinhalten. Diese hängen von der Sättigung (Strategie 2) bzw. von der relativen Permeabilität (Strategy 3) ab oder verteilen die Differenz zwischen globaler aktueller und globaler potentieller Aufnahme gleichmässig auf ungestresste Stellen um (Strategie 4). Der Kompensationsprozess ist so implementiert, dass die globale (über das Gebiet integrierte) Menge an aufgenommenem Wasser dem potentiellen, von der Atmosphäre vorgegebenem Wert entspricht. Lokal verwelkte Stellen treten auch mit den alternativen Ansätzen für Wasserwurzelaufnahme auf, wobei die Bildung mit Strategie 2 und 3, die, im Vergleich zum Standard-Modell, zu einer geringeren Aufnahme an ungünstigen und einer erhöhten Aufnahme an günstigen Stellen führen, abgeschwächt wird. Das Auftreten der trockenen Stellen wird mit diesen Strategien somit in einigen Fällen, jedoch nicht grundsätzlich, verhindert.

Im Allgemeinen erscheinen die mit den oben beschriebenen Modellansätzen erlangten Ergebnisse diskussionswürdig. Eine nach dem Standard-Modell vorhergesagte Verringerung des Ernteertrags erscheint unrealistisch, vor allem bei stationären Randbedingungen und unter Anbetracht dass die trockenen Stellen lokal auftreten und der Gesamtwassergehalt im Gebiet einen gewissen Grenzwert nicht unterschreitet. Daher gewinnt die Einbeziehung von Kompensationsmechanismen in heterogenen Böden an Bedeutung. Dies könnte möglicherweise zu einer Überschätzung des Ernteertrags führen, falls Pflanzen eine Reduktion der Wasserwurzelaufnahme aufgrund von Stress nicht vollständig ausgleichen können. Zudem treten ausgetrocknete Stellen mit Druckwerten am Welkpunkt auch bei Verwendung der alternativen Modelle für Wasseraufnahme von Wurzeln auf. Da diese trockenen Stellen von nassem Material umgeben sind, erscheinen sie ebenfalls unrealistisch. Das eigentliche Problem ist jedoch, dass die nötigen Informationen, solche Effekte als realistisch oder unrealistisch einzuordnen zu können, nicht vorhanden sind. Dies lässt schlussfolgern, dass makroskalige Modelle für die Wasseraufnahme von Wurzeln, deren Aufnahmerate lokal festgelegt wird, in homogenen Böden zwar gut verwendbar sein mögen, jedoch in heterogenen Böden zu Effekten führen, die die generelle

Gültigkeit des konzeptionellen Modells in Frage stellen. Für heterogene Medien wären Wurzelaufnahmemodelle, die die Reaktion des Gesamtsystems berücksichtigen, besser geeignet. Ob das Auftreten lokal ausgetrockneter Stellen in bestimmten Bodenstrukturen tatsächlich ein Modellartefakt ist und in welchem Ausmaß Kompensation existiert, kann nur unter Miteinbeziehung boden-physikalischer und pflanzen-physiologischer Vorgänge beurteilt werden. Diese sind auf größeren Skalen einerseits schwierig einzubeziehen und anderseits in heterogenen Medien kaum erforscht.

Schadstofftransport

Die, aus den Strömungssimulationen abgeleiteten, stationären Verteilungen der Darcy-Flüsse (in Gaußschen und nicht-Gaußschen Feldern) werden für die Durchführung eines numerischen Transportexperiments verwendet. An der Oberfläche wird ein Schadstoffpuls ins Gebiet eingelassen und unterhalb der Wurzelzone, oberhalb des Grundwasserspiegels aufgezeichnet. Fluss-gemittelte Durchbruchskurven (die zeitliche Ableitung der gesamten, normalisierten Konzentration im Gebiet) werden mit Blick auf Einfluss der Wasseraufnahme von Wurzeln und nicht-Gaußscher Strukturen untersucht. Es zeigt sich, dass beide Faktoren den Transport von Schadstoff in den durchgeführten Szenarien beeinflussen.

Der Schadstoff durchquert Felder, die unter den angelegten Bedingungen verbundene Pfade aus gut durchlässigem Material und Linsen aus schlecht durchlässigem Material besitzen, am schnellsten und Felder, die das entgegengesetzte Muster aufweisen, am langsamsten. Generell ist die Fließzeit durch die Infiltrationsrate an der oberen Randbedingung bestimmt. Zwischen den einzelnen Strukturen beobachtete Unterschiede nehmen mit fallender Infiltrationsrate zu. Daher befinden sich, bei Miteinbeziehung der Wasseraufnahme von Wurzeln, sowohl die Ankunftszeiten der Hauptmasse des Schadstoffs als auch beobachtete Unterschiede zwischen den verschiedenen Strukturen zwischen den Werten die sich mit Szenarien ohne Wurzelaufnahme ergeben, deren Infiltrationsraten der Infiltrationsrate an der oberen Randbedinungen bzw. der Netto-Infiltrationsrate im Wurzelszenario entsprechen. Beim Vergleich zweier Szenarien im bewachsenem und unbewachsenem Boden mit derselben Grundwasserneubildungsrate, führt die Wasseraufnahme von Wurzeln in allen in Betracht gezogenen Strukturen zu schnelleren Fließpfaden durch die Wurzelzone. Die Konzentration, die von stagnanten Zonen im Boden zurückgehalten wird, ist in Feldern mit nassen Linsen (unter den gegebenen Bedingungen) höher als in Feldern mit trockenen Linsen. Da Wasserwurzelaufnahme die Durchlässigkeit in Linsen aus grobem Material verringert, so dass weniger Schadstoff in diese Regionen gelangt, könnte die Wasseraufnahme von Wurzeln die von der Struktur zurückgehaltene Konzentration in Feldern mit Linsen aus grobem Material, die unter den angelegten Randbedingungen trocken sind, erniedrigen.

Die vorliegende Studie zeigt, dass Unterschiede im Transportverhalten zwischen den einzelnen, betrachteten Strukturen existieren. Die oft gemachte Annahme einer multi-Gaußschen Verteilung der Bodenparameter kann somit in einer Über- oder Unterschätzung der Ankunftszeiten des Schadstoffs resultieren. Die Unterschiede bei der Ausbreitung des Schadstoffs in Gaußschen und nicht-Gaußchen Strukturen spielen eine wichtige Rolle für die Reaktionen, die der Schadstoff auf seinem Weg durch die ungesättigte Zone unterläuft. Umso langsamer die Ausbreitungsgeschwindigkeit ist, desto mehr Reaktionen laufen

ab und desto weiter schreitet der Abbau des Schadstoffs voran. In diesem Sinne ist die Einbeziehung von Struktur sehr wichtig für die Abschätzung des Schadstoffeintrags ins Grundwasser. Da sich bei gleicher Grundwasserneubildungsrate, unter Berücksichtigung von Wurzeln schnellere Fließpfade ergeben, was wiederum den Abbau des Schadstoffs beeinflusst, darf der Schadstoffeintrag ins Grundwasser nicht allein auf Neubildungsraten basierend bestimmt werden. Beide Faktoren, das Vorhandensein von Wurzeln und der Bodenstruktur sollten deshalb in der Modellierung berücksichtigt werden, wenn die Studie auf Umweltprobleme in Verbindung mit Schadstofftransport gerichtet ist.

Variabilität von Druck und Sättigung

Die Verteilung des Wassergehalts im Boden, unter anderem durch Mittelwert und Varianz beschrieben, charakterisiert das Strömungsverhalten von Wasser und geht in gekoppelte Systeme, wie z.B. Klimamodelle, als wichtiger Parameter ein. Als weiterer Punkt wird daher der Einfluss der Wasseraufnahme von Wurzeln und der Heterogenität der Bodenparameter auf den Mittelwert und die Varianz der Druckhöhe und der Sättigung diskutiert.

Simulationen mit stationären Randbedingungen in 2D heterogenen Feldern ergeben, dass die Varianz der Druckhöhe unter sehr nassen und sehr trockenen Bedingungen groß ist. Da die hydraulische Leitfähigkeit von grobem Material mit zunehmender Trockenheit schneller abnimmt als die hydraulische Leitfähigkeit von feinem Material, gibt es einen Bereich in dem die Leitfähigkeit von grobem und feinem Material sehr ähnliche Werte annimmt, so dass die Struktur wenig ausgeprägt und die Varianz der Druckhöhe klein ist. Außerhalb dieses Bereichs (bei niedrigeren Wasserdruckwerten), sind trockenere Zustände generell mit einer höheren Variabilität verbunden.

Unter transienten Bedingungen, während Trocknungsphasen, erhöht sich die Variabilität von Druck und Sättigung. Während der Bewässerung ist der Trockenheitszustand des Bodens nicht zwangsläufig mit der Variabilität verbunden, da sich in mehrdimensional strukturierten Böden eine heterogene Bewässerungsfront entwickelt, welche bei Eintreffen in einer bestimmten Bodenschicht, die Varianz von Druck und Sättigung in dieser Schicht erhöht. Wenn die Infiltrationsfront die jeweilige Schicht passiert hat, sinkt die Varianz von Druck und Sättigung wieder ab. Je nach Aufnahmestrategie der Wurzeln werden während des Trocknens und Bewässerns leicht erhöhte oder erniedrigte Varianzen des Drucks und der Sättigung im Vergleich zum unbewachsenen Fall beobachtet. Die betrachteten Strukturen der Bodenparameter beeinflussen Mittelwert und Varianz von Druck und Sättigung nur wenig. Da Wasserwurzelaufnahme, im Vergleich zu einem gleich trockenen Zustand im unbewachsenen Boden, Einfluss auf die Varianz der Sättigung nimmt, ändert sich die Beziehung von Mittelwert und Varianz der Sättigung im bewachsenen Boden.

Der Punkt, an dem der mittlere Druck in einer bestimmten Bodenschicht nach einer Trocknungsphase anzusteigen beginnt (Minimum der Druckhöhe), entspricht dem ersten Eintreffen von Regenwasser in dieser Schicht. Das Maximum der Varianz kann als Maß für das Eintreffen der mittleren Front in dieser Schicht gesehen werden. Der beobachtete Zeitversatz zwischen Minimum des Mittelwerts und Maximum der Varianz des Drucks oder der Sättigung kann somit als Maß für die Breite der Infiltrationsfront dienen. Die Frontbreite nimmt

mit abnehmener Netto-Infiltrationsrate ab. Somit ist die Breite der Infiltrationsfront beim Durchqueren der ungesättigten Zone im unbewachsenen Fall eher konstant, während die Frontbreite im bewachsenen Fall mit der Tiefe zunimmt. Da sich die Frontbreite in Szenarien mit Wasserwurzelaufnahme mit steigender Tiefe weitet, werden Vorhersagen von Ankunftszeiten der Infiltrationsfront, die auf gewöhnlichen, effektiven Bodenparametern beruhen, zunehmend schwieriger und ungenauer mit der Tiefe.

Der Variationskoeffizient der Druckhöhe ist in den analysierten Testfällen hauptsächlich von der Varianz bestimmt, so dass er im Bezug auf das Minimum des mittleren Drucks zeitlich versetzt sein Maximum erreicht. Der Variationskoeffizient der Sättigung hingegen wird vom Mittelwert dominiert und erreicht seinen Höchstwert nur mit sehr kleinem Zeitversatz zum Minimum der mittleren Sättigung.

Zusammenfassend lässt sich sagen, dass die Wasseraufnahme von Wurzeln und die Heterogenität der Bodenparameter gemeinsam Strömungsprozesse in der ungesättigten Zone beeinflussen, so dass keiner der Faktoren vernachlässigt werden kann, was bei gross-skaligen Anwendungen oft der Fall ist. Die Schwierigkeit, das Auftreten lokal verwelkter Stellen, die hier mit allen berücksichtigten Wurzelmodellen auftreten, als realistisch oder unrealistisch einordnen zu können, die Tatsache dass der Einfluss von Wurzeln auf die Variabilität von Druck und Sättigung von der Aufnahmestrategie abhängt und die vorherrschende Wissenslücke, tatächliche Entwicklungs- und Aufnahmemechanismen von Wurzeln in heterogenen Böden betreffend, verdeutlichen die Notwendigkeit eines tieferen Verständnisses für die Funktionsweise von Wurzeln auf kleinen Skalen bevor makroskalige Modelle für die Wasseraufnahme von Wurzeln für verlässliche Vorhersagen von Stömungsprozessen in heterogenen Böden verwendet werden können.

Ausblick

Ein konzeptionelles Verständnis für die Funktionsweise von Wurzeln in heterogenen Böden könnte mittels physikalischer Experimente und numerischer Studien vorangetrieben werden. Experimente auf der Labor- und Feldskala, aber vor allem auch mikroskalige biologische Erkenntnisse über Wurzelverhalten in heterogenen Strukturen könnten von Wert sein. Besonders interessant wäre die Messung kritischer Druckwerte unterhalb derer reduzierte oder keine Aufnahme stattfindet, und deren Abhängigkeit von Bodenparametern.

Auf der numerischen Seite erscheint die Verwendung von makroskaligen Modellen, die Wurzelaufname als Optimierungsproblem behandeln, oder die Verwendung von mikroskaligen Modellen, die Wasserwurzelaufnahme in Folge von Druckgradienten zwischen Boden und Wurzel simulieren, vielversprechend. Nach den Ergebnissen dieser Arbeit zufolge sollte sich die Analyse auf das Verhalten eines Wurzelsystems in der Nähe von Linsen aus grobem Material konzentrieren. Desweiteren wäre die Entwicklung der Varianz von Druck und Sättigung in unterschiedlich strukturierten Böden unter Verwendung eines mikroskaligen Modells interessant.

1 Introduction

1.1 Motivation

The development of efficient crop-production and sustainable irrigation strategies is of major importance due to a growing world population and decreasing water resources. In order to increase the agricultural yield, fertilizers and pesticides are often intensively used, which could contaminate groundwater resources. Finding solutions for environmental problems such as the agricultural use of arid regions or groundwater contamination becomes more difficult in the future since heat waves and heavy rainfall are expected to intensify (IPCC, 2007). The formation of cracks in the soil during dry periods makes groundwater resources more vulnerable for contamination during events of heavy rainfall. Reduced availability of water in the soil limits the uptake of water by roots and causes restricted growth or even wilting of plants. To be able to handle these problems, reliable model predictions of flow and transport processes in the upper part of the soil are necessary.

The part of the soil between aquifer and atmosphere is referred to as unsaturated zone. Flow processes are controlled by precipitation, evapotranspiration and groundwater recharge. Figure 1.1 shows a sketch of the unsaturated soil zone including relevant flow processes. Water movement is indicated by dark blue arrows, exchange with the atmosphere additionally by light blue arrows. Two important factors for unsaturated flow, which are in the focus of this work, are the soil heterogeneity and the vegetation whoose roots extract soil water (denoted by 'root water uptake' (RWU)). Note that the terms 'heterogeneity' and 'soil structure' are used interchangeably in this study.

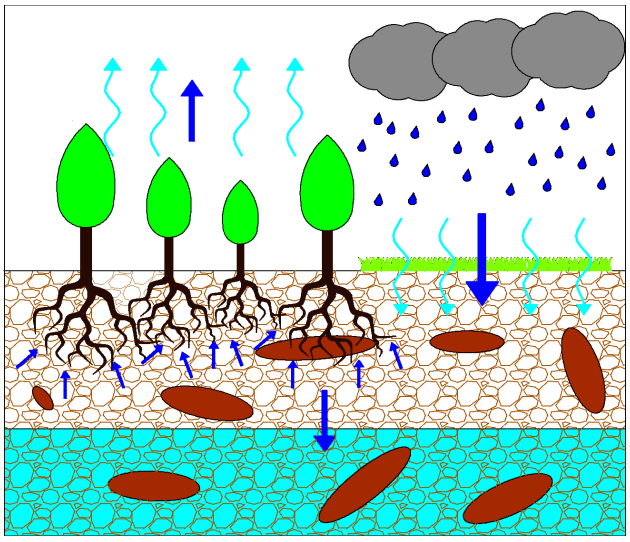

Figure 1.1: *Sketch of the unsaturated zone. Flow processes are determined by precipitation, evapotranspiration and groundwater recharge. Movement of water is indicated by dark blue arrows, exchange with the atmosphere additionally by light blue arrows.*

Motivated by different fields of interest, root water uptake and heterogeneity of the soil have often been analyzed separately. Studies on large-scale root water uptake usually address crop production while studies which include soil heterogeneity are mostly motivated by contaminant transport. However, root water uptake and soil structure have combined effects on unsaturated flow. As the supply of water is essential for plants to live and grow, root water uptake is affected by soil heterogeneity. Conversely, plant roots influence the soil structure by changing the soil moisture and by growing into the soil. Therefore, this work jointly considers the influence of root water uptake and soil heterogeneity on unsaturated flow.

The approach used to model the system depends on the scale of interest. Root water uptake and heterogeneity affect unsaturated water flow on a local scale: Roots extract water at distinct locations and flow pathways of water depend on the pore geometry of the soil matrix. However, for most environmental applications, larger scales of several meters or kilometers are relevant. With increasing size of the system, factors which are crucial on small scales may become less important and large-scale pattern such as the variation of soil properties or percentage of root mass per depth might dominate. Small-scale processes are thus often neglected, and simplified or averaged approaches, so-called upscaled models, are preferably used when environmental problems are treated. These model approaches also vary with respect to the considered level of complexity. Artificial terms, which are supposed to represent small-scale processes on larger scales, are sometimes introduced to governing equations. When choosing a model for large-scale environmental applications, it is important that the considered approach be as simple as possible but does not lead to a loss of relevant information. The use of large-scale models gets problematic if effects exist that cannot be reproduced by the simplified model for example due to neglected interactions between flow-influencing factors. Using more complex large-scale approaches can be problematic as well because ar-

tifacts may be introduced to predictions by insufficiently represented processes which originate on smaller scales. Nevertheless, such approaches are used on large scales, but to make reliable predictions, conditions which restrict the applicability of upscaled models should be well defined.

In the following sections, micro- and macroscale model concepts for root water uptake and heterogeneity are explained.

1.2 Root water uptake

Soil water enters the root induced by pressure and osmotic gradients between the surface and the inner part of the root. Subsequently, water travels to the xylem where it is transported up to the foliage. There, water evaporates into the atmosphere through openings at the leaves, so called stomata. Figure 1.2 illustrates the water cycle in a plant.

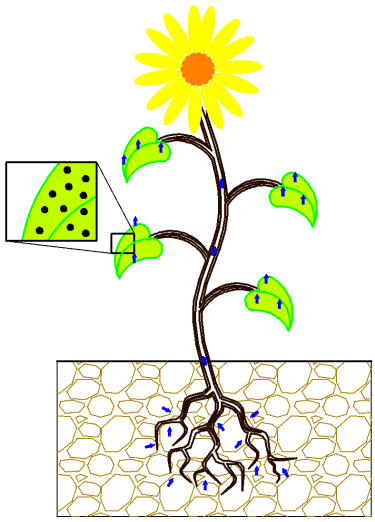

Figure 1.2: *Water cycle in a plant: water is taken up at the roots of a plant and transported to the leaves where it evaporates into the surrounding air.*

Thus, stomata control the transpiration of plants. If they are covered with water during rainfall cycles, transpiration is assumed to be inhibited. If the stomata are exposed to the atmosphere, the demand of water by plants is driven by meteorological variables, such as solar radiation, air temperature and wind speed, but also plant parameters, such as an average leaf area. Root water uptake is assumed to be controlled by the highest occurring resistance. Under wet conditions, the highest hydraulic resistance occurs in the leaf with water evaporation into the surrounding air and uptake is demand-controlled (Hopmans and Bristow, 2002). Depending on the geometry and distribution of the root system as well as the uptake strategy, the extraction rate is distributed over the root zone such that the integrated global uptake rate equals the atmospheric demand. Measurement data suggest that the root

surface area rather than the root length distribution is the measure of root geometry that determines uptake. Furthermore, uptake takes place predominantly within $30\,\mathrm{cm}$ from the root tip (Varney and Canny, 1993). As roots grow and decay, the active root distribution in the soil develops with time. Very little is known about the strategies how roots develop and take up water in a variably saturated soil.

As the soil dries out, the decreasing unsaturated soil hydraulic conductivity and the possibly decreasing root-soil contact lead to an increased flow resistance. Unfavorable conditions, such as water scarcity or lack of oxygen that occur under extremely wet conditions, can induce stomata closure and thereby cause a reduction of the uptake rate (Augé and Moore, 2002). Under so-called stressed conditions, root water uptake is, therefore, supply-controlled (Hopmans and Bristow, 2002). Experimental data suggest, that root systems can compensate local reduction of the water uptake rate by increased extraction at other locations where sufficient water is available (e.g. Taylor and Kleppner, 1978; Hasegawa and Yoshida, 1982; English and Raja, 1996; Stikic et al., 2003; Leib et al., 2006). The exact mechanism is, however, barely understood.

Clearly, the extraction of water by plant roots is a complex process. Moreover, knowledge gaps exist regarding the exact mechanisms of root functioning.

Model concepts for root water uptake were developed on different scales. Reviews on water transpiration have been given by, e.g., Nimah and Hanks (1973), Molz (1981), Passioura (1988), Hopmans and Bristow (2002), Cardon and Letey (1992), Wang and Smith (2004) and Raats (2007). Generally, complexity of models decreases with domain size. Approaches to model water uptake by plant roots are mainly divided into two types: Microscopic models where root water uptake is determined by radial water flow in response to water potential gradients, and macroscopic approaches which consider extraction of water by the root zone as a volumetric sink term in the water mass balance.

On the scale of a single root, three types of models are used to model water flow. The first accounts for water flow inside the root, the second type deals only with water flow in the soil (both are described by, e.g., Hopmans and Bristow (2002) and Raats (2007)). The third type combines both (Roose and Fowler, 2004; Doussan et al., 2006). These models are based on the work of, e.g., Gardner (1960), Philip (1966), Dalton et al. (1975) and Herkelrath et al. (1977a,b). Gradients between the water potential inside the root and water potential in the soil at the root surface are assumed to drive radial flow of water towards the root. Water flux into the root is balanced by the axial flux along the root. Water flow from roots to leaves through the xylem is often assumed to be described by Poiseuilles law (Roose and Schnepf, 2008).

Models for a single root can be extended to work on the root-system (plant) scale. Additionally, growth mechanisms are considered in different ways. Initially, such models were used to compare observed root systems with simulated ones. Later, the goal was rather, to obtain average properties and characteristics of root water uptake (Roose and Schnepf, 2008). Recently, models on a root-system scale were developed which couple micro- and macro approaches, in particular the flow of soil water, determined by Richards' equation and water transport in the xylem of a three-dimensional root network. A volumetric sink term for

each soil node is determined by summation over the radial fluxes of root segments, which are located in the corresponding soil voxel (Javaux et al., 2008). Compensation patterns occur due to the root architecture and an optimized distribution of the extraction rate. Javaux et al. (2008) illustrated that the macroscopic extraction rate derived from the fully resolved three-dimensional root uptake model follows the root density distribution as long as sufficient water is available. As the soil is depleted by water, the extraction pattern changes and the maximum average uptake rate moves further down.

In macroscale approaches, the water extraction by plant roots is usually modeled as a spatio-temporally uniform or variable sink term in the water balance equation (Whisler et al., 1968; Molz and Remson, 1970; Verburg et al., 1996). Hopmans and Bristow (2002) reviewed larger scale crop models, water and nutrient uptake models. The volumetric sink term is obtained in two ways, referred to as so-called Type 1 and Type 2 models.

Based on the radial water flow to a single root, Type 1 models, introduced by Nimah and Hanks (1973), use an Ohm's law analogy where uptake is determined by three factors. First, a difference in water potential between the soil and the plant, second, a network of resistances, consisting of the resistance to flow in the soil and the resistance to flow across the root surface and through the roots, and third, a water flow- geometry term (e.g. Guswa, 2005; Green et al., 2006). Since the root resistance is included to determine the transition from potential to reduced uptake, compensation of reduced uptake due to local stress is not introduced to the model but results automatically as a consequence of the root water uptake formulation (e.g. Hopmans and Bristow, 2002; Guswa, 2005). However, microscale-modeling as well as macroscale-Type1 approaches require information about root geometry which is generally not available in detail. Moreover, on larger scales of several meters or kilometers, such detailed models would overload current computation power and strongly simplified approaches need to be used. Type 1 models are thus more suitable for water flow calculations on the root system scale.

On the plot and field scale, Type 2 models, which are based on empirical relations, are favored. In such models, root water uptake is commonly assumed to be dependent on available water in the soil and the root distribution function that describes the relative presence of roots as a function of depth. The root distribution function can be modeled either as a one-dimensional (e.g. Molz, 1981; Hoffman and Genuchten, 1983) or a multi-dimensional root density distribution function (e.g. Coelho and Or, 1996; Vrugt et al., 001a,b). Beyond the one-dimensional descriptions, an exponentially decreasing function with depth is most common. Specific active root distributions that take only the parts of roots into accout, which are actively involved in root water uptake, were reported e.g. by Hoogland et al. (1981) and Raats (1974). A temporally changing root distribution function was investigated by Clausnitzer and Hopmans (1994). If root distribution functions are, however, too complex, they run into the same problems as Type 1 models. Data on root geometry is not available and simulations are extremely demanding which restricts such models to a scale of root systems.

To account for water stress, the reduction factor approach, proposed by Feddes et al. (1976) is the most popular. In this approach, the potential transpiration is multiplied by a factor which is equal to one if conditions are favorable and, depending on water pressure head or saturation, decreases under unfavorable conditions. Different parametrizations and shapes

are discussed (e.g. Skaggs et al., 2006). Feddes et al. (1976) proposed a linear reduction of uptake with pressure head under extremely wet and dry conditions due to oxygen or water deficit, characterized by four critical values of pressure head. In the range of intermediate values, the reduction factor is constant and equals one. An alternative smooth, S-shaped reduction function was suggested by van Genuchten (1987).

Compensation for stressed conditions was rarely included in macroscale vadose zone models. In the study of Li et al. (2001) and Bouten (1995), the potential transpiration rate was weighted according to a stress index which was depending on root distribution and soil water availability or saturation. Katul et al. (1997) compared different weighting factors, amongst others, a factor depending on the saturation with a weighting factor determined by the hydraulic conductivity. Jarvis (1994), Pang and Letey (1998) and Simunek and Hopmans (2009) also used a weighted stress index and allowed for partial compensation beyond a critical value. A section about macro-models which include compensation mechanisms can be found in the review of Skaggs et al. (2006).

Analytical solutions for unsaturated flow in homogeneous soil with water extraction by plant roots modeled by a sink term were first presented by Warrick (1974) and extended by, e.g., Basha (1999), Braddock and Parlange (2000), Braddock and Parlange (2003) and Yuan and Lu (2005). The dynamics of vegetation at the scale of ecosystems were analyzed by, e.g., Rodriguez-Iturbe et al. (1999), Laio et al. (2001), Porporato et al. (2001) and Guswa et al. (2002). The mean intensity, duration and frequency of periods with water deficit could be quantitatively described to derive optimal conditions for vegetation (e.g. Porporato et al., 2004).

1.3 Flow in heterogeneous soil

Soil heterogeneity and structure were often neglected in vadose zone models which consider root water uptake (Wang and Smith, 2004). However, variability of soil hydraulic properties significantly affects flow processes. An overview of possibilities to describe soil heterogeneity is given in this section.

Natural soils show spatial and temporal variations in the arrangement of pore sizes and consisting materials. Soil hydraulic properties, thus differ in space and show various structures. Samples of different soil profiles are illustrated in Figure 1.3.

One distinguishes between micro-heterogeneity which refers to the heterogeneity at the pore-scale, like the existence of macropores and elements which form a separate pore network, and macro-heterogeneity which comprises the spatial variability of macroscopic soil properties which determine flow at a macroscopic scale. The two types of soil heterogeneity require different modeling approaches (Feyen et al., 1998). Reviews on different descriptions, upscaling approaches and model concepts were given by, e.g., Feyen et al. (1998), Vereecken et al. (2007b) and Harter and Yeh (1998).

Figure 1.3: *Pictures of soil columns illustrating the heterogeneity of the soil. Note that the two profiles on the right side are grown with roots. The pictures were taken in the Soil Museum Wageningen.*

On the pore scale, detailed knowledge of the soil parameter distribution is available by methods such as magnetic resonance imaging (MRI). Due to the large differences between the flow behavior in the soil and in macropores, the classical continuum approach cannot be applied to micro-heterogeneous structures. Often dual - porosity models are used and have shown potential to reproduce measured data on flow and transport.

On the macroscale, soil parameters are assumed to vary continuously and Richards equation can be applied to model flow. However, field tracer tests have demonstrated that flow patterns are extremely complex and irregular (Feyen et al., 1998). Amongst others, effects such as horizontal redistribution of solutes (Schulin et al., 1987), preferential movement through macropores (Flury et al., 1995) or fingered flow (Ritsema et al., 1993), were observed. Several concepts have been developed to model flow in a macroscale heterogeneous soil, they can be divided into two main classes. First, a deterministic approach, where definite values of the varying property are attributed to each point of space assuming that slight variations are unimportant or assumed to be represented by an equivalent homogeneous medium obtained by upscaling techniques. A field specific distribution of measured soil parameter values can be used as well. The second class comprises stochastic approaches which essentially differ from deterministic approaches by assuming that each property is described by a distribution at each point of space. In contrast to the deterministic approach, the stochastic approach accounts for the variability of soil parameters and is able to quantify emerging uncertainties which is crucial on the field scale, since only few measurement points contribute to the estimation of soil properties.

In the stochastic approach, flow processes are modeled by the same continuum equations that are used in a homogeneous field (Feyen et al., 1998). The soil hydraulic parameters are assumed to be random space functions. Often, based on the concept of Miller-similar soils (Miller and Miller, 1956) only differing in scale but not in pore geometry, variability of soil properties is described by a scale factor which relates the constitutive relationships at

different locations to an average hydraulic function. In fact, only the linear components of hydraulic functions such as the saturated hydraulic conductivity are described by scaling factors (Tillotson and Nielsen, 1984). The scale factors in the similarity concept are modeled as random fields. As a consequence, the hydraulic variables such as pressure and saturation are also random space functions, representing the spatial heterogeneity of the system.

For unsaturated flow without root water uptake, this topic has been addressed by, e.g., Dagan and Bresler (1979). Their pioneering work resulted in a large body of literature. The objective is generally to derive stochastic properties of flow variables (pressure head, water content, water flux) and effective flow parameters which are constant in space and predict mean water flow. Approaches to reach this goal mainly differ between analytical solutions and numerical studies.

Steady state flow was analyzed analytically by, e.g., Yeh et al. (1985a,b,c) using a perturbation approximation. The variance of hydraulic variables and effective hydraulic conductivity were analyzed as function of the statistical properties and mean flow characteristics. Analytical solutions for the mean and the variance of pressure head in a multiple layered unsaturated soil were derived by Lu and Zhang (2004) and Lu et al. (2007). Mantoglou and Gelhar (1987a,b,c) extended the solutions of Yeh et al. (1985a,b,c) to transient conditions emphasizing the effects of vertical heterogeneity on the effective soil hydraulic properties.

The most common way to numerically approach stochastic models is the Monte Carlo method. For a Monte Carlo study, numerous realizations of parameter fields with the desired statistical properties, representing the soil, need to be generated. In each field, the flow equation is numerically solved. Subsequently, mean and variance of the obtained hydraulic variables are calculated by averaging over the realizations. They provide a measure on the mean flow behavior in a parameter field with variable soil hydraulic properties including uncertainties of predictions. Since the computational effort is high if flow in higher dimensional domains is analyzed, research is increasingly conducted in the direction of alternative stochastic approaches where analytical expressions or measurement data are included to reduce the necessary computation power.

Various numerical studies on unsaturated flow in heterogeneous soils (Warrick et al., 1977; Warrick and Amoozegar-Fard, 1979; Peck et al., 1977; Hopmans et al., 1988) tested the performance of effective parameters derived by analytical solutions (Anderson and Shapiro, 1983; Hopmans et al., 1988; Polmann et al., 1991) or investigated more complex structures such as preferential flow in 2D isotropic heterogeneous domains (e.g. Roth, 1995; Birkholzer and Tsang, 1997). It was found, that the analytical predictions, made by the stochastic theory, agree well with the averaged profiles of the simulated heterogeneous pressure head distributions. The underlying assumptions of the perturbation approximations such as small variability of the soil parameters were found not to be critical in the test cases examined. Observations on variance of pressure, hysteresis and large-scale anisotropy of effective hydraulic conductivities could be confirmed by the detailed simulations as well (Polmann et al., 1991). The standard deviation of the pressure head increases generally with increasing variance of the loghydraulic saturated conductivity and with decreasing water content. With increasing dimensionality of the soil domain, the standard deviation of the pressure head decreases (Hopmans et al., 1988).

In the early studies, scaling factors were assumed to be statistically independent. As analysis of data on soil parameters show that scale factors can be autocorrelated (e.g. Hopmans, 1987), correlated random fields were used in later work (e.g. Hopmans et al., 1988). Variability of soil parameters has been described mostly with multi-Gaussian correlated random fields. In two dimensions, multi-Gaussian structure manifests as isolated extreme values. Nevertheless, under very dry conditions, processes such as the formation of cracks or shrinking of roots may create macropores which result in connected pathways that are not captured by multi-Gaussian fields. Neuweiler and Cirpka (2005) and Neuweiler and Vogel (2007) considered non-multi-Gaussian fields with connected high and low extreme values in comparison with Gaussian fields. Effective hydraulic conductivities were determined by homogenization theory. It was found that connectivity of extreme values does only have a significant influence on the mean flow if the soil is very dry.

The flow pattern in two-dimensional Miller-similar random parameter fields was analyzed by, e.g., Roth (1995) and Birkholzer and Tsang (1997). Miller-similarity involves a correlation of the saturated hydraulic conductivity and the entry pressure. Depending on the relative specific discharge (compared with saturated conductivity), a network of flow channels develops. The hydraulic conductivity of coarse material is under saturated conditions larger than that of fine material but decreases due to the lower air entry pressure stronger with decreasing saturation than that of fine material. This leads to a crossover of the hydraulic conductivity of coarse and that of fine material at a specific saturation, as illustrated by Roth (1995). This means that the hydraulic conductivity of coarse material is smaller than the hydraulic conductivity of fine material for saturations lower than the crossover point. At intermediate saturations close to the crossover, the variance of the conductivity has a minimum and the soil structure behaves as rather homogeneous. At very dry states, the pattern of the conductivity at fully saturated conditions is inverted. Correspondingly changes the location and pattern of the flow channels.

The standard deviation of soil moisture as function of the mean value was analyzed intensively by experimental and numerical studies. Increasing (e.g. Bell et al., 1980; Famiglietti et al., 1998; Oldak et al., 2002) as well as decreasing (e.g. Famiglietti et al., 1999; Choi and Jacobs, 2007) variability with decreasing mean saturation was found. During drying from very wet states, $\sigma_S(< S >)$ was shown to follow a parabolic curve. σ_S initially increases until a maximum is reached and decreases during further drying, (e.g. Ryu and Famiglietti, 2005; Choi and Jacobs, 2007; Choi et al., 2007; Harter and Zhang, 1999). Explanations were given based on empirical (Hu and Islam, 1998) and statistical analysis of field data (e.g. Ryu and Famiglietti, 2005) as well as stochastic theories (Vereecken et al., 2007a). It was shown that $\sigma_S(< S >)$ depends on the soil hydraulic parameters and that the pore-size distribution determines the maximum value of σ_S.

1.4 Root water uptake in heterogeneous soils

In heterogeneous media, the assumptions of a uniform distribution and uptake ability of roots might not be given. On the pore-scale, roots are found clustered in cracks and biopores (Taylor, 1974; Wang and Smith, 2004). The results by Hatano et al. (1988) and Hatano and Sakuma (1990) indicate that the root distribution depends on the distribution of macropores. The effect of macropores on root water uptake pattern is, however, unclear. On one hand, the soil volume explored by a root system is much smaller compared to a uniform root distribution. Additionally, roots may be in poor contact with the soil (Herkelrath et al., 1977b) and unfavorable soil structure might induce roots to send growth reducing signals (Passioura, 2002). On the other hand, macropores provide the opportunity to reach deeply located wet layers and nutrients (Cornish, 1993). The non-uniform distribution of roots and uptake ability is assumed to influence root water uptake also on the macroscale. However, a large knowledge gap exists regarding this topic. According to Wang and Smith (2004), the use of strongly simplified models on the field scale is likely to lead to an overestimation of root water uptake in structured soils.

The interaction of root water uptake and flow in random heterogeneous soils has been considered in few studies only. The topic was addressed by Rubin and Or (1993), who derived an analytical steady-state solution for a one-dimensional column model with root water uptake in a stochastic framework. They found that root water uptake has a strong influence on the mean and variance of pressure and saturation. In the root-zone, where water is continuously extracted by plant roots, the mean water content decreases with increasing depth, and increases with depth below this zone. The variance of saturation and pressure head follow the mean profile, high saturations relating to low variances and vice versa. Soil heterogeneity with root water uptake was also analyzed by Kim et al. (1996, 1997) who showed that the consideration of soil heterogeneity is relevant for the spatial average of evapotranspiration using a one-dimensional water budget model. Katul et al. (1997) compared predicted and measured time series of mean and variance of the soil moisture with different uptake models. A root water uptake term that depends on water content consistently gave good agreement with the measurements but differences between the different strategies were found to be small. The variability of pressure head, however, depends on the uptake model, as demonstrated by Hopmans et al. (1988).

Transpiration dynamics influence the variability of flow. Albertson and Montaldo (2003) analyzed the temporal changes of soil moisture variability in the unsaturated zone using a one-dimensional model that includes vegetation. It was concluded that transpiration and infiltration may increase or decrease the variance of soil moisture depending on the soil moisture state. Teuling and Troch (2005) compared model results with measurements at three different sites. Contradictory observations of increasing as well as decreasing standard deviation of soil moisture with decreasing mean value, earlier reported (e.g. Famiglietti et al., 1998, 1999), were explained by the temporal dynamics of the interaction between soil, vegetation, and topography controls. The main factor between both cases (creating or destroying spatial variance) was found to be whether or not the soil dries below a critical moisture content which defines the transition between unstressed and stressed transpiration. Rodriguez-Iturbe et al. (2006) found that vegetation heterogeneity significantly affects spatio-temporally averaged

soil moisture in comparison to a homogeneous vegetation. Ivanov et al. (2010) analyzed the temporal development of the soil moisture variability in comparison to the temporal behavior of the mean in a slope experiment. It was concluded that in vegetated soils, perturbations from an attractor state can be balanced more easily than in bare soils. This is referred to as a homogenizing effect of vegetation.

1.5 Overview of the work

Modeling of root water uptake has been focused to homogeneous domains, and consideration of spatial variability in more than one dimension has remained quite limited. The scope of this work is to assess the effect of soil heterogeneity in combination with root water uptake on the variability of pressure head in the water unsaturated zone numerically. Different approaches for root water uptake and soil structure are considered.

For root water uptake, standard approaches on large scales that are determined by the distribution of roots and atmospheric demand or which additionally account for soil moisture are considered. On the next level, heterogeneous uptake strategies are included which compensate local reduction of the uptake rate by increased extraction at other locations to maintain the global actual uptake at the potential value. As base case, in order to determine the influence of vegetation, scenarios where root water uptake is neglected (and the same net infiltration rate is assumed) are analyzed.

Soil structure is described by effective homogeneous or simplified one-dimensional media. Furthermore, variation of soil parameters in two directions is included. Water flow including root water uptake in 1D structures can be solved with analytical solutions. In this work, we provide an analytical steady-state approximation for mean and variance of pressure head in a layered soil, for comparison with our numerical results and with the solutions for a medium consisting of parallel streamtubes, derived by Rubin and Or (1993). As a variety of patterns exist in the soil, differently structured fields are taken into account for the 2D simulations. We consider non-Gaussian random fields, to determine whether the assumption of Gaussian heterogeneity limits the generality of conclusions on the impact of variability of flow.

It is assumed that essential features of three-dimensional water flow are reproduced by two-dimensional calculations (Roth, 1995). In view of large computational demand of transient 3D modeling, simulations are, therefore, carried out in two dimensions. The simplification is supported by the finding that under saturated conditions, one- and two-dimensional flow are qualitatively different but that the difference between two- and three-dimensional flow is only of a quantitative nature (Dagan, 1989).

An overview of model concepts for root water uptake and soil structure is illustrated in Figure 1.4.

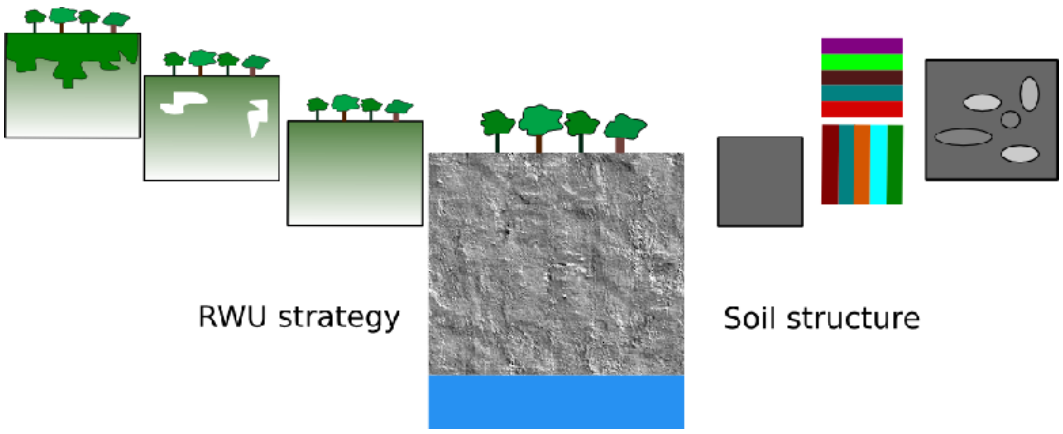

Figure 1.4: *Sketch of unsaturated flow problem and different models for root water uptake strategy and soil structure. In the simplest case, the heterogeneity of the soil is assumed to be homogeneous and root water uptake is determined by the root density. In more advanced models, the soil is modeled to vary in one, two or three dimensions. For root water uptake models, the reduction of uptake due to stress or preferential, compensating strategies can be considered.*

The main goal of this work is to identify the phenomena of unsaturated flow, introduced by the interaction of root water uptake and soil structure, where models with different complexity are considered. Constant and temporally variable precipitation rates are analyzed, (evaporation is not considered). Mean and variance of soil hydraulic variables as well as fastest flow tracks are the parameters of interest.

In particular, this study focuses on the following issues:

1. Which influence of structure becomes important under the consideration of root water uptake?
2. Which features of structure are sensitive to the influence of root water uptake?
3. Which conditions do limit simplified models, such as the analytical solutions for layered media?
4. Are the conclusions made under steady state conditions extendable to transient cases?

In chapter 2, the theoretical basics of unsaturated flow, stochastic modeling and the numerical scheme used for the simulations, are given. In chapter 3, semi-analytical (first-order second-moment) solutions for mean and variance of pressure head in layered media are derived. Chapter 4 explains the numerical setup of the water flow simulations. In chapter 5, steady state simulations are analyzed. It is tested under which conditions the analytical solutions for layered media gives good estimates of the mean and the variance of the pressure head distribution for unsaturated flow in an isotropic, two-dimensional structured domain. The joint effect of (Gaussian and non-Gaussian) soil structure and root water uptake on the steady state mean and variance of the hydraulic variables is analyzed for wet conditions, and for drier conditions that are still typical for Germany or the Netherlands. Arid or semi-arid conditions are not considered. It is furthermore discussed, which features of structure

are sensitive to the influence of root water uptake where different uptake strategies are tested. The influence of heterogeneity and root water uptake on the time series of the hydraulic variables with dynamic boundary conditions, such as drydown and rewetting and periodic cycles, is assessed in section 6.

Since little is known about the exact mechanisms of root water uptake, this study provides a qualitative analysis on the influence of root water uptake and soil structure, points out the limitation of large scale root water uptake approaches and determines which features of structure are critical.

2 Modeling of flow in the subsurface

In this chapter, the theoretical background for flow in the subsurface is given. We introduce the basic concepts of flow in porous media and treat flow in the unsaturated zone. We present how heterogeneity of soil hydraulic properties can be modeled and finally explain the discretization scheme for the numerical solution of the unsaturated flow problem.

2.1 Flow in porous media

This section provides an insight on the concepts of porous media which rely on an averaged macroscopic description of the soil. We roughly explain how modeling is transferred from the micro- to the macroscale and what measures characterize flow on the macroscale. Moreover, the interaction between porous matrix and fluid is discussed and basic flow equations to describe flow in porous media are presented.

2.1.1 Transition from the micro- to the macroscale

The volume of a porous medium, a material which contains pores, is divided into solid matrix and pore space. On the pore level, each point belongs either to the pore space or to the matrix, described by a pore distribution. The pore space is typically filled by one or several fluids. Flow on the pore scale is described by the Navier-Stokes equation and depends on the properties of the solid matrix and the properties of the fluids. Besides the pore-size distribution, particle sizes of grains and friction coefficients of pore channels are important parameters of the matrix. Fluids are predominantly described by their density $\rho\,[\mathrm{kg/m^3}]$, the mass per unit volume, and the dynamic viscosity $\mu\,[\mathrm{kg/ms}]$ which is a measure of a fluid's resistance to shear stresses and represents the internal friction within a fluid.

To describe flow on scales that are relevant for environmental applications, a transition from the pore scale to the continuum scale is necessary. This is performed by averaging over the pore distribution. The volume from which on averaging over the pore distribution leads to a macroscopic value that neither depends on the form nor on the size of the averaging volume, is called representative elementary volume (REV). Down to this characteristic size it is assumed that every element contains solid matrix and pore space (Roth, 2007).

At the continuum scale, the porous matrix is characterized by the volume fraction of interconnected pore space referred to as the porosity ϕ [-] and by the pore-size-distribution index which indicates whether a rather wide (small values) or a more uniform distribution

(large values) of pore sizes is on hand. The microscopic properties of the matrix, such as friction coefficient and tortuosity of pores lead to a macroscopic resistance of the solid matrix, described by the intrinsic permeability $\mathbf{k}_s$ [m^2]. A rigorous definition is given in equation (2.13). Taking the properties of a fluid into account, the saturated conductivity $\mathbf{K}_s$ [m/s] with $\mathbf{K}_s = \frac{\rho \cdot g}{\mu}\mathbf{k}_s$ describes the ability of the porous medium to transmit a fluid under fully saturated conditions.

In general, flow behavior and fluid properties depend on the pressure p and the temperature T. However, in this work, such variations are neglected and incompressible, isothermal flow is considered.

The macroscopic state of a fluid is characterized by the amount of the fluid and its potential energy. The amount of the fluid is described by the water content Θ [$-$] which equals the volume fraction of the fluid,

$$\Theta = \frac{\text{Volume of fluid in REV}}{\text{Total volume in REV}}, \tag{2.1}$$

or the saturation [-]

$$S = \frac{\Theta}{\phi} \tag{2.2}$$

where ϕ is the porosity. The saturation is a measure for the fraction of pore space that is filled with fluid. Its value is between zero and one.

The potential energy density of a pure fluid in a porous medium is the energy which is required to move a unit volume of fluid from a reference state to a particular state in the porous media. Considering isothermal incompressible flow of pure fluid, a particular state of an element of the fluid is defined by height z and the pressure p. The reference state is assumed to be characterized by z_r, p_r, (Roth, 2007).

The potential energy Ψ per unit volume of the fluid is then determined by the pressure difference and gravity.

$$\Psi(\mathbf{x}) = \Psi_p + \Psi_g \tag{2.3}$$

$$= p(\mathbf{x}) - p_r + \int_{z_r}^{z} \rho(z')g dz' \tag{2.4}$$

$$= p(\mathbf{x}) - p_r + \rho g(z - z_r) \tag{2.5}$$

where p [Pa] is the pressure at location $\mathbf{x}$ [m], ρ [kg/m^3] the density, g [m/s^2] the gravitational acceleration, and z [m] is the upwards-pointing vertical vector of $\mathbf{x}$.

2.1.2 Interaction between fluid and matrix

At the surface of a fluid, an interfacial energy density, so called surface tension γ $[\mathrm{J/m^2}]$, acts due to the difference of attractive forces (cohesion) acting on molecules which are located within the fluid and close to the surface. Surface tension leads to a restoring force which acts to minimize the interfacial area between the fluid and its surrounding. When a fluid is in contact with a solid, the fluid tends to adhere to the solid due to attractive forces between the molecules of the solid and the fluid (adhesion).

For a system of two fluids, cohesion leads to the formation of droplets of one fluid in the other fluid. In a thin tube, filled with two fluids, cohesion and adhesion can cause the fluid to rise against gravity. The interface between the fluids is described by the contact angle a, illustrated in Figure 2.1. The competition between cohesive and adhesive forces determines whether an acute or an obtuse contact angle develops (Tipler, 1999). The force F resulting from interfacial tension is directed tangentially to the interface. The fluid with the acute contact angle is called wetting fluid, and the fluid with the obtuse contact angle is called non-wetting fluid. The fluid rises until gravitational forces acting on the risen mass of fluid are large enough to balance the vertical component of F.

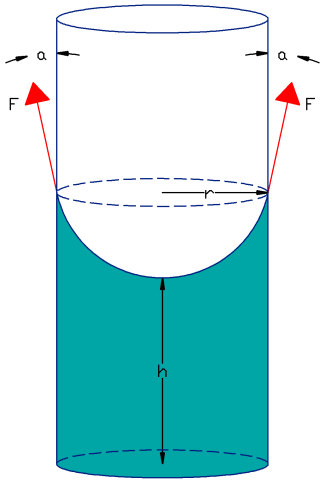

Figure 2.1: *Capillary tube filled with water.*

The height is inversely proportional to the radius of the capillary. Hence, the narrower the tube is, the higher does the wetting fluid rise and the larger is the required energy to break the meniscus.

The pressure jump at the interface between the two fluids is called capillary pressure

$$p_c = p_1 - p_2 = \frac{2\gamma}{r} \tag{2.6}$$

where r $[\mathrm{m}]$ is the radius of the capillary.

The most simplified model for porous media consists of a bundle of capillaries with different diameters. In the same way as for the idealized case, surface tension exists due to intermolecular forces such that menisci form within the solid matrix of real soils. The emerging pressure discontinuity across the interface of two immiscible fluids in a porous medium on the micro scale is described on the macroscale by the difference of pressures of wetting and non-wetting fluid.

$$p_c = p_{non} - p_{wet} \tag{2.7}$$

This energy density induced by the interaction of porous medium and fluid contributes to the pressure potential in equation (2.5). The capillary pressure can be seen as a measure of the tendency of the porous medium to suck in the wetting or to repel the non-wetting fluid (Bear, 1972). For a single tube, the capillary pressure can explicitly be determined. In the soil, which consists of a network of capillaries, a distribution of capillary pressures is found. Depending on the degree of saturation, pores with different sizes are filled. For low saturation values, the water is mainly located in narrow pores with high capillary pressures. As the saturation increases, larger pores are included which lowers the capillary pressure (Cirpka, 2007). The macroscopic capillary pressure represents an average pressure in the REV. Figure 2.2 illustrates the idealized case of the soil represented by a bundle of capillaries filled with water and air. On average, a constitutive relationship between macroscopic capillary pressure and saturation, also called retention curve, can be obtained. Generally, the retention curve needs to be determined experimentally. To account for residual air or water in the soil, the retention curve is usually set for the effective saturation which is defined as

$$S_e = \frac{\Theta - \Theta_r}{\Theta_s - \Theta_r} \tag{2.8}$$

where Θ_r [-] is the minimum (residual) water content and Θ_s $[-]$ the maximum water content.

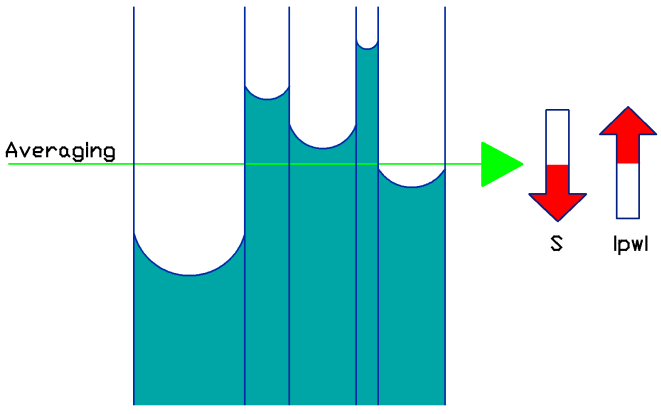

Figure 2.2: *In a porous medium, saturation and pressure head are average quantities. Averaging over different pore sizes is illustrated for a bundle of capillaries. With increasing height, the absolute value of the water pressure head increases and the saturation decreases.*

Models for the capillary pressure-saturation relationship were suggested, for example, by Russo (1988), Brooks and Corey (1966) and van Genuchten (1980). A very commonly used relation is the parametrization by van Genuchten (1980):

$$S_e(p_c) = (1 + (\alpha p_c)^n)^{-1+\frac{1}{n}} \tag{2.9}$$

where $p_c\,[\mathrm{m}]$ is the capillary head. $\alpha\,[1/\mathrm{m}]$ and $n > 1$ [-] are model parameters which influence the shape of the curve. α represents the retention ability and n the pore-size distribution. Typical values of these parameters for different soils can be found in Carsel and Parrish (1988). The capillary pressure-saturation relationship is shown in Figure 2.3.

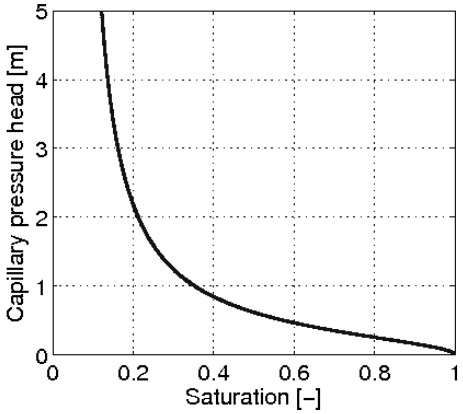

Figure 2.3: *Parametrization of the saturation according to Van Genuchten (for* $\alpha = 3.04\,\mathrm{m}^{-1}$ *and* $n = 2\,[-]$*).*

Note, that the presented concept of a macroscopic capillary pressure-saturation relationship is based on equilibrium conditions. Such conditions might not hold under transient, quickly changing infiltration patterns. Furthermore, real pore networks have a very complex structure such that residual water or air is entrapped in the soil at drainage and imbibition. This leads to a hysteretic behavior of the retention curve, meaning that the relationship between capillary pressure and saturation on the macroscale depends on the history of imbibition and drainage. Alternative approaches are currently being discussed where, e.g. a dynamic, temporally variable term is introduced into relation (4.3) (e.g. Manthey et al., 2005) or where the classic concept is replaced by relations based on the distinction between percolating and non-percolating fluid (Hilfer, 2006).

2.1.3 Flow equations

In the following, the most important equations which describe flow in a porous media are introduced.

Mass Balance

In an arbitrary volume of the porous medium, the mass of a fluid is always conserved. Conservation of the mass means that the rate of change of mass within a volume equals the mass that flows across the volume boundary plus the amount of water that is extracted per unit time and per unit volume.

The specific mass of the fluid is given by its volume fraction $\Theta\,[-]$ multiplied by the density $\rho\,[\mathrm{kg/m^3}]$.

$$\frac{\partial}{\partial t}\int_V \Theta\rho dV + \oint \rho\mathbf{j}\cdot d\mathbf{A} = -\int_V \rho R dV \tag{2.10}$$

with $\mathbf{j}\,[\mathrm{m^3/sm^2}]$ being the volume flux per cross-sectional area, $d\mathbf{A}$ the area element pointing outwards, and $R\,[1/\mathrm{s}]$ the (positive) volumetric extraction rate due to sinks.
Using Gauss' theorem, the advective term can be transformed to an integral over volume.

$$\frac{\partial}{\partial t}\int_V \Theta\rho dV + \int_V \nabla\cdot\rho\mathbf{j} dV = -\int_V \rho R dV \tag{2.11}$$

Since equation (2.11) has to be fulfilled for any arbitrary volume, it follows that

$$\frac{\partial}{\partial t}[\Theta\rho] + \nabla\cdot[\rho\mathbf{j}] = -\rho R \tag{2.12}$$

Darcy's Law

The volume flux of a pure fluid in a porous medium under fully saturated conditions was found to depend linearly on the driving forces which are the pressure gradient for horizontal flow, and gravity and pressure gradient for vertical flow.

$$\begin{aligned}\mathbf{j} &= -\frac{1}{\mu}\mathbf{k}_s\nabla\Psi \\ &= -\frac{1}{\mu}\mathbf{k}_s(\nabla p + \rho\mathbf{g})\end{aligned} \tag{2.13}$$

Equation (2.13) is an empirical flux law which dates back to Henry Darcy (1803-1858) who studied the water flow through a sand column. Under the assumption of slow

(i.e. a low Reynolds number) and stationary flow of an incompressible Newtonian fluid, Darcy's law can be derived from the Navier-Stokes equation (Gray and Hassanizadeh, 1998).

The Buckingham-Darcy Law

For a system of several fluids, the interaction of the two phases has to be taken into account. To include the increased resistance to flow for a given phase due to the presence of the other phase, the permeability $\mathbf{k}$ is composed of an intrinsic part $\mathbf{k}_s$ which is a property of the matrix, and a temporally variable part k_r, the relative permeability, which is a function of the phase saturation.

$$\mathbf{k} = \mathbf{k}_s \cdot k_r(S) \tag{2.14}$$

The volume flux of one fluid is then described by the so-called Buckingham-Darcy equation,

$$\mathbf{j} = -\frac{\mathbf{k}}{\mu}\nabla\Psi. \tag{2.15}$$

In the same way as for the retention curve, a relationship can be obtained for $k_r(S)$. Examples of models which parametrize the relative permeability are the Gardner model,

$$k_r(p_c) = \exp(-\alpha p_c) \tag{2.16}$$

or the Mualem-van Genuchten model

$$k_r(p_c) = (1 + (\alpha p_c)^n)^{a(1-1/n)}(1 - (\alpha p_c)^{n-1}(1 + (\alpha p_c)^n)^{-1+1/n})^2. \tag{2.17}$$

In both relations, $p_c\,[\mathrm{m}]$ is the capillary head, and $\alpha\,[1/\mathrm{m}]$ and $n\,[-]$ are parameter influencing the shape of the curve. In Figure 2.4, the Gardner-parametrization is illustrated.

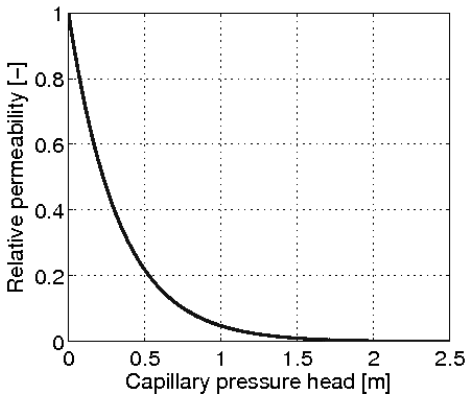

Figure 2.4: *Relative permeability-capillary head relationship after Gardner (for $\alpha = 3.04\,\mathrm{m}^{-1}$).*

2.2 Flow in the unsaturated zone

In the unsaturated zone, the pore space is filled with water and air. Since the volume fraction and movement of water is affected by the volume fraction of air, water flow in the unsaturated zone has to be treated as a multiphase process. This means, that the conductivities of the porous medium for both water and air need to be described by the Buckingham-Darcy law. Furthermore, the air phase needs to be considered in the total potential of fluids in the porous medium. While the hydrostatic pressure in the air is negligible due to its much lower density compared to water, the air pressure may contribute to the pressure term in equation (2.5).

2.2.1 Richards' equation

It is assumed that the volume fraction of air in the unsaturated zone exceeds a critical value, such that the air phase becomes continuous and connected to the surface. As the mobility of air is much larger than the mobility of water, pressure gradients of p_a, induced by a change of water content, are much smaller than those of p_w. The system reacts quasi-instantaneously and is always at equilibrium such that the water decouples from the air phase, and the pressure of the air phase can be assumed to be constant throughout the domain (Roth, 2007). Hence, flow of water in the unsaturated zone can be considered as quasi one-phase flow, and the only contribution to the pressure potential comes from the interfacial forces, given by

$$\Psi_p = p_w - p_a \tag{2.18}$$

The pressure of the air phase p_a corresponds to the atmospheric pressure which is, for simplicity, set to zero $p_a = 0$. The pressure potential is, therefore, given by the soil water pressure.

$$\Psi_p = p_w \tag{2.19}$$

For $z = z_0$, the potential of water is

$$\Psi = p_w + \rho g z \tag{2.20}$$

The volume flux of water in the unsaturated zone is then,

$$\mathbf{j} = -\frac{\mathbf{k}}{\mu}(\nabla p_w + \rho \mathbf{g}). \tag{2.21}$$

Combining the Buckingham-Darcy equation and the mass balance (equation (2.12)) leads to the Richards equation which describes the dynamics of unsaturated water flow. Under the assumption that porosity is constant and that water is an incompressible fluid, density cancels out and Richards' equation becomes

$$\phi \frac{\partial S(p_w)}{\partial t} - \nabla \cdot [\mathbf{k}_s \lambda (\nabla p_w + \rho \mathbf{g})] = -R \tag{2.22}$$

where $\phi\,[-]$ is the porosity, $S\,[-]$ is the saturation, $\mathbf{k}_s\,[\mathrm{m}^2]$ is the intrinsic permeability, $\lambda = k_r/\mu\,[\mathrm{ms/kg}]$ the mobility and $R\,[1/\mathrm{s}]$ the sink term due to root water uptake, having positive values. The parametrization for R is explained in section 2.2.2.

In terms of water pressure head ψ with

$$\psi = \frac{p_w}{\rho g} \tag{2.23}$$

Richards' equation reads

$$\phi \frac{\partial S(\psi)}{\partial t} - \nabla \cdot [\mathbf{K}(\psi)(\nabla\psi + \mathbf{e}_z)] = -R \tag{2.24}$$

where $\mathbf{K}(\psi)\,[\mathrm{m/s}]$ is the hydraulic conductivity with $\mathbf{K} = \frac{\rho g}{\mu}\mathbf{k} = \mathbf{K}_s \cdot k_r$. $\mathbf{K}_s\,[\mathrm{m/s}]$ is referred to as the saturated hydraulic conductivity, the hydraulic conductivity under fully saturated conditions.

2.2.2 Root water uptake

The soil surface is covered with vegetation. The extraction of water by plant roots affects the dynamics of water flow, especially in the upper part of the soil and needs to be accounted for in the flow equation.

On the macroscale, root water uptake R is commonly accounted for as a sink term of the Richards equation (2.24). Approaches to model root water uptake can be arbitrarily complex. On large scales, the goal is, however, to keep models preferably simple. The complexity depends on the number of processes taken into account. Generally, the uptake rate is assumed to be determined by atmospheric demand and presence of roots. Additionally, soil water status or compensation mechanisms, where locally reduced uptake can be compensated by increased uptake at other locations, are considered.

According to the simplest approach, the water extraction rate is determined by the transpiration demand $\tau\,[\mathrm{m/s}]$ and the root distribution function $d_r\,[1/\mathrm{m}]$. The root distribution function distributes the atmospheric demand according to the relative presence of plants throughout the domain. The resulting extraction rate equals the local potential uptake rate R_p.

$$R(z) = \tau d_r(z) = R_p \tag{2.25}$$

In this work, the root distribution function is modeled by an exponentially decreasing function with depth.

$$d_r = \frac{1}{\delta}\exp(\frac{z-H}{\delta}) \tag{2.26}$$

where H [m] is the height of the domain, and δ [m] is a parameter characterizing the length of the roots.

Accounting for soil water status

On the next level, the availability of soil water is considered. Unfavorable soil conditions such as water or oxygen scarcity are, on the macroscale, commonly modeled by a stress-reduction factor f_F which ranges between zero and one and depends on the pressure head or saturation. This factor is multiplied with the uptake rate R such that, under stressed conditions, the uptake rate R_1 is locally reduced compared to the potential root water uptake rate R_p.

$$R_1(\psi, z) = R_p f_F(\psi) \tag{2.27}$$

Root water uptake modeled according to equation (2.27) is in the following referred to as Strategy 1, also basic or standard approach. In this work, the stress-function was modeled according to the so-called Feddes-function, proposed by Feddes et al. (1978), where the reduction of water uptake is characterized by four critical values of the pressure head, $h_1 - h_4$, and a linear dependence of the reduction factor on pressure head:

$$f_F = \begin{cases} -\frac{1}{h_1 - h_2}\psi & h_1 < \psi < h_2 \\ 1 & h_2 < \psi < h_3 \\ \frac{1}{h_3 - h_4}\psi & h_3 < \psi < h_4 \\ 0 & \text{for } \psi < h_1 \text{ or } \psi > h_4 \end{cases} \tag{2.28}$$

The Feddes-function is illustrated in Figure 2.5.
Typical values for the critical pressure heads $h_1 - h_4$ can be found in Taylor and Ashcroft (1972).

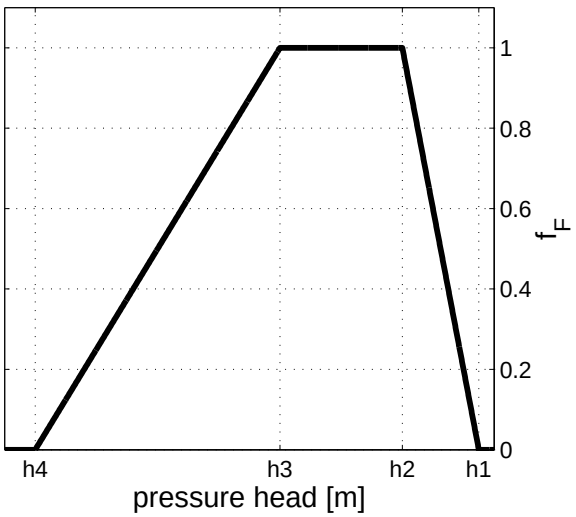

Figure 2.5: *Sketch of the Feddes-Function with critical values h_1, h_2, h_3 and h_4 (wilting point).*

Accounting for compensation mechanisms

Since experimental data support the occurrence of compensation mechanisms for local stress within the root zone (e.g. Taylor and Kleppner, 1978; Hasegawa and Yoshida, 1982; English and Raja, 1996; Stikic et al., 2003; Leib et al., 2006), it is expected that roots can react in response to unfavorable soil conditions in order to maintain the overall uptake at the potential rate. The global actual uptake in the whole domain $T_{act} = \int_V R_1(\psi, z)dV$ $[\mathrm{m}^2/\mathrm{s}]$ is then equal to the global potential transpiration $T_{pot} = \int_V R_p dV$ $[\mathrm{m}^2/\mathrm{s}]$ where R_1 $[1/\mathrm{s}]$ is the local actual uptake rate and R_p $[1/\mathrm{s}]$ the local potential uptake rate. The process of compensation is very complex and barely known. In micro-models or Type 1 macro-models for root water uptake, compensation results automatically since the extraction rate is determined through a chain of resistances. These approaches are, however, better suited for the plant scale. A sound understanding of the mechanisms ruling compensation or macroscopic pattern could not yet be derived which makes modeling of compensation processes on larger scales difficult. Into macro-approaches that are based on a prescribed uptake rate, compensation has to be artificially introduced. The global loss of root water uptake due to stress in comparison to the potential value needs to be calculated and taken up elsewhere. This is either possible by distributing (adding) the loss to unstressed locations or by multiplying the reduced uptake rate R_1 at each location by a scaling factor, such that the global amount of extracted water equals the atmospheric demand.

In this work, three strategies (Strategy 2, 3, 4), which include compensation mechanisms for local reduction of uptake due to stress by increased uptake at other places, are tested. The corresponding root water uptake terms are denoted by R_2, R_3 and R_4. In order to maintain the global uptake rate at the potential value under occurrence of local stress, Strategy 2&3 use a scaling factor and Strategy 4 adds the global loss of uptake, which is the uptake demand minus the actual uptake summed over all nodes, to unstressed locations.

Strategy 2 and 3 additionally assume that root water uptake is increased at favorable locations and decreased at unfavorable locations. They are modeled by a factor M_i by which equation (2.27) is extended.

$$R_i(\psi, z) = R_p f_F(\psi) M_i \tag{2.29}$$

In Strategy 2, root water uptake is proportional to the saturation, thus more water is extracted where more water is available.

$$M_2 = S \cdot f_{c_2}; \text{ full compensation}$$

Strategy 3 reflects that permeability could be the limiting factor for root water uptake. In this case the extraction rate is proportional to the relative permeability.

$$M_3 = k_r \cdot f_{c_3}; \text{ full compensation}$$

To keep a constant global root water uptake rate, the extraction rate is in both strategies multiplied by a factor f_c in such a way that the global actual water uptake T_{act} $[\mathrm{m}^2/\mathrm{s}]$ equals the global potential demand T_{pot} $[\mathrm{m}^2/\mathrm{s}]$, $f_{c_2} = \frac{T_{pot}}{\int R_p f_F S dV}$ and $f_{c_3} = \frac{T_{pot}}{\int R_p f_F k_r dV}$.

These approaches are permanent mechanisms which compensate the local decrease of the root water uptake rate due to stress (reduction with f_F) and unfavorable locations (proportional to S or k_r) by enhanced uptake at other locations.
The strategies correspond to the model for root water uptake by Katul et al. (1997) who used a weighting function equal to one, depending on the water content or related to the hydraulic conductivity, but neglected a water stress function. The strategy depending on the water content was proposed by Warrick (1974) and Markar and Mein (1987). Strategy 2 and 3 are also similar to the approach of Jarvis (1989), Jarvis (1994) and Simunek and Hopmans (2009). Their inverse dimensionless water stress index $1/\omega$ corresponds to our f_c. In comparison to their model, we add a dependence of S or k_r and neglect a critical threshold value to account for partial compensation. Stress in the sense of a decreased global actual uptake rate T_{act} cannot occur with Strategy 2 and 3. Furthermore, the transpiration demand and root distribution function is independent of time in our approach.

The fourth uptake strategy cannot be formulated in terms of equation (2.29) since it equally redistributes the difference between global actual uptake and global potential uptake which occurs with Strategy 1, to the remaining unstressed parts. Thus, stressed and unstressed locations are treated differently in the fourth root water uptake term R_4:

$$R_4 = \begin{cases} R_1 & \text{for stressed nodes} \\ R_p + \triangle R_{loss} & \text{for unstressed nodes} \end{cases} \text{; full compensation}$$

$\triangle R_{loss}$ is the global deficit of the uptake rate (summed up over all nodes) which is, according to Strategy 4, equally distributed over the unstressed nodes, $\triangle R_{loss} = \frac{\sum_{nodes}(R_p - R_1)}{nb_{unstr}}$ with nb_{unstr} being the number of unstressed nodes.
A decrease of the total actual transpiration rate T_{act} occurs with this modification only if not enough water is available in the whole domain, i.e. if all locations are stressed.

2.2.3 Derivation of time scales

Soil moisture dynamics are modeled with the Richards equation. Boundary conditions, soil hydraulic properties and sink term determine steady state and temporal behavior of water flow in the soil. Dimensionless groups as well as characteristic timescales of the system, which both determine the flow behavior, can be calculated by means of dimensional analysis. A dimensionless form of the Richards equation is obtained in the following way. All parameters and variables are written in dimensionless form by dividing the variable u by a characteristic quantity u_0.

$$u^* = \frac{u}{u_0} \tag{2.30}$$

where u^* denotes the dimensionless variable. The variables in the Richards equation can thus be split into a dimensionless quantity and a characteristic quantity.

This leads to the following expressions for time t [s] and the spatial vector (in 1D) x [m],

$$t = t_0 \cdot t^* \tag{2.31}$$

$$x = x_0 \cdot x^* \tag{2.32}$$

It follows that

$$\begin{aligned} \frac{\partial}{\partial t} &= \frac{\partial t^*}{\partial t}\frac{\partial}{\partial t^*} = \frac{1}{t_0}\frac{\partial}{\partial t^*} \\ \frac{\partial}{\partial x} &= \frac{\partial x^*}{\partial x}\frac{\partial}{\partial x^*} = \frac{1}{x_0}\frac{\partial}{\partial x^*} \end{aligned} \tag{2.33}$$

$$\nabla = \frac{1}{x_0}\nabla^* \tag{2.34}$$

In the same way, the other variables such as the sink term, the hydraulic conductivity and the pressure head can be expressed by the product of a characteristic and a dimensionless quantity

$$\begin{aligned} R &= R_0 \cdot R^* \\ K &= K_0 \cdot K^* \\ \psi &= \psi_0 \cdot \psi^* \end{aligned} \tag{2.35}$$

Inserting the dimensionless parameters into Richards' equation yields

$$\phi_0\phi^*\frac{S_0}{t_0}\frac{\partial S^*}{\partial t^*} - \frac{1}{x_0}\nabla^* K_0 K^* \frac{1}{x_0}\nabla^*\psi_0\psi^* - \frac{1}{x_0}K_0K^*e_z = -R_0R^*. \tag{2.36}$$

Rearranging the terms such that the dimensionless equation has the same form as the original equation leads to

$$\phi^*\frac{\partial S^*}{\partial t^*} - \frac{t_0K_0\psi_0}{S_0x_0^2\phi_0}\nabla^*K^*\nabla^*\psi^* - \frac{K_0t_0}{S_0x_0\phi_0}K^*e_z = -\frac{t_0R_0}{S_0\phi_0}R^*. \tag{2.37}$$

The Richards equation (2.24) and equation (2.37) differ only by the coefficients of each term. By setting these factors equal to one, a time scale for each term is derived. The time scales characterize the temporal behavior of the different processes, which the terms reflect.

The characteristic time scales are

$$t_1 = \frac{S_0x_0^2\phi_0}{K_0\psi_0} \tag{2.38}$$

$$t_2 = \frac{S_0x_0\phi_0}{K_0} \tag{2.39}$$

$$t_3 = \frac{S_0\phi_0}{R_0} \tag{2.40}$$

t_1 is related to capillary flow, t_2 to gravity flow and t_3 to root water uptake. These timescales are used and explained in more detail in chapter 6.1.

2.3 Heterogeneity

On the macro scale, soil parameters can vary strongly and have very diverse patterns. Their full distribution, which is not accessible by measurement devices, contains a high level of uncertainty that makes it extremely difficult to describe the flow behavior in such soils. It is, however, a major task of environmental modelers to include the variation of soil parameters on large scales into their applications, but keep the computational effort small at the same time. For the development of such effective models, it is necessary to quantify the effect of soil structure. In this section, it is shown how the variation of soil parameters on large scales is usually put into a mathematical framework, how different patterns of soil parameters can be realized in this description, and what measures this framework provides to characterize these patterns.

2.3.1 Stochastic Approach

As, on larger scales, only few measurement points contribute to the estimation of soil parameters such as hydraulic conductivity and retention parameter, it is impossible to obtain a detailed distribution. Often, stochastic methods are used to describe the variations of soil parameters. A stochastic description allows to quantify the emerging uncertainty by different measures. Some of these measures will be explained in the first part of this section. Basic terms and definitions used in the stochastic approach will be given to provide some background knowledge for the following chapters. In the second part, the concept of the soil as a stochastic ensemble will be introduced.

2.3.1.1 Terms and definitions

To assure that the reader has a basic knowledge of the terms used in later chapters, a list of definitions, which are constantly used in the field of stochastic modeling, is provided in the following. The definitions should give an insight rather than be mathematically rigorous. They are taken from chapter two of Zhang (2002), chapter two of Gelhar (1993) and chapter two of Neuweiler (2005).

- **Random variable**: In most natural processes, a variable at a distinct location is unknown, but the possible values can be restricted to a certain interval or set. A random variable u is the collection of all possible outcomes of a given experiment. The classic sample experiment is the throw of a die. The random variable is then $u = \{1, 2, 3, 4, 5, 6\}$. The concept of a random variable forms the basis of the stochastic approach.

- **Random space function**: A random space function describes the variation of an observed quantity in space. At each point in space, the quantity is uncertain but the possible outcomes are given. A random space function is thus a random variable, $u_1, .., u_n$, at each point in space. The collection of all possible records is called ensemble. One particular trial is denoted as one realization of the random space function. If the spatial index is multidimensional, one refers to a random space function also as random field. Note, that the variation of an observed quantity with time is denoted by a stochastic process. As done in Zhang (2002), the three names are used as interchangeable terms in the following.

- **Cumulative distribution function (cdf)**: The cdf of a random variable characterizes the likelihood of each possible outcome of a given experiment. $cdf(u)$ is the probability that a random variable is found at a value smaller or equal to u.
Probability density function (pdf) $\mathbf{p}_u$: $p_u(u)du$ is the probability that the random variable lies in a small interval du, in between u and $u + du$. For a random space function, which is a random variable $u_1, ...u_n$ at each point in space, the probabilistically interrelation of the variables has to be taken into account. A complete probabilistic description of a random field requires the probability density function at each point in space. The joint or multivariate probability density function gives the probability of each random variable to be in a certain range, i.e. the probability that u_1 lies in du_1, u_2 in du_2, ... and u_n in du_n.

- **Moments**: The probability distribution of a random variable is characterized by its infinite number of moments

$$\mu_n = \langle u^n \rangle = \int_{-\infty}^{\infty} u^n p_u(u) du \tag{2.41}$$

or centralized moments

$$\mu'_n = \langle (u - \mu_1)^n \rangle = \int_{-\infty}^{\infty} (u - \mu_1)^n p_u(u) du \tag{2.42}$$

A random field is composed of multiple random variables. The moments are determined from each random variable and the joint pdf.

$$\langle U(\mathbf{x})^n \rangle = \int_{-\infty}^{\infty} u_1 u_2 ... u_n p_u(u_1, \mathbf{x}_1; u_2, \mathbf{x}_2; ....; u_n, \mathbf{x}_n) du_1 du_2 ... du_n \tag{2.43}$$

In practice, the stochastic properties of a random field are mostly reduced to the first two statistical moments.

The **first moment** is the mean or expected value

$$\langle U(\mathbf{x}) \rangle = \int_{-\infty}^{\infty} u p_u(u, \mathbf{x}) du \tag{2.44}$$

The **second central moment** is defined as

$$C_U(\mathbf{x}_1, \mathbf{x}_2) = \langle U'(\mathbf{x}_1)U'(\mathbf{x}_2)\rangle = \langle U(\mathbf{x}_1)U(\mathbf{x}_2)\rangle - \langle U(\mathbf{x}_1)\rangle\langle U(\mathbf{x}_2)\rangle$$
$$= \int_{-\infty}^{\infty}\int_{-\infty}^{\infty} u_1 u_2 p_u(u_1, \mathbf{x}_1; u_2, \mathbf{x}_2)du_1 du_2 - \langle U(\mathbf{x}_1)\rangle\langle U(\mathbf{x}_2)\rangle \tag{2.45}$$

where $U'(\mathbf{x}_i) = U(\mathbf{x}_i) - \langle U(\mathbf{x}_i)\rangle$ is the fluctuation of U at $\mathbf{x}_i$. Equation (2.45) describes the covariance of the random field U at two space points, also called the autocovariance function.

When $\mathbf{x}_1 = \mathbf{x}_2 = \mathbf{x}$, the autocovariance reduces to the variance function which gives the deviation from the mean at each point in space.

$$\sigma_U^2(\mathbf{x}) = C_U(\mathbf{x}, \mathbf{x}) = \int_{-\infty}^{\infty} u^2 p_u(u, \mathbf{x})du - \langle U(\mathbf{x})\rangle^2 \tag{2.46}$$

The coefficient of variation is the variance devided by the squared mean, $CV_U = \frac{\sigma_U^2}{\langle U\rangle^2}$.

The autocorrelation coefficient is given by

$$\rho_U(\mathbf{x}_1, \mathbf{x}_2) = \frac{C_U(\mathbf{x}_1, \mathbf{x}_2)}{\sigma_U(\mathbf{x}_1)\sigma_U(\mathbf{x}_2)} \tag{2.47}$$

ρ_U is a measure for the correlation of outcomes at $\mathbf{x}_1$ and $\mathbf{x}_2$, it describes the likelyhood to sample similar values at the two locations.

- **Gaussian random field:** A random field $U(\mathbf{x})$ is called normal (Gaussian or multi-Gaussian) if the random variables $U(\mathbf{x}_1), U(\mathbf{x}_2), ..., U(\mathbf{x}_n)$ are jointly normal for any set of n points. A normal process is completely characterized by its mean $\langle U(\mathbf{x})\rangle = \mu_U(\mathbf{x})$ and autocovariance $C_U(\mathbf{x}_i, \mathbf{x}_j)$.

The normal univariate pdf of a random variable is:

$$p_u(u) = \frac{1}{2\pi\sigma^2}\exp\left(-\frac{(u-\mu_1)^2}{2\sigma^2}\right) \tag{2.48}$$

The normal joint pdf of two random variables (bivariate) at two locations $\mathbf{x}_1, \mathbf{x}_2$ of the same stochastic process $U(\mathbf{x})$ is:

$$p_u(\mathbf{x}_1, \mathbf{x}_2) = \frac{1}{2\pi\sigma_U(\mathbf{x}_1)\sigma_U(\mathbf{x}_2)\sqrt{1-\rho^2}}$$
$$\exp\left(-\frac{1}{2(1-\rho^2)}\left(\frac{\mathbf{x}_1-\mu_1}{\sigma(\mathbf{x}_1)}\right)^2 - 2\rho\frac{(\mathbf{x}_1-\mu_1)(\mathbf{x}_2-\mu_2)}{\sigma_U(\mathbf{x}_1)\sigma_U(\mathbf{x}_2)} + \left(\frac{\mathbf{x}_2-\mu_2}{\sigma_U(\mathbf{x}_2)}\right)^2\right) \tag{2.49}$$

- **Function of a random variable** g(U(**x**)): If g is a function of a random variable, the stochastic properties of g(U(**x**)) can be derived from the moments of U(**x**)

$$\langle g^n \rangle = \int_{-\infty}^{\infty} g(u)^n p_u(u) du \tag{2.50}$$

- The **correlation of two random fields** in space is derived from the cross-covariance between two random fields U and V which is defined as

$$\begin{aligned} C_{UV}(\mathbf{x}_1, \mathbf{x}_2) &= \langle U'(\mathbf{x}_1) V'(\mathbf{x}_2) \rangle \\ &= \langle U(\mathbf{x}_1) V(\mathbf{x}_2) \rangle - \langle U(\mathbf{x}_1) \rangle \langle V(\mathbf{x}_2) \rangle \\ &= \int_{-\infty}^{\infty} \int_{-\infty}^{\infty} uv p_{UV}(u, \mathbf{x}_1; v, \mathbf{x}_2) du dv - \langle U(\mathbf{x}_1) \rangle \langle V(\mathbf{x}_2) \rangle \end{aligned} \tag{2.51}$$

where $p_{UV}(u, \mathbf{x}_1; v, \mathbf{x}_2)$ is the joint probability density function of $U(\mathbf{x}_1)$ and $V(\mathbf{x}_2)$. The cross-correlation coefficient is then

$$\rho_{UV}(\mathbf{x}_1, \mathbf{x}_2) = \frac{C_{UV}(\mathbf{x}_1, \mathbf{x}_2)}{\sigma_U(\mathbf{x}_1) \sigma_V(\mathbf{x}_2)} \tag{2.52}$$

The normal joint pdf of two random fields is:

$$\begin{aligned} p_{UV}(u, \mathbf{x}_1; v, \mathbf{x}_2) = & \frac{1}{2\pi \sigma_U(\mathbf{x}_1) \sigma_V(\mathbf{x}_2) \sqrt{1 - \rho_{UV}^2}} \\ & \exp\left[-\frac{1}{2(1-\rho_{UV}^2)} \left[\left(\frac{u(\mathbf{x}_1) - \mu_1}{\sigma_U(\mathbf{x}_1)^2} \right)^2 - 2\rho_{UV} \frac{(u(\mathbf{x}_1) - \mu_1)(v(\mathbf{x}_2) - \mu_2)}{\sigma_U(\mathbf{x}_1) \sigma_V(\mathbf{x}_2)} + \left(\frac{v(\mathbf{x}_2) - \mu_2}{\sigma_V(\mathbf{x}_2)} \right)^2 \right] \right] \end{aligned} \tag{2.53}$$

- **Stationarity**:
  - **Second-order stationarity** requires the process to have no trends which means that the mean and the variance are finite and constant in space and the two-point covariance depends only on the separation vector,

$$\begin{aligned} U(\mathbf{x}) = \langle U \rangle &= const, \\ \sigma_U^2(\mathbf{x}) &= const, \\ C_U(\mathbf{x}_1, \mathbf{x}_2) = C_U(\mathbf{r}) &= C_U(-\mathbf{r}). \end{aligned} \tag{2.54}$$

– **Statistically isotropic** are second-order stationary fields where the covariance additionally fulfills

$$C_U(\mathbf{x}_1, \mathbf{x}_2) = C_U(|\mathbf{r}|). \tag{2.55}$$

Apart from chapter 5.2.3, the random fields considered in this work are modeled as statistically isotropic.

- **Integral scale**: The integral scale is the integral of the autocovariance over distance normalized with the variance. For statistically isotropic fields, it becomes

$$I_U = \int_0^\infty \frac{C_U(\mathbf{r})}{\sigma_U^2} d\mathbf{r}. \tag{2.56}$$

The integral scale is a measure of the distance over which values at two different locations are correlated.

2.3.1.2 Probabilistic description of the soil

The stochastic approach is used to include the variation of soil parameters into the unsaturated flow problem. The distribution of soil hydraulic properties is then described by an ensemble of realizations of parameter fields. In this study, the variation of the loghydraulic saturated conductivity $F = \ln(K_s)$ and the retention parameter α is considered. F and α are thus random fields, given by the mean and the fluctuation about the mean:

$$\begin{aligned} F &= \langle F \rangle + f, \\ \alpha &= \langle \alpha \rangle + \alpha'. \end{aligned} \tag{2.57}$$

All other input parameters of the model are for simplicity assumed to be deterministic. From f and α being stochastic parameters follows that the output variables S and ψ as well as the dependent functions such as the saturation-pressure-relationship $S(\psi)$ and the relative conductivity-pressure relationship $K(\psi)$ are random space functions.

Miller similarity

To be able to consistently describe soil classes regarding structure, Miller and Miller (1956) introduced a similarity concept which states that two porous media are similar if they have identical microscopic geometries and differ only in their length scale. For Miller similar soils, the soil water retention curve and the unsaturated hydraulic conductivity of a soil u can then be related to a reference soil ^{r} by a scaling factor b_u which varies in space. The scaling factor b_u 'contains' the heterogeneity and is modeled as a random field. The variation of soil

hydraulic properties can thus be described by defining the reference state and the scaling factor. Soil hydraulic properties of the soil u and the reference state are interrelated by the dependency of a typical grain size diameter d. The value ψ needed to retain a given amount of water, is assumed to be inversely proportional to a characteristic grain size diameter d since capillary forces decrease with increasing radius,

$$\psi(S) \sim \frac{1}{d}. \tag{2.58}$$

As the flux per cross-section through a capillary increases quadratically with the radius, the conductivity of a soil is assumed to increase proportionally with the squared diameter,

$$K_s \sim d^2. \tag{2.59}$$

Based on these explanations, scaling relations for the retention curve and the hydraulic conductivity between a soil u and the reference soil, (denoted by ^{r}), were proposed,

$$\psi_u(S) = \frac{\psi^r(S)}{b_u}, \tag{2.60}$$

$$K_u(S) = b_u^2 K^r(S). \tag{2.61}$$

According to Birkholzer and Tsang (1997), with a deterministic pore-size distribution n and a scaling factor b_u equal to

$$b_u = \sqrt{\frac{K_s}{K_s^r}}, \tag{2.62}$$

the following relation is obtained from equation (2.60) and (2.61) after 'some mathematical rearrangements',

$$\frac{\alpha}{\alpha^r} = \sqrt{\frac{K_s}{K_s^r}}. \tag{2.63}$$

α [1/m] is a measure for the retention ability used in the hydraulic conductivity parametrization.

The assumption that the similarity concept holds, thus entails a correlation of f and α. The theoretical concept is supported by measurements of soil parameters indicating an existing correlation between f and α and has the advantage that mathematical expressions describing the flow in Miller similar soils with only one random input parameter are easier to handle. Note, that real data does not suggest a perfect correlation which is here the case. The other extreme would be to assume totally independent random fields representing f

and α. The cross-correlation of real soils is in the range of 0.7 (e.g. Hopmans, 1987) and varies from soil to soil.

Stochastic properties of α

The second order stochastic parameters of α, being a function of f, can be derived from the stochastic properties of f. Expressions for the mean and the standard deviation of α, σ_α, the two-point autocorrelation function of α, ρ_α and the two-point crosscorrelation function $\rho_{f\alpha}$ of f and α and corresponding integral scales I_α, $I_{f\alpha}$ for a Gaussian distribution of f are presented.

From relation (2.63) follows

$$\alpha = C\sqrt{K_s} = C\sqrt{K_{s,g}}\exp(\frac{1}{2}f) = A\exp(\frac{1}{2}f), \tag{2.64}$$

where C is a proportionality factor and $K_{s,g}$ the geometric mean of the saturated hydraulic conductivity.

Using relation (2.64) and assuming $\langle f\rangle = 0$, the zeroth moment of α becomes

$$\begin{aligned}\langle\alpha\rangle &= \int \alpha(f)p_u(f)df \\ &= \int A\exp(\frac{1}{2}f)\frac{1}{\sqrt{2\pi\sigma_f^2}}\exp(-\frac{f^2}{2\sigma_f^2})df \\ &= A\exp(\frac{\sigma_f^2}{8})\end{aligned} \tag{2.65}$$

where $p_u(f)$ is the probability density of f. The variance is

$$\begin{aligned}\sigma_a^2 &= \int(\alpha - \langle\alpha\rangle)^2 p_u(f)df \\ &= \int(A\exp(\frac{1}{2}f) - \langle\alpha\rangle)^2\frac{1}{\sqrt{2\pi\sigma_f^2}}\exp(-\frac{f^2}{2\sigma_f^2})df \\ &= A^2\exp(\frac{\sigma_f^2}{4})(\exp(\frac{\sigma_f^2}{4}) - 1)\end{aligned} \tag{2.66}$$

The dependency of the coefficient of variation of α, CV_α with $CV_\alpha = \frac{\sigma_\alpha^2}{\langle\alpha\rangle^2}$, on σ_f^2 is illustrated in Figure 2.6.

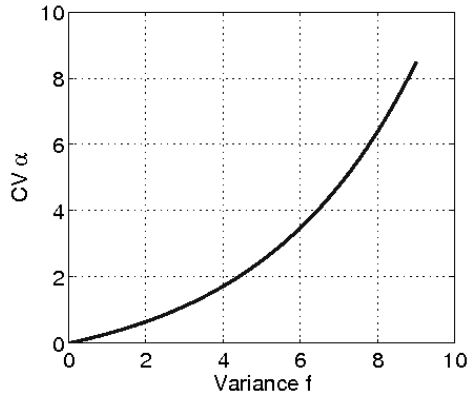

Figure 2.6: *Coefficient of variation of α as function of variance of f.*

The covariance function of α is

$$\begin{aligned} C_{aa}(z'-z'') &= \int\int \big(\alpha(z')-\langle\alpha\rangle\big)\big(\alpha(z'')-\langle\alpha\rangle\big)\, p_u(f(z'),f(z''))df(z')df(z'') \\ &= \int\int \left(A\exp(\frac{1}{2}f(z'))-\langle\alpha\rangle\right)\left(A\exp(\frac{1}{2}f(z''))-\langle\alpha\rangle\right) \\ &\quad \left(\frac{1}{2\pi\sigma_f^2\sqrt{1-\rho_f^2}}\exp(-\frac{f(z')^2-2\rho_f f(z')f(z'')+f(z'')^2}{2\sigma_f^2(1-\rho_f^2)})\right)df(z')df(z'') \\ &= A^2\exp(\frac{\sigma_f^2}{4})(\exp(\frac{1}{4}\rho_f\sigma_f^2)-1) \end{aligned} \tag{2.67}$$

where $p_u(f(z'),f(z''))$ is the Gaussian joint probability density of $f(z')$ and $f(z'')$ and ρ_f is the correlation function of f.

$$\rho_f(h) = \frac{C_{ff}(h)}{\sigma_f^2} \tag{2.68}$$

$h = z'-z''$ is here the distance vector between z' and z'' and $C_{ff}(h)$ is the two-point autocovariance of f. The correlation function of α is the autocovariance C_{aa} normalized with the variance.

$$\rho_a(h) = \frac{C_{aa}(h)}{\sigma_a^2} = \frac{\exp(\frac{\sigma_f^2\rho_f(h)}{4})-1}{\exp(\frac{\sigma_f^2}{4})-1} \tag{2.69}$$

The crosscovariance of f and α is

$$\begin{aligned} C_{fa}(z'-z'') &= \int\int f(z')\left(\alpha(z'')-\langle\alpha\rangle\right)p_u(f(z'),f(z''))df(z')df(z'') \\ &= \int\int f(z')\left(A\exp(\frac{1}{2}f(z''))-\langle\alpha\rangle\right) \\ &\quad \left(\frac{1}{2\pi\sigma_f^2\sqrt{1-\rho_f^2}}\exp(-\frac{f(z')^2-2\rho_f f(z')f(z'')+f(z'')^2}{2\sigma_f^2(1-\rho_f^2)})\right)df(z')df(z'') \\ &= \frac{1}{2}A\rho_f\exp(\frac{\sigma_f^2}{8})\sigma_f^2 \end{aligned} \tag{2.70}$$

The corresponding correlation function is then

$$\rho_{fa}(h) = \frac{C_{fa}(h)}{\sigma_f\sigma_a} = \frac{\rho_f(h)\sigma_f}{2\sqrt{\exp(\frac{\sigma_f^2}{4})-1}} \tag{2.71}$$

The correlation function of f, α and $f\alpha$ is shown in Figure 2.7 for $\sigma_f^2 = 1.0$.

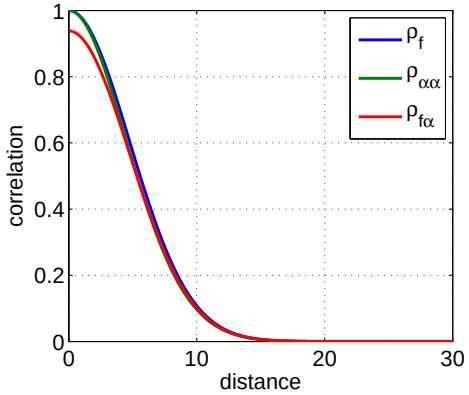

Figure 2.7: *Correlation function of f, α and $f\alpha$ vs. distance (for $\sigma_f^2 = 1.0$).*

The equations are based on a multi-Gaussian pdf and cannot be used for non-multi Gaussian fields.

2.3.2 Gaussian and Non-Gaussian soil structure

Only multi-Gaussian fields (random fields with a normal multivariate pdf) are fully described by their first order second moment properties, (see section 2.3.1.1). Random fields with other pdfs can have the same first two moments as multi-Gaussian fields but a completely different, eventually more realistic pattern, characterized by features which are only contained in higher order moments. Such features can be related to the arrangement of extreme values. Multi-Gaussian fields are symmetric and have therefore spatially isolated extreme values. Non-Gaussian fields can be generated from Gaussian fields by applying certain transformations such that extreme values appear differently. In this work, non-Gaussian fields with connected extreme values and fields with large patches of extreme values are considered. In the following, the generation of such fields and the corresponding transformations of multi-Gaussian fields are explained.

2.3.2.1 ZH-transformation

It is recently discussed that fields with connected extreme values better represent natural spatial pattern of soil parameters. Such two-dimensional parameter fields, namely Gaussian fields and fields with connected high or connected low extreme values, were used in the study of Neuweiler and Vogel (2007). Fields with connected extreme values are non-Gaussian and can be generated through transformation of Gaussian fields according to Zinn and Harvey (2003)

$$y_j = \sqrt{2}\mathrm{erf}^{-1}(2\mathrm{erf}(\frac{x_j}{\sqrt{2}}) - 1), \tag{2.72}$$

where x_j is the value at node j of a Gaussian field and y_j the value of the resulting non-Gaussian field.

Transformation (2.72) projects positive and negative extreme values onto positive extreme values. Intermediate values, which are connected in the Gaussian field, become the minimum extreme values in the transformed field. Thus, the transformed field has connected low extreme values. The transformed field is referred to as T1-field. The inverse of the T1-field (with the value $-y_j$ at node j), referred to as IT1-field, shows connected high extreme values. One realization, representing the saturated loghydraulic conductivity of T1- and IT1-fields, in comparison to Gaussian fields, denoted by G1-fields, with the same univariate and two-point autocorrelation function, is shown in Figure 2.8.

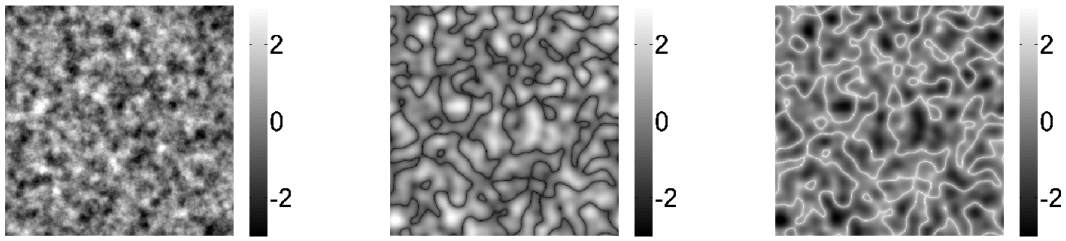

(a) G1 (b) T1 (c) IT1

Figure 2.8: *One realization of the saturated loghydraulic conductivity f, representing the three structures of G1- (a), T1- (b) and IT1-fields (c).*

2.3.2.2 V-transformation

Fields with large patches of coarse or fine material can be generated from Gaussian fields using a so-called V-transformation, described in Li (2010):

$$\begin{aligned} y_j &= k \cdot (x_j - m)^a, x_j \geq m \\ y_j &= (m - x_j), x_j < m \end{aligned} \tag{2.73}$$

where x_j is the value at node j of a multi-Gaussian field, y_j is the value of the transformed field and $m > 0$, $a > 0$ and $k > 1$ are transformation parameters. Transformation (2.73) turns values that are smaller than m into postive values, m becomes the smallest value of the resulting distribution and values larger than m become either more concentrated ($k < 1$) towards or more deviated from m ($k > 1$), (Li, 2010). The particular pattern depends on the choice of m, k and a. In a multi-Gaussian field, the intermediate values (around zero) form the connected background material. These values can be shifted to higher values, depending on m, but remain connected in the transformed field. Isolated patches of high conductive material emerge from the right (for $x_j \geq m$) and the left branch (for $x_j < m$) of transformation (2.73). While the steepness of the slope of the right branch is controlled by a and k, the left slope is always constant which results in two kinds of isolated patches. The patches emerging from the left branch have moderately high values and smooth edges. The patches emerging from the right branch are the more sharp-edged and larger, the smaller a is, and the larger and more extreme, the larger k is. Figure 2.9 shows the V-transformation for different parameters of a and k.

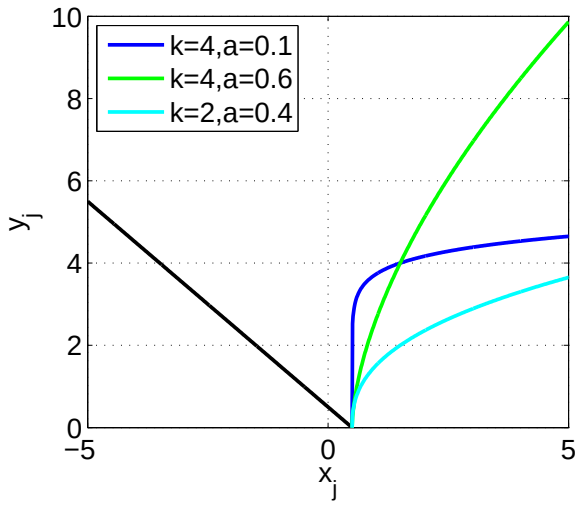

Figure 2.9: *Left branch (for $x_j < m$; black line) and right branch (for $x_j \geq m$) of transformation (2.73) for $m = 0.5$ and different values of a and k. Small values of a and large values of k (e.g. dark blue line) lead to fields with large patches of high conductive material.*

In the same way as for T1- and IT1-fields, transformed fields (referred to as T2-fields) and the inverse of the transformed fields (IT2-fields) are obtained using transformation (2.73). T2- and IT2-fields show the opposite pattern. One realization, representing the saturated loghydraulic conductivity of T2-, IT2- and Gaussian G2-fields, with the same univariate and two-point autocorrelation function, is shown in Figure 2.10.

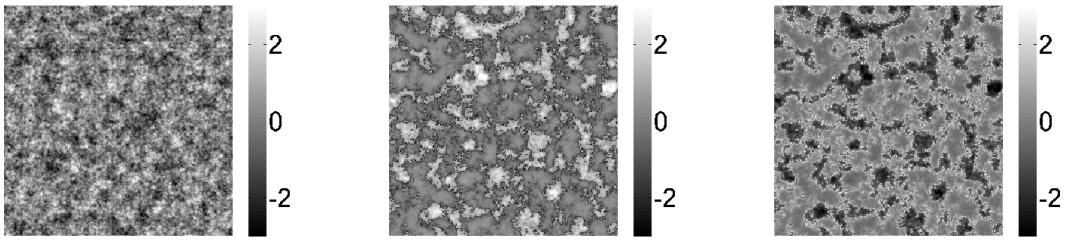

(a) G2 (b) T2 (c) IT2

Figure 2.10: *One realization of the saturated loghydraulic conductivity f, representing the three structures of G2- (a), T2- (b) and IT2-fields (c). Transformation parameters, $a = 0.1$, $m = 0.5$, $k = 4.0$, were used.*

Note that the ZH-transformation preserves the univariate, while the V-transform does not.

2.3.3 Measures to characterize the soil structure

This section briefly introduces measures which can be used to characterize the soil structure. An important measure captured by the first two moments, discussed first, is the anisotropy of soil parameters, which means the asymmetry of soil properties in space. The variety of occurring soil structures in nature and the fact that first order second moment properties are not sufficient to fully characterize a random variable, call for other measures to describe the soil heterogeneity, which take e.g. the arrangement of extreme values into account. For example, the saturated loghydraulic conductivity fields introduced in chapter 2.3.2 are not distinguishable by their mean and variance. Two examples of such measures, the copula and the connectivity function, are presented in the following. These measures are certainly not able to represent all existing features of heterogeneity but involve the alignment of extreme values, thus describe a spatial property of non-Gaussian fields which is not included in the first two moments.

2.3.3.1 Anisotropy

The fields shown in section 2.3.2 are isotropic, meaning that the saturated loghydraulic conductivity has the same stochastic properties in both directions and that the covariance of f depends only on the distance vector. Natural fields often show a slightly layered structure where the integral scale in the horizontal direction is larger than in the vertical direction. Anisotropy introduces a flow component orthogonally to the mean flow direction and can thus severly influence flow. It is a classical first-order second-moment measure.

2.3.3.2 Copulas

An empirical bivariate copula is a scale-invariant measure which captures the dependence of two random variables as a full distribution meaning that the dependence or correlation can be distinguished according to the different quantile of the variables (Li, 2010). Any two variables can be observed by means of a copula. When referring to an empirical bivariate spatial copula, usually the random variables at two space points of a random field are considered. In this study, the term copula refers to an empirical bivariate spatial copula density. It is defined as the bivariate probability density function related to the marginal distribution.

To give a more illustrative explanation, the construction of a copula for one particular distance vector h from a sample of values is explained in the following. The cumulative density function (cdf) of the empirical distribution $f(\mathbf{x})$ is calculated. Pairs of values which are separated by the distance h are identified and transformed into a scatter plot $cdf(f(\mathbf{x}))$ vs. $cdf(f(\mathbf{x}+h))$. Figure 2.11 illustrates an example for $cdf(f(\mathbf{x})) = 0.3$ and $cdf(f(\mathbf{x}+h)) = 0.89$. The scatter plot is visualized by a contour plot. From the copula density, the characteristic features of the underlying structure can be inferred e.g. which values form larger patches. For example, a maximum in the copula density at a specific pair of cdf-values for a series of distance classes $h1$-$h5$ means that the parameter values,

belonging to such cdf-values, are correlated up to a distance of $h5$.

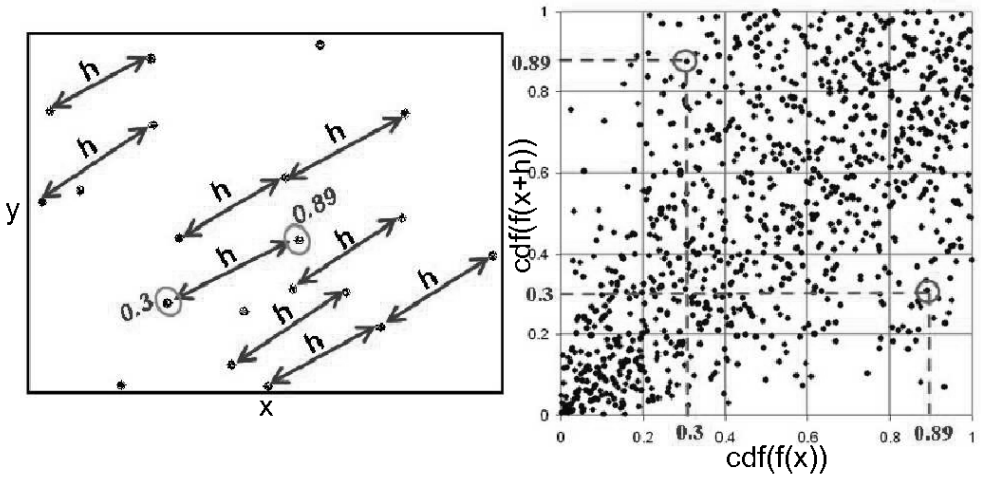

Figure 2.11: *Construction of an empirical copula from a sample. (a) shows the empirical distribution after the cdf is calculated. Pairs* $(cdf(f(\boldsymbol{x})), cdf(f(\boldsymbol{x}+h)))$ *which are separated by the distance* h *are identified and put into a scatter plot (b). Taken from Li (2010).*

The dependence of two space points of a random field can also be described with an autocovariance function. The covariance function does, however, neither image the frequency nor the values of the observed pair but only the correlation. Thereby the information about the typical cluster size of extreme values is lost.

The parameter fields for the saturated loghydraulic conductivity, presented in section 2.3.2, can be classified according to their copula: The copula of the Gaussian fields is symmetrical and rugby-shaped. In contrast, the copulas of the non-Gaussian fields are asymmetric with a maximum at high values for a series of distance classes if large clusters of high extreme values are present (T1,T2) and a maximum at low values if large clusters of low extreme values are present (IT1, IT2). Figure 2.12 shows examples of copulas (for one distance class) of Gaussian and non-Gaussian fields with clusters of high or low extreme values.

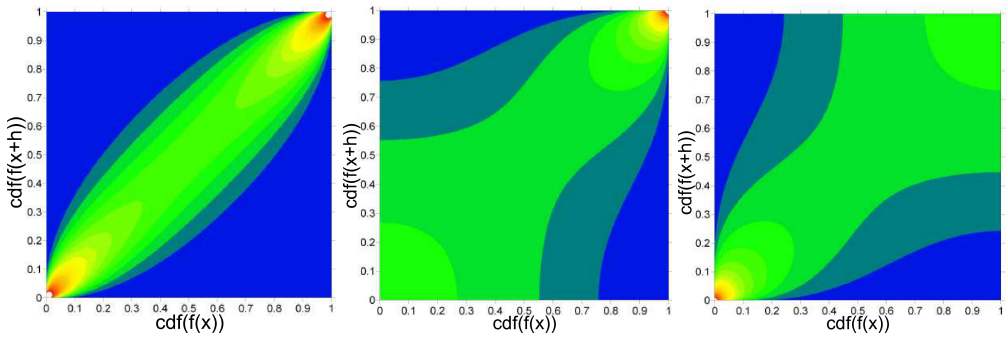

Figure 2.12: *Copulas of a Gaussian field (a) and non-Gaussian fields with patches of high extreme values (b) and patches of low extreme values (c). Taken from Li (2010).*

2.3.3.3 Connectivity

From a copula, the typical cluster size can be identified. Another feature of structure, which is not captured by a copula and also not contained in the mean and the variance of a random field, is the connectivity of regions with similar parameter values.

To find the values that are connected over larger distances, the parameter of interest is, in a continuous field, first transformed into a binary field by means of a threshold value t. Values which are larger than t are set to one and values below the threshold value to zero, or vice versa. Connectivity is analyzed as a function of the threshold value t. Therefore, it is determined whether values equal to one form connected clusters in the binary field. Depending on the objective of the connectivity analysis, different methods are used. One possibility is the Euler characteristic χ which is, in two dimensions, calculated from the number of isolated objects N and the number of redundant connections C (Li, 2010).

$$\chi = N - C \tag{2.74}$$

While the threshold t is continuously lowered (or increased), the number of isolated objects N and number of connections C and, thus, χ changes. In this way, the connectivity function $\chi(t)$ is obtained. Values which are equal to the threshold value, at which $\chi(t)$ is zero, are connected in the parameter field. Connectivity is, hence, defined by the equality of N and C. The Euler characteristic is thus a global measure to quantify connectivity as a whole. It is a proper measure to characterize the saturated hydraulic conductivity, but might not always be of interest, e.g. when heterogeneous hydraulic variables such as water fluxes are analyzed for connectivity. Then, it is rather meaningful to determine the threshold, from which on a connected pathway from the surface to the groundwater resources exists. As illustrated in Figure 2.13, this might be independent from the number of isolated objects and number of connections.

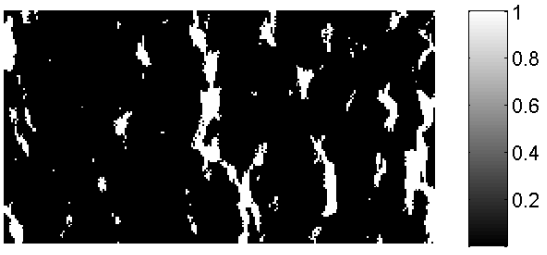

Figure 2.13: *Example of a binary field. The Euler method would not predict that values equal to the applied threshold value are connected.*

To determine which range of values of a parameter field form connected pathways from top to bottom, the parameter field, to be observed, is transformed into a binary indicator field according to a certain threshold value, as in the previous case. In the second step, the clusters

of values equal to one are identified and labeled. This procedure is carried out according to the Hoshen-Kopelman-Algorithm (Hoshen and Kopelman, 1976; Fricke, 2004). A connected path from top to bottom exists, if a cluster with the same label appears at the top and bottom of the output field, (see Figure 2.14). The threshold value is scanned through all possible values of the parameter field to find the minimum and maximum threshold value for which the values are connected.

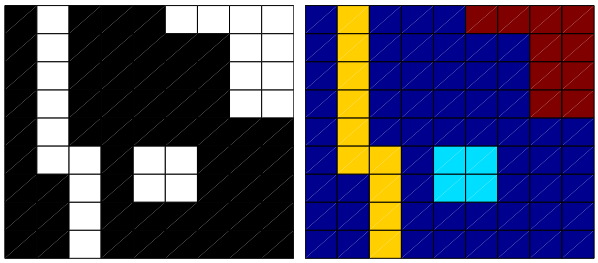

Figure 2.14: *Illustration of Hoshen-Kopelman procedure. In the binary field (a), clusters of values equal to one (white fields) are identified and labeled (b). Different colors correspond to different labels. In this example only the yellow cluster is connected from top to bottom.*

2.3.4 Methods to solve stochastic flow equations

There are a number of methods to solve the stochastic flow equations. Generally, the goal is to make predictions about the moments of hydraulic variables such as pressure head and saturation. Approaches can be divided into analytical solutions, where often the method of small perturbations is used, or numerical simulations. Beyond numerical approaches, performance of Monte Carlo simulations is the most common method. Recently, alternative, more efficient methods are explored (e.g. Oladhyshkin and Novak, 2010). In this work, we focus on the two main approaches, perturbation method on the analytical side and Monte Carlo Method on the numerical side, which are introduced in the following.

2.3.4.1 Perturbation Method

In this section the basics of perturbation approximations, following the book of Zhang (2002) are explained. It is shown how to make approximate predictions of mean and variance of flow variables. As explained in the previous section, variability of the flow problem is described with one random parameter, the loghydraulic saturated conductivity F. The fluctuations of the soil parameters (equation (2.57)) propagate to the dependent variables. ψ can be described by a formal Taylor expansion in terms of the standard deviation σ_f

$$\psi = \psi^0 + \psi^1 + \psi^2 + ... \tag{2.75}$$

Note, that if the variation of the sink term and the boundary conditions was considered as well, $\psi^{(n)}$ would be a function of σ, a combination of the standard deviations of f, of the sink term and of the boundary conditions.

In case the pressure head field varies weakly, ψ can be approximated to first order. To first order in σ_f, the mean head is $\langle\psi\rangle = \psi^0$ and the head fluctuation is $\psi' = \psi^1$. The head covariance is, hence, $C_\psi(\mathbf{x}_1, \mathbf{x}_2) = \langle\psi^1(\mathbf{x}_1)\psi^1(\mathbf{x}_2)\rangle$ to first order in σ_f. Thus, to make predictions about the mean and fluctuations of the head to first order in σ_f, a set of equations for each order has to be derived which can be solved for ψ^0 and ψ^1. Therefore, the decomposed random variables and the expansion of the dependent variables are inserted into the Richards equation and conditions for initial and boundary conditions. Then, terms at separate order are collected. The resulting sets of equations, consisting of zeroth or first order Richards' equations, boundary and initial conditions, are solved for ψ^0 and ψ^1, respectively.

Method of Greens function

Applying the perturbation method to the unsaturated flow problem results in a linear, inhomogeneous partial differential equation for each order. One possibility to solve these equations is the Method of Greens function which is a mathematical tool to solve inhomogeneous linear equations of the form

$$Au = g \tag{2.76}$$

where A is some linear operator and u the unknown.

The equation is solved by

$$u(z) = \int_{-\infty}^{\infty} G(z - z')g(z')dz' \tag{2.77}$$

where G is the Greens function defined by

$$AG(x) = \delta(x) \tag{2.78}$$

with $\delta(x)$ being the Dirac delta function. To determine the Greens function might be very difficult. For standard equations, G can be found in the literature, it can also be derived for simple cases e.g. using mirror functions.

2.3.4.2 Monte Carlo method

In this method, a deterministic flow problem is solved numerically for each realization of an ensemble of parameter fields. From the resulting ensemble of hydraulic variables, the moments such as mean, variance and covariance are derived.

The numerical method to solve the flow equation, which is in our case the Richards equation, is explained in the next section.

2.4 Numerical model for the Richards equation

Unsaturated flow is modeled by the Richards equation which is a non-linear partial differential equation. First-order second-moment perturbation approximations for the unsaturated flow problem including root water uptake exist for steady flow and simple soil structures (see chapter 3). However, these solutions underlie restrictions as small variability of the soil parameters and are only able to capture the influence of soil structure characterized by the first two moments (mean and variance) which means a loss of information. Transient problems, large variations of soil parameters or more complex structure have to be analyzed using numerical solutions.

Numerical schemes approximate the continuous problem in space and time with a discrete solution. The procedure to obtain the discrete distribution can be grouped into three steps. First, the domain of interest is divided into subunits by means of a grid. Second, the flow-determining equations, in our case the Richards equation, is discretized, which means that it is formulated for all subunits (in space and time). And third, the resulting system of non-linear equations is linearized and solved for each successive time level based on the information given at the boundaries and in the initial state.

In order to represent the real problem appropriately, the following conditions have to be met. The discretization scheme should lead to stable solutions, meaning errors are not amplified. Furthermore, it has to be convergent which means that with a refinement of the grid spacing, the numerical solution tends towards the exact solution of the differential equations. And last, the discretization scheme has to be mass conservative.

In the following, the discretization scheme in time and space is explained in more detail. These methods are implemented in the flow simulator MUFTE-UG (Multiphase Flow, Transport and Energy model) (Helmig et al., 1998) and used for the numerical simulations in 2D fields.

2.4.1 Temporal discretization

For the time discretization, a fully implicit Euler scheme is used which corresponds to a backward finite-difference scheme where the time derivative is approximated by the difference of the solution at two successive time levels,

$$\frac{\partial u}{\partial t} = \frac{u^{n+1} - u^n}{t^{n+1} - t^n} = f(u^{n+1}), \tag{2.79}$$

where n and $n+1$ denote the time level and $f(u^{n+1})$ the system of equations evaluated at the next time level. Consequently, the full system of equations has to be solved at each time level which is computationally expensive but guarantees stability.

2.4.2 Spatial discretization

The spatial discretization of the Richards equation is done using a vertex-centered finite-volume scheme, the so-called Box method (Helmig, 1997).

As in finite-element methods, a discrete solution for the potential is obtained on the nodes of a finite-element mesh using the weak form of the Richards equation. The fluxes are balanced over the boundaries of a control volume which is defined by a dual (finite-volume) mesh. In this sense, the Box method combines the advantages of finite-volume methods as it is locally mass conservative and finite-element schemes being applicable to complicated meshes.

In the following, we consider unsaturated flow in the domain Ω. The domain is discretized with a finite-element mesh into elements E. The elements are further divided into subcontrol elements to obtain a dual mesh - the finite-volume mesh. This mesh is constructed by connecting the element barycenters with the barycenters of the element faces. Each element consists then of n subcontrol volumes, where n is the number of vertices or nodes of the element. The volume of each finite-volume box is denoted by B. The grid is illustrated in Figure 2.15.

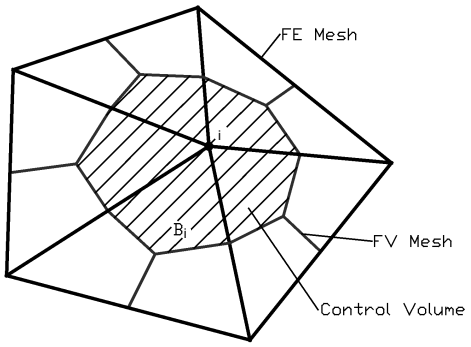

Figure 2.15: *Construction of Finite Element and Finite Volume mesh.*

A numerical, discrete solution approximates the real, continuous solution at distinct points, defined by the finite-element mesh. In our case, the unknown is the total potential Ψ, defined in equation (2.20). Within one element, Ψ is approximated using first-order Ansatz functions N_j which have to be equal to unity at the node j and zero at all other nodes. In between two nodes, the Ansatz functions N_j are chosen as piecewise linear (see Figure 2.16).

$$\tilde{\Psi} = \sum_{j=1}^{n} N_j \Psi_j \tag{2.80}$$

Gradients are described by

$$\nabla\tilde{\Psi} = \sum_{j\in\eta_i}^{n} \nabla N_j (\Psi_j - \Psi_i) \tag{2.81}$$

where η_j is the set of neighboring nodes of the node i in a given element.
The geometry of the domain is discretized with the same Ansatz functions as the unknowns.

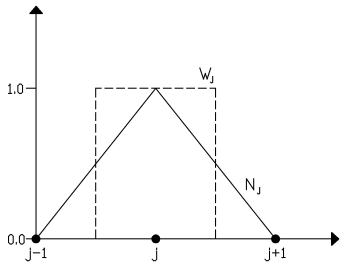

Figure 2.16: *Sketch of Ansatz functions N_j and weighting functions W_j.*

The weak formulation requires the Richards equation (2.24) not to hold absolutely but on average and with respect to some test function W_i which has to vanish on the boundaries of the domain.

$$\int_\Omega W_i \frac{\partial(\rho\Theta(p_w))}{\partial t} - \int_\Omega W_i \nabla \cdot [\rho\lambda k_s \nabla\Psi] - \int_\Omega W_i \rho R = 0 \tag{2.82}$$

Approximating the solution by discrete values (equation 2.80) results in an error or residual ϵ when employed in equation 2.82. The weighted residual which is the residual multiplied by the test function becomes, however, zero on the average if the test functions, also called weighting functions, are chosen appropriately,

$$\int_\Omega W_i \epsilon d\Omega \stackrel{!}{=} 0. \tag{2.83}$$

With equation 2.80, 2.81 and the weighing functions W_i, the weak formulation of the Richards equation (2.82) for the approximate solution is as follows

$$\int_\Omega W_i \frac{\partial \sum_{j\in\eta_i}(\rho\Theta_j)N_j}{\partial t} d\Omega - \int_\Omega W_i \nabla \cdot [\rho\lambda k_s \sum_{j\in\eta_i}(\Psi_j - \Psi_i)\nabla N_j] d\Omega$$
$$- \int_\Omega W_i \sum_j N_j \rho R_j d\Omega = W_i \epsilon d\Omega \stackrel{!}{=} 0. \tag{2.84}$$

As S_j, Ψ_j and R_j are node values, not depending on the spatial coordinates, the summations can be pulled out of the volume integral. Assuming incompressible flow, the density of water is constant and drops out in each term,

$$\frac{\partial \sum_{j\in\eta_i}\Theta_j}{\partial t}\int_\Omega W_i N_j d\Omega - \sum_{j\in\eta_i}(\Psi_j-\Psi_i)\int_\Omega W_i\nabla\cdot[\lambda k_s \nabla N_j]d\Omega$$
$$-\sum_j R_j\int_\Omega W_i N_j d\Omega = W_i\epsilon d\Omega \stackrel{!}{=} 0. \tag{2.85}$$

Using a mass lumping technique, the properties of a finite-volume-formulation are gained. The mass matrix M_{ij} is defined as

$$M_{ij} := \int_\Omega W_i N_j d\Omega \tag{2.86}$$

and it is assumed that this 'mass' is concentrated at the nodes. Correspondingly, M_{ij} can be replaced by the matrix M_{ij}^{lump} where the coefficients of each row of M_{ij} are summed onto the diagonals

$$M_{ij}^{lump} = \delta_{ij}\sum_k M_{ik}, \tag{2.87}$$

with δ_{ij} being the Kronecker delta.

In the Box method, the weighting functions are chosen to be piecewise constant (equal to unity) within the control volume box B_i of the node i and zero otherwise, i.e. the characteristic function of the box B_i. Weighting and Ansatz-functions are shown in Figure 2.16. Due to the definition of W_i and N_k, one gets

$$M_{ij}^{lump} = \delta_{ij}\sum_k\int_\Omega W_i N_k d\Omega = \delta_{ij}\int_\Omega W_i d\Omega = \delta_{ij}\int_\Omega dB_i d\Omega = \delta_{ij}\|B_i\|, \tag{2.88}$$

where $\|B_i\|$ is the volume of B_i. The assignment of the 'mass' to a subvolume, in this case B_i, is typical for finite-volume methods.

The storage term (term 1) becomes then

$$\frac{\partial \sum_{j\in\eta_i}\Theta_j}{\partial t}\int_\Omega W_i N_j d\Omega$$
$$= \frac{\partial \sum_{j\in\eta_i}\Theta_j}{\partial t}\delta_{ij}\|B_i\| = \frac{\partial\Theta_i}{\partial t}\|B_i\|. \tag{2.89}$$

The sink term (term 3) becomes

$$\int_\Omega W_i R d\Omega = R_i \|B_i\|. \tag{2.90}$$

The flux term (term 2) can be simplified using the product rule of differentiation (equation (2.91))

$$\int_\Omega W_i \nabla \cdot \mathbf{F} d\Omega = \int_\Omega \nabla \cdot (W_i \mathbf{F}) d\Omega - \int_\Omega \nabla W_i \mathbf{F} d\Omega, \tag{2.91}$$

with W_i being a scalar field and **F**, a vector field,

and the Green-Gauss integral theorem (equation (2.92))

$$\int_\Omega \nabla \cdot (W_i \mathbf{F}) d\Omega = \oint_{\partial\Omega} W_i \mathbf{F}, \cdot \mathbf{n} d\Gamma \tag{2.92}$$

where **n** denotes the outer unit normal vector.

Term 2 can then be reformulated to yield

$$\begin{aligned} &\sum_{j \in \eta_i} (\Psi_j - \Psi_i) \int_\Omega W_i \nabla \cdot \lambda k_s \nabla N_j d\Omega \\ &= \sum_{j \in \eta_i} (\Psi_j - \Psi_i) \int_\Omega \nabla \cdot (W_i \lambda k_s \nabla N_j) d\Omega \\ &\quad - \sum_{j \in \eta_i} (\Psi_j - \Psi_i) \int_\Omega \nabla W_i \lambda k_s \nabla N_j d\Omega. \end{aligned} \tag{2.93}$$

Using the definition of W_i, which implies $\nabla W_i = 0$, and using the Green-Gauss theorem, the flux term reduces to

$$\begin{aligned} &\sum_{j \in \eta_i} (\Psi_j - \Psi_i) \int_\Omega W_i \nabla \cdot \lambda k_s \nabla N_j d\Omega \\ &\qquad = \sum_{j \in \eta_i} (\Psi_j - \Psi_i)(\lambda)_{ij} \int_{\partial B_i \cap \partial B_j} k_s \nabla N_j \cdot \mathbf{n}_{\partial B_i} d\Gamma_{B_i}. \end{aligned} \tag{2.94}$$

The flux into a box boundary segment is thus determined by the difference of the total potential of the two adjacent nodes, the mobility and the intrinsic permeability at the interface of two boxes. To guarantee that the fluxes are continuous with the applied discretization scheme, the intrinsic permeability k_s is defined at the nodes and is harmonically averaged

to obtain the value at the interface of two boxes. The mobility is assigned according to a fully upwinding scheme which takes the properties of the upstream node. Considering the direction of the advective transport in this way leads to a more stable solution.

$$(\lambda)_{ij} = (\lambda)_j \text{ if } \Psi_{w,i} < \Psi_{w,j} \tag{2.95}$$

$$(\lambda)_{ij} = (\lambda)_i \text{ if } \Psi_{w,i} \geq \Psi_{w,j} \tag{2.96}$$

Applying term 1, term 2 and term 3 to equation (2.85) and taking the time discretization into account finally leads to the discretized form of the Richards equation:

$$\frac{\Theta_i^{n+1} - \Theta_i^n}{t^{n+1} - t^n} \|B_i\| - \sum_{j \in \eta_i} (\Psi_j - \Psi_i)^{n+1} (\lambda)_{ij}^{n+1} \bar{k_s}^{n+1} \int_{\partial B_i \cap \partial B_j} \nabla N_j \cdot \mathbf{n}_{\partial B_i} d\Gamma_{B_i} - R_i^{n+1} \|B_i\| = 0 \tag{2.97}$$

where $\bar{k_s}$ is the harmonic mean of $k_{s,i}$ and $k_{s,j}$.

2.4.3 Linearization

The discretization scheme results in a system of non-linear equations of the form

$$\mathbf{f}(\mathbf{u}) = 0, \tag{2.98}$$

where $\mathbf{u}$ is the set of unknowns and $\mathbf{f}$ a non-linear function of $\mathbf{u}$. Non-linearity emerges from the constitutive relationships as the relative permeability - pressure head relationship or the pressure head - saturation relationship. The non-linearity is treated with the **Newton-Raphson** method where the function is linearized in the following way,

$$\mathbf{u}_{r+1} = \mathbf{u}_r - \left(\frac{\partial \mathbf{f}}{\partial \mathbf{u}} \right)_r^{-1} \cdot \mathbf{f}(\mathbf{u}_r), \tag{2.99}$$

where r indicates the iteration step.
The matrix of partial derivatives is defined as Jacobian matrix,

$$\mathbf{J} = \frac{\partial \mathbf{f}}{\partial \mathbf{u}}. \tag{2.100}$$

For the transient solutions, the Jacobian is evaluated numerically.

3 First order second moment solutions for unsaturated flow

For simple soil structures, such as layered media or a medium consisting of parallel streamtubes (parallel column medium) and for the standard root water uptake parametrization, first order second moment solutions of the steady state unsaturated flow problem including root water uptake can be derived using a perturbation approximation. The mathematical procedure to derive such solutions in general, was explained in section 2.3.4.1. The dependent flow variables are expanded in terms of the systems standard deviation σ. In this work, the random space functions in the Richards equation, Θ and $K(\psi)$, are functions of the pressure head $\psi(f, \alpha)$, the saturated loghydraulic conductivity f, and the soil parameter α which is related to f via the Miller similarity, (equation (2.64)). Hence, only one random soil parameter, f, determines the variability of the system. The mean and the variance of the pressure head ψ can thus be expressed in terms of the statistical properties of f. Assuming small variability of the soil parameters and dependent variables, the steady state first order second moment solution can be determined using a perturbation approach.

In this chapter, analytical solutions for mean and variance of pressure head in a parallel column medium, derived by Rubin and Or (1993), are shown and compared to semi-analytical expressions for the first two moments in a layered medium.

3.1 Column media

In Rubin and Or (1993), the stochastic Richards equation with water extraction by roots modeled as sink term in a parallel column medium is analytically solved for the mean and the variance of pressure head. The solution describes one-dimensional flow in independent homogeneous streamtumbes where no interactions between media with different properties takes place. The upper boundary corresponds to the surface and is modeled as a Neumann boundary with constant inflow q. The lower boundary corresponds to the water table and is modeled by a Dirichlet boundary condition with ψ equal to zero. The root water uptake parametrization is as in equation (2.25) with an exponentially decreasing root density distribution (equation (2.26)),

$$R(z) = \frac{\tau}{\delta} \exp \frac{z - H}{\delta}, \tag{3.1}$$

where $\tau\,[\mathrm{m/s}]$ is the atmospheric demand, $\delta\,[\mathrm{m}]$ the root depth and $H\,[\mathrm{m}]$ the vertical extension of the domain. Note that in the work of Rubin and Or (1993), δ is treated as a random

variable as well while in this work, δ is assumed to be deterministic.
After Rubin and Or (1993), the mean of pressure head is given by

$$\psi^0(z) = \frac{1}{\langle\alpha\rangle} \ln\left(\frac{\langle\alpha\rangle}{\langle K_s\rangle}\left[\frac{q_n}{\langle\alpha\rangle} + \left[\frac{\langle K_s\rangle}{\langle\alpha\rangle} - \frac{q_n}{\langle\alpha\rangle} - \frac{\delta}{1+\langle\alpha\rangle\delta}\tau e^{-H/\delta}\right]e^{-\langle\alpha\rangle z} + \frac{\delta}{1+\langle\alpha\rangle\delta}\tau e^{-\frac{H-z}{\delta}}\right]\right). \tag{3.2}$$

With a deterministic δ, the variance of pressure head reads,

$$\langle\psi^1(z), \psi^1(z)\rangle = \int_0^z (F_4(z')\alpha'(z) + F_5(z')f(z'))^2 dz' \tag{3.3}$$

with

$$F_4 = \frac{\partial\psi}{\partial\alpha} - \frac{1}{\langle\alpha\rangle^2}\ln\left(\frac{\exp(\langle F\rangle + 1)}{\langle\alpha\rangle\langle\phi_{tc}\rangle}\right) + \frac{F_1}{\langle\alpha\rangle\langle\phi_{tc}\rangle} \tag{3.4}$$

$$\begin{aligned} F_1 &= -\frac{\partial\phi_{tc}}{\partial\alpha} \\ &= -\frac{q_n}{\langle\alpha\rangle^2} - \frac{\delta^2\tau\exp\left(-(H-z)/\delta\right)}{(1+\delta\langle\alpha\rangle)^2} \\ &\quad - \frac{[1+\langle\alpha\rangle z]\exp[-\langle\alpha\rangle z + \langle F\rangle]}{\langle\alpha\rangle^2} \\ &\quad + \frac{q_n[1+\langle\alpha\rangle z]\exp[-\langle\alpha\rangle z]}{\langle\alpha\rangle^2} \\ &\quad + \frac{[\delta + z(1+\delta\langle\alpha\rangle)]\delta\tau\exp[-\frac{H}{\delta} - \langle\alpha\rangle z]}{(1+\delta\langle\alpha\rangle)^2} \end{aligned} \tag{3.5}$$

$$F_5 = \frac{\partial\psi}{\partial F} = \frac{F_2 - \langle\phi_{tc}\rangle}{\langle\alpha\rangle\langle\phi_{tc}\rangle} \tag{3.6}$$

$$F_2 = \frac{\partial\phi_{tc}}{\partial F} = \frac{\exp(\langle F\rangle - \langle\alpha\rangle z)}{\langle\alpha\rangle} \tag{3.7}$$

where ϕ_{tc} is the matric flux potential with $\phi_{tc} = \int_{-\infty}^{\psi} K(\psi)d\psi$, $\langle\phi_{tc}\rangle = \frac{K_s\exp(\alpha\langle\psi\rangle)}{\alpha}$ and $q_n = q - \tau$.

Mean and variance of pressure head depend on the vertical position $z\,[\mathrm{m}]$. Figure 3.1 illustrates mean and variance profile of pressure head for different values of $q\,[\mathrm{mm/d}]$, $\tau\,[\mathrm{mm/d}]$ and $\delta\,[\mathrm{m}]$. At the groundwater table, the medium is fully saturated. With increasing vertical position, the saturation and ψ decrease due to capillary suction. Above this region, which is called the capillary fringe, the shape of the profile depends on the water extraction by

plants. Without root water uptake, the saturation or water pressure remain constant above the capillary fringe up to the surface. This value depends on the infiltration rate at the top boundary. Under consideration of root water uptake, water is continuously extracted within the root zone, the saturation and ψ thus decrease from the surface downwards. The particular shape depends on the atmospheric demand τ and the rooting depth δ. Thus, scenarios where root water uptake is taken into account are reflected in a 'bent' shape of mean and variance of water pressure head or saturation vs. vertical position. Figure 3.1 shows profiles of the mean and the variance of pressure head for an infiltration rate of q equal to $3\,\mathrm{mm/d}$ and an extraction rate of τ of $2\,\mathrm{mm/d}$ with different values of δ (dashed lines). The solid lines in Figure 3.1 are obtained without root water uptake and an infiltration rate of q (black line) or $q - \tau = 1\,\mathrm{mm/d}$ (green line). For a certain infiltration rate q and transpiration demand τ, the mean and variance profiles for all values of δ are bounded between the profiles which are obtained for the case without root water uptake and an infiltration rate of q or an infiltration rate of $q - \tau$ (Rubin and Or, 1993).

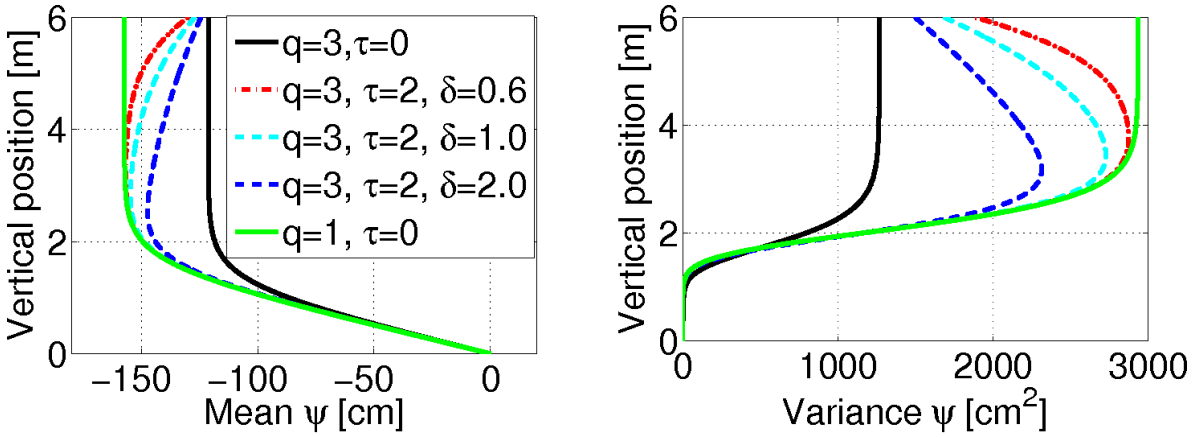

(a) Mean of pressure head (b) Variance of pressure head

Figure 3.1: *Analytical solution for mean (a) and variance (b) of pressure head in a column soil according to the solution of Rubin and Or (1993). In the legend, q denotes the infiltration rate [mm/d], τ the transpiration rate [mm/d] and δ [1/m] the rooting depth.*

3.2 Layered media

A similar solution for mean and variance of pressure head, as derived by Rubin and Or (1993) for a medium consisting of parallel streamtubes, can be determined for a layered medium. In the following, the derivation is outlined.

As in the previous chapter, root water uptake is parameterized according to equation (3.1) and depends only on the potential transpiration rate which equals the, over the root-zone distributed, atmospheric demand.

The conductivity K and the water pressure head ψ are expanded around the homogeneous solution into different orders in terms of the standard deviation of f.

$$\psi = \psi^0 + \psi^1 + \psi^2 + ...$$
$$K = K^0 + K^1 + K^2 + ...$$

Inserting the expressions into the 1D steady state Richards equation, where the time derivative is omitted, leads to

$$\frac{\partial}{\partial z}[(K^0 + K^1 + ...)(\frac{\partial \psi^0}{\partial z} + \frac{\partial \psi^1}{\partial z} + ... + 1)] = R. \tag{3.8}$$

Under consideration of the variation of f, α and ψ, the hydraulic conductivity K is written as

$$\begin{aligned} K &= K_s \exp(\alpha\psi) \\ &= K_{s,g}(1 + f + \frac{1}{2}f^2 + ...) \exp\left((\langle\alpha\rangle + \alpha')(\psi^0 + \psi^1 + ...)\right). \end{aligned} \tag{3.9}$$

The zeroth and first order hydraulic conductivity is obtained from equation (3.9) by taking only zeroth respectively first order terms into account,

$$\begin{aligned} K^0 &= K_{s,g} \exp(\langle\alpha\rangle\psi^0), \\ K^1 &= K_{s,g} f \exp(\langle\alpha\rangle\psi^0) + K_{s,g} \exp(\langle\alpha\rangle\psi^0)(\alpha'\psi^0 + \langle\alpha\rangle\psi^1). \end{aligned} \tag{3.10}$$

Zeroth order solution

At zeroth order, we obtain from equation (3.8)

$$\frac{\partial}{\partial z}[K^0(\frac{\partial \psi^0}{\partial z} + 1)] = R, \tag{3.11}$$

where the boundary conditions are

$$q^0(z = H) = q,$$
$$\psi^0(z = 0) = 0.$$

With K^0 (equation (3.10)), R (equation (3.1)) and transformation,

$$\varphi^0 = \exp(\langle\alpha\rangle\psi^0), \tag{3.12}$$

the zeroth order Richards equation (3.11) results in

$$\frac{\partial^2 \varphi^0}{\partial z^2} + \langle\alpha\rangle \frac{\partial \varphi^0}{\partial z} = \frac{\tau\langle\alpha\rangle}{K_{s,g}\delta} \exp(\frac{z - H}{\delta}). \tag{3.13}$$

Equation (3.13) is solved by

$$\begin{aligned}\varphi^0 &= \exp(-\langle\alpha\rangle z)(1+\frac{q}{K_{s,g}}+\frac{\tau}{K_{s,g}})-\frac{q}{K_{s,g}}+\frac{\tau}{K_{s,g}} \\ &+\frac{\langle\alpha\rangle\delta\tau}{(1+\langle\alpha\rangle\delta)K_{s,g}}(\exp(\frac{z-H}{\delta})-\exp(-\frac{H}{\delta}-\langle\alpha\rangle z)).\end{aligned} \tag{3.14}$$

The zeroth order pressure head follows from

$$\psi^0=\frac{1}{\langle\alpha\rangle}\ln(\varphi^0). \tag{3.15}$$

The solution ψ^0 represents the pressure head profile for a homogeneous soil where the conductivity equals its geometric mean $K_{s,g}$. As the mean only depends on the averaged soil parameters, ψ^0 agrees with the zeroth order solution of Rubin and Or (1993).

First order solution

The variance of the pressure head ψ^1 results from the solution of the first order equation, which is obtained by taking only first order terms of the flow equation (3.8),

$$\frac{\partial}{\partial z}[K^0\frac{\partial\psi^1}{\partial z}+K^1(\frac{\partial\psi^0}{\partial z}+1)]=0. \tag{3.16}$$

As the sink term R is deterministic, it does not depend on first order terms, hence the right hand side equals zero.

With K^1 from equation (3.10), the first order Richards equation becomes

$$\begin{aligned}&\frac{\partial}{\partial z}[K_{s,g}\exp(\langle\alpha\rangle\psi^0)\frac{\partial\psi^1}{\partial z}+(K_{s,g}f\exp(\langle\alpha\rangle\psi^0) \\ &+K_{s,g}\exp(\langle\alpha\rangle\psi^0)(\alpha'\psi^0+\langle\alpha\rangle\psi^1))(\frac{\partial\psi^0}{\partial z}+1)]=0.\end{aligned} \tag{3.17}$$

Using the zeroth order flux,

$$q^0=-K_{s,g}\exp(\langle\alpha\rangle\psi^0)(\frac{\partial\psi^0}{\partial z}+1), \tag{3.18}$$

and the following transformations,

$$\varphi^1 = \phi_t^0\psi^1, \tag{3.19}$$

$$\phi_t^0 = \exp(\langle\alpha\rangle\psi^0), \tag{3.20}$$

yields

$$\frac{\partial^2}{\partial z^2}\varphi^1+\langle\alpha\rangle\frac{\partial}{\partial z}\varphi^1=\frac{\partial}{\partial z}\frac{q^0}{K_{s,g}}(f+\psi^0\alpha'). \tag{3.21}$$

This expression can be further simplified by integration where the integration constant is assumed to be zero as the average over the fluctuations has to be zero,

$$\frac{\partial}{\partial z}\varphi^1 + \langle\alpha\rangle\varphi^1 = \frac{q^0}{K_{s,g}}(f + \psi^0\alpha'). \tag{3.22}$$

With the boundary conditions,

$$q^1(z = H) = 0,$$
$$\psi^1(z = 0) = 0,$$

equation (3.22) can be solved using the Greens function, which results in

$$\varphi^1 = \int_0^z G(z - z')g(z')dz' \tag{3.23}$$

with

$$g = \tfrac{q^0}{K_{s,g}}(f + \psi^0\alpha')$$

and

$$G(z - z') = \exp(-\langle\alpha\rangle(z - z')).$$

With $\psi^1 = \varphi^1/\phi_t^0$, it follows

$$\psi^1 = \exp(-\langle\alpha\rangle\psi^0)\int_0^z \exp(-\langle\alpha\rangle(z - z'))g(z')dz'. \tag{3.24}$$

The first order second moment approximation for the variance of the pressure head ψ as a function of the stochastic properties of f and α can be calculated by taking the expectation value of $\psi^1(z) \cdot \psi^1(z')$ at the same location, $z = z'$, i.e.

$$\begin{aligned}\sigma_\psi^2 &= \langle\psi^1(z)\psi^1(z)\rangle \\ &= e^{-2\langle\alpha\rangle(\psi^0(z)+z)}\int_0^z\int_0^z exp^{2\langle\alpha\rangle(z'+z'')}\langle g(z')g(z'')\rangle dz'dz''.\end{aligned} \tag{3.25}$$

The term $\langle g(z')g(z'')\rangle$ contains the covariance function of f, α and αf. As the covariances of f and α are in the integral multiplied by ψ^0, the integrals in equation (3.25) cannot be solved analytically and are solved numerically.

Note, that a deterministic root water uptake term affects the zeroth order solution within the root zone, and the first order solution through the zeroth order solution. The first order solution of pressure head consequently follows the zeroth order solution. Thus, the assumed model for root water uptake results in a bent shape of mean and variance pressure head profile in comparison to solutions without root water uptake, which was already observed by Rubin and Or (1993) for a medium that consists of an ensemble of parallel streamtubes.

The variance of pressure head in layered soil depends on the correlation length. For decreasing correlation lengths, the pressure head variance tends towards zero, (see Figure 3.2). Thus, for small correlation lengths, the variances of the pressure head in a layered soil, are much smaller than the variances in a soil consisting of independent homogeneous stream-tubes.

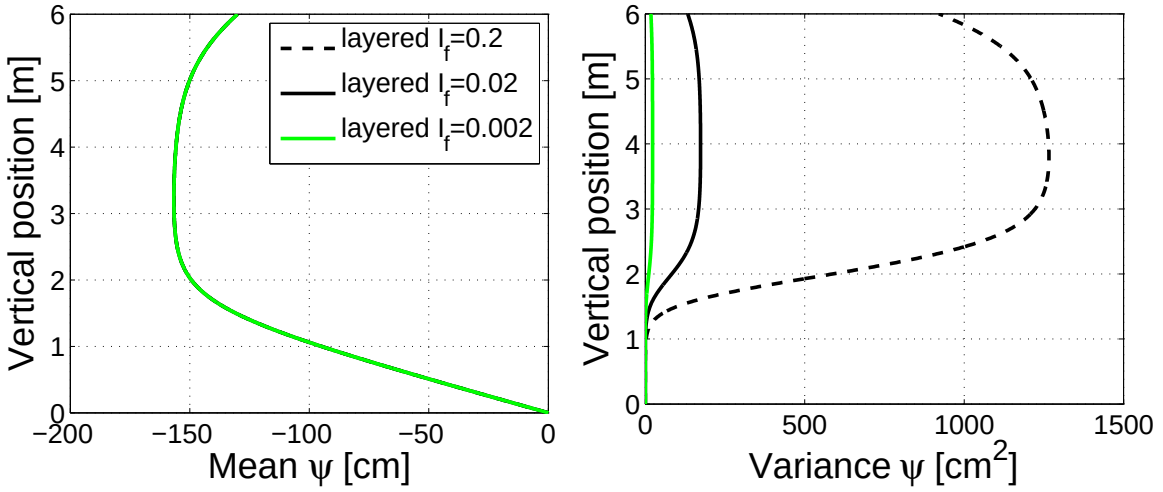

(a) Mean of pressure head (b) Variance of pressure head

Figure 3.2: *Analytical solution for mean (a) and variance (b) of pressure head in a layered soil with different integral scales of f.*

For increasing correlation length, one realization of the layered ensemble tends towards a homogeneous field and the layered solution approaches the solution of Rubin and Or (1993), as shown in Figure 3.3.

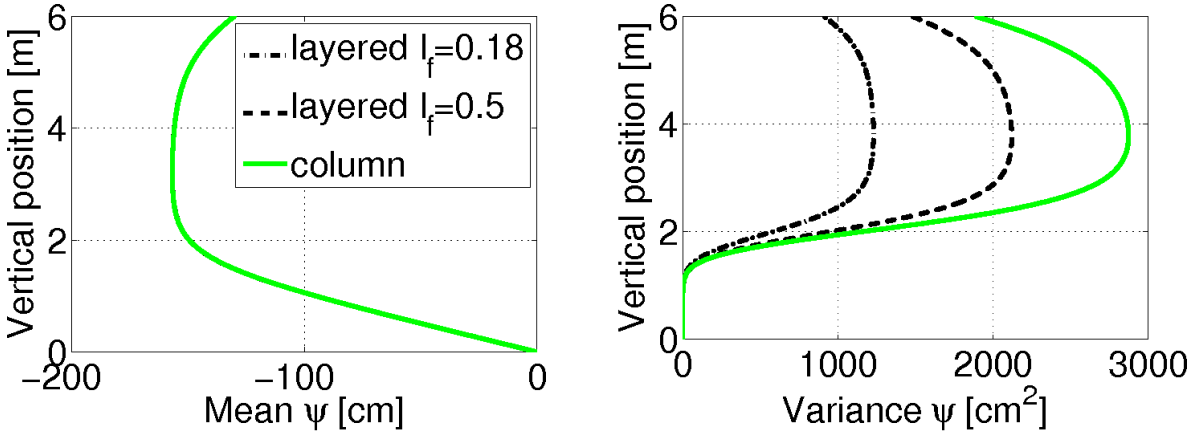

(a) Mean of pressure head (b) Variance of pressure head

Figure 3.3: *Analytical solution for mean (a) and variance (b) of pressure head in a column and layered medium with different integral scales of f.*

High variances of the saturated loghydraulic conductivity

The semi-analytical solutions for mean and variance of pressure head in layered media are derived with the assumption that variances of the hydraulic parameters are smaller than 1. To test the limitation of this assumption, the solutions are compared to 1D numerical steady state simulations. Layered parameter fields with increasing variance of f, from $\sigma^2 = 0.5$ to $\sigma^2 = 3$ were used.

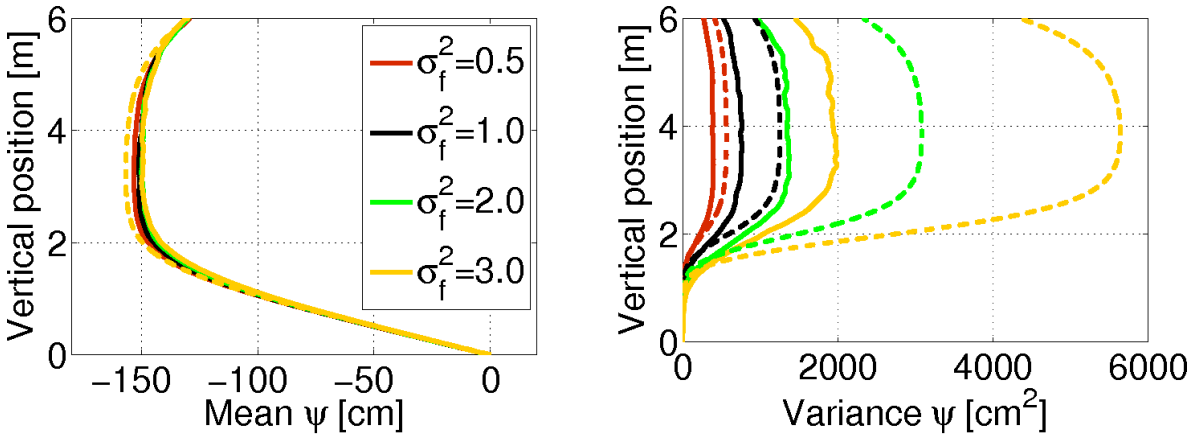

(a) Mean of pressure head (b) Variance of pressure head

Figure 3.4: *Numerical (solid lines) and semi-analytical (dashed lines) solutions for mean (a) and variance (b) of pressure head for a layered soil. The variance of f is 0.5, 1, 2, and 3.*

Figure 3.4 shows the numerically obtained mean and variance of the steady state pressure head distribution in comparison with the perturbation approximations for different values of the variance of the saturated loghydraulic conductivity f. The mean profile of the pressure head is well described by the semi-analytical solutions for all values of the variance of f. The agreement between the numerical and semi-analytical solutions for the variance of pressure head is not too poor for $\sigma_f^2 = 0.5$, but is rapidly getting worse as the variance of f increases. Thus, the assumption of small variances of f is irrelevant for the mean, but is a severe restriction where the variance of pressure head is considered. Saturated flow is, in contrast, less sensitive to σ_f^2 such that agreement between analytical and numerical solutions is found up to high variances of f. The extreme sensitivity of the pressure head ψ to changes in σ_f^2 in the unsaturated case reflects the high non-linearity of the problem.

Since water has to pass through low conductive parts of the soil in both 1D cases (column and layered media), the solution for the variance of pressue head in 1D is expected to overestimate flow in isotropic 2D fields where water can bypass less permeable strata and lenses. A medium consisting of independent streamtubes and a layered medium are, thus, not the two extremes regarding the variability of unsaturated flow.

The applicability of the presented 1D analytical solutions to two dimensional, isotropic Gaussian and non-Gaussian media is discussed in chapter 5.

4 Setup of numerical test case

To assess the joint impact of soil structure and root water uptake, unsaturated flow in simple soil domains is compared to flow in more complex structures. In simply structured media such as layered soil, unsaturated flow including root water uptake is approachable with analytical solutions. More complex parameter fields or root water uptake strategies including compensation are analyzed by means of numerical simulations.

Parameter fields with different patterns of extreme values (Gaussian and non-Gaussian fields) as well as root water uptake strategies with and without compensation mechanisms are tested. In this chapter, the numerical setup, the parametrization of the constitutive relationships and the parameter fields, which are used for the numerical simulations, are shown. Finally an overview of the performed simulations is given.

4.1 Numerical setup

Unsaturated flow in a vegetated soil with the groundwater table at the bottom and constant or variable inflow at the top is discussed.

The size of the domain is $8x8\,\mathrm{meters}$ with a discretization of $256x256\,\mathrm{cells}$. The upper two meters of the domain are used to model infiltration appropriately as described in the following. Thus, the flow domain of interest amounts $6\,\mathrm{m}$ in the vertical and $8\,\mathrm{m}$ in the horizontal direction.

Boundary conditions

Infiltration is modeled as a Neumann boundary condition. The infiltration in a heterogeneous field with variation of soil parameters in two directions can lead to local ponding if the local infiltration capacity is exceeded. So that all water can infiltrate and naturally redistribute before it reaches the domain of interest, the upper boundary of the domain is mimicked by an artificial top layer with a thickness of $2\,\mathrm{m}$. The first $12\,\mathrm{cm}$ of the artificial top layer are homogeneous and of very high conductivity such that no water ponds on top, the remaining part is heterogeneous such that the flow field can develop. At the bottom of this artificial top layer, which is the top boundary of the domain of interest, the flow field is at equilibrium. Figure 4.1 illustrates the model concept for infiltration.

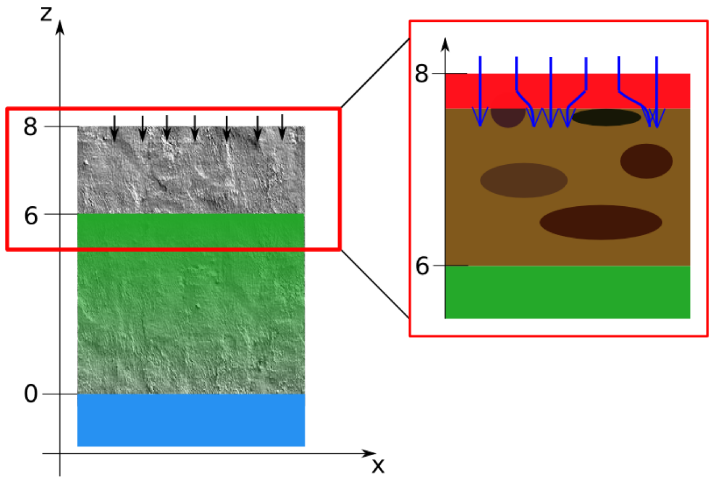

Figure 4.1: *Modeling of infiltration using an artificial layer that consists of a very conductive layer on top and a heterogeneous part; the domain of interest extends from a vertical position of zero to a vertical position of 6m.*

To analyze steady state scenarios, the inflow rate is modeled as constant. For the dynamic scenarios, the inflow rate is temporally variable. We distinguish here between drydown and rewetting scenarios where a constant infiltration rate is applied from a certain point of time, which is illustrated in Figure 4.2a, and periodic cycles where the inflow rate follows a periodic function. For the periodic cycles, a sine-function with variable frequency $f_d\,[1/\mathrm{s}]$ is chosen in this work. Since we only consider infiltration (and neglect evaporation), the negative part of the sine-function is set to zero. The modified function is illustrated in Figure 4.2b (blue line) and is later referred to as sin'.

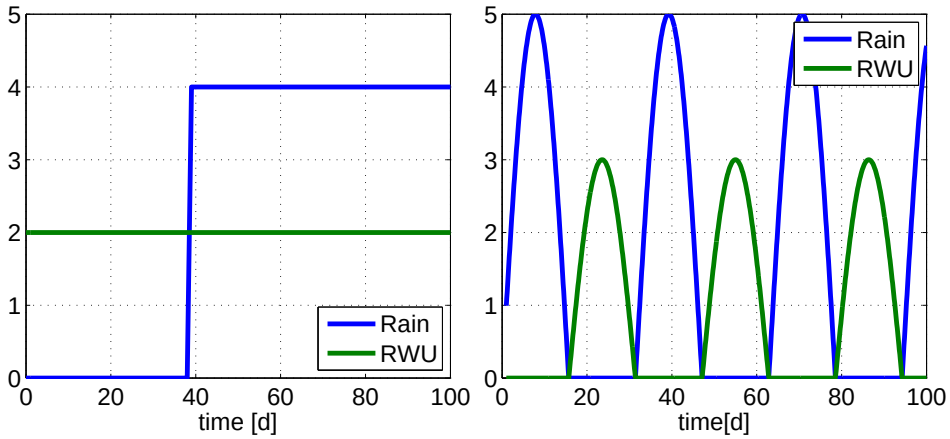

(a) (b)

Figure 4.2: *Sketch of temporally varying infiltration (blue) and root water uptake (green) rate over time in drydown and rewetting scenarios (a) and periodic cycle scenarios (b). In (b), no transpiration occurs during infiltration phases and vice versa.*

The lower boundary ($z = 0$) is the water table and is a Dirichlet type boundary with ψ being zero. The left and the right side of the domain are no-flow boundaries.

Sink Term

Root water uptake is modeled as a sink term with a pre-described extraction rate at each node and starts directly at the top boundary of the domain of interest (at a vertical position of $z = 6\,\mathrm{m}$). Different root water uptake terms, R_1 - R_4, explained in chapter 2.2.2, are used. The parameter δ, which describes the e-folding depth of root water uptake, constantly equals $0.6\,\mathrm{m}$ in this work. Figure 4.3 shows the resulting root density for δ equal to $0.6\,\mathrm{m}$ and a domain height H of $6\,\mathrm{m}$.

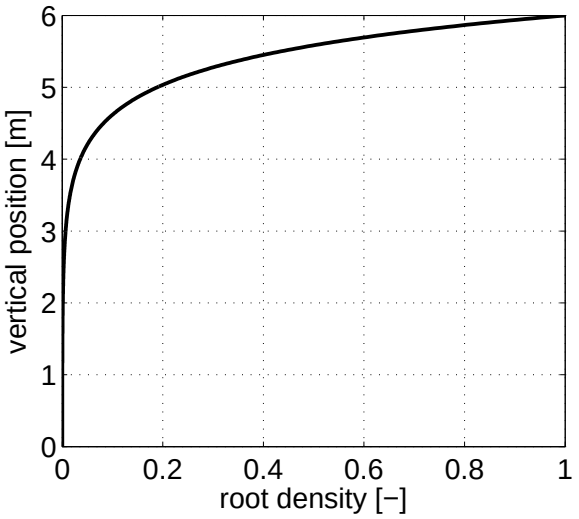

Figure 4.3: *Exponentially decreasing density of roots vs. vertical position for* $\delta = 0.6m$ *and* $H = 6m$.

The considered strategies account for unfavorable conditions by a locally decreased uptake rate if the pressure head is below or beyond critical values. In this so-called stressed regime, the soil is so dry that root water uptake is reduced due to water scarcity or so wet that root water uptake is decreased because of anaerobic conditions. The corresponding stress-response-function is modeled according to the Feddes-Function (Feddes et al., 1978) illustrated in Figure 2.5. For the critical values $h_1 - h_4$, typical values of $h_1 = -0.1\,\mathrm{m}$, $h_2 = -0.25\,\mathrm{m}$, $h_3 = -4.0\,\mathrm{m}$ and $h_4 = -150.0\,\mathrm{m}$ were used (e.g. Taylor and Ashcroft, 1972).

Strategy 1 does not compensate for stressed conditions and, thus, leads to a reduced global transpiration rate. Strategy 2-4 compensate for local stress by increased uptake at more favorable locations. In Strategy 2 the uptake rate depends on the saturation, in Strategy 3 on the relative permeability. To maintain the global transpiration rate at the potential value, a scaling factor is multiplied in Strategy 2 and 3. This factor is calculated in the postprocessing of each timestep and multiplied with the extraction rate of the next timestep. In the fourth uptake strategy, the difference between the uncompensated uptake and (global) potential

demand is also determined in the postprocessing. The difference is divided by the number of unstressed nodes and, in the next timestep, added to the potential extraction rate at each unstressed node. As the results of the last timestep are used to calculate the scaling factor (Strategy 2&3) or the increase of uptake (Strategy 4) of the present timestep, the timestep is limited not to introduce a systematic error and achieve satisfactory accuracy of results.

The atmospheric demand τ is modeled as constant value in the steady state scenarios. In the dynamic scenarios, τ follows a sine function which has the same frequency as the inflow rate, but is shifted by half a period with respect to the infiltration function such that during infiltration no transpiration occurs and vice versa. The temporally changing atmospheric demand is illustrated in Figure 4.2 (green line).

4.2 Parametrization of constitutive relationships

Different approaches exist to parametrize the water retention curve and the relative permeability-pressure head relationship. In chapter 2.1, examples were given for both relationships. These models were derived semi-empirically. There is evidence that the Mualem-Van Genuchten model leads to better agreement with experimental data than other parametrizations. The approach of Mualem for the relative permeability has, however, the disadvantage to be mathematically very complex. In the derivation of the analytical expressions for the mean and the variance of pressure head, the relative permeability is hence parametrized according to the easier-to-handle Gardner-relation (equation (4.1)). For compatibility with the analytical solutions, the Gardner parametrization is chosen for the steady state simulations.

$$\mathbf{K}(\psi) = \mathbf{K}_s \exp(\alpha\psi) \tag{4.1}$$

In the transient simulations (chapter 6) which should reproduce a natural scenario, the relative permeability is modeled according to the Mualem-relationship.

$$\mathbf{K}(\psi) = \mathbf{K}_s(1 + (\alpha\psi)^n)^{a(1-1/n)}(1 - (\alpha\psi)^{n-1}(1 + (\alpha\psi)^n)^{-1+1/n})^2 \tag{4.2}$$

The saturation is given by the Van-Genuchten model.

$$S(\psi) = (1 + (\alpha\psi)^n)^{-1+\frac{1}{n}} \tag{4.3}$$

4.3 Parameter fields

Following the stochastic approach (chapter 2.3.1), the saturated hydraulic conductivity K_s and the parameter α in the constitutive relationships are described by spatially correlated random fields. Parameter fields with multi-Gaussian and different non-Gaussian probability density functions are considered. Gaussian fields have isolated patches of extreme values and connected intermediate values. In chapter 2.3.2, transformations were presented which lead to Non-Gaussian fields with connected low extreme values (referred to as T1-fields) or to fields with large patches of low extreme values (referred to as T2-fields). Fields with the opposite pattern are obtained by taking the inverse value $y_j^{IT} = -y_j^T$ of the transformed fields. The fields with connected high extreme values are referred to as IT1-fields, and the fields with large patches of high extreme values are referred to as IT2-fields. Transformed fields (T1 or T2-fields) and inverse transformed fields (IT1- or IT2-fields) are compared to multi-Gaussian fields (G1- or G2-fields) with the the same univariate and two-point autocorrelation function. One realization representing the saturated loghydraulic conductivity of each structure of field set 1 and field set 2 is shown in Figure 2.8 and 2.10, respectively.

Statistical Properties

The statistical properties of the saturated loghydraulic conductivity, F and the parameter α (of both field sets) that were used in the following case studies, are $\langle F \rangle = -13.4934\,\ln(\mathrm{m/s})$, $\sigma_f^2 = 1.0$, $\langle \alpha \rangle = 3.04\,\mathrm{m}^{-1}$ and $CV_\alpha = 0.28 - 0.29$. The integral scales of field set 1 are $I_f = 0.187m - 0.189\,\mathrm{m}$, $I_\alpha = 0.180m - 0.182\,\mathrm{m}$ and $I_{f\alpha} = 0.176m - 0.178\,\mathrm{m}$.

The Gaussian fields are generated for a given integral scale of f. To avoid that variations are averaged out when solving Richards equation numerically, the computation grid has to be sufficiently small. According to Tompkins et al. (1994), the correlation length should comprise at least 5 nodes. Therefore, the correlation length is, at a resolution of 256 by 256 elements on 8 by 8 meters, larger than $0.1562\,\mathrm{m}$. Correlation length and integral scale are (for a Gaussian field) related by a factor $\frac{1}{2\pi}$.

When creating non-Gaussian fields with transformation (2.72) and (2.73), the autocorrelation function of f changes slightly. As Gaussian and non-Gaussian fields are supposed to have the same autocorrelation function of f, Gaussian fields with the same correlation length as the transformed fields are generated after the transformed fields are obtained. Therefore, the autocorrelation functions of f for the Gaussian and the non-Gaussian fields are determined numerically. Subsequently, a Gaussian correlation function is fitted onto the numerically determined correlation function of f. Equation (2.65) - (2.71) are applied to derive the autocorrelation function of α and the crosscorrelation function of α and f. The integral scales are then calculated by integration of the correlation functions according to equation (2.56). A comparison of the numerically and theoretically derived correlation functions are shown in Figure 4.4.

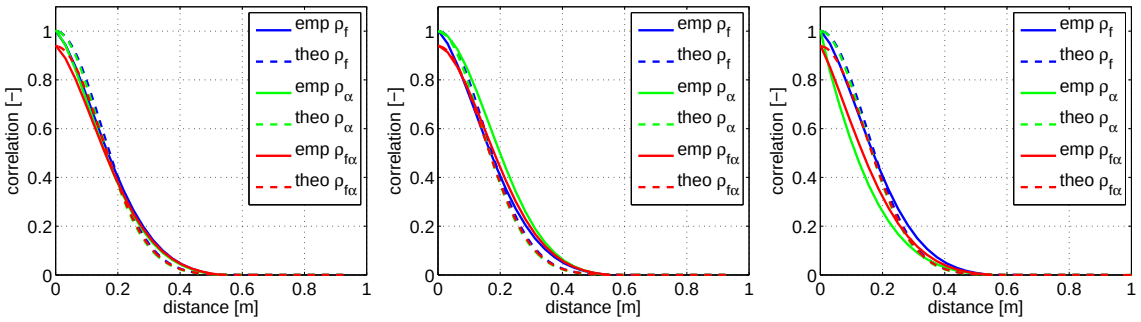

Figure 4.4: *Comparison of theoretically and empirically determined correlation function of f, α and $f\alpha$ for G1 (a), T1 (b) and IT1 (c) fields.*

4.4 Performed simulations

Simulations are carried out with the flow model MUFTE-UG. This code solves the Richards equation using a node-centered finite volume (so-called box) method with an implicit backward Euler discretization in time (Helmig et al., 1998), explained in chapter 2.4. Ensembles of 100 or 40 realizations with a resolution of $256x256\,\mathrm{cells}$ on domains of $8x8\,\mathrm{m}$ are taken as parameter fields for each structure.

The numerically obtained mean and variance profiles of the pressure head distribution are calculated by averaging over all realizations and in the horizontal direction. To exclude boundary effects, $1.5\,\mathrm{m}$ (which equals approximately $7-8$ correlation lengths) are cut off the lateral sides of the domain of each realization before the output fields are averaged (Bosma et al., 1993).

With the setup described above, the following scenarios are analyzed. The performed simulations can be divided into two parts, steady state and dynamic simulations.

On one hand, simulations with constant infiltration rate q [mm/d] and transpiration demand τ [mm/d] are carried out until quasi-steady state is reached. Their purpose is to test the first order second moment solutions for layered media and find the joint effect of Gaussian and non-Gaussian soil structure and root water uptake on the steady state mean and variance of pressure head. Moderate dry and wet conditions are analyzed. For comparison with the scenarios including root water uptake, simulations without root water uptake considering the same net infiltration rate (q-τ) are performed. Under dry conditions, both field sets are used as input for the soil hydraulic properties. Different strategies for root water uptake R_1 - R_4 are tested for T2-fields and a dry scenario.

On the other hand, dynamic simulations with temporally variable top boundary and sink term are performed to assess the influence of heterogeneity on the time series of the hydraulic variables under consideration of root water uptake. Root water uptake term R_1 and R_2 are applied for a drydown and rewetting scenario in parameter fields G1, T1 and IT1. In there, root water uptake depletes the root-zone for $40\,\mathrm{days}$ with a constant rate τ, subsequently infiltration, with a constant rate q, is considered on the artificial boundary. The

initial condition is equal to $35\,\mathrm{cm}$. A comparative scenario without roots and with the same net infiltration rate ($q - \tau$) is carried out where the initial condition is equal to $50\,\mathrm{cm}$. Furthermore, periodic cycle scenarios where top boundary q and atmospheric demand τ follow a modified sine-function are done. A low frequency case where one period equals approximately $30\,\mathrm{days}$ and a high frequency case where one period equals approximately $3\,\mathrm{days}$ are tested. An overview of applied settings are given in Table 4.1 and 4.2.

No.	Description	$q\,[\mathrm{mm/d}]$	$\tau\,[\mathrm{mm/d}]$	R	Fields
S1	wet, w. roots	16	7	1	G1,T1,IT1
S2	wet, no roots	9	0	-	G1,T1,IT1
S3	dry, w. roots	3	2	1	G1,T1,IT1,G2,T2,IT2
S4	dry, no roots	1	0	-	G1,T1,IT1
S5	dry, w. roots	3	2.5	1-4	T2
S6	med dry, no roots	3	0	-	G1,T1,IT1

Table 4.1: *Steady state simulation settings. q is the infiltration rate, τ the transpiration rate, R the model for root water uptake.*

No.	Description	$q\,[\mathrm{mm/d}]$	$\tau\,[\mathrm{mm/d}]$	ψ_{init}	R	Fields
D1	dryd.-rew., w. roots	4, after 40 days	2	35	1-2	G1,T1,IT1
D2	dryd.-rew., no roots	2, after 40 days	0	50	-	G1,T1,IT1
D3	dryd.-rew., no roots	4, after 40 days	0	50	-	G1,T1,IT1
D4	per.cylces, high frequ.	$6sin'(t)$	$-4sin'(t)$	35	1	G1,T1,IT1
D5	per.cycles, low frequ.	$6sin'(10 \cdot t)$	$-4sin'(10 \cdot t)$	35	1	G1,T1,IT1

Table 4.2: *Dynamic simulation settings. q is the infiltration rate, τ the transpiration rate, R the model for root water uptake. sin' corresponds to the modified sine-function explained above.*

5 Steady state flow in 2D Gaussian and non-Gaussian fields

The objective of this chapter is to demonstrate the joint effect of soil structure and root water uptake on steady state unsaturated flow. The simulations specified and listed in chapter 4 are analyzed. We are primarily interested if characteristics of root water uptake gained from 1D analytical solutions are also valid for 2D Gaussian and furthermore non-Gaussian fields. Wet and dry conditions are distinguished. To point out which effects of structure are only observed in combination with root water uptake, simulations without root water uptake are presented as a reference case in comparison to simulations where root water uptake is included in the model. To make sure conclusions are not limited to the standard root water uptake term R_1, different uptake strategies, explained in chapter 2.2.2, are compared for a specific test case.

In the first part, mainly mean and variance of pressure head are analyzed. In the last section of this chapter, the maximum connected velocity (fastest track) is analyzed to illustrate the potential risk for contaminant transport estimations of neglecting transpiration of plants and non-Gaussian soil structures. First of all, the pattern of the hydraulic conductivity, which determines the flow behavior and depends on the saturation, is characterized at wet and dry states.

5.1 Saturation dependent flow pattern

When analyzing flow under variably saturated conditions, one needs to be aware that the hydraulic conductivity is a function of pressure head and saturation, respectively. The dependency of the hydraulic conductivity and of the flow patterns on the saturation in Miller-similar Gaussian fields was discussed by Roth (1995). Figure 5.1 illustrates the hydraulic conductivity according to the parametrization by Gardner (equation (4.1)) as a function of pressure head for coarse and fine material. Under fully saturated conditions, which corresponds to a pressure head value of zero, the hydraulic conductivity is largest and equal to the saturated hydraulic conductivity. With decreasing pressure head, the volume fraction of water decreases and the volume fraction of air increases. Thus, the hydraulic conductivity of the porous medium for water decreases (see chapter 2.1). The hydraulic conductivity of coarse material decreases due to the lower air entry pressure stronger with decreasing water pressure head than that of fine material. This leads to a crossover of the hydraulic conductivity of coarse and fine material at a specific water pressure head. At intermediate states close to the crossover, the variance of the conductivity has a minimum and the soil structure

is rather homogeneous. It was shown that the pattern of the hydraulic conductivity of the fully saturated state in Miller-similar Gaussian fields is inverted for pressure head values much larger than the crossover point (Roth, 1995).

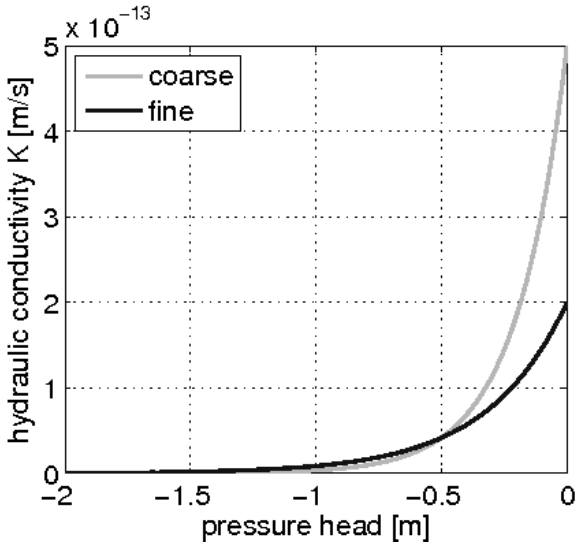

Figure 5.1: *Crossover of the loghydraulic conductivity of coarse and fine material.*

Such a crossover occurs also in G1-, T1- and IT1-fields. Under saturated conditions, the pattern of the conductivity in T1- and IT1-fields is characterized by connected extreme values, isolated opposite extreme values and intermediate values. The material with intermediate values is here called background material. To illustrate the change of pattern, the values of the saturated loghydraulic conductivity f can be considered as separated into these three classes. To be more precise, a threshold value f_{thr_1} is defined such that one class captures the values of the saturated loghydraulic conductivity that form the connected pathways. Here, f_{thr_1} was chosen such that in a parameter field with connected pathways of high extreme values, f_{thr_1} corresponds to the maximum possible value, at which the values larger than f_{thr_1} appear as connected paths. Figure 5.2 shows three examples of binary fields which were obtained according to a threshold value equal to f_{thr_1} (a), larger than f_{thr_1} (b) and smaller than f_{thr_1} (c). f_{thr_1} is meant as an estimate to roughly characterize the pattern of the considered parameter fields and should not be mixed with the measures to quantify connectivity. Its negative value, $f_{thr_2} = -f_{thr_1}$, is used to separate the parameter range into the second class. The arithmetic average of the total parameter range represents the background material and is assigned to the third class.

Figure 5.3 shows the loghydraulic conductivity versus pressure head for these three classes. The unsaturated conductivity of the coarse material crosses that of the background material at pressure head h_c. At pressure head h_f (with $h_f < h_c$), the unsaturated conductivity of the fine material crosses that of the background material. Thus, for values of the pressure head inbetween h_c and h_f, both coarse and fine material are less conductive than the background material. In this regime of pressure heads, both fields, T1- and IT1-fields, have therefore connected pathways of material with a low conductivity such that similar results for the

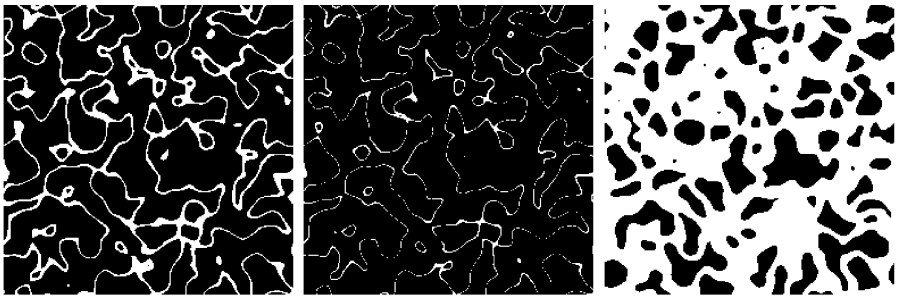

(a) (b) (c)

Figure 5.2: *Binary fields obtained by cutting all values below a certain threshold. In (a), the threshold value is equal to f_{thr_1} such that values above this threshold value form pathways. In (b) and (c), the threshold value is above and below f_{thr_1}, respectively.*

T1- and IT1-fields are expected in the steady state. For the parameters chosen here, this range of pressure heads is obtained for net infiltration rates of approximately $4 - 40\,\mathrm{mm/d}$. Note that these 'crossover points', h_c and h_f, are only a rough estimate and the range of pressure head values which lead to the same patterns are strongly dependent on the chosen soil parameters. Different patterns of the unsaturated conductivity in T1- and IT1-fields are obtained for dry conditions ($1\,\mathrm{mm/d}$ net infiltration rate), as shown on the right hand side in Figure 5.4.

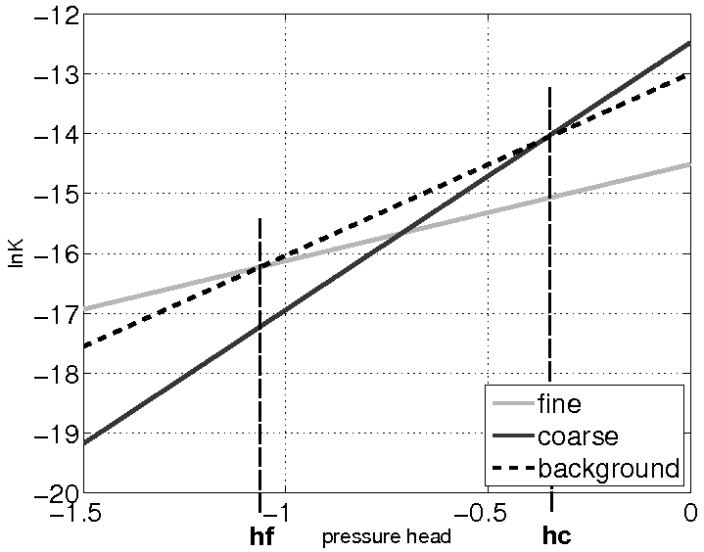

Figure 5.3: *Crossover of the loghydraulic conductivity of coarse and background material at pressure head $h_c\,[\mathrm{m}]$ and of fine and background material at $h_f\,[\mathrm{m}]$.*

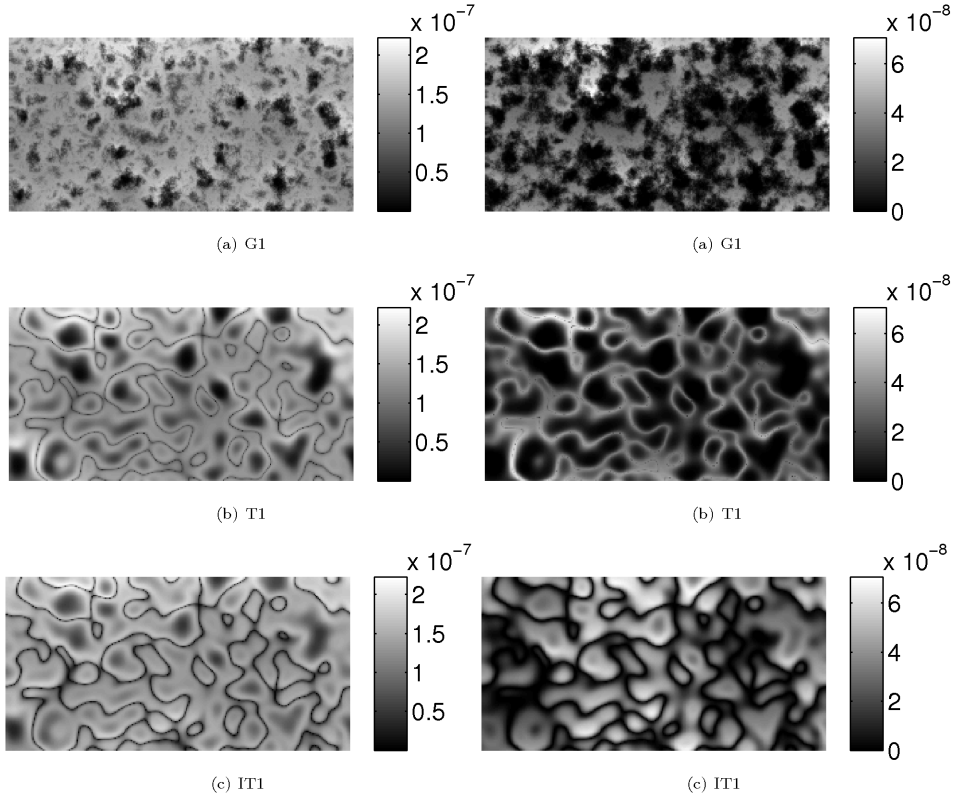

Figure 5.4: *Hydraulic conductivity* K $[\mathrm{m/s}]$ *in G1-, T1- and IT1-fields, for wet conditions with* $q = 16\,\mathrm{mm/d}$, $\tau = 7\,\mathrm{mm/d}$ *(left) and for dry conditions with* $q = 3\,\mathrm{mm/d}$, $\tau = 2\,\mathrm{mm/d}$ *(right).*

5.2 Joint influence of structure and root water uptake

It is analyzed under which conditions the first order second moment solutions give good estimates in two-dimensional fields and what effects non-Gaussian soil structures introduce in comparison to multi-Gaussian fields if root water uptake is considered. It is furthermore discussed, which features of structure are sensitive to the effect of root water uptake.

5.2.1 Wet conditions

Using analytical solutions, it was demonstrated that in 1D fields root water uptake leads, in comparison to a scenario without root water uptake and with the same net infiltration rate, to an increase of the mean (and correspondingly to a decrease of the variance) of pressure head within the root-zone which results in a bent shape of the mean and the variance pressure head profile (chapter 3). Figure 5.5 shows the numerically obtained mean and variance of pressure head versus the vertical position in differently structured 2D-fields (G1, T1- and IT1-fields) for two very wet scenarios with and without root water uptake.

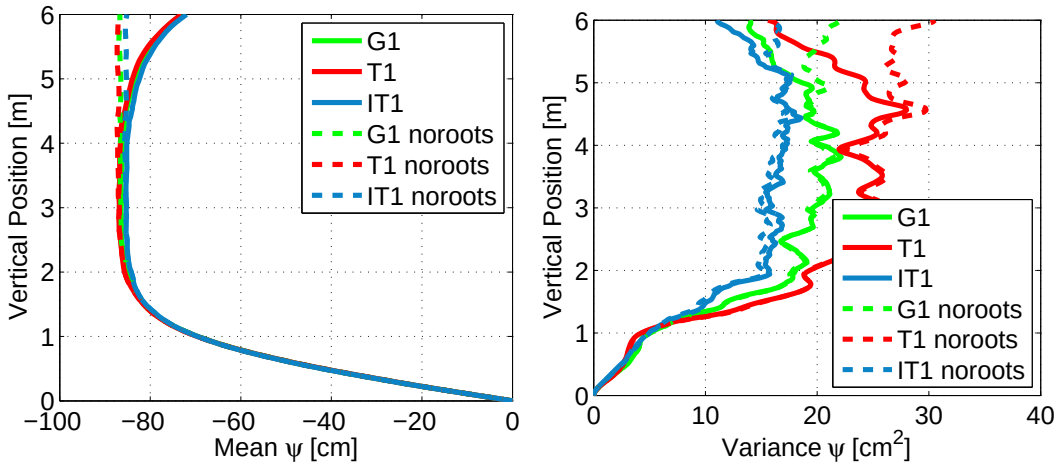

(a) Mean of Pressure Head (b) Variance of Pressure Head

Figure 5.5: *Simulated mean* $[\mathrm{cm}]$ *(a) and variance* $[\mathrm{cm}^2]$ *(b) of pressure head vs. vertical position* $[\mathrm{m}]$ *in G1-, T1-, IT1-fields for wet conditions with (solid lines) and without root water uptake (dashed lines) (scenarios S1 and S2 in Table 4.1).*

The bent shape, discussed for the analytical solutions, is also seen in the three numerically obtained mean and variance profiles of pressure head and is the only difference in comparison to a scenario without root water uptake and the same net inflow rate. Below the root zone, the scenarios with root water uptake and without root water uptake lead to the same profile of mean and variance of pressure head. As for the case without root water uptake, no influence of the considered structures is expected under wet conditions due to the same effective value and small variances of the hydraulic conductivity in G1-, T1- and IT1-fields. Furthermore, T1- and IT1-fields have a similar pattern of hydraulic conductivity, which is connected values of low conductive material (see chapter 5.1).

A comparison of the mean and the variance of pressure head in G1-, T1- and IT1-fields with the layered analytical solution, illustrated in Figure 5.6, yields that the numerically obtained mean pressure head is predicted well by the analytical solutions. Due to a variance of the loghydraulic conductivity, σ_f^2, equal to 1.0 (see chapter 3) and the possibility to bypass low conductive lenses in a 2D-field, the variances of pressure head in G1-, T1- and IT1-fields are overestimated by the analytical solutions.

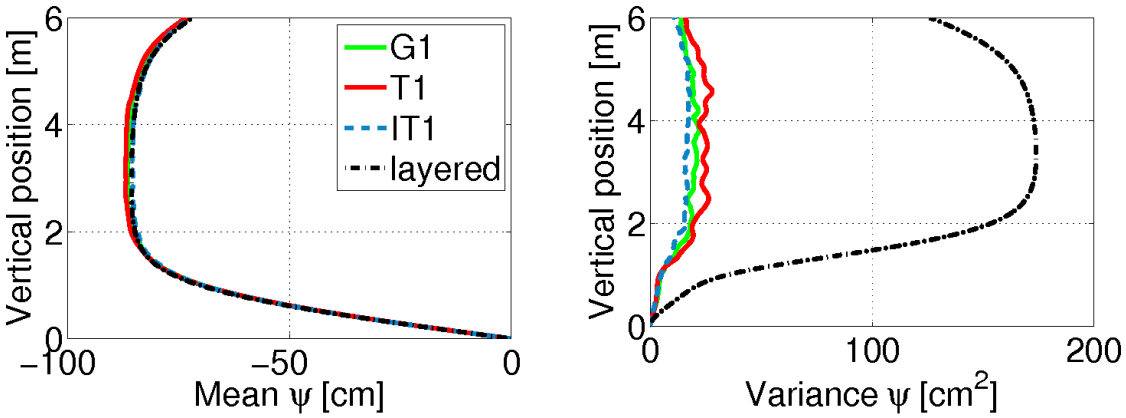

(a) Mean of pressure head (b) Variance of pressure head

Figure 5.6: *Simulated mean* [cm] *(a) and variance* [cm^2] *(b) of pressure head vs. vertical position* [m] *for G1-, T1-, IT1-fields, in comparison to the layered analytic solutions (black dashed line) for scenario S1. The numerically obtained mean pressure head is well estimated, the variance of pressure head is overestimated by the analytical solution.*

5.2.2 Dry conditions

Flow without root water uptake

Under dry conditions, the hydraulic conductivity of IT1-fields has connected pathways of low conductive material, and the hydraulic conductivity of G1- and T1-fields has large low conductive patches (right hand side of Figure 5.4). The low conductive pathways in IT1-fields can act as barriers for flow in the vertical direction such that little pools of higher pressure pond up (see Figure 5.7, 5.8).

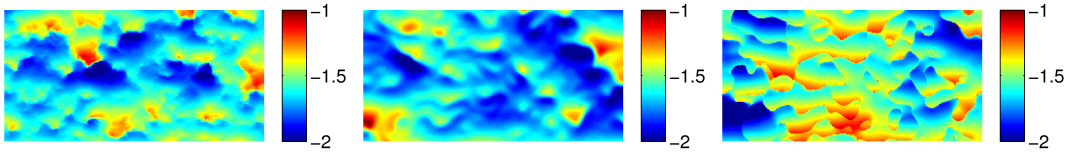

(a) G1 (b) T1 (c) IT1

Figure 5.7: *Pressure head* ψ [m] *for G1-, T1- and IT1-fields under dry conditions (scenario S4).*

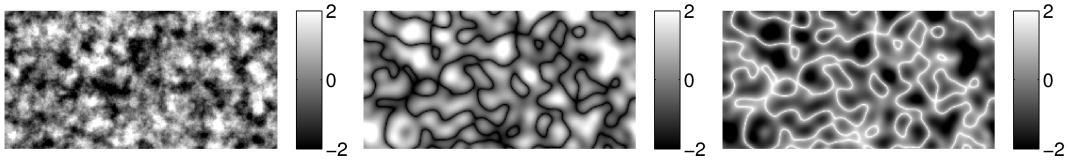

(a) G1 (b) T1 (c) IT1

Figure 5.8: *Saturated loghydraulic conductivity* f [$-$] *for G1, T1 and IT1-fields.*

The ponding in IT1-fields leads to a difference between the mean pressure head of IT1-fields and G1-/T1-fields of about $10\,\mathrm{cm}$. A comparison of the mean and the variance of pressure head in the three 2D fields with the analytical solution for layered media, illustrated in Figure 5.9, yields that the mean pressure head in the field with connected pathways of coarse material (IT1) is most similar to the first-order second-moment solution which inherently assumes an underlying Gaussian distribution. The variances of pressure head in G1-, T1- and IT1-fields are in the same order of magnitude and are all strongly overestimated by the analytical solution.

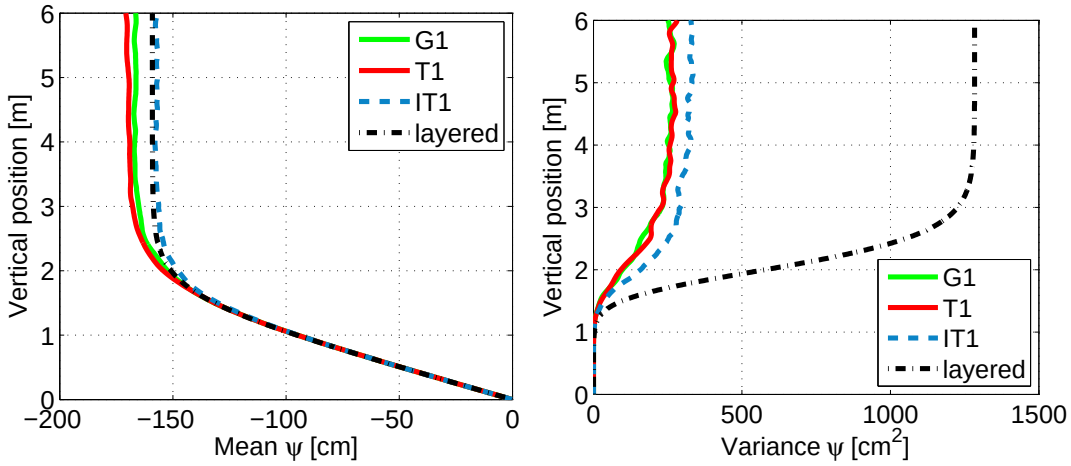

(a) Mean of Pressure Head (b) Variance of Pressure Head

Figure 5.9: *Comparison of simulated mean* $[\mathrm{cm}]$ *(left) and variance* $[\mathrm{cm}^2]$ *(right) of pressure head for three structures (G1, T1 and IT1), in comparison to analytical solutions (black dashed line); dry conditions (scenario S4).*

Flow with root water uptake

The low conductive patches in G1- and T1-fields, illustrated on the right hand side of Figure 5.4, impede flow towards their inner parts and lead to very dry regions in the soil if root water uptake is considered. These regions form in the following way, while the steady-state distribution of pressure head develops.

In coarse lenses, a limited amount of water is present. Such lenses continuously dry, if more water is taken up by roots than is replenished across their boundaries. The flow into a coarse lens from its surrounding depends on the conductivity and the pressure gradient between the lens and its surrounding. Due to low conductivities, water ponds above coarse lenses to supply water into the inner parts of such patches. However, the deviation of pressure head values on top of coarse lenses from their surrounding is limited due to lateral equalization of pressure head. The pressure head value in the surrounding of coarse lenses depends in turn on the inflow rate.

Limited ponding above such lenses leads to a maximum replenishment rate from the top of a coarse lens into its inner part. If the replenishment rate is not sufficient to meet

the extracted amount of water, a drying front proceeds upwards into coarse lenses from its lower boundary, leading to decreasing conductivities. Thus, conductivities of lenses of coarse material monotonously decrease such that increasing pressure gradients are required to draw water into coarse lenses. At some point, required pressure head values in coarse lenses increase infinitely given the pressure head on top and bottom is limited. An analytic steady state solution is derived for a sample setup in one dimension, where a lens of thickness $L\,[\mathrm{m}]$ with hydraulic properties of $K_s\,[\mathrm{m/s}]$ and $\alpha\,[\mathrm{m}^{-1}]$ is considered. At the boundaries, top and bottom of the lens, the pressure head ψ is fixed to $h_t\,[\mathrm{m}]$ and $h_b\,[\mathrm{m}]$, respectively. The relative permeability is modeled after Gardner. The root water uptake rate $R\,[1/\mathrm{s}]$ is assumed to be constant and uniformly distributed. Reduction of uptake due to stressed conditions is not taken into account.

In the vertical direction, Richards equation (at steady-state) reads,

$$\frac{\partial}{\partial z} K_s \exp(\alpha\psi)(\frac{\partial \psi}{\partial z} + 1) = R. \tag{5.1}$$

With the following transformation,

$$\phi_t = \exp(\alpha\psi), \tag{5.2}$$

Richards equation becomes

$$\frac{1}{\alpha}\frac{\partial^2 \phi_t}{\partial z^2} + \frac{\partial \phi_t}{\partial z} = \frac{R}{K_s}. \tag{5.3}$$

Boundary conditions are

$$\phi_t(z=0) = H_1, \tag{5.4}$$

$$\phi_t(z=L) = H_2, \tag{5.5}$$

with

$$H_1 = \exp(\alpha h_b), \tag{5.6}$$

$$H_2 = \exp(\alpha h_t). \tag{5.7}$$

This set of equations is solved by

$$\phi_t = \frac{e^{-\alpha z}(e^{\alpha L}(H_1 K_s - H_2 K_s + LR) - e^{\alpha z}(H_1 K_s + Rz) + e^{\alpha(L+z)}(H_2 K_s + R(-L+z)))}{(-1+e^{\alpha L})K_s}. \tag{5.8}$$

Figure 5.10a illustrates the solution of equation (5.3) for a typical length of coarse patches of $L = 0.175\,\mathrm{m}$, a saturated conductivity of $K_s = 1.6618E-6\,\mathrm{m/s}$ and α equal to $3.3452\,\mathrm{m}^{-1}$. The root water uptake rate is $R = 1.676E-8\,\mathrm{s}^{-1}$ and the pressure head at top and bottom of the lens was estimated with the analytical solution for layered soil to $h_b = 1.264\,\mathrm{m}$

and $h_t = 1.24\,\mathrm{m}$ (with simulation settings of scenario S3 in Table 4.1). Negative values of the variable ϕ_t are unphysical, as they correspond to imaginary values of the pressure head. These regions with imaginary pressure head values increase with increasing saturated conductivity of the lens, which is illustrated in Figure 5.10b where coarser material, with $K_s = 1.9777E-6\,\mathrm{m/s}$ and $\alpha = 3.6493\,\mathrm{m}^{-1}$, is used in solution (5.8).

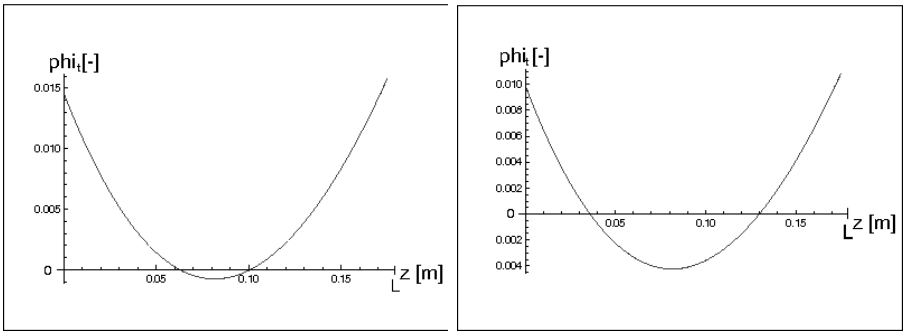

(a) (b)

Figure 5.10: *Analytical 1D solution of equation (5.3) for* $\phi_t = \exp(\alpha\psi)\,[-]$ *vs.* $z\,[\mathrm{m}]$ *including root water uptake if the pressure head at top and bottom of the domain is fixed. Two sets of hydraulic properties are used: (a)* $K_s = 1.6618E-6\,\mathrm{m/s}$, $\alpha = 3.3452\,\mathrm{m}^{-1}$ *(b)* $K_s = 1.9777E-6\,\mathrm{m/s}$, $\alpha = 3.6493\,\mathrm{m}^{-1}$.

In our model, water uptake is only restricted if the wilting point ($h_4 = -150\,\mathrm{m}$) is reached which leads to wilted spots in large patches of coarse material. Such a case is illustrated in Figure 5.11, which shows the pressure head distribution in one realization of T1-fields in comparison to the loghydraulic saturated conductivity and the distribution of the root water uptake term. In two of the patches of coarse material, the pressure head is decreased to the wilting point of $h_4 = -150\,\mathrm{m}$ and the uptake rate is zero, while the surrounding is still relatively wet.

The localized wilted areas in T1-fields are reflected by a decrease of the mean of pressure head and by very large variances in the upper part of the domain where a considerable part of the rainwater has been taken up but the water extraction rate by roots is still large. Figure 5.12 shows the mean and the variance profiles of pressure head in the three structures, G1-, T1- and IT1-fields, for a relatively dry scenario with $q = 3mm/d$, $\tau = 2mm/d$ and $\delta = 0.6m$ (scenario S3 in Table 4.1). In contrast to the case without root water uptake, large differences between the structures are seen in the upper part of the profile. T1-fields, which have connected values of fine material and large isolated patches of coarse material, show the lowest mean values and highest variances of pressure head meaning that such dry spots develop heavily in T1-fields. Corresponding to the size of low conductive patches, dry wilted spots develop less in G1-fields and only very weakly in IT1-fields. Clearly, the analytical solutions, derived in section 3, make poor predictions for the pressure head under dry conditions if local wilting occurs.

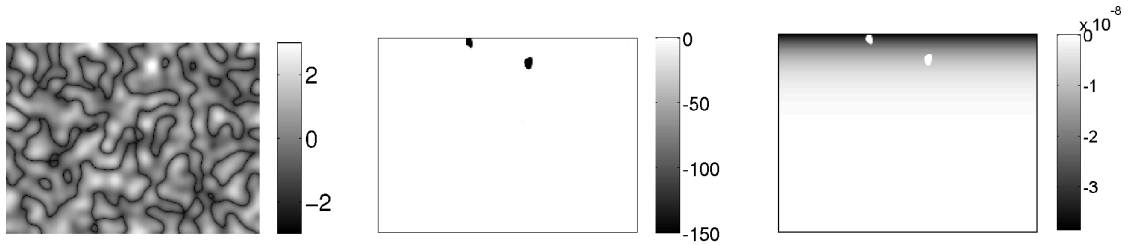

(a) Loghydr. sat. conductivity (b) Pressure head (c) Root water uptake

Figure 5.11: *Formation of dry regions in coarse lenses of T1-field: distribution of saturated loghydraulic conductivity f (a), pressure head (b) and (negative) root water extraction rate (c).*

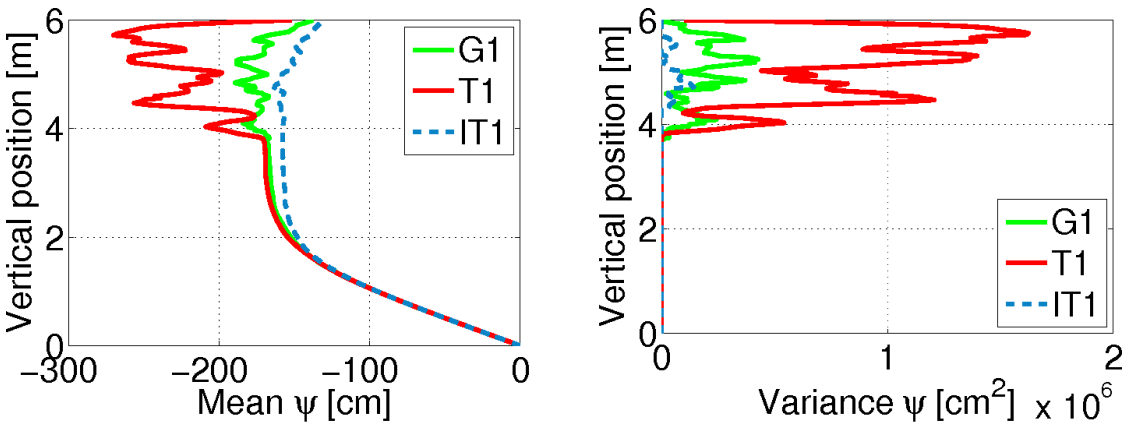

(a) Mean of pressure head (b) Variance of pressure head

Figure 5.12: *Comparison of simulated mean* [cm] *(a) and variance* [cm^2] *(b) of pressure head in G1-, T1- and IT1-fields for scenario S3 in Table 4.1. Dry spots lead to extremely large variances of pressure head.*

Since the replenishment from the surrounding is limited, the occurrence of local wilting is related to the length scale over which water can be drawn by roots. The analytical solution, shown in Figure 5.10, and the numerical results, shown in Figure 5.11, illustrate that the length scale of coarse patches is the limiting factor. This aspect is further analyzed using a second set of parameter fields (G2-, T2-, IT2-fields), introduced in chapter 2.3.2 and 4.3, where the asymmetry of structure length scales is more pronounced. The fields are constructed such that they agree in mean and variance of the saturated loghydraulic conductivity but differ in their copulas which results in patterns with large patches of coarse or fine material. One realization of G2-, T2-, and IT2-fields is shown in Figure 2.10. Such fields can be generated from Gaussian fields using a so-called V-transformation (Li, 2010), which is described in chapter 2.3.2.

The larger the patches of coarse material in the parameter fields are, the more susceptible the structure is to the drying process at distinct locations. With the applied settings, only T2-fields have large enough structures of coarse material so that dry spots develop. Figure 5.13

shows the mean and the variance of pressure head in G2-, T2-, and IT2-fields for scenario S3 in Table 4.1. (Low values of the mean and extreme values of the variance of pressure head indicate the formation of dry spots). Thus, the susceptibility for the effect of local wilting is sensitive to the asymmetry of structure length scales and develops much more if large patches of coarse material exist. For other structures, root water uptake only bents the mean pressure head in the upper part of the soil, compared to cases without root water uptake.

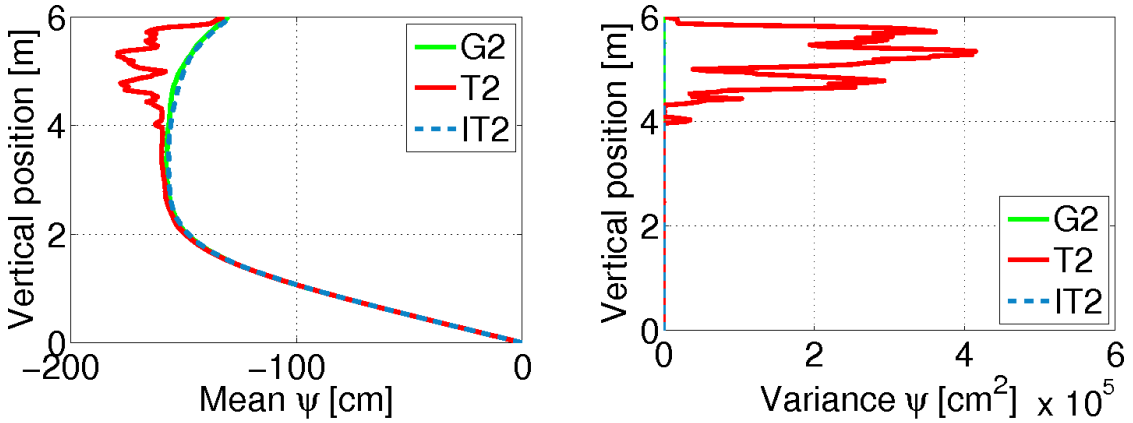

(a) Mean of pressure head (b) Variance of pressure head

Figure 5.13: *Comparison of simulated mean* [cm] *(a) and variance* [cm^2] *(b) of pressure head in G2-, T2- and IT2-fields for scenario S3. In T2-fields, dry spots lead to extremely large variances of pressure head.*

Soil structures with large patches of coarse material can be found in nature. For example, the las Cruces Trench Site dataset, which was parametrized by Li (2010) has such a structure. The existence of large coarse lenses, compared to the size of structures of other material, is captured by spatial bivariate copulas of the saturated hydraulic conductivity. For details, we refer to the paper of Bárdossy (2006). From the bivariate copula, it can be inferred which parameter values are correlated over what length scale. In comparison to Gaussian copulas that are symmetric, large patches of high extreme values are reflected in an asymmetric shape of the bivariate copula. Examples of copula density distributions for different parameter fields are shown in chapter 2.3.3, Figure 2.12. Hence, copulas could eventually serve as an indicator for the susceptibility of a structure to the formation of dry patches when standard root uptake models are used.

Using the standard root water uptake model, local wilting affects the integrated (global) actual transpiration such that the atmospheric demand cannot be met anymore. Such a continued water uptake, even from relatively dry patches in an otherwise moist soil, does not seem realistic. Instead, since sufficient water may be available at other locations nearby, water uptake should be shifted to those locations. The applied root water uptake model R_1 is quite broadly used for simple soil structures where such effects are not relevant. However, for heterogeneous media, this uptake strategy is limited to wet scenarios, as demonstrated above.

5.2.3 Formation of dry regions in anisotropic media

In the previous section, isotropic parameter fields are used to illustrate that root water uptake can lead to extreme values of the pressure head distribution under dry conditions. The critical feature of structure which is related to the formation of dry regions is the length scale over which water can be drawn from the surrounding of coarse lenses. This length scale depends on the soil hydraulic properties and the driving forces for flow. In nature, the heterogeneity of soil parameters is often anisotropic, layered or column like. Moreover, the driving forces differ between the vertical and horizontal direction. In the horizontal, capillary forces facilitate the flow of water, in the vertical, gravity must be additionally taken into account. The typical length scale over which water can be drawn by roots in the horizontal or vertical direction, thus, differs.

Whether roots can draw water in the horizontal direction over a distance that is smaller or larger than in the vertical direction is analyzed by means of analytical solutions. The same simplified test model as for the vertical case (section 5.2.2) is used to predict the distribution of pressure head in a horizontally aligned lens of length $L\,[\mathrm{m}]$ with fixed pressure head at its boundaries.

In the horizontal direction, Richards equation is

$$\frac{\partial}{\partial x} K_s \exp(\alpha\psi) \frac{\partial \psi}{\partial x} = R \tag{5.9}$$

The solution for $\phi_t = \exp(\alpha\psi)$ reads then

$$\phi_t = \frac{2H_1 K_s (L - x) + x(2H_2 K_s + \alpha L R(-L + x))}{2K_s L} \tag{5.10}$$

Figure 5.14 shows the solution of the pressure head $\psi\,[\mathrm{m}]$ for flow in the horizontal direction (red) in comparison to the solution in the vertical direction (blue). The difference of the potential $\triangle\Psi$ between the two boundaries of the lens matches in both cases. With the parameters chosen, regions with imaginary pressure head values form in the vertical direction at smaller values of K_s and α than in the horizontal direction. One has to mention that for a sound analysis, the water content in the lenses should be compared, the adjustment is here done by eye.

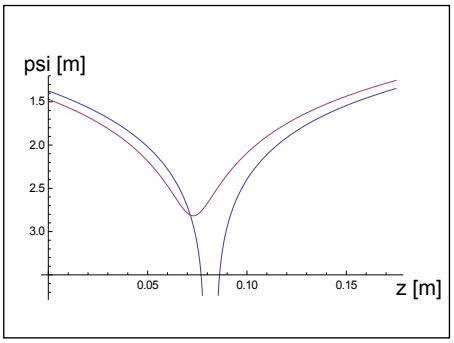

Figure 5.14: *Analytical 1D solution for pressure head $\psi\,[\mathrm{m}]$ vs. $z\,[\mathrm{m}]$ in a vertically aligned lens (blue) and a horizontally aligned lens (red) with fixed pressure head at the boundaries and the same soil hydraulic properties α and K_s.*

With these restrictions, our simplified test model predicts that the maximum distance over which roots can draw water in the vertical direction may be smaller than in the horizontal direction. This means that the effect of local wilting in patches of coarse material can be further specified. Large lenses of coarse material may in the vertical direction be more susceptible to the formation of wilted regions than in the horizontal direction. Thus, in anisotropic media with vertically aligned lenses of coarse material, extremely dry parts of the soil may occur more distinct than in anisotropic media with horizontally aligned coarse lenses.

To test the conclusions, flow simulations are carried out in anisotropic parameter fields with coarse lenses in the vertical as well as in the horizontal direction. The results confirm the analysis above. In a field with vertically aligned lenses of coarse material, dry patches form heavily. Only in few cases horizontal lenses dry up. In such cases, the thickness of the horizontal lenses is large. Figure 5.15 shows two sample realizations of the saturated loghydraulic conductivity and the corresponding pressure field in media with horizontal (a) or vertical coarse lenses (b). In the field with horizontal anisotropy, local stress does not occur while in the field with vertical coarse lenses, several patches with pressure head values in the stressed regime (pressure head values smaller than $-4\,\mathrm{m}$) develop.

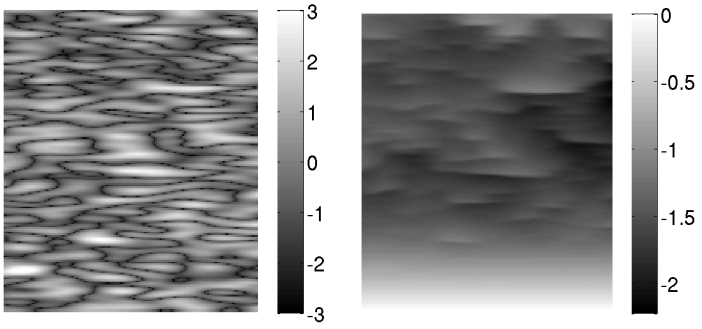

(a) Horizontal anisotropy

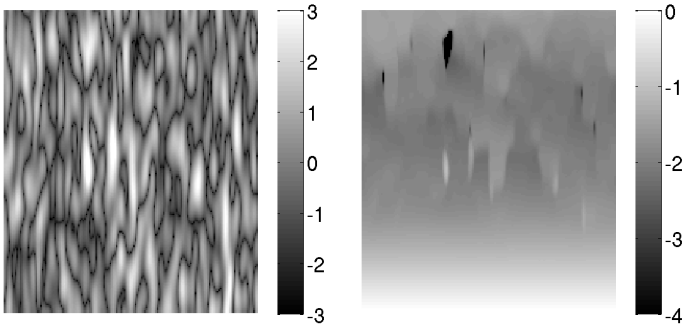

(b) Vertical anisotropy

Figure 5.15: *Saturated loghydraulic conductivity f (left) and pressure head $\psi\,[\mathrm{m}]$ (right) in (a) anisotropic horizontal and (b) anisotropic vertical media. Values smaller than $-4m$ (dark spots) correspond to stressed regions. The effect of local wilting occurs more severe in fields with vertical lenses of coarse material.*

5.2.4 Formation of dry regions in non-Miller similar media

The parameter fields K_s and α are in this work assumed to be correlated with each other via the Miller-similarity. The theoretical concept was explained in chapter 2.3.1.2. In Miller-similar fields α is proportional to $\sqrt{K_s}$ such that high values of K_s and high values of α occur at the same location. In this way, few spots of the hydraulic conductivity exist which might rapidly decrease while the steady-state develops. In this section, it is tested, whether the assumption of Miller-similar soils enhances the susceptibility to the formation of local wilting.

If K_s and α are modeled as two independent, lognormally distributed random fields, large values of α and K_s that are not located at the same place, contribute to low values of the hydraulic conductivity K under dry conditions. Low conductive regions get thereby larger and also lower due to the lognormal distribution of α such that dry spots form more easily if Miller-similarity is not assumed. Figure 5.16 illustrates the hydraulic conductivity K in a Miller-similar and non Miller-similar media.

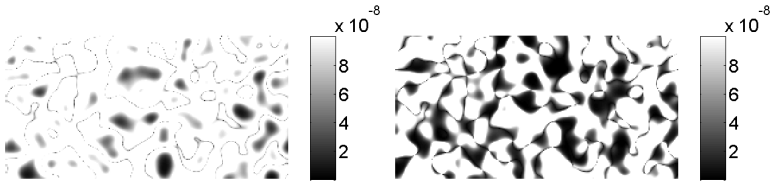

(a) (b)

Figure 5.16: *Hydraulic conductivity* $K\,[\mathrm{m/s}]$ *in Miller-similar media (a) and non-Miller similar media (b).*

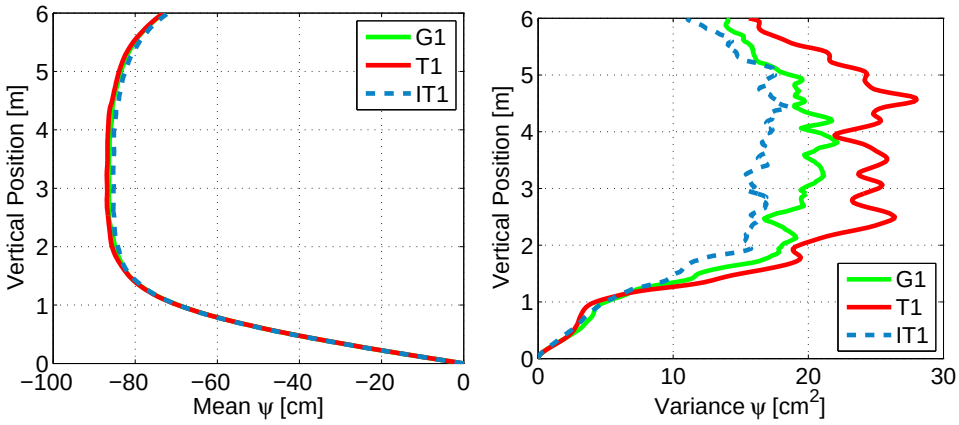

(a) Miller similar media

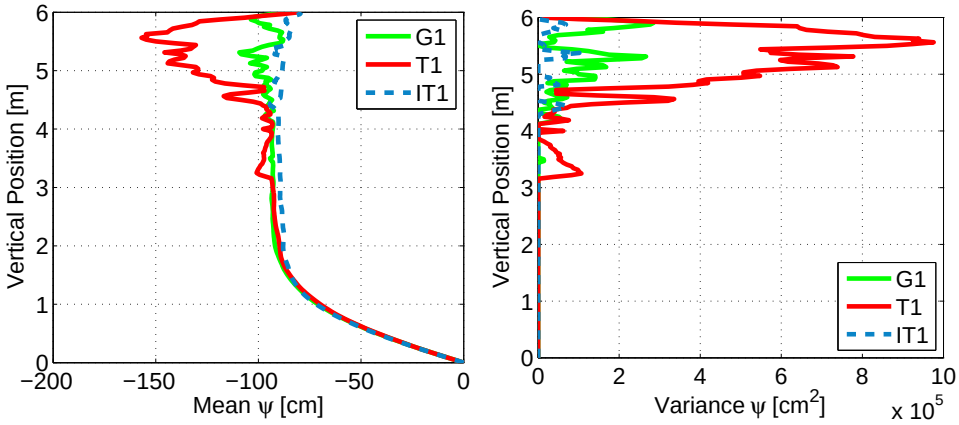

(b) non-Miller similar media

Figure 5.17: *Mean* $[\mathrm{cm}]$ *(left) and variance* $[\mathrm{cm}^2]$ *(right) of pressure head in Miller-similar media (a) and non-Miller simlar media (b) for relatively wet conditions (scenario S1). Large values of the variance of pressure head indicate the formation of dry regions.*

Since regions of low conductive material are larger in non-Miller similar media, the susceptibility to the formation of dry regions is increased. Numerical simulations confirm that dry patches form in non-Miller similar media under wetter conditions or at higher infiltration

rates, compared to scenarios in Miller-similar media. Figure 5.17 shows the profile of ensemble mean and variance of pressure head for scenario S1 in Table 4.1, which was conducted in a Miller-similar parameter field (a) and a non Miller-similar media (b). The large variances of pressure head in part (b) indicate that dry regions extensively form in the simulation where K_s and α are not related to each other. The effect of local wilting is thus not an artifact of Miller-similar media.

5.3 Comparison of root water uptake strategies

Since experimental data support the occurrence of compensation mechanisms for local stress within the root zone (Taylor and Kleppner, 1978; Hasegawa and Yoshida, 1982; English and Raja, 1996; Stikic et al., 2003; Leib et al., 2006), it is expected that roots can react in response to an impeding soil structure in order to maintain the overall uptake at the potential rate. For this reason, the basic root uptake term R_1 (in equation (2.27)) is compared to three strategies which include compensation mechanisms for local drying. The corresponding root water uptake terms are denoted by R_2, R_3 and R_4.

The uptake models, R_1 to R_4, are compared using the settings of scenario S5 in Table 4.1 (slightly drier conditions than in the previous section) and one realization of a T2-field where a resolution of 128x128 on 8x8m was chosen. The distribution of the saturated loghydraulic conductivity and the parameter α are shown in Figure 5.18.

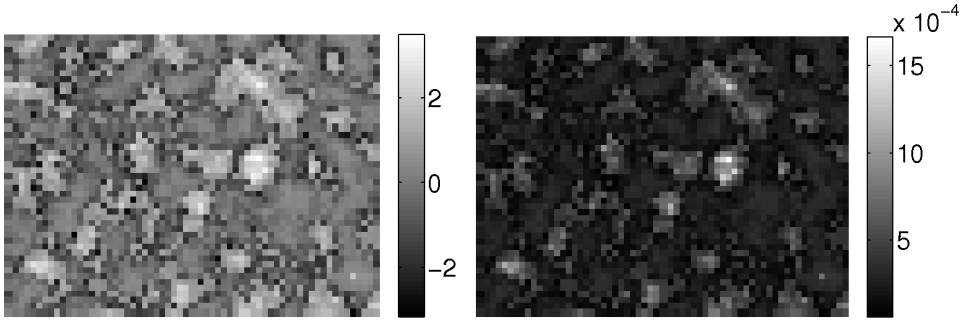

(a) Loghydr. sat. conductivity (b) α-parameter

Figure 5.18: *Saturated loghydraulic conductivity f $[-]$ (a) and parameter α $[\mathrm{Pa}^{-1}]$ (b).*

In Figure 5.19, the simulation results are shown. The distribution of pressure head (left) and corresponding root water uptake (right) are illustrated for the different uptake strategies R_1-R_4 (from top to bottom). The basic model leads to wilting within the two largest uppermost patches, (Figure 5.19a,b). In case Strategy 2 ($M_2 = S$) is considered, the resulting relationship between root water uptake and pressure head in the water limited part of the Feddes function is non-linear. Thus the formation of extremely dry spots is attenuated in comparison to Strategy 1. But local wilting is in general also possible. In Figure 5.19c and d it can be seen, that the stressed area is smaller compared to the basic model and the extreme values of pressure head are equal to $-4.1\,\mathrm{m}$ instead of $-150\,\mathrm{m}$ with the basic model.

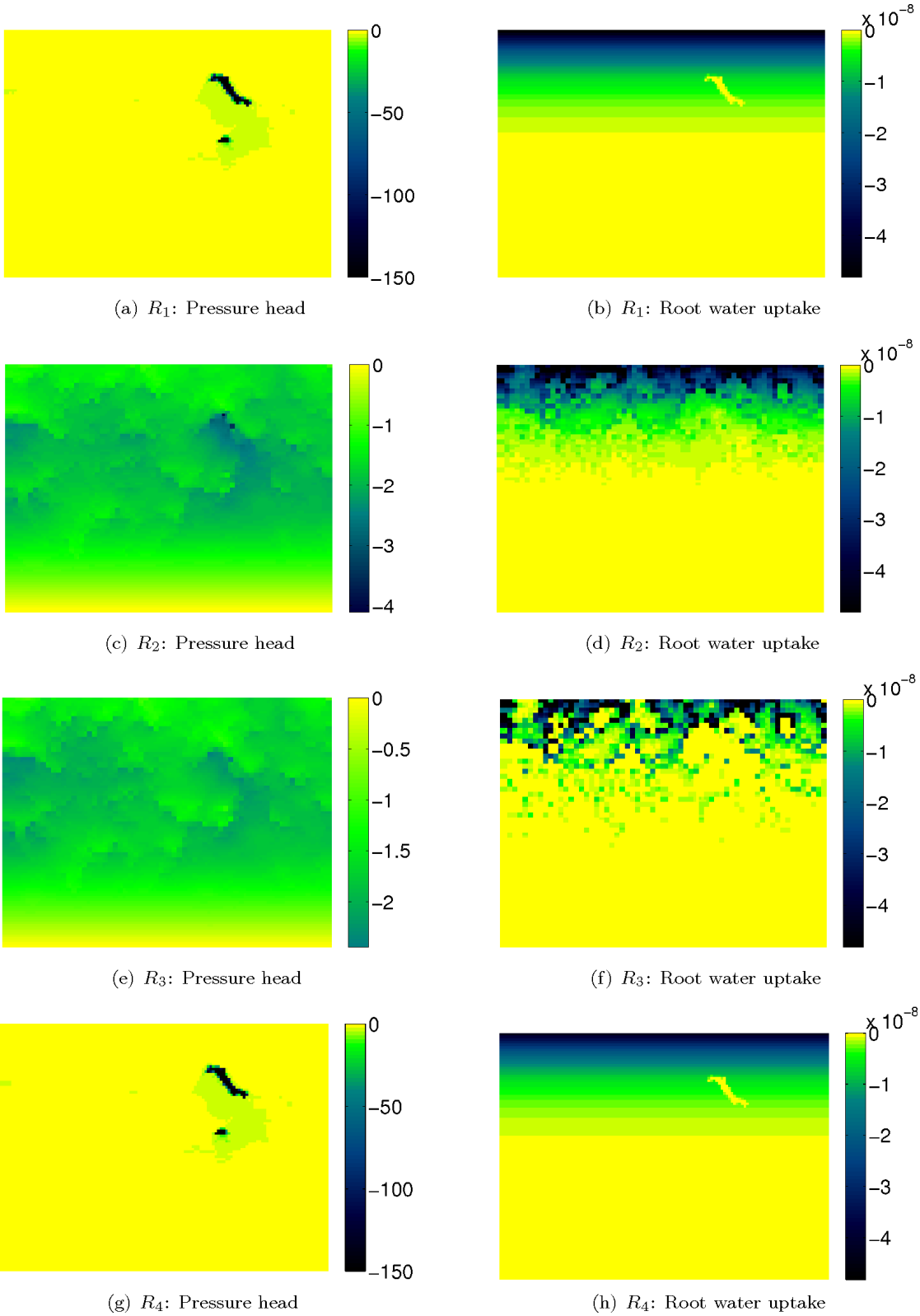

(a) R_1: Pressure head

(b) R_1: Root water uptake

(c) R_2: Pressure head

(d) R_2: Root water uptake

(e) R_3: Pressure head

(f) R_3: Root water uptake

(g) R_4: Pressure head

(h) R_4: Root water uptake

Figure 5.19: *Distribution of pressure head ψ [m] (left) and (negative) root water extraction rate R [1/s] (right) with uptake models R_1, (a,b), R_2 (c,d), R_3 (e,f) and R_4 (g,h) for scenario S5 in Table 4.1*

In case preferential uptake depends on the relative permeability (Strategy 3), the resulting extraction rate decreases stronger with the pressure head in the water limited range of the Feddes-function than with Strategy 2. Therefore, the formation of dry areas is even more attenuated and occurs less often. In the test case examined in this study, dry regions did not form when Strategy 3 was applied, (see Figure 5.19e, f). This effect is, however, in principle still possible if the conditions are dry enough or the patches of coarse material large enough. In contrast, Strategy 4 does not diminish the stressed or wilted area since the uptake rate at stressed locations is not decreased compared to Strategy 1 (see Figure 5.19g,h). By increasing the uptake rate at neighboring nodes in order to meet the atmospheric demand, the opposite effect might be the case. Counting the number of stressed nodes yields that the number of stressed nodes is slightly increased if compared to the standard approach R_1.

Concluding, stress and wilting can develop locally in lenses of coarse material, although surrounded by fine, wet material even when root water uptake strategies that compensate for local wilting by increased uptake at wet locations and decreased uptake at stressed locations, are considered. However, with the root water uptake strategies 2-3, the effect is attenuated and the global uptake is not affected by the wilted locations in coarse material. When the fourth approach is employed, the global uptake rate is maintained at the potential value, but the stressed area is not reduced compared to the standard model.

Considering the adaptability that plants can generally show in nature, the formation of wilted areas within a relatively wet surrounding seems unreasonable. Obviously, our modeling approaches, and also the current state of knowledge of compensation mechanisms, lack essential aspects, such as the consideration of soil physical and plant physiological processes. Whatever strategy applies, compensation mechanisms do probably not work over long distances, such as few kilometers. Thus, locally wilted spots could eventually occur in large fields if the cultivated crops are not able to access the groundwater system. Though, to preestimate the local range of influence for compensation is difficult since plants may transmit signals within one root system, and even communicate indirectly with neighboring plants by changing the soil moisture status. The natural range of influence is hence likely to depend strongly on the observed species and location. Compensation is probably not only limited in space, but also in time. The implemented strategies assume immediate adaptation to changing conditions. Since the mechanisms driving compensation are still unclear and compensatory growth or signaling might require some processing-time, an immediate response might not be realistic under quickly changing infiltration pattern. Furthermore, compensation certainly depends on the soil moisture state. If a threshold dryness is exceeded such that the bulk of the soil becomes stressed, the uptake rate is reduced if groundwater resources cannot be accessed. Otherwise, in the extreme case, the whole atmospheric demand would be extracted from few locations which seems unreasonable.

Finally, one needs to add, that it is questionable how well macroscopic compensation models for local stress represent natural processes in general. Compensation usually means the enhanced uptake at deeper layers for stress close to the surface. Additionally, hydraulic variables are often monitored as average quantity. In heterogeneous media, little data on e.g. resolved uptake pattern is currently available. In particular, local occurring stress at specific locations and corresponding compensation has not been observed, to our knowledge, and

remains until then speculative.

5.4 Impact on solute transport: Flow velocities

Solute, released into water at the surface, travels through the unsaturated zone. To estimate the potential risk for groundwater contamination, it is crucial to predict the transport behavior of a solute. This topic has been addressed by numerous studies (e.g. Birkholzer and Tsang, 1997). Root water uptake and non-Gaussian soil structures are often neglected in such work.

In this section, Darcy fluxes of the steady state simulations in G1-, T1- and IT1-fields, with and without root water uptake, treated above, are discussed. In the scenario without root water uptake, the infiltration rate at the top boundary corresponds to the net infiltration rate below the root zone, $q - \tau$, of the scenario where root water uptake is accounted for. In these stationary flux fields, solute transport is investigated using two methods. First, maximum connected transport velocities are studied, second, a numerical tracer experiment is conducted. It is analyzed whether connected velocities and breakthrough curves are influenced by root water uptake and non-Gaussian soil structures.

5.4.1 Stationary water flow field

Within the root-zone, root water uptake continuously decreases the infiltration rate q at the top boundary with increasing depth such that the net infiltration rate corresponds to $q - \tau$ below the root-zone. Thus, ensemble mean and variance of the total Darcy flux ($\sqrt{j_x^2 + j_y^2}$), which are shown in Figure 5.20 and Figure 5.21, agree below the root zone in the scenario with root water uptake (solid lines) and in the scenario without root water uptake where a infiltration rate of $q - \tau$ (dashed lines) is used. The coefficient of variation decreases with increasing mean and is thus, in the upper part of the domain, smaller as in the case without root water uptake.

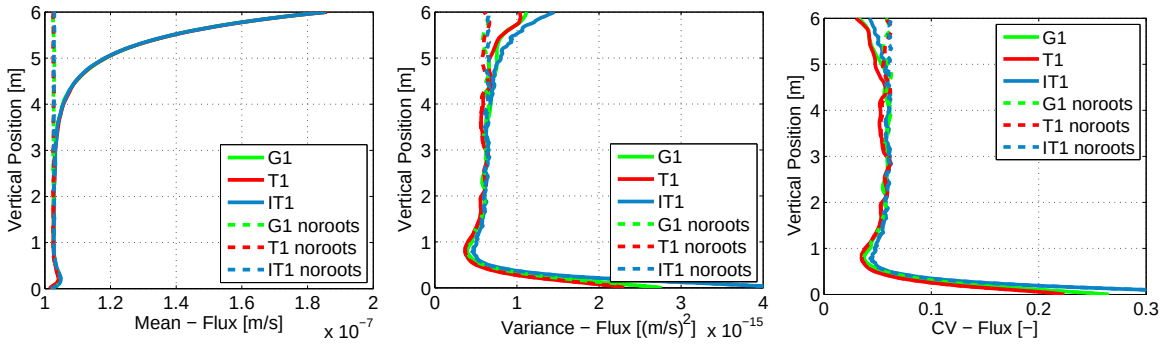

(a) (b) (c)

Figure 5.20: *Mean* $[\mathrm{m/s}]$ *(a), variance* $[(\mathrm{m/s})^2]$ *(b), and coefficient of variation* $[-]$ *(c) of total Darcy flux profile with and without roots; wet conditions (scenario S1 and S2).*

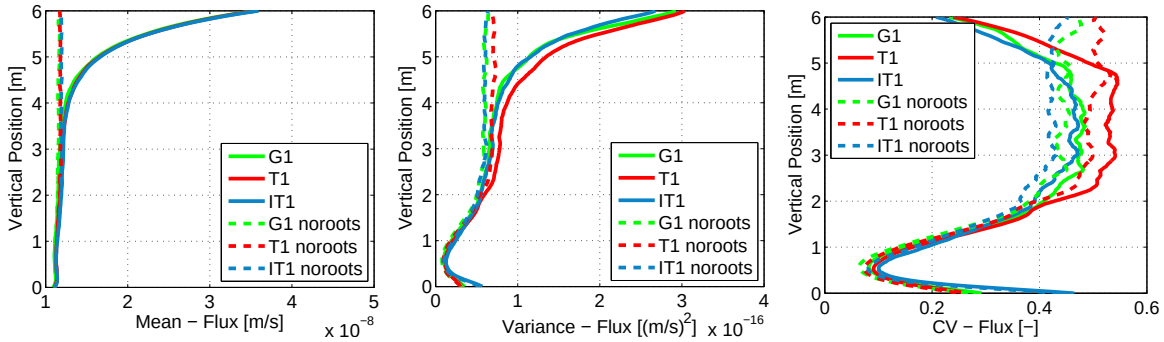

(a) (b) (c)

Figure 5.21: *Mean* $[\mathrm{m/s}]$ *(a), variance* $[(\mathrm{m/s})^2]$ *(b), and coefficient of variation* $[-]$ *(c) of total Darcy flux vs. vertical position* $[\mathrm{m}]$ *in G1, T1 and IT1-fields with and without roots; dry conditions (scenario S3 and S4).*

The flow network depends on the pattern of the hydraulic conductivity which was shown to be dependent on the infiltration rate at the top boundary, (see section 5.1). Under wet conditions, the water flux field, illustrated in Figure 5.22, is similar in the non-Gaussian fields T1 and IT1, corresponding to the pattern of the hydraulic conductivity. As reported by Roth (1995), the variability of fluxes is small and the distributions are rather uniform close to the crossover where coarse and fine material have similar conductivities. Under drier conditions, the flow fields, illustrated in Figure 5.23, show distinct channels and T1- and IT1-fields have different patterns. Ensemble mean and variance of Darcy fluxes are hardly affected by the considered structures.

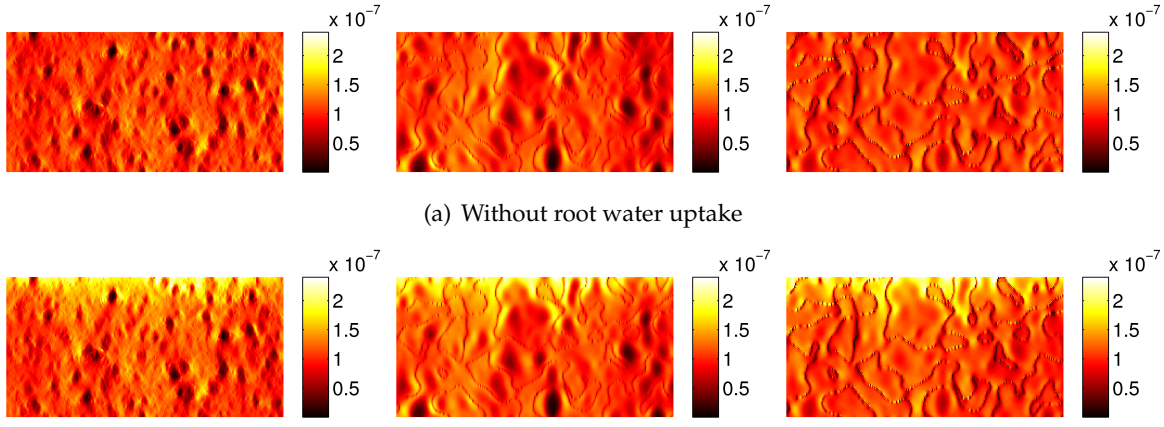

(a) Without root water uptake

(b) With root water uptake

Figure 5.22: *Darcy flux in one realization of G1-, T1- and IT1-fields; wet conditions, without root water uptake (a), and with root water uptake (b).*

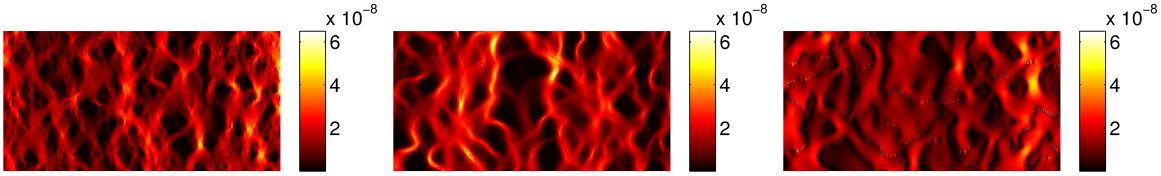

(a) Without root water uptake

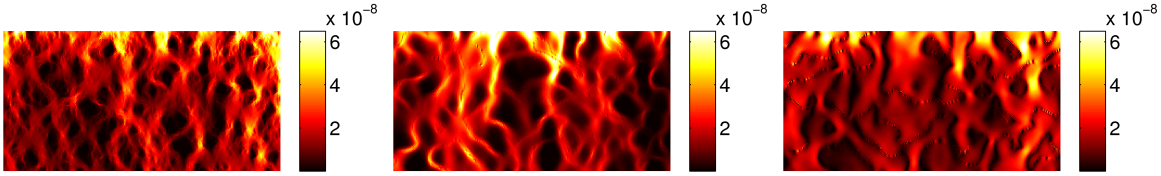

(b) With root water uptake

Figure 5.23: *Darcy flux in one realization of G1-, T1- and IT1-fields; dry conditions, without root water uptake (a), and with root water uptake (b).*

5.4.2 Transport velocities

The transport velocity of solutes is related with the number of occurring reactions and plays, thus, a role for the degradation process of hazardous compounds. This is important for environmental problems such as the leaching of pesticides. Therefore, in solute transport analysis, one is mainly interested in preferential flow paths, where solute can travel quickly, or the arrival of the bulk of solute.

If solute is released into the stationary flow field, it is transported with a velocity of $\mathbf{j}/\Theta$ where $\mathbf{j}$ is the Darcy flux in x- and z-direction and Θ, the water content. The arrival time of solute at a certain depth depends on the velocity of the tracks along which solute is transported. In order to identify the role that root water uptake and non-Gaussian soil structures play for fast tracks of solute transport problems, the transport velocity fields are searched for cluster with high values (preferential paths) which are connected from top to bottom. The fastest track is related with the connected cluster with the highest velocity. The velocity at which most connected cluster are found can be considered a measure related with the velocity of the bulk mass. The number of connected cluster as function of a threshold velocity is obtained using the Hoshen-Kopelman-Procedure, introduced in chapter 2.3.3. The threshold velocity is set equal to the highest velocity and is subsequently stepwise decreased. For each threshold velocity, values which are smaller than this value, are set equal to zero, the remaining values are set equal to one. To find and label connected cluster of values equal to one in each realization, the Hoshen-Kopelman-Algorithm implemented by Fricke (2004) (in the programming language C) is included into a Matlab code. In this work, processes in the upper part of the unsaturated zone (above the capillary fringe) and the influence of root water uptake are of interest, hence, transport velocities are analyzed in a subdomain, which extends from the surface (vertical position of $z = 6\,\mathrm{m}$) to a location which is below the root-zone and $2\,\mathrm{m}$ above the groundwater table (vertical position of $z = 2\,\mathrm{m}$). Two scenarios, with and without root water uptake, which have the same net infiltration rate are compared

under dry conditions. With and without root water uptake, the considered structures have only little influence on the maximum threshold velocity and bulk velocity. In IT1-fields, the bulk velocity is slightly smaller than in G1- and T1-fields. This difference is slightly larger in the scenario without root water uptake than in the scenario with root water uptake. Both, the maximum and the bulk velocity are in all structures larger with root water uptake which indicates that solute travels faster in the scenario with root water uptake. Figure 5.24 shows the number of connected cluster as function of the threshold value according to which the binary field is obtained for a dry scenario with and without root water uptake, which have the same net infiltration rate.

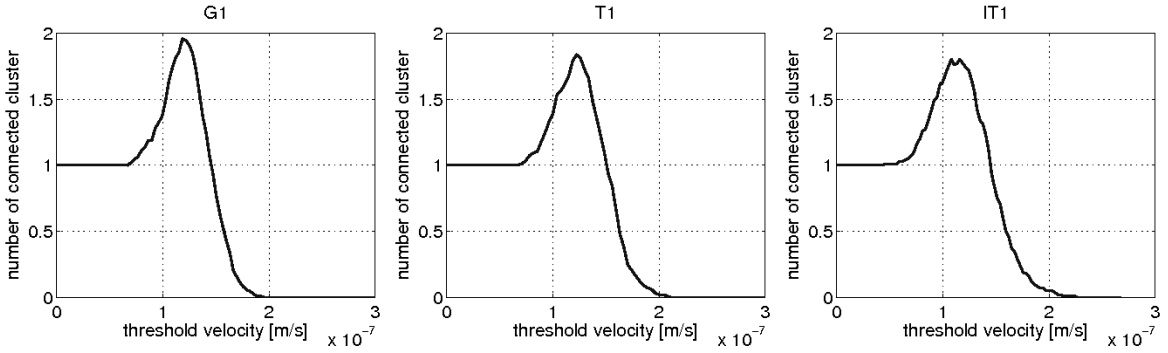

(a) Without root water uptake

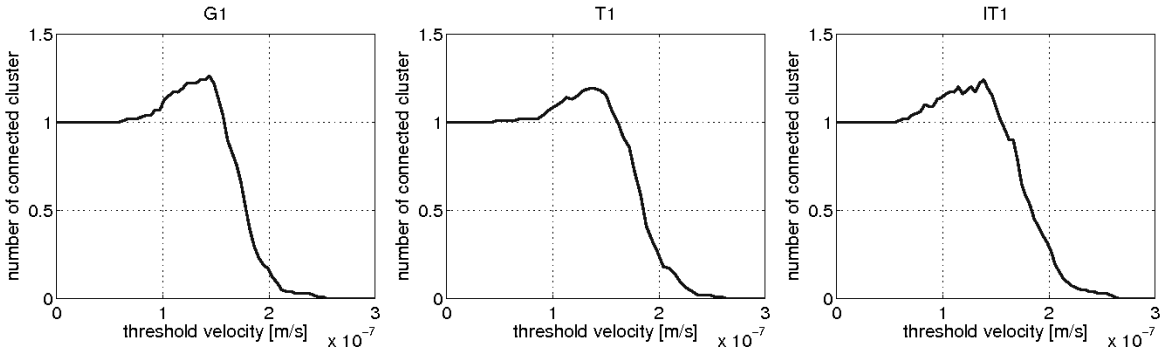

(b) With root water uptake

Figure 5.24: *Number of cluster vs. threshold velocity, averaged over all realizations. Without root water uptake (a) and with root water uptake (b).*

To test the above applied method of connected cluster, results are compared to arrival times of solute derived from a numerical tracer experiment. At the top boundary of the velocity fields, an initial pulse of solute is released. The total (accumulated) concentration in the subdomain (from a vertical position of $z = 2\,\mathrm{m}$ to $z = 6\,\mathrm{m}$) is calculated and normalized (denoted as $c\,[-]$). The change of concentration over time at a plane located $2\,\mathrm{m}$ above the groundwater table is derived by differentiation of the accumulated concentration with respect to time. This curve is referred to as the flux-averaged breakthrough curve in this work.

We concentrate on the influence of root water uptake and non-Gaussian soil structures on first arrival and arrival of bulk of the solute, but also on the tail of the flux-averaged break-

through curves and the concentration held back by stagnant zones (here called residual concentration). The tail of a breakthrough curve implies that small transport velocities exist which lead to a retarded arrival of the solute. To evaluate the impact of root water uptake and soil structure more clearly, we consider, in addition to the scenario without root water uptake and an infiltration rate at the top boundary equal to $q - \tau$, a case without root water uptake and an infiltration rate of q.

Note that in the numerical tracer experiment only advective transport is considered. Numerical dispersion occurs, but does not affect the measures of interest (peak arrival and tailing).

Naturally, with higher infiltration rates at the top boundary, solute propagates faster through the domain than at lower infiltration rates. Since the flux continuously decreases with increasing depth in scenarios with root water uptake, the arrival time of the bulk of solute is in between the two cases (inflow rate q and $q - \tau$) without root water uptake. The tail of the flux-averaged breakthrough curve depends on the infiltration rate at the top boundary as well. At higher infiltration rates, the arrival of solute at the lower boundary of the subdomain is less retarded and the tail less distinct than at lower infiltration rates. Thus, solute mass passes the lower boundary of the domain the earlier and more concentrated, the higher the infiltration rate at the top boundary is. In the scenario with root water uptake, the tailing of the flux-averaged breakthrough curve is in between both no-root cases.

Figure 5.25, 5.26 and Figure 5.27 show the normalized concentration (in the subdomain) over time (a) as well as flux-averaged breakthrough curves (b-d) in G1- (green), T1- (red) and IT1-fields (blue) for a scenario with roots (scenario S3 in Table 4.1) and the corresponding scenarios without root water uptake, with an infiltration rate equal to q, and $q - \tau$, respectively (scenario S4 and S6). In (c) and (d) different sections of the breakthrough curves are shown to illustrate the peak arrival or tailing more clearly. Single realizations are indicated by light colored, dashed lines, ensemble means are represented by dark colored, solid lines. In the scenario with root water uptake, solute arrives approximately $110\,\mathrm{days}$ ahead of the no-root case if an infiltration rate of $q - \tau$ is applied and approximately $190\,\mathrm{days}$ later if an infiltration rate of q is considered.

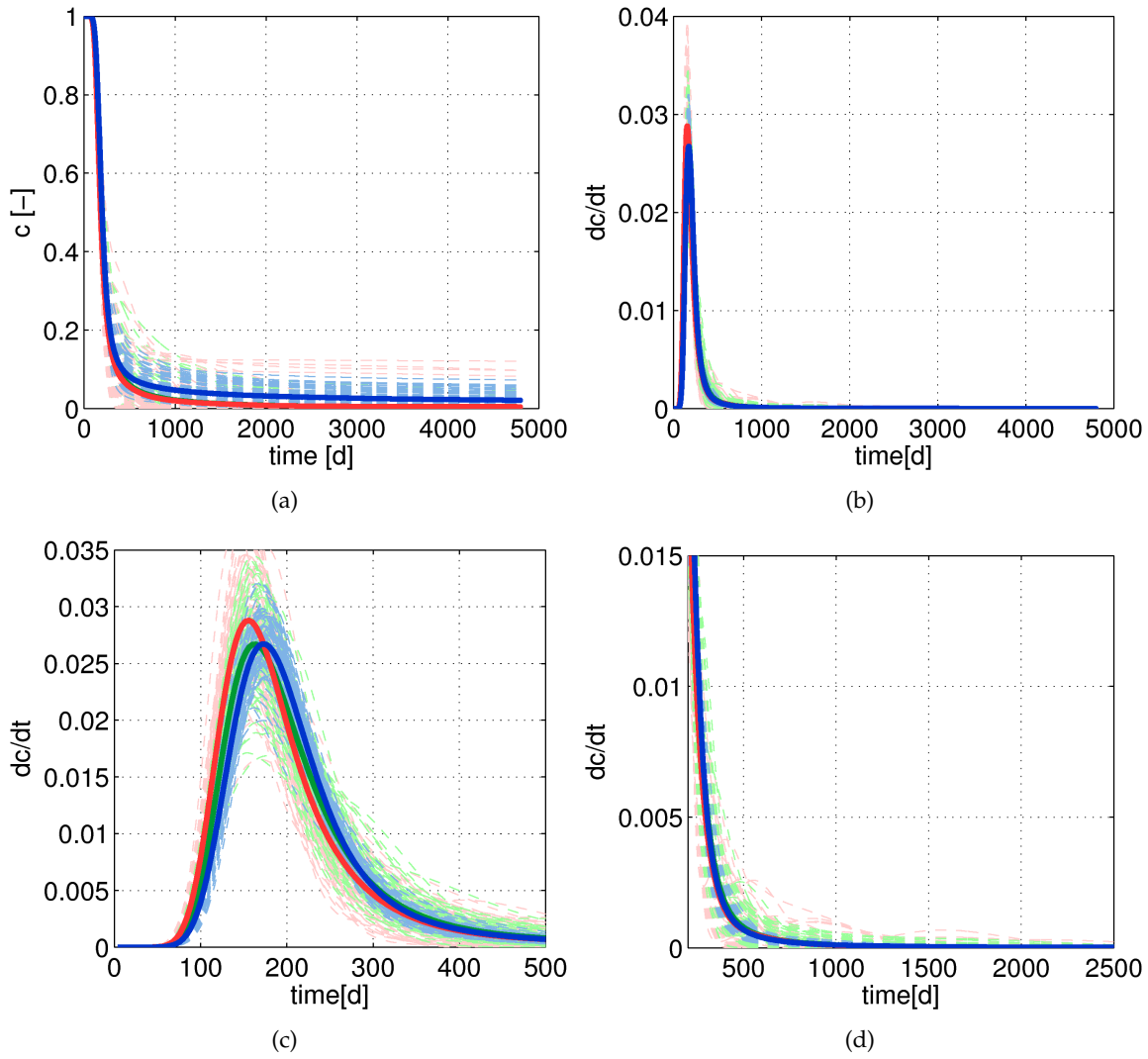

Figure 5.25: *Normalized concentration (in the subdomain) over time (a) and flux-averaged breakthrough curves (b-d) (monitored* $2\,\mathrm{m}$ *above the groundwater table) in G1- (green), T1- (red) and IT1-fields (blue). Root water uptake is not considered, the infiltration rate at the top boundary is equal to* q.

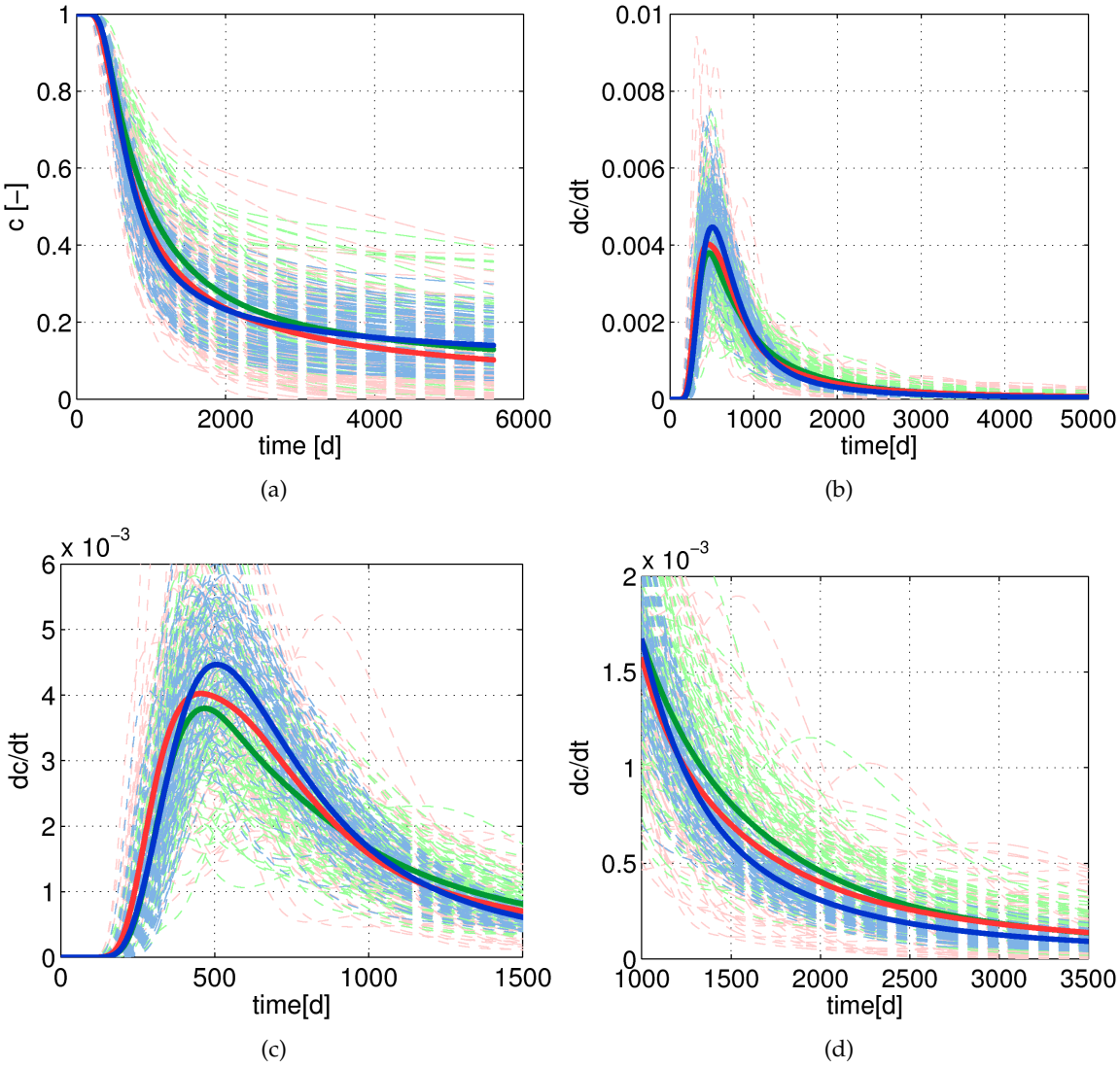

Figure 5.26: *Normalized concentration (in the subdomain) over time (a) and flux-averaged breakthrough curves (b-d) (monitored* $2\,\mathrm{m}$ *above the groundwater table) in G1- (green), T1- (red) and IT1-fields (blue). Root water uptake is not considered, the infiltration rate at the top boundary is equal to* $q - \tau$.

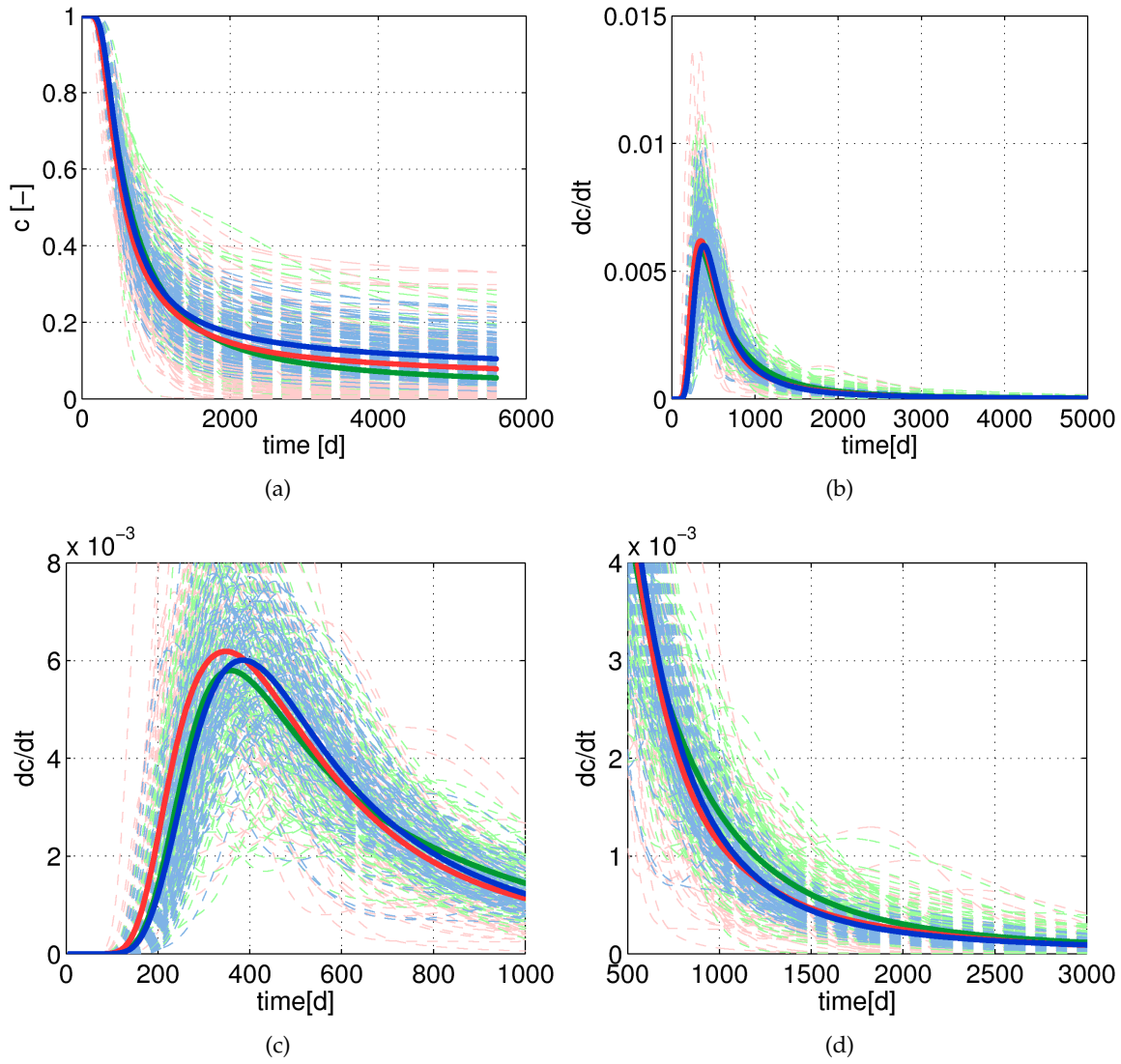

Figure 5.27: *Normalized concentration (in the subdomain) over time (a) and flux-averaged breakthrough curves (b-d) (monitored* $2\,\mathrm{m}$ *above the groundwater table) in G1- (green), T1- (red) and IT1-fields (blue), including root water uptake.*

In T1-fields, particles travel on average faster than in G1- or IT1-fields such that, at early times, more solute per unit time is detected. Correspondingly, the slope of T1-fields (red line) is steeper at the onset of the breakthrough curve and the maximum occurs earlier than in G1- and IT1-fields. In IT1-fields, solute arrives on average later than in G1-fields. Differences between the considered structures increase with decreasing infiltration rate applied at the top boundary. Thus, comparing two scenarios with and without root water uptake where averaged fluxes and pressure heads are equal below the root-zone (same net infiltration rate), differences between G1-, T1- and IT1-fields are smaller if root water uptake is considered. Table 5.1 summarizes the times (in days of simulation time) at which dc/dt is maximum in G1-, T1- and IT1-fields in the performed scenarios.

RWU	$G1$	$T1$	$IT1$
no - high	164	156	172
no - low	468	456	508
yes	356	348	384

Table 5.1: *Times [days] at which dc/dt is maximum in G1-, T1- and IT1-fields with and without root water uptake (high and low infiltration rate), monitored $2\,\mathrm{m}$ above the groundwater table.*

With and without root water uptake, the residual concentration is highest in IT1-fields, which have large patches of fine material. With increasing infiltration rates, the residual concentrations decrease.

In G1- and T1-fields, which have lenses of coarse material, the conductivity of coarse patches is lowered by root water uptake such that these regions are bypassed by downwards streaming water. The flow around dry lenses might lead to a lower residual concentration and a decrease of the tail such that dc/dt approaches zero more quickly in such fields if root water uptake is taken into account, in comparison to the case without root water uptake and the same net infiltration rate of $q - \tau$. However, which feature of structure is, with respect to solute transport, most sensitive to the influence of root water uptake, needs to be analyzed more detailed in future studies.

Comparing the results obtained with the numerical tracer experiment and the results of the above used method of connected clusters, the latter can predict an earlier arrival of solute under consideration of root water uptake but is not able to capture the differences between the considered structures. Thus, algorithms based on the search for connected clusters can only provide approximate measures for transport problems.

5.5 Intermediate summary 1: Steady states

In this chapter, steady state simulations on unsaturated water flow including infiltration and root water uptake in differently structured soils are analyzed. In the following the main findings of this chapter are listed:

- The pattern of the hydraulic conductivity is dependent on saturation. With the parameters chosen in this work, a wide range of infiltration rates exist which lead to similar pattern of the hydraulic conductivity of T1- and IT1-fields. With very low infiltration rates, the hydraulic conductivity of T1- and IT1-fields show inverse pattern (5.1). This needs to be considered when steady state or dynamic simulations under varying conditions are conducted.
- Section 5.2.1 shows that under wet conditions, root water uptake bents the profile of mean and variance of pressure head by extracting water within the root zone. Only small differences of mean and variance of pressure head exist between the considered structures.
- Without root water uptake, structure slightly influences the pressure head distribution under dry conditions. Including root water uptake, local wilting occurs in some structures, which decreases the mean pressure head and leads to extremely large values of the variance of pressure head (section 5.2.2).
- The feature of structure which is sensitive to local wilting is the length scale of coarse lenses. This feature is more critical in the vertical direction. The sensitivity to local wilting is also increased if non-Miller similar media is considered.
- The occurrence of local wilting under steady state conditions leads to unreasonable results and is likely to be a model artifact due to the use of oversimplified model approaches for root water uptake.
- Section 5.3 demonstrates that compensating root water uptake mechanisms maintain the global potential uptake rate and attenuate the effect of local wilting but do not prevent local stress. We currently lack a sufficient understanding of uptake and compensation mechanisms with respect to the involvement of soil-physical and plant-physiological processes.
- Flux-averaged breakthrough curves obtained from transport calculations yield that in dry scenarios with and without root water uptake, particles cross T1-fields slightly faster, while IT1-fields retain more concentration over a long period of time. Arrival times of bulk solute (i), tailing of the flux-averaged breakthrough curves (ii) as well as differences between G1-, T1- and IT1-fields (iii) increase with decreasing infiltration rate at the top boundary. Thus, in comparison to a case without root water uptake and the same net infiltration rate, (i)-(iii) are smaller if root water uptake is considered since the top infiltration rate is larger and water is continuously extracted over depth (section 5.4).

6 Transient flow in 2D Gaussian and non-Gaussian fields

In the previous chapter, the influence of soil structure and root water uptake on steady state unsaturated flow was discussed. In reality, weather patterns are not constant over a long period of time but vary strongly and drying and rewetting cycles take turns. Under such conditions, conclusions drawn at steady state might not hold due to e.g. changing flow patterns or preferential flow, and factors such as structure and root water uptake might become more important. In this section, the joint influence of structure and root water uptake on transient unsaturated flow during drying and rewetting phases is discussed.

We particularly focus on the phenomenon of locally occurring stress at distinct locations, which has been shown to be the most severe effect of soil structure on steady state distributions of pressure head under consideration of root water uptake. Timescales for formation and recovery of dry spots as well as the impact of the occurrence of local wilting on crop yield is assessed. The second issue to be investigated deals with the development of variability of pressure head and saturation over time during drying and rewetting and the impact of root water uptake in the process. Special attention is paid to the state of largest variability of pressure head, which is related to the driest state under steady state conditions.

In the following, pressure head and saturation are analyzed in G1-, T1- and IT1-fields at three different depths of the root zone, illustrated in Figure 6.1, for test cases where drying and subsequent rewetting is considered. The root water uptake terms R_1 and R_2, described in section 2.2.2, are applied and compared to cases without root water uptake.

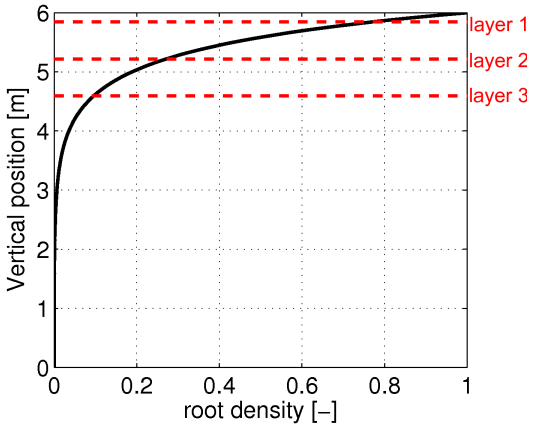

Figure 6.1: *Exponentially decreasing root density and layers (in red) at which variables are analyzed.*

Test case

The joint influence of structure and root water uptake on transient flow is illustrated for a scenario where first drying due to drainage and root water uptake is considered, and subsequently rewetting with a constant flux at the top boundary. In this drydown-rewetting scenario (scenario D1 in Table 4.2), root water uptake (with $\tau = 2\,\mathrm{mm/d}$ and $\delta = 0.6\,\mathrm{m}$) is applied from the beginning of the simulation. From the 40th day forward, both, root water uptake and infiltration, with a rate of $4\,\mathrm{mm/d}$ (on the artificial boundary), are considered until a steady state profile develops. (Recall that infiltration on the soil surface is modeled by an artificial layer of $2\,\mathrm{m}$. If infiltration is considered from the 40th day forward on the artificial top boundary, the infiltration front arrives accordingly later at the top boundary of the model domain.) The initial condition at the beginning of the simulation is uniform with ψ equal to $-35\,\mathrm{cm}$.

Figure 6.2 shows time series of the mean of pressure head or saturation (solid line) in comparison to the coefficient of variation (dashed line) for the three structures, G1- (green), T1- (red) and IT1-fields (blue), in layer 1 (a), layer 2 (b) and in layer 3 (c).

In each layer, the infiltration pattern at the top boundary is reflected. Through root extraction and drainage of the initial water mass, the upper part of the soil dries down until infiltrating rainwater arrives. A rewetting front proceeds from the surface to the groundwater table which subsequently reaches all layers. The minimum of mean pressure head or saturation corresponds to the driest state before rewetting starts. The rainwater arrives at layer 1, approximately after $70\,\mathrm{days}$, at layer 2, after $87\,\mathrm{days}$ and at layer 3, after $105\,\mathrm{days}$. More deeply located layers dry over a longer period of time and less water arrives due to water extraction by plant roots above. This leads to a slower achievement of the steady state value such that the drydown-rewetting curve widens with depth. Apart from the pressure head in layer 2 where the mean in T1-fields has lower values from $100 - 150\,\mathrm{days}$ than the mean in G1- and IT1-fields, the mean of pressure head and saturation behave very similarly in the considered structures.

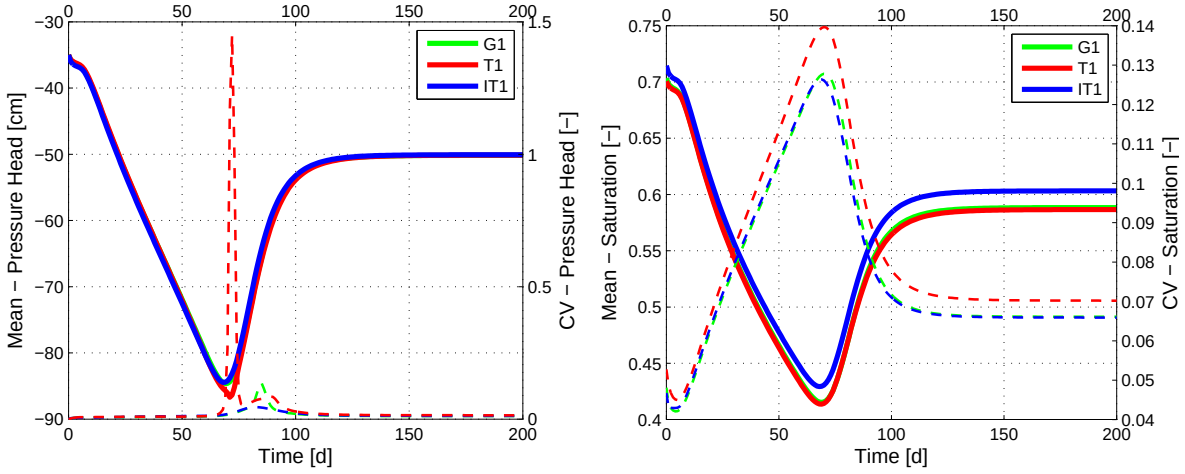

(a) layer 1

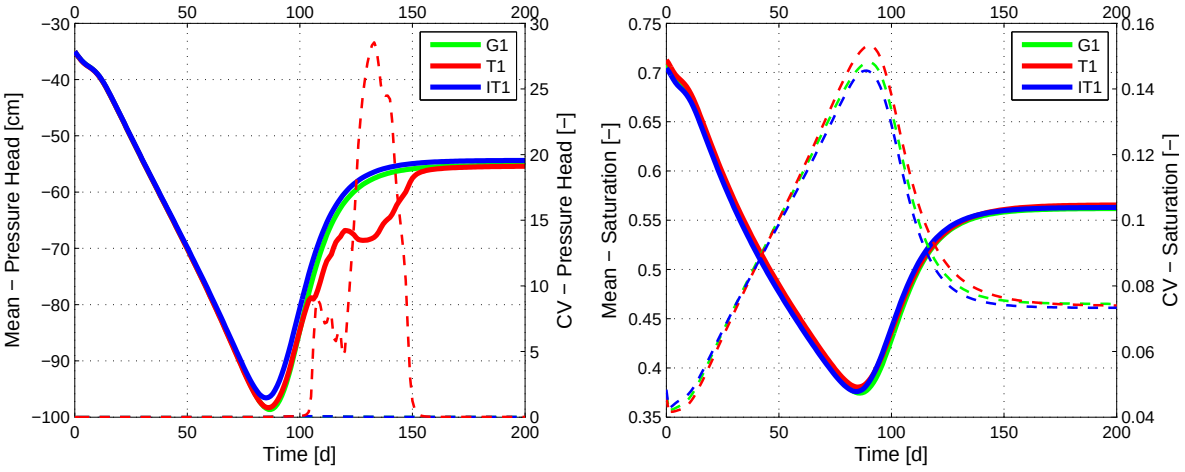

(b) layer 2

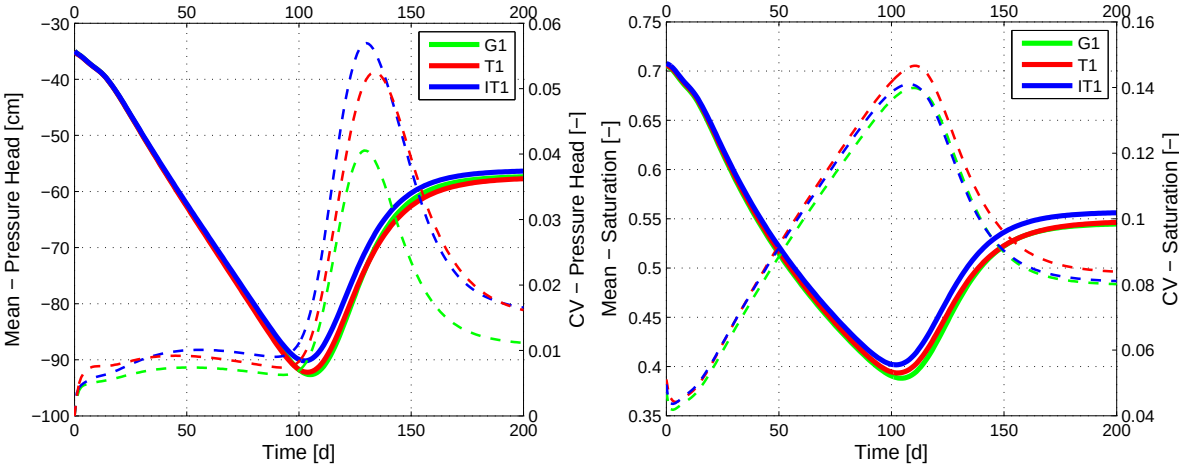

(c) layer 3

Figure 6.2: *Mean (solid line) and coefficient of variation (dashed line) of pressure head (left) and saturation (right) vs. time for G1 (green), T1 (red) and IT1-fields (blue) in layer 1 (a), layer 2 (b) and in layer 3 (c).*

The coefficient of variation of pressure head versus time shows two distinct features. Particularly striking are, first, the large peaks of the coefficient of variation of T1-pressure fields (red dashed line) in layer 1 and 2, which occur at the same time as the mean pressure head in T1-fields deviates from the mean pressure head in G1- and IT1-fields. From the results of the previous chapter it can be concluded that these peaks are related to the formation of dry regions in lenses of coarse material. The mean and variance of saturation is not affected by these dry regions. The formation of dry spots depends on the local root water uptake rate and the length scale of patches of coarse material. In layer 3, where root water uptake is small, dry spots do not form. In G1- and IT1-fields, lenses of coarse material are smaller than in T1-fields which leads to a smaller susceptibility to the formation of dry regions. Figure 6.3 shows again time series of $< \psi >$ and CV_ψ in the three structures, but with differently scaled axis. In G1- and IT1-fields, the coefficient of variation of pressure head has moderate values, which indicates that patches with extreme pressure head values do not form in layer 1 to layer 3.

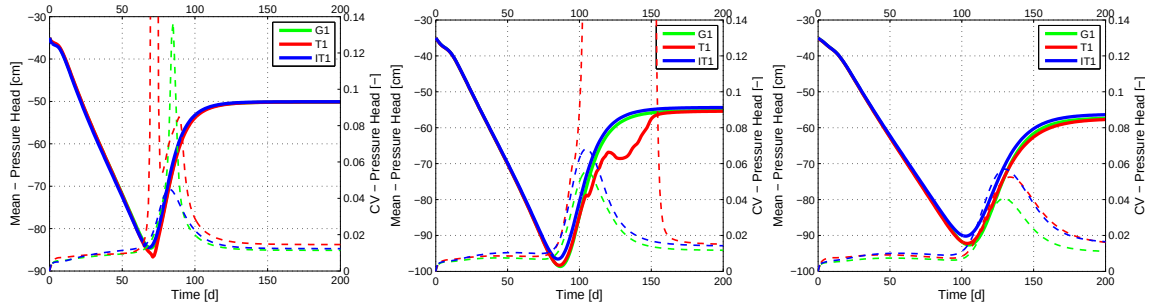

(a) layer 1 (b) layer 2 (c) layer 3

Figure 6.3: *Mean (solid line) and coefficient of variation (dashed line) of pressure head vs. time for G1- (green), T1- (red) and IT1-fields (blue) in layer 1 (a), layer 2 (b) and in layer 3 (c).*

The second distinctive feature in Figure 6.2 or Figure 6.3 is, that the maximum of the coefficient of variation of pressure head follows the minimum of the mean pressure head with a remarkable time lag. Extremes of mean and CV of saturation occur also with a small shift (which is however much smaller than for the pressure head). Thus, the driest state and the state with the maximum variability of pressure head and saturation do not occur simultaneously as expected from steady state solutions. Both phenomena are investigated more closely in the following sections.

6.1 Formation of dry spots

Section 5.2 demonstrates that root water uptake, modeled according to the standard macro-approach, can cause local wilting in soil structures with large patches of coarse material under dry steady state conditions with constant infiltration at the top boundary and constant water extraction by roots. These locations are permanently wilted spots, situated in a wet surrounding. The mechanism of formation is explained as well. This section focuses on the estimation of timescales for the formation of dry spots during drying and the recovery during rewetting. Such timescales give the opportunity to estimate a critical frequency for periodic cycle scenarios above which dry spots should not form. Before the formation and recovery during drying and rewetting is analyzed, we recall how dry patches form.

- Under dry conditions, conductivities of coarse lenses have very low values which leads to ponding of water above coarse lenses to supply water into the coarse material.
- Pressure head values on top of coarse lenses cannot deviate from their surrounding by any value due to lateral equalization of pressure. Pressure head values in the surrounding of coarse lenses are determined by the infiltration rate at the top boundary. A limited pressure head on top of a coarse lens leads to a maximum inflow rate from the top of a coarse lens into its inner part.
- If the replenishment rate is not sufficient, a drying front proceeds into coarse lenses from below, leading to decreasing conductivities. At some point infinite pressure gradients are required to draw water into coarse lenses.
- In our model, root water uptake is limited at the wilting point. Such locations, thus, dry up to the wilting point which is equal to $-150\,\mathrm{m}$.
- Localized dry spots with extremely low pressure head values lower the mean pressure head and lead to extreme values of the variance of pressure head.

In this section, transient conditions are analyzed using scenario D1, where a drying phase is followed by a rewetting phase.

During drying, no infiltration at the top boundary is applied. Depending on the local extraction rate, the distribution of soil parameters, and the time over which drying is considered, critical pressure heads are reached at some point such that stressed patches develop. As root water uptake decreases exponentially with depth, the extraction rate is largest close to the surface. Thus, dry regions form first in upper layers. As water depletion of the soil is continued, the formation of such regions moves downwards. Regarding the distribution of soil hydraulic parameters, the length scale of lenses of coarse material was found to be the critical feature of structure to which the formation of dry spots is sensitive. Hence, in structures with large patches of coarse material (T1-fields), dry spots are expected to form earlier than in structures where coarse material is arranged in pathways (IT1-fields) or smaller patches (G1-fields).

During rewetting, dry spots get replenished if the infiltration rate at the top boundary is large enough to cause pressure gradients, which enable sufficient flow into coarse lenses.

Root water uptake continuously diminishes the rain rate at the top boundary within the root zone such that less water arrives in deeper layers. Replenishment is therefore the less efficient, the deeper dry spots are located. The point of time at which the rewetting front arrives, differs between locations in one soil layer, since the rewetting front is heterogeneous and reaches some locations later.

In Figure 6.2, which shows time series of mean and coefficient of variation of pressure head and saturation, extreme values of the coefficient of variation of pressure head indicate the formation of dry spots. Dry spots emerge only in T1-fields in layer 1 and layer 2. Rewetting occurs before dry locations develop in G1- and IT1- structures. Dry spots form close to the surface (layer1) shortly after the driest state is reached. The rewetting front is able to refill these regions such that the coefficient of variation recovers within approximately $5\,\mathrm{days}$. In layer 2, stressed, dry patches form from approximately $110\,\mathrm{days}$-$150\,\mathrm{days}$ simulation time. The minimum of pressure head and saturation occurs after $88\,\mathrm{days}$, it corresponds to the driest state in the scenario and indicates that the infiltration front reaches layer 2, on average, after $88\,\mathrm{days}$ simulation time. Hence, dry spots form after downwards moving rainwater has already reached layer 2. The formation of dry spots during rewetting can be explained by a heterogeneous infiltration front. Dry regions with low pressure head values are bypassed by the front at first and continue to dry. Such a case is illustrated in Figure 6.4 which shows the distribution of pressure head after $128\,\mathrm{days}$. At about $150\,\mathrm{days}$, these regions can be replenished. Figure 6.5 shows the distribution of the pressure head in the same realization after $128\,\mathrm{days}$ (with differently scaled axis) and $160\,\mathrm{days}$. The black bar marks the vertical position of layer 2. After $128\,\mathrm{days}$, one dry spot exists in layer 2 where pressure head values are equal to $-150\,\mathrm{m}$. After $160\,\mathrm{days}$, this location is not in the stressed, uptake reduced regime anymore, but has still pressure head values equal to $-3\,\mathrm{m}$.

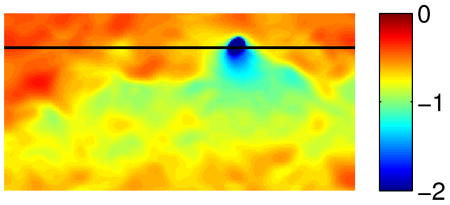

Figure 6.4: *Distribution of pressure head* $[\mathrm{m}]$ *in sample realizations of T1-fields after* $128\,\mathrm{days}$ *(black bar at layer 2). The rewetting front (indicated by high, red values) bypasses dry locations with low (blue) pressure head values.*

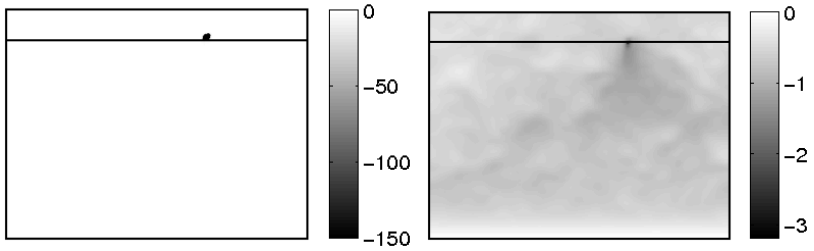

(a) (b)

Figure 6.5: *Distribution of pressure head* $[\mathrm{m}]$ *in sample realizations of T1-fields after* $128\,\mathrm{days}$ *(a) and after* $160\,\mathrm{days}$ *(b) (black bar at layer 2).*

To be able to predict how long the formation and recovery of dry spots take in each layer, typical timescales for it are estimated in the next section.

6.1.1 Estimation of time scales

Typical time scales for the formation and recovery of dry patches depend on the simulation settings such as the considered initial condition, infiltration rate and hydraulic properties of coarse lenses. A transient analytical solution of the heterogeneous 2D problem would provide the opportunity to derive a timescale over which critical pressure head values are reached. Such estimates are currently not available from the literature. However, timescales for capillary flow, gravity flow and root water uptake, which were derived in chapter 2.2.3 by means of a dimensionless form of the Richard's equation, can be used to obtain rough estimates. These are:

- Capillary flow: $t_1 = S_0 \frac{x_0^2 \phi_0}{K_0 h_0}$
- Gravity flow: $t_2 = \frac{S_0 \phi_0 x_0}{K_0}$
- Root water uptake: $t_3 = \frac{\phi_0 S_0}{R_0}$

t_3 corresponds to the time that is needed to entirely deplete spots with a given initial saturation S_0 by root water uptake with extraction rate R_0. Under the assumption that coarse lenses do not get refilled by capillary flow, t_3 can be used to approximate a timescale for the formation of dry spots.

t_2 corresponds to the time which is necessary to drain or imbibe a volume of water equal to $\phi_0 S_0$, at a flow rate which is equal to the saturated hydraulic conductivity, the maximum flux that can be driven by gravity. t_2 can be used to estimate the time needed to refill water depleted spots up to a saturation of S_0.

t_1 describes the time which water takes to flow over a distance of x_0, at a conductivity of K_0, driven by pressure forces.

Formation of dry spots

The timescale for the formation of dry spots corresponds to t_3 and is, in the following, referred to as t_{DS},

$$t_{DS} = \frac{\phi_0 S_0}{R_0} \tag{6.1}$$

where ϕ_0 is the porosity and R_0 the local root water uptake rate, depending on the vertical position. For S_0, the saturation in coarse lenses at the beginning of the simulation (initial saturation) is chosen. Figure 6.6 illustrates a cross-section of the initial saturation at the vertical position of layer 1 along 40 realizations. (The vertical position of layer 1-layer 3 is illustrated in Figure 6.1). At a mean saturation of 0.7, coarse lenses have an initial saturation in the range of 0.3-0.4.

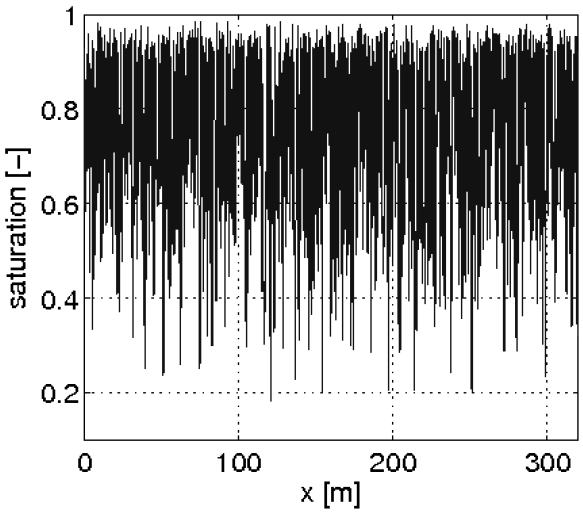

Figure 6.6: *Horizontal cross-section of initial saturation* $[-]$ *at vertical position of layer 1 along* 40 *realizations. At dry locations consisting of coarse material, the saturation is in the range of* 0.3.

With an initial saturation of 0.3 and 0.4, the characteristic timescales for the formation of dry spots are:

layer	$t_{DS}[d]$ $(S_0 = 0.3)$	$t_{DS}[d]$ $(S_0 = 0.4)$
layer 1	40.87	54.49
layer 2	115.82	154.43
layer 3	328.24	437.65

Table 6.1: *Timescales [in days] for formation of dry spots (for* $S_0 = 0.3$ *and* $S_0 = 0.4$*) in layer 1, layer 2 and layer 3.*

Note, that the estimated timescales can only be a rough estimate for the time at which dry spots form. t_{DS} depends on the initial saturation in coarse lenses, which, being a function

of the soil hydraulic parameters, varies between different coarse lenses. Furthermore, the estimate for t_{DS} implies that coarse lenses do not get replenished by the surrounding due to capillary flow. This is the case, if the time for capillary flow into coarse lenses is much larger than the time over which dry regions form. t_1 can be used to approximates the time for flow into coarse lenses due to pressure forces. If we choose $K_0 = K_{s0}\exp(-\alpha_0 h_0)$, t_1 is

$$t_1 = \frac{\phi_0 S_0 x_0^2}{h_0 K_{s0}\exp(-\alpha_0 h_0)} \tag{6.2}$$

where S_0 is the saturation and h_0, the pressure head in coarse lenses. x_0 is half the typical length scale of coarse lenses, which is here equal to $0.1\,\mathrm{m}$. For sample properties of coarse lenses ($K_{s0} = 1.4E-12\,\mathrm{m}^2$ and $\alpha_0 = 8.5E-4\,\mathrm{Pa}$), t_1 is approximately $1.3\,\mathrm{days}$ if h_0 is equal to $-1.0\,\mathrm{m}$, but approximately $85\,\mathrm{days}$ for a pressure head of $h_0 = -1.6\,\mathrm{m}$.

Thus, t_1 becomes very large, if the pressure head in coarse lenses exceeds a certain value. Since such conditions are not given at the beginning of the simulation, the estimated timescales t_{DS} tend to underestimate the time at which dry spots form. At layer 2 of test scenario D1, dry spots form approximately after $110\,\mathrm{days}$ which is estimated well by the calculated timescales in Table 6.1. In contrast, the theoretical timescales do not predict the temporal behavior at layer 1. Dry spots form approximately after $70\,\mathrm{days}$ instead of after 40 to $50\,\mathrm{days}$.

One has to be aware that the timescale for the formation of dry spots does not directly include the material properties, which omits the fact that local wilting occurs only in coarse lenses and is the more severe, the higher K_s and α in coarse lenses are. However, by assuming that the critical regions cannot be replenished, soil hydraulic properties as well as structure features are inherently considered. In our test case, this is obviously only given for T1-structures.

Recovery of dry spots

In the following, the time over which dry spots get replenished is estimated by the timescale for gravity flow, t_2 (see equation (2.40)). For S_0, we use the saturation in coarse lenses at steady state, x_0 is the typical length of a coarse lens. The net flow rate q_l of downwards streaming rainwater at a distinct layer z_0 is determined by the infiltration rate at the top boundary q and the amount of water potentially extracted by roots from the surface up to $z = z_0$, which equals $T_{z_0} = \int_{z_0}^{H} R_p dz$. Thus, in the equation for t_2, K_0 is replaced by the local net infiltration rate q_l in each layer which is given by $q - T_{z_0}$.

$$t_{RC} = S_{st}\frac{x_0\phi_0}{q_l} = \frac{S_{st}\phi_0 x_0}{q - T_{z_0}} \tag{6.3}$$

With x_0 equal to $0.2m$ and S_{st} equal to 0.2-0.3, we get the following timescales for each layer

layer	$T_{z_0}[mm/d]$	$t_{RC}(S_{st} = 0.2)$	$t_{RC}(S_{st} = 0.3)$
layer 1	0.4585	3.9532	5.9298
layer 2	1.4561	5.5033	8.2549
layer 3	1.8081	6.3871	9.5806

Table 6.2: *Timescales for replenishment of dry spots ($S_{st} = 0.2/0.3$) in layer 1, 2 and 3.*

The estimates for t_{RC} roughly agree with the observations from Figure 6.2 only in layer 1. In layer 1 the coefficient of variation recovers within approximately $5\,\mathrm{days}$, while it recovers in layer 2 within approximately $20\,\mathrm{days}$ if the time for recovery is estimated by the period of time which passes by from the occurrence of the peak value of CV_ψ until CV_ψ is back at moderate values. Formula 6.3 does not take into account that fluxes in coarse lenses are smaller than $q - \tau$ due to very low conductivities, especially in the beginning of the replenishment process, such that dry spots are initially bypassed by the infiltration front. Hence, the calculated timescales t_{RC} underestimate the observed period for recovery.

6.1.2 Periodic weather pattern

Natural weather patterns constantly fluctuate, rainy periods follow dry periods and vice versa. Depending on the season and geographical location, the frequency between raining and drying phases can differ from hours to months. In this work, it is illustrated that during drying cycles and in the beginning of rewetting periods, local stress may occur in lenses of coarse material, which leads to extreme values of the pressure head and a reduction of the uptake rate. The time over which locally dry regions form, can be roughly estimated by t_{DS} (equation (6.1)). If critical locations are refilled by rainwater before t_{DS}, wilted or locally stressed regions should not occur. With periodic infiltration patterns, it is assumed that transpiration is inhibited by rainwater covering the plant leaves' stomata during rainfall periods such that root water uptake phases have the same frequency but are shifted by half a period, compared to the infiltration pattern. In this way, root water uptake is zero during rainfall periods and non-zero in the absence of infiltrating rainwater at the top boundary. Since the timescale for formation is much larger than the observed timescale for recovery of dry spots, wilted regions, which form if the drying phase exceeds a time of t_{DS}, are always replenished during the rewetting phase. Thus, t_{DS} corresponds to a critical frequency for periodic infiltration pattern below which dry spots form. If drying and rewetting cycles are modeled with different frequencies, the timescale for recovery of dry spots t_{RC} has to be taken into account as well.

In the following we consider a scenario where both, root water uptake and infiltration are modeled according to a modified sine-function with frequency $f_d\,[\mathrm{d}^{-1}]$. The infiltration rate at the top boundary is given by $q = q_A sin'(t \cdot f_d)$ (negative values are set to zero, see chapter 4) where t is the time in days and q_A the amplitude of the infiltration pattern. The temporal pattern of the local root water uptake rate has the same frequency as the infiltration rate and is described by $\tau = -\tau_A * sin'(t \cdot f_d)$ (negative values are set to zero). q_A is equal to $6\,\mathrm{mm/d}$ and τ_A equal to $4\,\mathrm{mm/d}$. Due to the observations in the previous drydown-rewetting

scenario, which has the same net infiltration rate, we assume that at the beginning of a drying scenario, the saturation in coarse lenses is in the range of 0.2. According to equation 6.1, timescales which predict the formation of dry spots are obtained for each layer. For the calculation of these timescales, the periodic root water uptake rate ($\tau = -4 * sin'(t \cdot f_d)\,\mathrm{mm/d}$) is approximated by a constant value of $2\,\mathrm{mm/d}$. In scenarios where the upper boundary condition and the sink term are prescribed by periodic functions consisting of drying and wetting phases, dry spots are assumed to form if the drying phase exceeds t_{DS}. Thus, the timescale in each layer corresponds to a critical frequency of $f_{d,c} = \frac{\pi}{t_{DS}}$. Critical timescales and frequencies are summarized in Table 6.3.

$layer$	$t_{DS}[d]$	$f_{d,c}[1/d]$
layer 1	27.25	0.1153
layer 2	77.22	0.0407
layer 3	218.83	0.0144

Table 6.3: *Timescales and critical frequency for formation of dry spots ($S_0 = 0.2$).*

The estimated timescales are only rough estimates. As the flow problem considered here is more complex than in scenario D1, additional difficulties regarding the estimation of timescales arise. With periodic boundary conditions, the mean of pressure head and saturation fluctuate in response to imposed infiltration and root water uptake cycles. Extreme values of mean pressure head and saturation depend on the frequency of applied cycles. Thus, S_0, the saturation at the beginning of the drying process is dependent on the frequency and difficult to properly estimate in advance.

Moreover, only at the surface, drying periods are clearly defined. Sink term and infiltration at the top boundary are prescribed by periodic cycles which are temporally shifted. Since the rewetting front proceeds from the surface downwards such that it arrives at deeper layers later whereas root water uptake cycles are simultaneous over the whole domain, the temporal pattern of drying and rewetting phases changes with depth. If drying and wetting phases overlap at deeper layers due to a retarded arrival of the rewetting front, pure drying phases are shortened which reduces the risk of dry spots. Thus, with increasing depth, the calculated frequencies overestimate simulated critical frequencies.

In the first layer, the critical frequency is $0.1153\,\mathrm{d}^{-1}$. Therefore, two cases are analyzed, one where the frequency is below the critical frequency in layer 1 ($f_d = 0.1\,\mathrm{d}^{-1}$) and one where it is above ($f_d = 1.0\,\mathrm{d}^{-1}$). With a low frequency of $f_d = 0.1\,\mathrm{d}^{-1}$, dry spots are expected to form in the first layer. In layer 2 and 3, dry spots are not expected since the applied frequency of drying cycles is above the theoretical frequencies in layer 2 and 3, which overestimate simulated critical frequencies.

Time series of mean and CV of pressure head and saturation are shown in Figure 6.7 for the high frequency case ($f_d = 1.0\,\mathrm{d}^{-1}$) and in Figure 6.8 for the low frequency case ($f_d = 0.1\,\mathrm{d}^{-1}$). In both cases, mean and CV of pressure head and saturation fluctuate in each layer around steady state values. Fluctuations of pressure head and saturation attenuate with depth. Superimposed to the fluctuations, the upper part of the domain first drains, due to

a uniform initial pressure head distribution, and is then rewetted since water enters the domain in total (q_A is larger than τ_A). For this reason, only times after $100\,\mathrm{days}$ simulation time are shown in Figure 6.7 and Figure 6.8. Very large values of CV_ψ indicate the occurrence of localized extreme values of the pressure head which is in turn related with local wilting or at least stress. As expected, dry regions form only in layer 1 if infiltration cycles with a frequency of $f_d = 0.1\,\mathrm{d}^{-1}$ are imposed. The pressure head dries up to a value of $12\,\mathrm{m}$ on average and the coefficient of variation reaches a value of 18. Extreme pressure head values occur in all structures, but first and most severely in T1-fields which have large patches of coarse material. Dry spots recover in IT1-fields slightly faster than in G1- and T1-fields. If boundary conditions vary with a frequency of $f_d = 1.0\,\mathrm{d}^{-1}$, mean and coefficient of variation of pressure head remain at moderate values indicating that local wilting does not occur in the test case considered here.

It should be mentioned that dry spots could generally still occur with frequently applied, but short rainfall cycles although the period of one drying phase does not exceed the estimated timescale t_{DS}. This is the case if less water is replenished into low conductive patches during (e.g. short) rainfall phases than is taken up by roots during (e.g. longer) drying phases, which might occur as the infiltration front initially bypasses low conductive regions. Then, dry spots form within several drying phases until they finally persist throughout the entire simulation time, also during rainfall events.

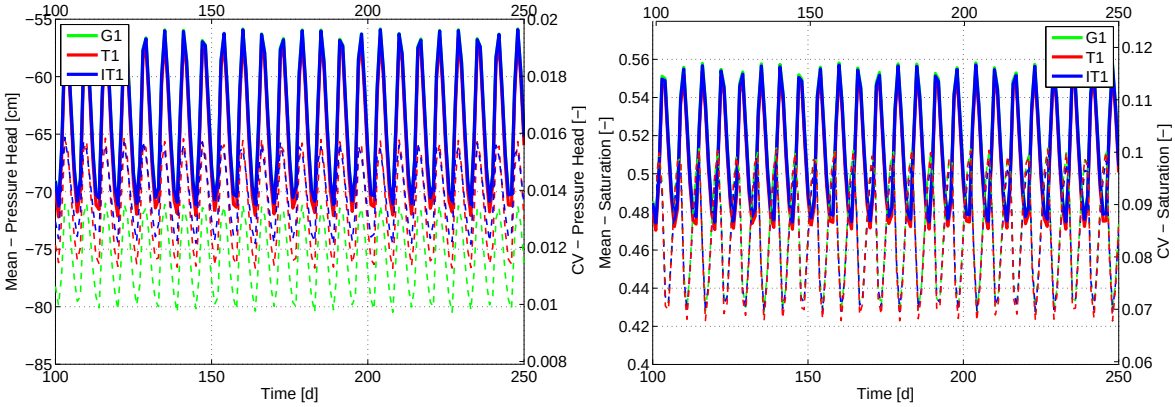

(a) layer 1

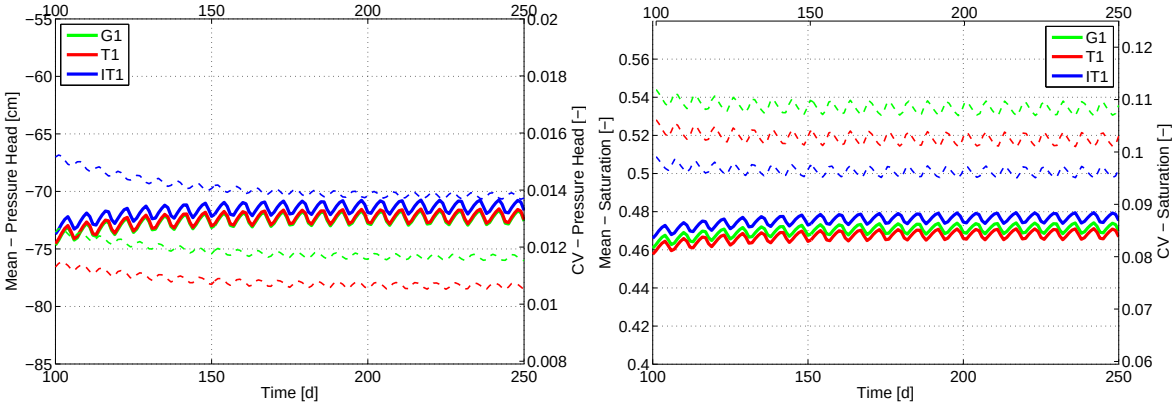

(b) layer 2

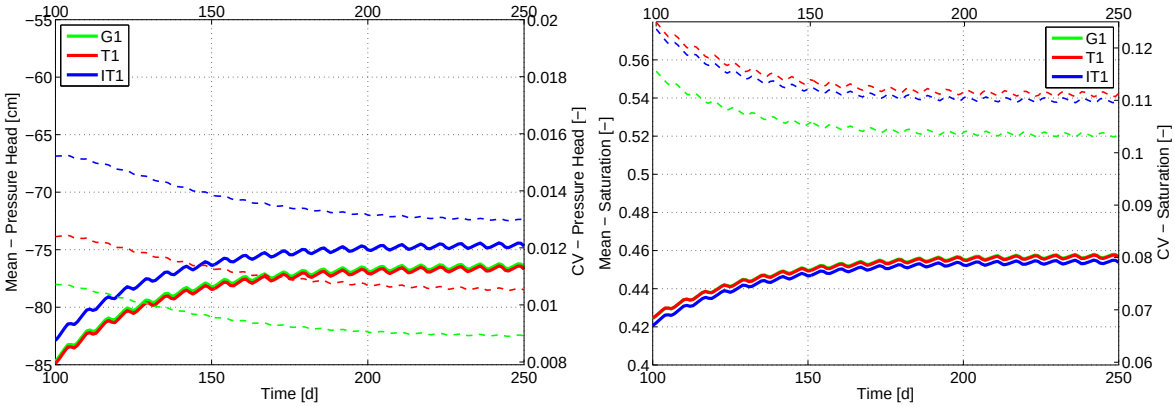

(c) layer 3

Figure 6.7: *Mean (solid line) and coefficient of variation (dashed line) of pressure head and saturation vs. time in layer 1 (a), layer 2 (b) and layer 3 (c). With a high frequency of* $f_d = 1.0\,\mathrm{d}^{-1}$*, dry spots do not form.*

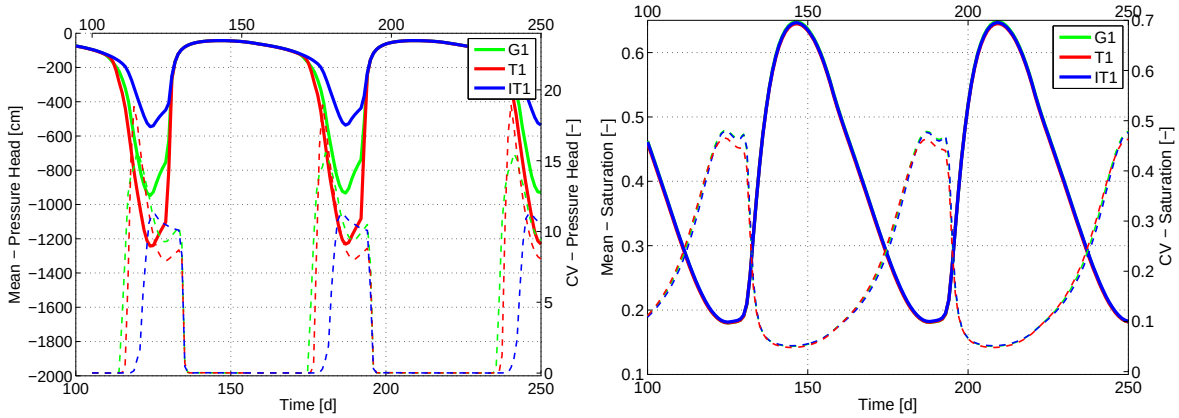

(a) layer 1

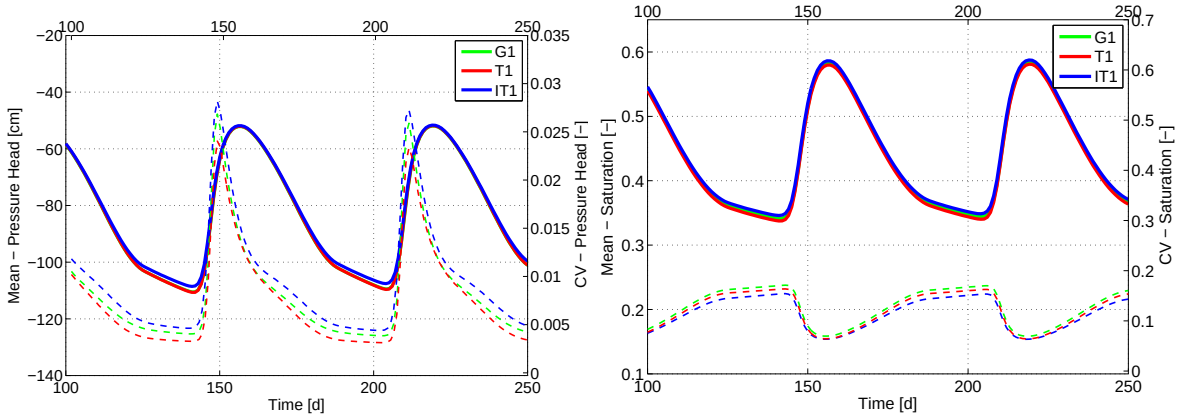

(b) layer 2

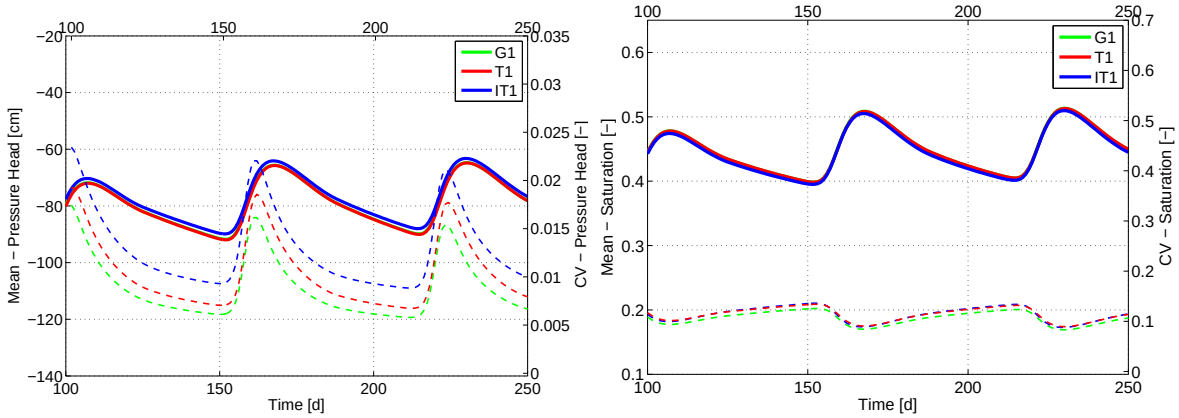

(c) layer 3

Figure 6.8: *Mean (solid line) and coefficient of variation (dashed line) of pressure head and saturation vs. time in layer 1 (a), layer 2 (b) and layer 3 (c). With a low frequency of* $f_d = 0.1\,\mathrm{d}^{-1}$*, dry spots form in the first layer during drying cycles.*

6.1.3 Crop yield

The yield of crop production is directly linked to the global actual transpiration $T_{act} = \int R_1 dV \, \mathrm{m}^2/\mathrm{s}$. With the standard model for root water uptake, where compensation mechanisms are not included, we predict a decrease of the local actual uptake rate and, thus, a decrease of the global actual uptake rate if locally wilted spots form. In the following, the impact of local wilting on the global actual uptake is quantified. In the considered drydown and rewetting scenario (scenario D1 in Table 4.2), local wilting occurs only in T1-structures and the stressed regions are very small. Figure 6.9 illustrates the summed up difference between local potential uptake rate and local actual uptake rate, $\sum_{layer}(R_p - R_1)$, versus time in layer 2 of T1-structures. The maximum reduction in layer 2 equals less than one percent of the potential value. Thus, the yield output is practically not affected in this scenario.

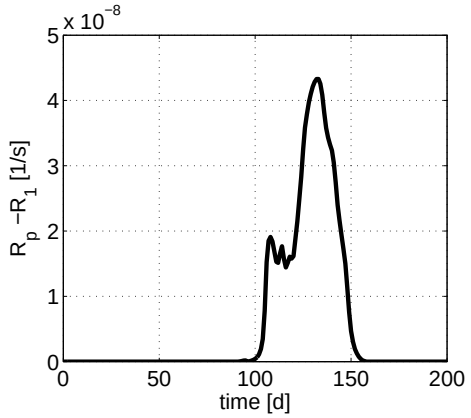

Figure 6.9: *Difference of local potential uptake rate R_p and local actual uptake rate R_1 vs. time for T1-fields in layer 2.*

With periodic weather patterns (low frequency case), dry spots form in the first layer. The difference of local potential uptake rate and local actual uptake rate in layer 1 is shown in Figure 6.10a. The local uptake rate is periodically reduced by approximately 4.5 percent of the potential value which leads to a reduction of the total yield, summed up over the entire simulation time, of only 0.7 percent. Figure 6.10b shows the global actual and global potential uptake. The deviation between global actual and global potential uptake is so small that it cannot be recognized in the graph.

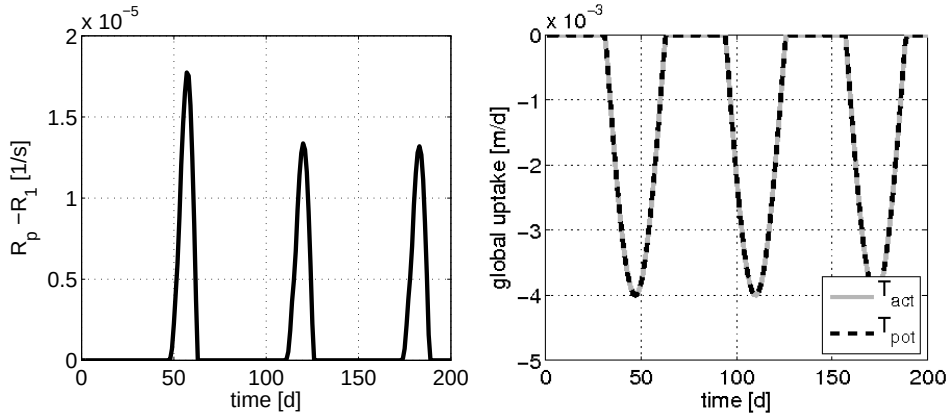

(a) (b)

Figure 6.10: *Difference of local potential uptake rate R_p and local actual uptake rate R_1 vs. time for T1-fields in layer 1 (a) and global actual and global potential uptake* $[\mathrm{m/d}]$ *vs. time (b). Periodic cycle scenario, low frequency* $f_d = 0.1\,\mathrm{d}^{-1}$.

In the considered test cases, crop yield is only remarkably decreased during drying periods, but hardly affected over the entire time. This would of course change, if longer drying periods, plants with deeper root systems or fields with larger lenses or lenses of coarser material are considered.

6.2 Variability of pressure head and saturation

This section treats the variability of pressure head and saturation in differently structured soils and under consideration of root water uptake, during drying and rewetting phases. Variability can be quantified by the coefficient of variation or by the variance. At steady state conditions, little influence of structure and root water uptake on the variance of pressure head is observed with the chosen model settings and unless dry spots form. Changes of the variance of pressure head vs. depth due to root water uptake are induced by changes of the mean value. Under transient conditions, larger sensitivity to factors such as structure and root water uptake is expected such that the standard deviation of saturation and pressure head as function of the mean value changes. The standard deviation of saturation as function of the mean value, $\sigma_S(< S >)$, is addressed by various experimental and numerical studies. During drying from very wet states, $\sigma_S(< S >)$ was shown to follow a parabolic curve. σ_S initially increases until a maximum is reached and decreases during further drying, (e.g. Ryu and Famiglietti, 2005; Choi and Jacobs, 2007; Choi et al., 2007; Harter and Zhang, 1999). Root water uptake influences drying patterns and might have a remarkable influence on the standard deviation of saturation and pressure head. Teuling and Troch (2005) emphasized the importance of root water uptake for the relationship of σ_S and $< S >$, the exact impact is however unclear. Another important issue is the change of variability during rewetting. During rewetting, the mean saturation changes from low to high values. However, with respect to the variability over time, rewetting cannot be regarded as reverse process of drying since, due to heterogeneous infiltration fronts, rewetting patterns differ substantially from drying patterns.

We focus in the following mainly on two questions. First, what influence does root water uptake have on the variability of pressure head and saturation during drying and rewetting. Second, when does the state of maximum variability occur with respect to the mean and which role does root water uptake and structure play for it. We analyze the coefficient of variation and the variance of pressure head and saturation versus time in comparison to the mean using test scenario D1, (simulation settings are listed in Table 4.2). Time series of mean and variance of pressure head and saturation are shown in Figure 6.11. In the following, we discuss the drying and rewetting part of the scenario separately.

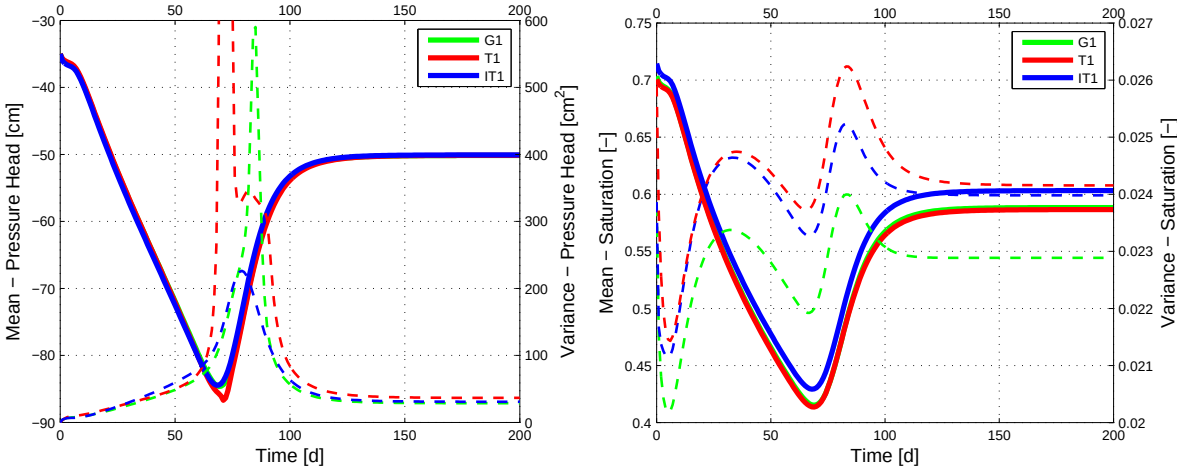

(a) layer 1

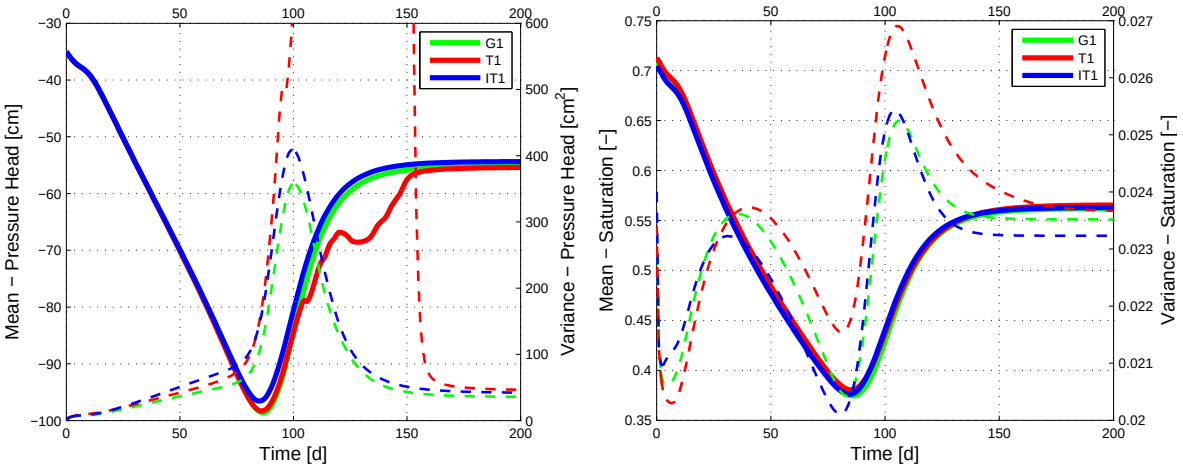

(b) layer 2

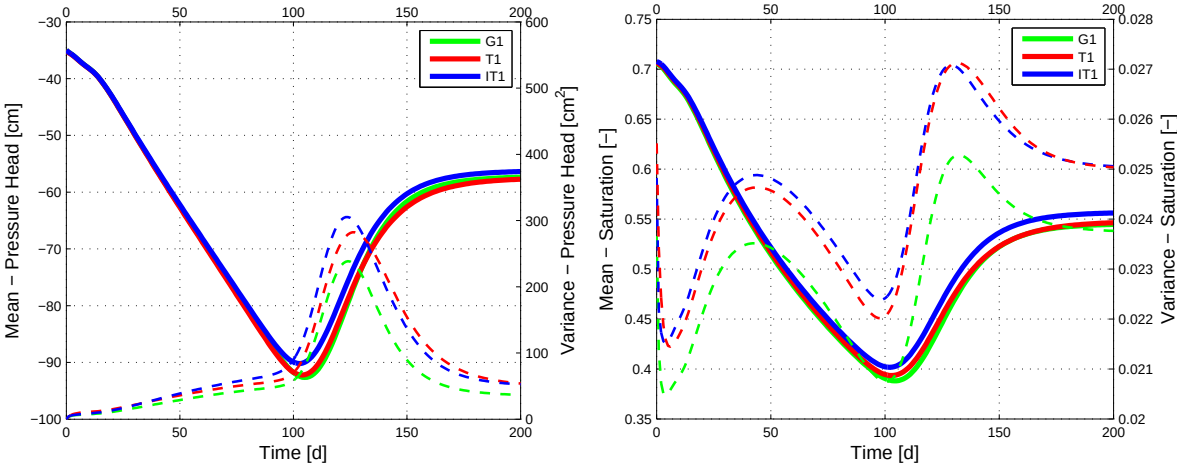

(c) layer 3

Figure 6.11: *Mean (solid line) and variance (dashed line) of pressure head (left) and saturation (right) vs. time for G1-, T1-, and IT1-fields, at layer 1 (a), layer 2(b) and layer 3(c).*

6.2.1 Drying of the soil

In the first part of scenario D1, the domain dries due to drainage and root water uptake. In the following, we analyze the variance of pressure head and saturation in G1-, T1- and IT1-fields during drying where the focus is set on the impact of root water uptake in comparison to scenarios where the domain dries due to drainage alone.

Independent of the considered processes, the pattern of the hydraulic conductivity field depends on the water content and changes during drying. At some point, coarse material becomes less conductive than fine material such that the variance of the hydraulic conductivity is minimal at the crossover point. At drier states, the pattern of the hydraulic conductivity field under fully saturated conditions is reversed. For a more detailed description, we refer to chapter 5.1. Test scenario D1 starts at a uniform initial condition of $\psi = -35\,\mathrm{cm}$ where coarse material is already less conductive than fine material. With further drying, the variance of the conductivity field increases. The variance of pressure head increases accordingly as well and the variance of saturation follows a parabolic curve. Without root water uptake, the pressure head is in coarse material at higher pressure head values than in fine material. The saturation is at lower values in coarse material. An example is shown in Figure 6.12. The loghydraulic conductivity f and the cross-section of f at layer 2 of the sample realization is illustrated in Figure 6.13.

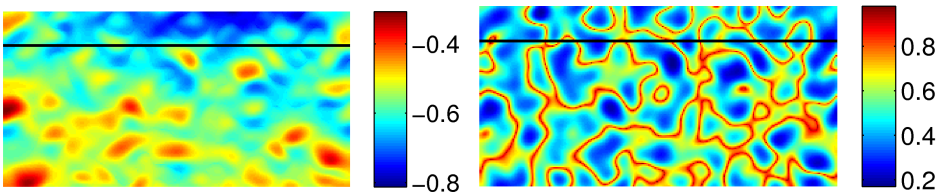

(a) (b)

Figure 6.12: *Sample realization of pressure head $\psi\,[\mathrm{m}]$ (a) and saturation $S\,[-]$ (b) without root water uptake. The black bar indicates the vertical position of layer 2.*

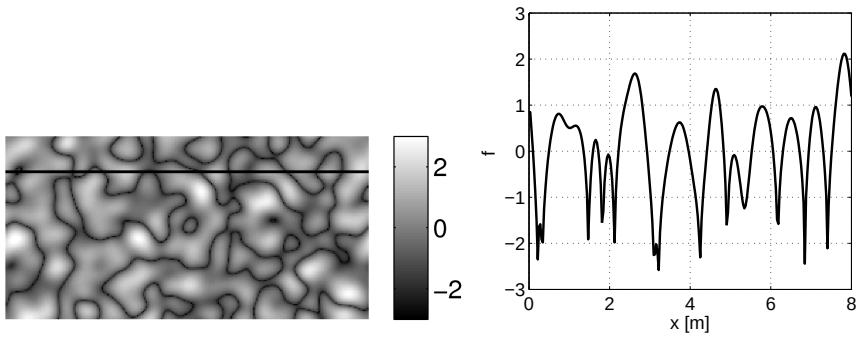

(a) (b)

Figure 6.13: *Sample realization of T1-fields: loghydraulic saturated conductivity f (a) and horizontal cross-section of f at layer 2 (b).*

Influence of root water uptake on pressure head

Root water uptake extracts water and decreases pressure head values at all locations. As explained in chapter 5.2.2, a drying front spreads from below, into coarse lenses if the replenishment rate from top is not sufficient to meet the water taken up by roots. Before the pressure head in coarse lenses is at lower values than the surrounding, the contrast between pressure head values in coarse and surrounding material is decreased by root water uptake such that the variance is smaller in scenarios with root water uptake than the variance in scenarios without root water uptake.

An example is shown in Figure 6.14 which compares the cross-section of pressure head in a sample realization of T1-fields in scenario D1 after $60\,\mathrm{days}$ with an equally dry scenario without root water uptake. Including root water uptake, high and low pressure head regions are slightly attenuated indicating a smaller variance in the sample realization. The ensemble variance at layer 2 after $60\,\mathrm{days}$ is also reduced by root water uptake.

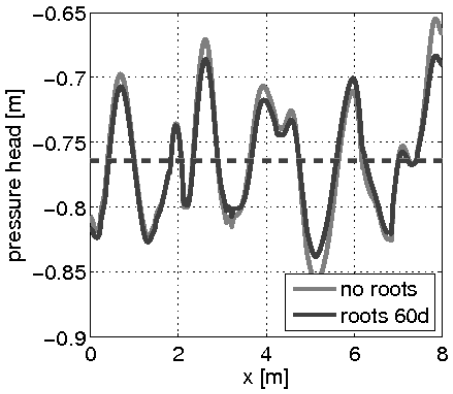

Figure 6.14: *Cross section of pressure head* $\psi\,[\mathrm{m}]$ *in T1-fields with and without roots after* $60\,\mathrm{days}$ *in layer 2. (The dashed line corresponds to the mean value of pressure head in layer2, which is identical for both scenarios.)*

By homogenizing the pattern temporarily, root water uptake may lead to a decrease of the variance of pressure head over time. As extraction is continued, pressure head values in coarse lenses become smaller than in the surrounding material. With further drying, critical values are reached such that dry spots form leading to extreme values of the variance of pressure head. Due to a continuous distribution of soil hydraulic parameters, the change of the distribution of pressure head during drying is complex and the onset of homogenizing and formation of dry spots differs between locations at one layer. It is therefore unlikely that the ensemble variance of pressure head decreases over time due to root water uptake. With the parameters chosen, we observe a decrease of the variance of pressure head only in single realizations. The ensemble variance, in contrast, increases always.

An example for the changing pressure head distribution is illustrated in Figure 6.15a, which shows a cross-section of the pressure head in layer 2 at different times for a scenario, where rewetting occurs later than in scenario D1. In the sample realization, the variance decreases from $80\,\mathrm{days}$ to $100\,\mathrm{days}$ simulation time. At the location marked by the red line, the pressure

head changes from values that are above to values below the mean such that the distribution of pressure head is homogenized. With further drying, pressure head values of $-2\,\mathrm{m}$ to $-3\,\mathrm{m}$ occur in layer 1 (Figure 6.15b) and in layer 2 after $120\,\mathrm{days}$ simulation time, which indicate the formation of dry spots and lead to an increase of the variance of pressure head from $100\,\mathrm{days}$ to $120\,\mathrm{days}$. (The vertical position of layer 1 and layer 2 with respect to the root density are illustrated in Figure 6.1).

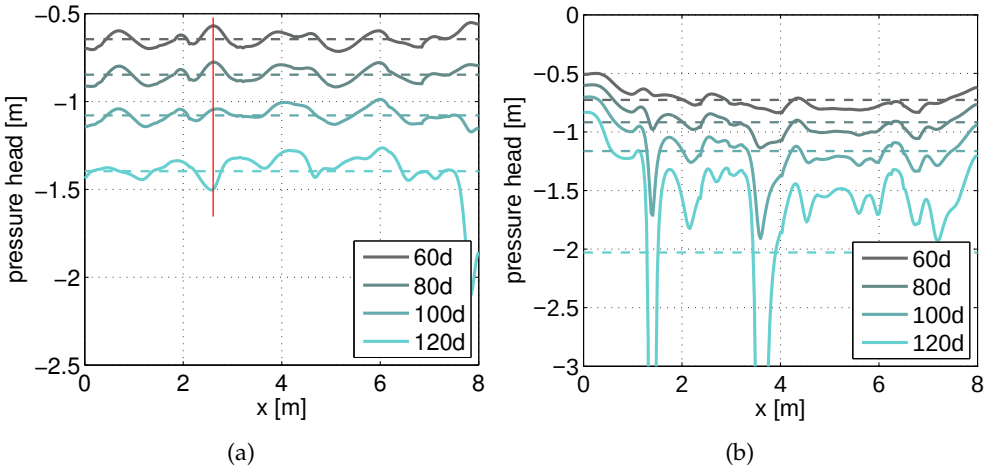

Figure 6.15: *Cross-section of pressure head* $\psi\,[\mathrm{m}]$ *in sample realizations of T1 fields at different times in layer 2 (a) and layer 1 (b) that is located* $62.5\,\mathrm{cm}$ *above layer 2.*

Thus, in our test case, root water uptake has a rather homogenizing effect on the distribution of pressure head during drying unless high extraction rates or long drying phases in T1-fields are considered, which lead to the formation of dry spots and, thus, to extreme values of the variance.

Influence of root water uptake on saturation

The distribution of saturation is uniquely related to the pressure head through the pc-S relationship that is modeled according to van Genuchten (1980) in this work (equation (4.3)). However, S depends also on the random parameter α. α is heterogeneously distributed due to the fact that a larger pore size diameter is related with smaller capillary forces. Water drains therefore faster and saturation is lower in coarse material than in fine material. While the pattern of pressure head might change during drying due to root water uptake, saturation is always lower at locations of coarse material since the influence of α dominates.

The pattern of saturation remains with changing pressure head values, but the variance of saturation is affected by root water uptake compared to equally dry states without root water uptake. Under consideration of root water uptake, local extremes of the pressure head distribution are attenuated. Since high pressure head values are related to coarse material and low values to fine material, wet locations are wetter and dry locations drier with root water uptake. Hence, the variance of saturation is larger if root water uptake is considered.

Figure 6.16 shows an example where the variance of saturation in the scenario with roots is slightly larger than in the case without roots. Figure 6.16a shows the cross-section of saturation in a sample realization of T1-fields of scenario D1 after $60\,\mathrm{days}$ in comparison to an equally dry scenario without root water uptake. As the two curves are almost identical, the line, representing the no-root case, can hardly be recognized. Figure 6.16b illustrates the difference between both cases, the saturation at layer 2 with roots (dark colored line in (a)) subtracted by the saturation at layer 2 without roots (light colored line in (a)). Positive values indicate that the saturation under consideration of root water uptake is larger, negative values indicate that it is smaller. A comparison of Figure 6.16(b) with a cross-section of the loghydraulic conductivity f at layer 2, Figure 6.13b, yields that the saturation in the scenario with root water uptake is higher at fine, wet locations and smaller than the saturation without root water uptake at coarse, dry locations.

Thus, with the parameters chosen, root water uptake increases the variance slightly during drying, in comparison to cases without root water uptake.

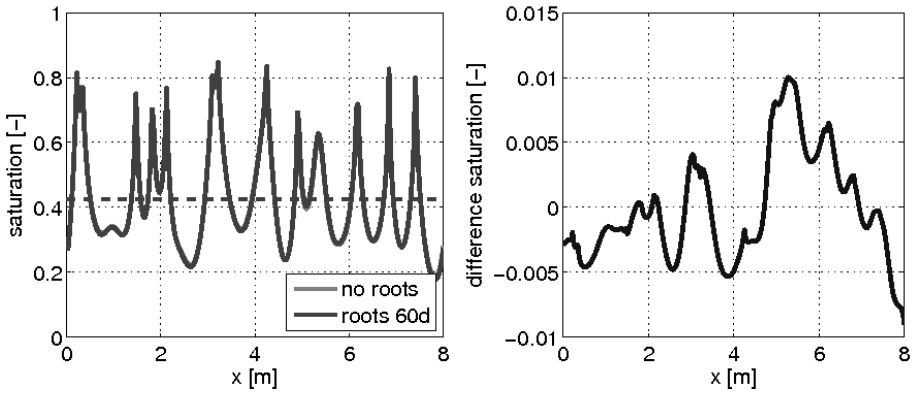

(a) (b)

Figure 6.16: *Cross section of saturation $S\,[-]$ in T1-fields with and without root water uptake after* $60\,\mathrm{days}$ *(a) in layer 2. (The dashed line corresponds to the (identical) mean value of saturation in layer2 of both scenarios.) (b) illustrates the difference between the saturation with and without root water uptake (dark colored line minus light colored line).*

6.2.2 Rewetting of the soil

The drying phase in test scenario D1, analyzed in the last section, is followed by a rewetting phase. During rewetting, rainwater infiltrates with a constant rate at the (artificial) top boundary and root water uptake continues as before. Time series of mean and variance of saturation and pressure head were presented in Figure 6.11. Due to the variation of soil hydraulic parameters, preferential flow paths and flow impeding parts of the soil exist which lead to a heterogeneous infiltration front. A heterogeneous front can be separated into first arrivals (in the following referred to as tips), mean front and tail. A sketch of a heterogeneous infiltration front is illustrated in Figure 6.17.

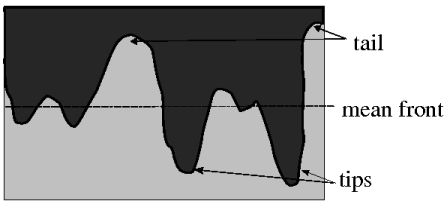

Figure 6.17: *Sketch of heterogeneous rewetting front.*

The rewetting phase is analyzed, as an example, using one sample realization of G1-fields. The loghydraulic conductivity and the corresponding cross-section at layer 2 is shown in Figure 6.18. In the following discussion, we distinguish between arrival of tips and arrival of the mean front.

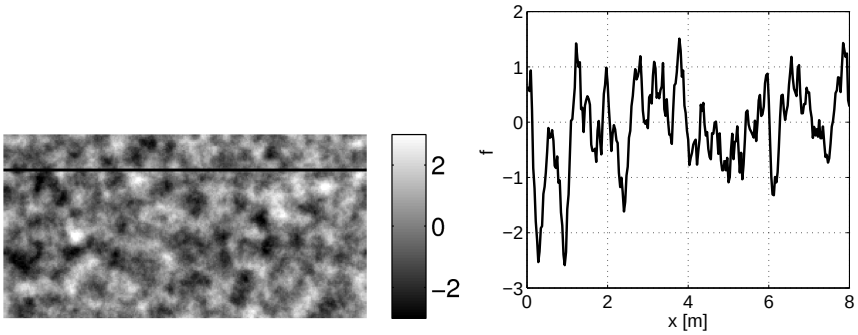

(a) (b)

Figure 6.18: *Loghydraulic conductivity f in sample realization of G1-fields (a), (the black bar indicates the vertical position of layer 2). Cross-section of f at layer 2 (b).*

Arrival of tips

The minimum of mean pressure head or saturation during a drying-rewetting scenario corresponds to the driest state before downwards moving rainwater arrives. Rewetting of one layer of the soil starts with the arrival of tips. The pressure head increases at locations which have been rewetted, while the pressure head continues to decrease (due to root water uptake and drainage) at locations which have not yet been rewetted. The time at which the minimum of mean pressure head (saturation) occurs, thus, represents the mean arrival time of tips of the pressure head (saturation) front.

Figure 6.19 illustrates the arrival of tips of the pressure head and saturation front at layer 2 for a sample realization of G1-fields. For better perceptibility, the distributions are illustrated referred to a distribution when the rewetting front has not reached the domain. Here, the distributions of pressure head and saturation at the arrival of tips are subtracted by the distributions after $60\,\mathrm{days}$ simulation time. The incoming infiltration front is clearly visible, first tips reach the vertical postition of layer 2 which is indicated by a black bar.

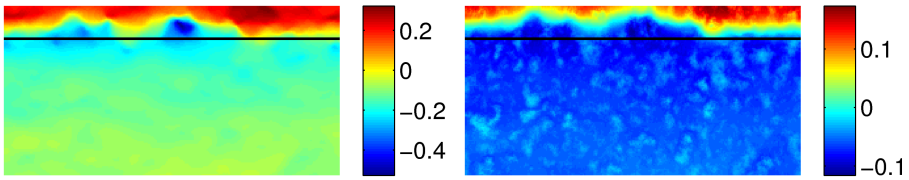

(a) (b)

Figure 6.19: *Distribution of pressure head* $[\mathrm{m}]$ *after* $88\,\mathrm{days}$ *(a) and saturation* $[-]$ *after* $87\,\mathrm{days}$ *(b) (with respect to the distributions after* $60\,\mathrm{days}$*) in a sample realization of G1-fields (black bar at layer 2) .*

Through the arrival of tips, the variance of pressure head and saturation in Figure 6.11 increases quickly since pressure head and saturation values increase at rewetted locations while values continue to decrease due to drainage and root water uptake at location that are not yet rewetted.

Arrival of mean front

The variance is maximum when rewetted and not yet rewetted locations balance each other. It decreases when most locations are rewetted such that also locations with low values of pressure head increase. Figure 6.20 shows a cross-section of ψ and S in layer 2 of a sample realization of G1-fields at three different times of the simulation, when $< \psi >$ and $< S >$ peak (red line), when σ^2_ψ and σ^2_S peak (green line) and when σ^2_ψ and σ^2_S are decreased again (blue line). After $101\,\mathrm{days}$, low pressure head values increase or do not decrease anymore such that the variance of pressure head starts to decrease.

The peak value of the variance of pressure head and saturation occurs therefore during the rewetting process and the time at which the variance of pressure head and saturation peaks, can be a measure for the arrival time of the mean infiltration front. Figure 6.21 illustrates the distribution of ψ and S at the time that σ^2_ψ and σ^2_S peak in layer 2 of G1-fields (subtracted by the distributions after $60\,\mathrm{days}$). The time lag between maximum of mean (arrival of tips) and maximum of variance (arrival of mean front) is a measure for the width of the horizontally averaged infiltration front (tail excluded). This aspect is discussed in section 6.2.3.

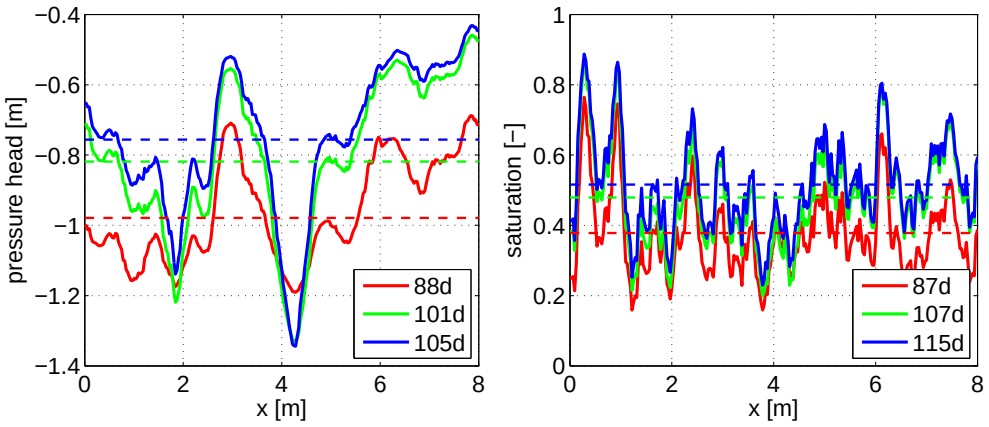

(a) (b)

Figure 6.20: *Cross section of pressure head* [m] *(a) and saturation* [−] *in sample realizations of G1-fields at different times. Since the pressure head front is heterogeneous and reaches dry locations later, low pressure head values are lower and high values are higher, which leads to a larger variance after* 101 days *than after* 88 days.

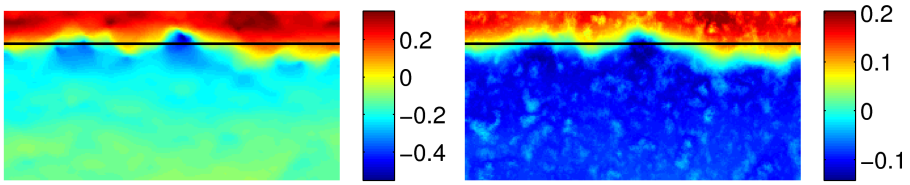

(a) (b)

Figure 6.21: *Distribution of pressure head* [m] *after* 101 days *(a) and saturation* [−] *after* 107 days *(b) (with respect to the distributions after* 60 days*) in a sample realization of G1-fields.*

Influence of root water uptake

The peak value of the variance of pressure head and saturation during rewetting is expected to be higher in scenarios with root water uptake than in scenarios without root water uptake which are at the arrival of the front at a comparable mean pressure head or mean saturation since, under consideration of root water uptake, locations that are reached later by the infiltration front continue drying by root water uptake and drainage instead of by drainage only. Therefore, if root water uptake is considered, not yet rewetted locations reach lower pressure head values while more tips arrive such that the variance has larger peak values than without root water uptake. Figure 6.22 illustrates the increase of variance of pressure head and saturation (at layer 1) due to a heterogeneous infiltration front for two scenarios with and without root water uptake which have a similar net infiltration rate q_l at layer 1. The peak values of the variance of pressure head and saturation are slightly enlarged by root water uptake. However, due to the sensitivity of the variance of saturation on the mean value and the applied infiltration rate at the top boundary, the variances of saturation, with

and without root water uptake, are difficult to compare. These aspects have to be analyzed more detailed in the future.

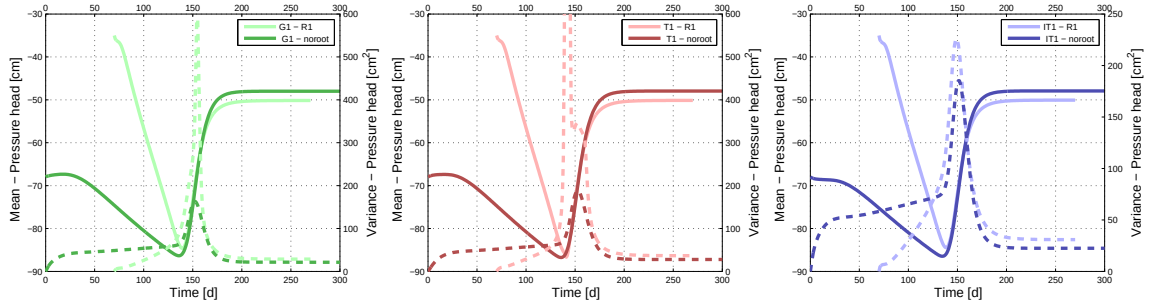

(a) Pressure head

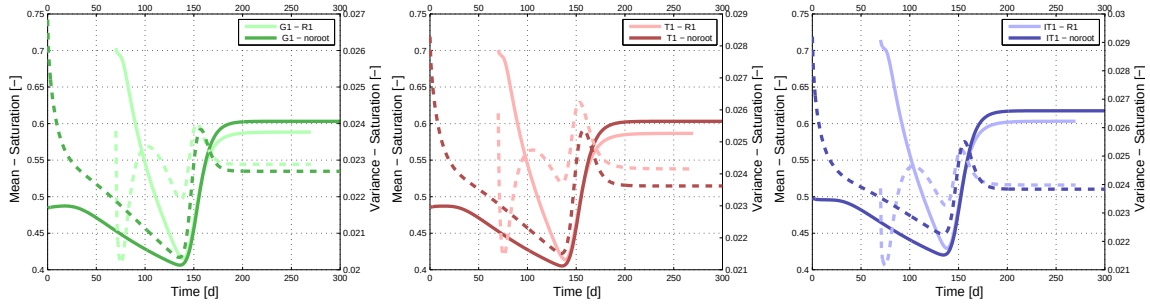

(b) Saturation

Figure 6.22: *Mean (solid line) and variance (dashed line) of pressure head (a) and saturation (b) vs. time in layer 1 of G1- (left), T1- (middle), and IT1-fields (right) with uptake strategy 1 (light colored lines) and without root water uptake (dark colored lines).*

Maximum variability

It was shown, that with a heterogeneous infiltration front, the extremes of mean and variance of pressure head and saturation occur temporally shifted. The variability can also be described by the coefficient of variation which is the variance divided by the squared mean. If the peak value of the variance of pressure head or saturation during rewetting is very high, the temporal development of the coefficient of variation is affected such that its maximum is shifted as well, compared to the minimum mean value.

Unless dry spots form, variations of the pressure head during drydown are rather small such that, during rewetting, the variance of pressure head (at a distinct layer) is strongly affected by the arrival of tips. The coefficient of variation of pressure head is thus dominated by the variance and peaks at about the same time as the variance of pressure head.

Due to the large retention of water in fine material, the distribution of the saturation is under dry conditions more heterogeneous than the pressure head distribution. Incoming rainwater infiltrates first into fine, already wet material which increases the mean value, but leads only to small changes of the variance. The temporal shape of the coefficient of variation of

saturation is therefore dominated by the temporal shape of the mean saturation. In scenario D1, the coefficient of variation of saturation peaks $1 - 7\,\mathrm{days}$ later than the minimum of the mean saturation, while the variance of saturation peaks approximately $14 - 28\,\mathrm{days}$ later. (Time series of mean and variance or coefficient of variation of pressure head and saturation are shown in Figure 6.11 and Figure 6.2).

6.2.3 Width of the horizontally averaged infiltration front

As explained in the previous section, the minimum of the mean of pressure head or saturation in Figure 6.11 represents the mean arrival time of tips and the maximum of the variance, the arrival time of the mean front. The time lag between extremes of mean and variance can be seen as a measure for the width of the front. The propagation of the infiltration front is affected by several factors such as dryness of the soil, soil hydraulic properties or precipitation. Root water uptake decreases the net infiltration rate with increasing depth by continuous extraction of water within the root-zone and therefore, influences the width of the front.

Figure 6.23 illustrates a widening of the front with depth in all structures. The times at which the extremes of $< \psi >$, σ^2_ψ and CV_ψ and the extremes of $< S >$, σ^2_S and CV_S occur are represented by colored symbols. The distance between peak times of mean and peak times of variance of pressure head or saturation increases from layer 1 to layer 3. In layer 1 and layer 2, symbols representing the peak time of pressure head in T1-fields are omitted since, due to the formation of dry spots during rewetting, the temporal shape of CV_ψ and σ_ψ is dominated by extreme values such that the arrival of the pressure head front cannot be assessed in such cases. Small differences of arrival times of tips and mean front exist between the structures, but a clear pattern is not evident.

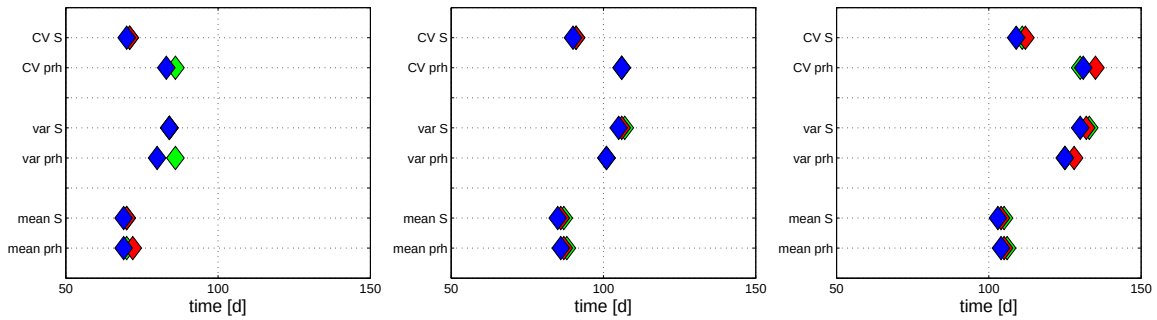

(a) layer 1 (b) layer 2 (c) layer 3

Figure 6.23: *Peak time of mean, variance and coefficient of variation of pressure head and saturation in layer 1(a), layer 2(b), layer 3(c). Green symbols represent G1-fields, blue, T1-fields and red symbols IT1-fields.*

If the net infiltration rate q_l, which reaches each layer, is the dominant factor controlling the width of the front, the time lag between peak time of mean and variance of

pressure head and saturation should be comparatively constant but dependent on the infiltration rate in cases without root water uptake. This aspect is discussed in the next section.

Flow without root water uptake

The influence of root water uptake on pattern and variability of pressure head and saturation during rewetting and drying was treated in the previous chapters. This section focuses on the time lag between mean and variance of pressure head or saturation in scenarios where root water uptake is not taken into account and where the infiltration rate at the top boundary is comparable to the net infiltration rate q_l in the upper or in the lower part of the root-zone in scenarios with root water uptake. It is tested, whether the infiltration rate is the dominant factor which determines the width of the front.

In scenarios which include root water uptake (with an infiltration rate of q_{root} and a root water uptake rate of τ), the amount of downwards moving rainwater is continuously decreased by root water uptake. Close to the surface, the net infiltration rate q_l is similar to q_{root} and in the lower part of the root zone, it is similar to $q_{root} - \tau$. If root water uptake is not considered, q_l is constant for all depth. Thus, in drydown and rewetting scenarios where rewetting with these infiltration rates (q_{root} and $q_{root} - \tau$) and drydown due to drainage, without root water uptake, is considered, the time lag between minimum of mean and maximum of variance of pressure head and saturation, which is taken as a measure for the width of the front, is expected to be relatively constant with increasing depth and larger for a smaller infiltration rate of $q_{root} - \tau$.

In the test scenarios without root water uptake, infiltration is applied from the 40th day forward (on the artificial boundary), starting with an uniform initial condition of ψ equal to $-50\,\mathrm{cm}$ (scenario D2, D3 in Table 4.2). The initial condition is chosen such that the mean pressure head profiles after $40\,\mathrm{days}$ (when infiltration starts on the artificial top boundary) have a similar shape in the scenario with root water uptake and without root water upake (see Figure 6.24).

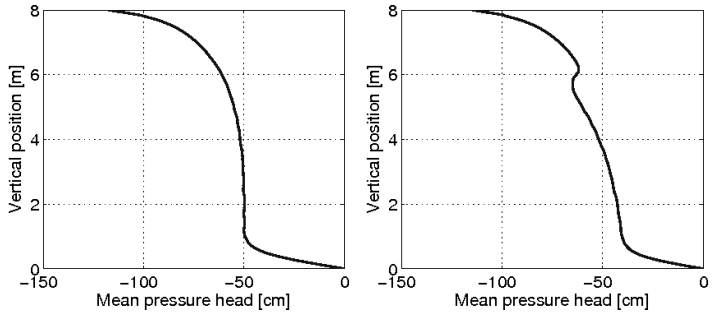

Figure 6.24: *The initial condition in the scenario without root water uptake is chosen such that the mean of pressure head vs. vertical position after* $40\,\mathrm{days}$ *(when infiltration starts) (a) is similar as in the scenario with root water uptake term* R_1 *(b). Note, that the artificial top boundary extends from a vertical position of* $6\,\mathrm{m}$ *to* $8\,\mathrm{m}$.

With the parameters of scenario D1, discussed in the previous section, q_{root} equals $4\,\mathrm{mm/d}$ and $q_{root} - \tau$ equals $2\,\mathrm{mm/d}$. Figure 6.25 and Figure 6.26 illustrate the times at which the extremes of mean and variance of pressure head and saturation occur for both infiltration rates. The time lag between minimum of $< \psi >$ and σ^2_ψ is more or less constant at all depth. It depends on the infiltration rate and increases with decreasing infiltration rate. For a high infiltration rate, the time lag between extremes of mean and variance is approximately $15 - 19\,\mathrm{days}$, which is similar to the time lag in layer 1 in scenario D1 with root water uptake. For a low infiltration rate, the time lag is approximately $24 - 30\,\mathrm{days}$, which is similar to the time lag below the root zone (layer 3) in scenario D1 with root water uptake. Thus, the time lags in the scenarios without root water uptake and an infiltration rate of q_{root} or $q_{root} - \tau$ bound the time lags in scenario D1 where root water uptake is accounted for.

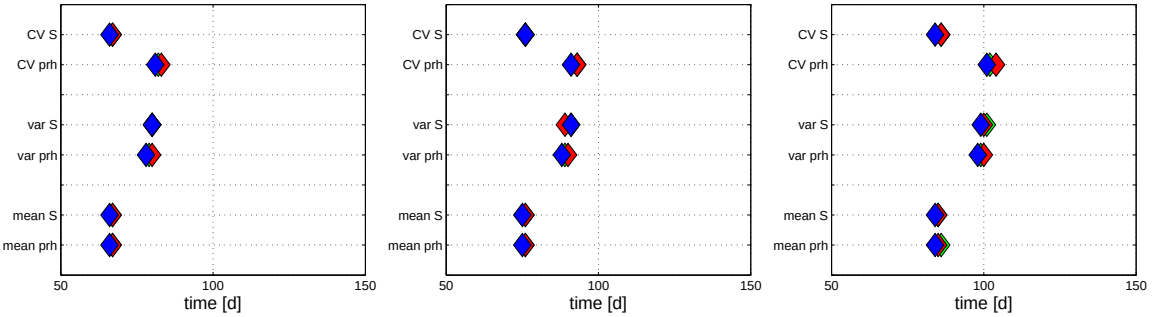

(a) layer 1 (b) layer 2 (c) layer 3

Figure 6.25: *Peak time of mean, variance and coefficient of variation of pressure head and saturation in layer 1 (a), layer 2 (b), layer 3 (c); no root water uptake, high infiltration rate of* $q = 4\,\mathrm{mm/d}$.

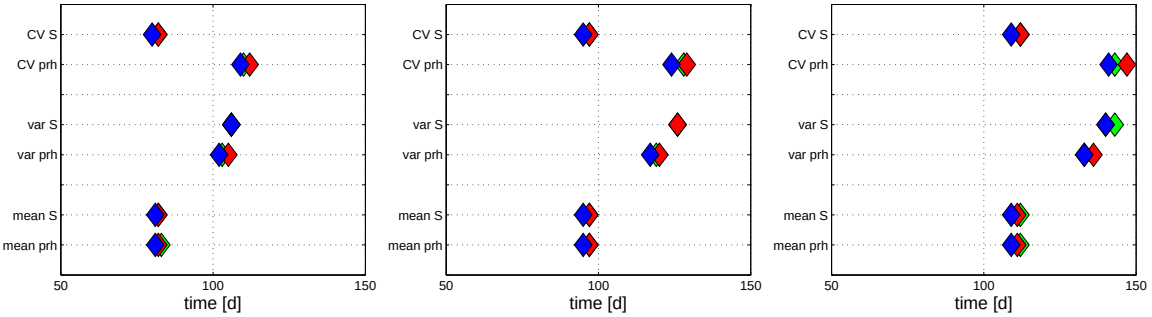

(a) layer 1 (b) layer 2 (c) layer 3

Figure 6.26: *Peak time of mean, variance and coefficient of variation of pressure head and saturation in layer 1 (a), layer 2 (b), layer 3 (c); no root water uptake, low infiltration rate of* $q = 2\,\mathrm{mm/d}$.

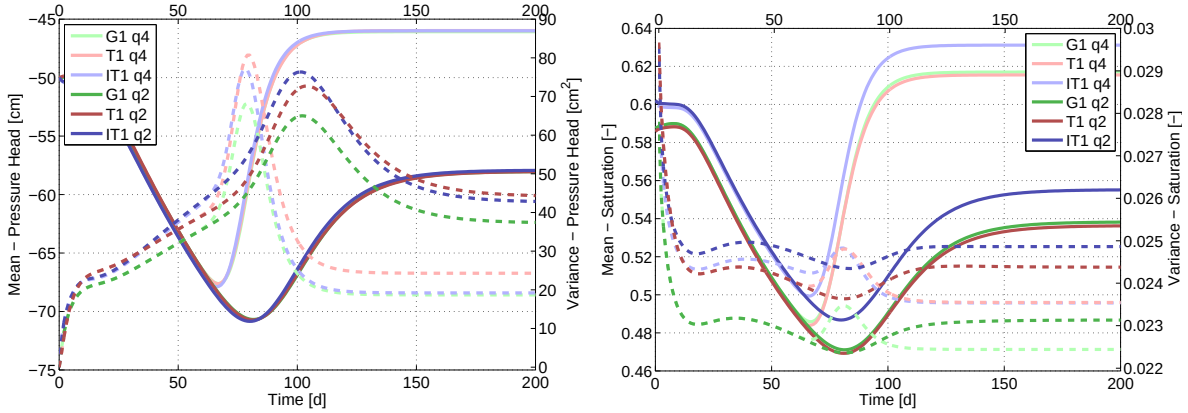

(a) layer 1

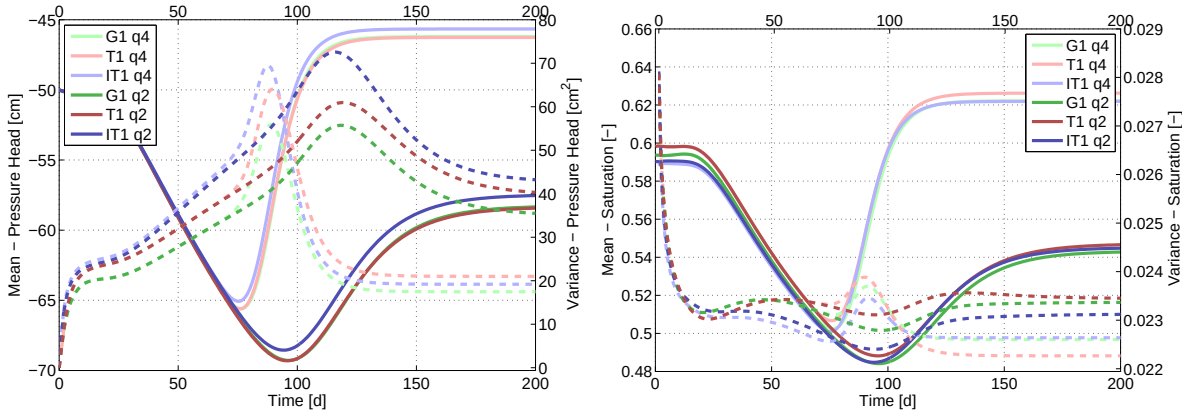

(b) layer 2

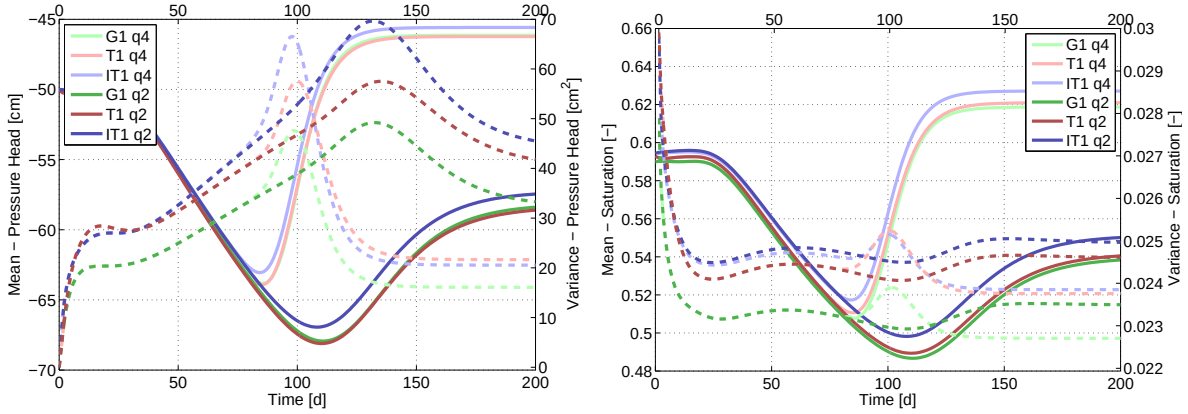

(c) layer 3

Figure 6.27: *Mean (solid line) and variance (dashed line) of pressure head (left) and saturation (right) vs. time in layer 1 (a), layer 2 (b) and layer 3 (c) for scenarios without root water uptake and an infiltration rate of* $4\,\mathrm{mm/d}$ *(light colored lines) and an infiltration rate of* $2\,\mathrm{mm/d}$ *(dark colored lines).*

It should be noted that an infiltration rate of $q = 2\,\mathrm{mm/d}$ at a mean saturation of approximately 0.5 is not sufficient to cause a remarkable increase of the variance of saturation at the arrival of tips of the front. This can be explained by a rather heterogeneous distribution of the saturation compared to pressure head. Hence, for an infiltration rate of $2\,\mathrm{mm/d}$, the maximum of the variance of saturation is almost not detectable. Figure 6.27 shows time series of mean and variance of pressure head and saturation in G1, T1 and IT1-fields at layer 1, 2 and layer 3 for an infiltration rate of $q = 4\,\mathrm{mm/d}$ (light colored lines) and an infiltration rate of $q = 2\,\mathrm{mm/d}$ (dark colored lines).

Since the changes of the variance of saturation during rewetting are relatively small with both infiltration rates, the coefficient of variation is not affected by the temporally shifted peak of the variance of saturation. The maximum of the coefficient of variation of saturation occurs, thus, concurrently to the minimum of the mean saturation.

If the initial condition for ψ is chosen as a hydrostatic pressure distribution, the variance of pressure head is zero before the infiltration front arrives. The width of the front during rewetting can then be clearly recognized. Figure 6.28 shows mean and variance of pressure head vs. depth at three different times for a scenario without root water uptake, hydrostatic initial condition for the pressure head and an infiltration rate of $q = 4\,\mathrm{mm/d}$. The propagation of tips and mean front is indicated by red lines.

In cases with root water uptake, the choice of a hydrostatic pressure distribution is not practical with the parameters chosen in this work as initial pressure head values in the upper part of the soil would be so low that extremely large variances of pressure head due to the formation of dry spots would dominate the profile.

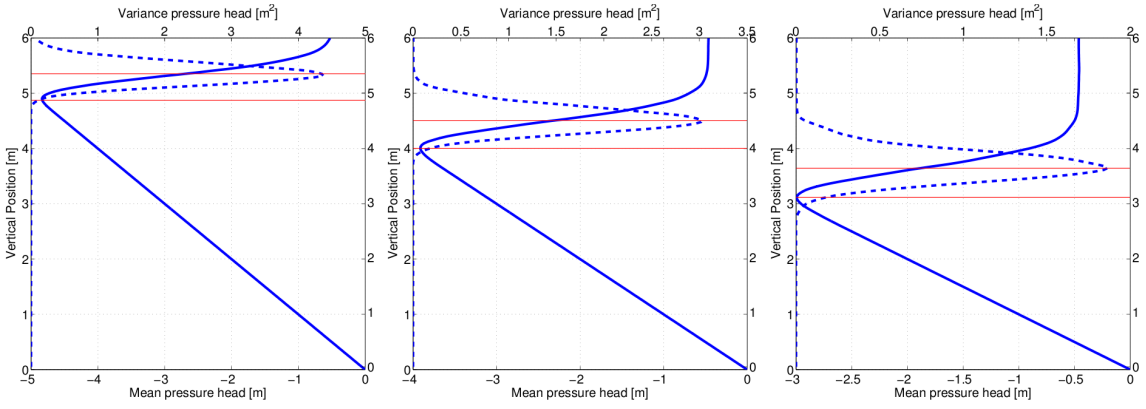

Figure 6.28: *Mean* $[\mathrm{m}]$ *(solid line) and variance* $[\mathrm{m}^2]$ *(dashed line) of pressure head vs. vertical position* $[\mathrm{m}]$ *for a scenario without root water uptake, a hydrostatic initial pressure distribution and an infiltration rate of* $4\,\mathrm{mm/d}$*. The red lines indicate the propagation of tips and mean front.*

Remark

It must be mentioned that taking the variance of pressure head as a measure for the mean front has certain limitations. The peak time of the variance depends on the pressure head or saturation values of locations which are not yet rewetted. For example, in the period between the arrival of tips and the arrival of the mean front, values which are not yet rewetted decrease more with root water uptake than without root water uptake. If the same rewetting front arrives, the variance peaks later and the width of the front is predicted to be larger if root water uptake is included, compared to scenarios with bare soil. One must therefore keep in mind that the time lag between extremes of mean and variance does not capture all differences between the rewetting front in cases with and without root water uptake. A quantitative comparison of the width of the front in cases with and without root water uptake should be seen as an approximate measure. The qualitative result that the width of the front depends on the net infiltration rate, widens with depth with root water uptake and is rather constant without root water uptake remains, however, valid.

6.2.4 Effective homogeneous soil

Instead of 2D heterogeneous fields, effective homogeneous models are often used in large scale applications. In heterogeneous fields, root water uptake was shown to influence the width of the front. When the front is wider such that distinct tips and tails exists, arrival times of the mean front are more difficult to predict with homogeneous effective models. In this section, it is tested how well the transient results in 2D heterogeneous fields with and without root water uptake, discussed in the previous section, agree with equivalent simulations in homogeneous effective soils. We do not aim at deriving effective parameters which capture dynamic effects during rewetting, but focus on the question if root water uptake improves or corrupts predictions of arrival times of the front with models which are based on standard effective parameters.

As discussed above, if root water uptake is included in the model, the net infiltration rate q_l decreases and the front widens with increasing depth due to continuous extraction of water within the root-zone. Hence, the deviation between homogeneous and heterogeneous media under consideration of root water uptake is expected to increase from layer 1 to layer 3. Accordingly, without roots, the deviation between arrival of the front in homogeneous and heterogeneous media is rather constant and depends on the infiltration rate.

Figure 6.29 illustrates the times at which pressure head or saturation are maximal for drydown and rewetting scenarios, with and without root water uptake (scenario D1-D3 in Table 4.2), in a homogeneous medium where for α and K_s, effective soil parameters are used. The saturated conductivity equals the geometric mean of the 2D heterogeneous K_s-fields and the α-parameter equals the arithmetic mean of the 2D α-field. Deterministic parameters and simulations settings agree in the heterogeneous and homogeneous case. Due to the absence of a heterogeneous α-parameter, pressure head and saturation peak at the same time.

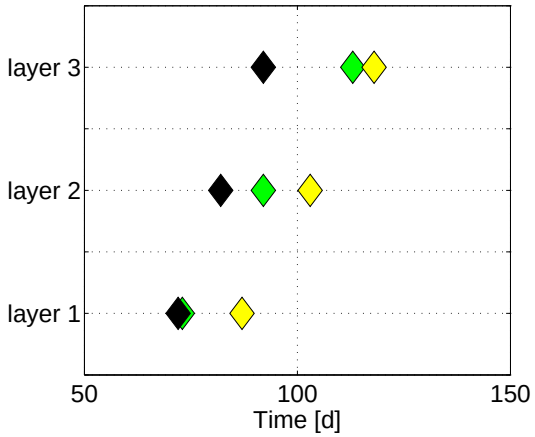

Figure 6.29: *Peak time of pressure head and saturation in layer 1, layer 2 and layer 3 of homogeneous domain for different scenarios: with root water uptake term R_1 (green), without root water uptake and an infiltration rate of $4\,\mathrm{mm/d}$ (black), and without root water uptake and an infiltration rate of $2\,\mathrm{mm/d}$ (yellow).*

The peak times in the homogeneous medium are in between the peak times of mean and variance of pressure head or saturation for the heterogeneous case. If the maximum of the variance of saturation is assumed to represent the mean infiltration front, the front arrives in the homogeneous scenario with roots approximately 11 (layer1), 15 (layer 2), 20 (layer3) days earlier than in the heterogeneous case.

For an infiltration rate of $q = 2\,\mathrm{mm/d}$, the front is in the homogeneous medium about 20 days ahead of the heterogeneous front. Since the variance of saturation does not have a distinct maximum, this case is difficult to evaluate. With an infiltration rate of $q = 4\,\mathrm{mm/d}$, the front in homogeneous and heterogeneous media arrive with a difference of approximately $8\,\mathrm{days}$.

Thus, using an effective homogeneous medium with standard parameters as substitute for the 2D structured fields, the arrival time of the front is underestimated, given the infiltration front is, in the heterogeneous case, assumed to be represented by the maximum of variance of saturation. The deviation of homogeneous and heterogeneous medium depends on the net infiltration rate and is therefore, in the scenario with root water uptake in between the two scenarios where root water uptake is not considered.

6.3 Influence of root water uptake strategy

This section analyzes in which way the model for root water uptake affects the time series of mean and variance of pressure head and saturation in Gaussian and non-Gaussian parameter fields (G1, T1 and IT1). Using the same drydown and rewetting scenario including root water uptake as above (scenario D1 in Table 4.2), root water uptake term R_2 depending on the saturation is compared to the standard approach R_1.

Uptake strategy 2 depends on the saturation and extracts hence more water at wet locations that consist of fine material than at dry locations that consist of coarse material. The impact of root water uptake strategy 1 on the pressure head of decreasing pressure head values in coarse lenses during drying phases (section 6.2.1), is therefore reduced with Strategy 2. Extracting water preferentially at wet, fine, locations, thus, leads to a distribution of pressure head and saturation which is more similar to distributions obtained with scenarios where root water uptake is not considered.

A sample realization of T1-fields, displayed in Figure 6.13, is used to illustrate the difference between pressure head and saturation obtained with Strategy 1 and Strategy 2. Figure 6.30 shows the distribution of pressure head (a) and saturation (b) with Strategy 1 (ψ_{R1}, S_{R1}) subtracted by the distribution with Strategy 2 (ψ_{R2}, S_{R2}) after $60\,\mathrm{days}$.

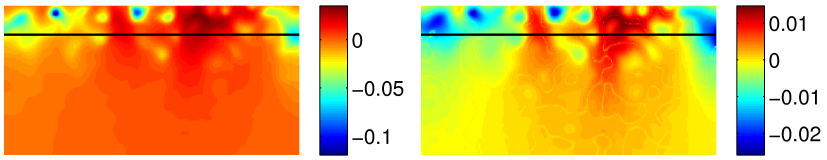

(a) (b)

Figure 6.30: *Difference of pressure head distributions* $[\mathrm{m}]$ *(a) and saturation distributions* $[-]$ *(b) with Strategy 1 and Strategy 2 after* $60\,\mathrm{days}$ *in a sample realization of T1-fields.*

At coarse locations, Strategy 1 leads to smaller saturations and lower pressure head values than Strategy 2. ψ_{R1} substracted by ψ_{R2} (or S_{R1} substracted by S_{R2}) has therefore negative values at such locations.

Since Strategy 1 and Strategy 2 differ only in their extraction pattern, but take up the same amount of water, the mean values of pressure head and saturation is hardly affected by the root water uptake strategy, unless dry spots form. The variance of pressure head and saturation is affected by root water uptake during drying and rewetting phases and if dry spots occur. As Strategy 2 leads to distributions which are similar to distributions obtained without root water uptake, these phenomena are attenuated with root water uptake model R_2. This is illustrated in Figure 6.31 and Figure 6.32 which compare time series of mean and variance of pressure head and saturation, obtained with Strategy 1 and Strategy 2 for the drydown-rewetting scenario D1, at layer 1 to layer 3, separately in each structure.

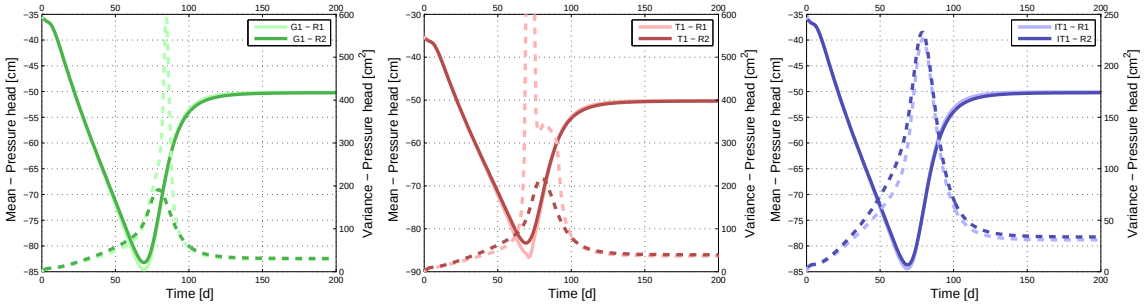

(a) layer 1

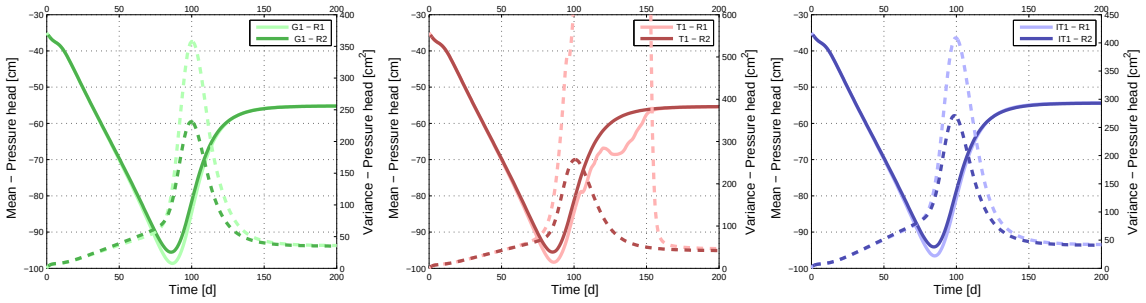

(b) layer 2

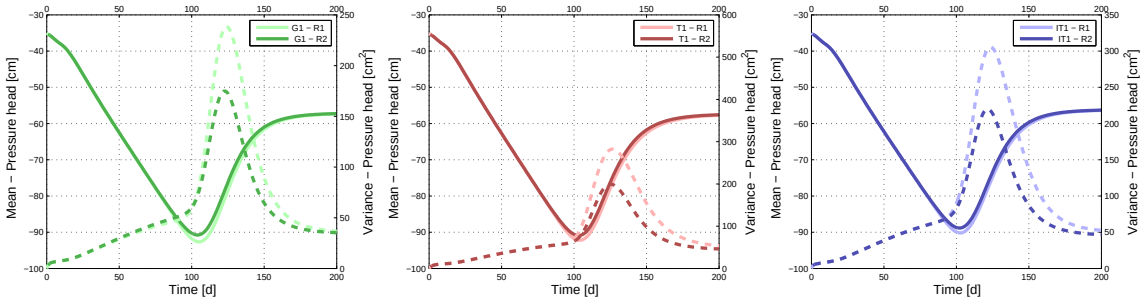

(c) layer 3

Figure 6.31: *Mean (solid line) and variance (dashed line) of pressure head* [m] *vs. time in layer 1 (a), layer 2 (b) and layer 3 (c) of G1- (left), T1- (middle) and IT1-fields (right) with Strategy 1 (light colored lines) and Strategy 2 (dark colored lines).*

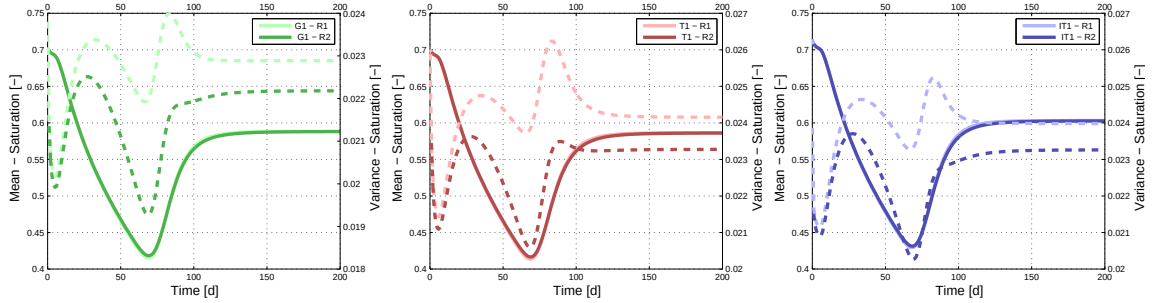

(a) layer 1

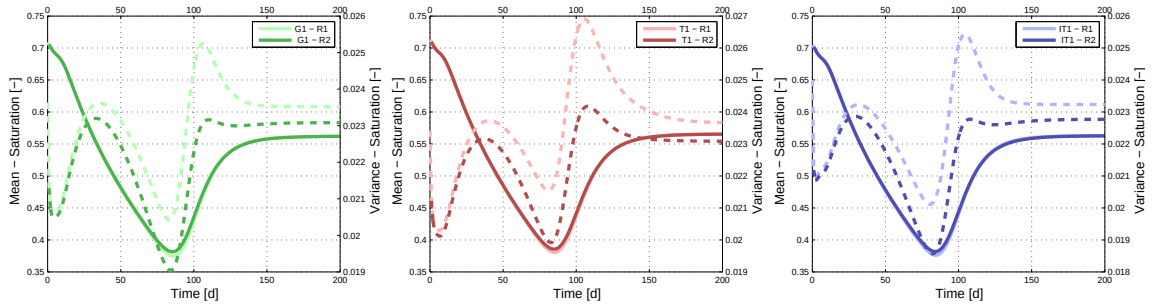

(b) layer 2

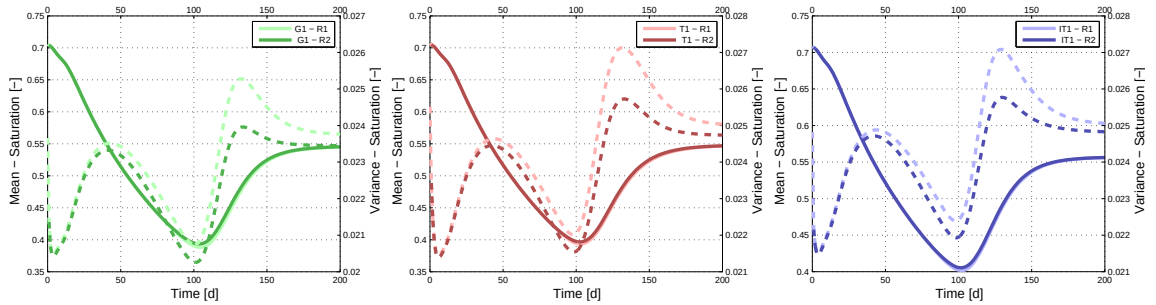

(c) layer 3

Figure 6.32: *Mean (solid line) and variance (dashed line) of saturation [–] vs. time in layer 1 (a), layer 2 (b) and layer 3 (c) of G1- (left), T1- (middle) and IT1-fields (right) with Strategy 1 (light colored lines) and Strategy 2 (dark colored lines).*

Formation of dry spots

In chapter 5.3 it was described that root water uptake strategies which increase uptake at favorable locations and decrease the uptake rate at unfavorable locations have an attenuating effect on the formation of dry spots. Since the root water uptake rate decreases with Strategy 2 more, at the onset of stressed conditions, than with Strategy 1, dry spots form later and less distinct with Strategy 2. In the test case observed here, the formation of dry spots is prevented if Strategy 2 is applied such that no extreme values of the variance of pressure head occur in T1-structures.

Variability during drying and rewetting

In the considered test case D1 where root water uptake is included, the variance of pressure head is slightly lower during drying (before patches of coarse material dry up) than at comparable states without root water uptake. The variance of saturation is with root water uptake slightly larger than at comparable states without root water uptake (see section 6.2.1). Peak values of the variance of pressure head and saturation during rewetting may be slightly larger with root water uptake (see section 6.2.2). As discussed above, root water uptake term R_2 leads to distributions of pressure head and saturation which are similar to the case without roots. Accordingly, the variance of pressure head is with Strategy 1 slightly lower during drying and higher during rewetting than with Strategy 2. The variance of the saturation is larger with Strategy 1 than with Strategy 2 during drying and rewetting.

As Strategy 2 leads, at the same mean saturation, to smaller variances of saturation, compared to Strategy1, the $\sigma_S(< S >)$-relationship at the surface is affected by the root water uptake strategy. This relationship is, for example, important for the parametrization of climate models (e.g. Vereecken et al., 2007a). Figure 6.33 shows a scatter plot of the variance vs. mean of saturation at the surface of T1-fields for test scenario D1 with Strategy 1 (light colored lines) and Strategy 2 (dark colored lines). The lower line of each curve corresponds to the drying process, the upper line to the rewetting process. With Strategy 2, both lines are shifted to lower variances and the maximum of the drying curves may be shifted to a higher saturation. The rewetting line differs from the drying line less with Strategy 2 corresponding to a lower peak value during rewetting than with Strategy 1.

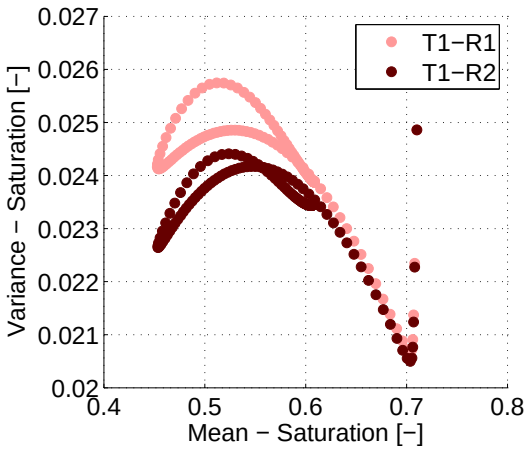

Figure 6.33: *Scatter plot of variance* $[-]$ *vs. mean* $[-]$ *of saturation (averaged at the surface of T1-fields) for Strategy 1 (*R_1*) and Strategy 2 (*R_2*).*

One reason for a smaller peak of the variance of pressure head and saturation during rewetting is that dry locations are less depleted with Strategy 2 than with Strategy 1, which diminishes the difference of dry and wet locations. Second, first arrivals of the infiltration front may be equalized by preferential water extraction at wet locations with Strategy 2. The saturation front is thereby slightly homogenized in comparison to Strategy 1. This is illustrated in Figure 6.34 which shows the difference of saturation fronts after $107\,\mathrm{days}$ simulation time

with both strategies. If Strategy 2 is applied, the saturation front reaches locations which have not been reached by the tail of the front with Strategy 1. On the other hand, the front with Strategy 2 does not reach locations which have been reached by tips of the front with Strategy 1.

Figure 6.35 illustrates the times at which minimum of mean and maximum of variance of pressure head and saturation occur. The variance of saturation peaks $3 - 4\,\mathrm{days}$ later with Strategy 2 which indicates that the front might propagate slightly slower than with Strategy 1. Changes of the variance of saturation are relatively small such that the coefficient of variation of saturation peaks at same time as the mean saturation.

To confirm these conclusion, the impact of root water uptake strategy 2 on a heterogeneous infiltration front and the $\sigma_S(< S >)$-relationship need to be analyzed more detailed in future work.

(a) (b) (c)

Figure 6.34: *Distribution of saturation after* $107\,\mathrm{days}$ *(substracted by the saturation after* $60\,\mathrm{days}$*) as binary field, with Strategy 1 (a), and Strategy 2 (b) as well as the difference of both (c). Values equal to* 1 *indicate locations which are only reached by the front with Strategy 1, values equal to* -1 *indicate locations that are only reached by the front with Strategy 2.*

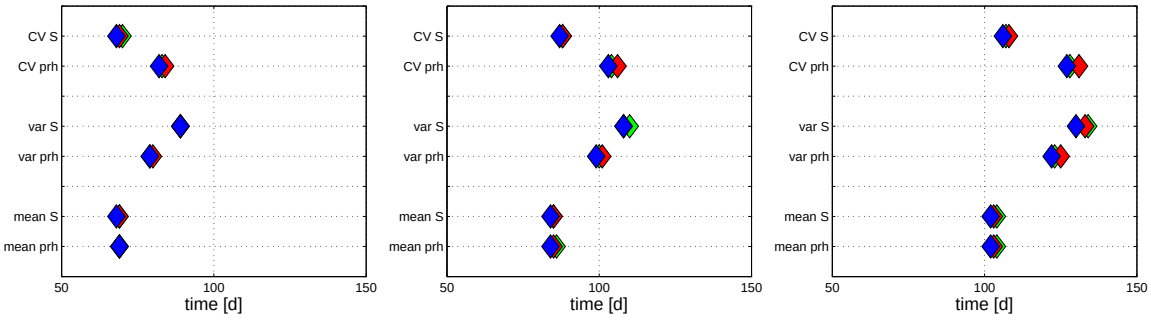

(a) layer 1 (b) layer 2 (c) layer 3

Figure 6.35: *Peak time of mean, variance and coefficient of variation of pressure head and saturation in layer 1(a), layer 2(b) and layer 3(c); for root water uptake term* R_2.

In summary, the modeling approach for root water uptake according to Strategy 2, leads during drying and rewetting to very similar results of the mean value as Strategy 1 but diminishes the impact of root water uptake on the variance of pressure head and saturation or may even change the impact of root water uptake by homogenizing the distribution of saturation. Thus, knowledge about the strategy how plant roots extract water is a crucial

factor to be able to assess the variability of pressure head and saturation. Using strongly simplified uptake models in heterogeneous fields, the influence of root water uptake might be overestimated.

6.4 Intermediate summary 2: Dynamic conditions

In this chapter, transient unsaturated flow with temporally variable infiltration and root water uptake rate is analyzed. The formation and recovery of dry spots as well as the development of the variability of pressure head and saturation at a specific depth during drying and rewetting phases is discussed. In the following, key findings are summarized.

- In section 6.1.1, timescales for the formation and recovery of dry spots are estimated based on characteristic timescales derived with the help of a dimensionless Richards equation (presented in section 2.2.3). The observed timescales for the formation of dry patches, which can be identified from Figure 6.11, agree roughly with the predicted timescales. In general, the timescales after which dry spots form tend to underestimate simulated times since in the estimation, replenishment from the surrounding of coarse patches is neglected which is actually not given. The timescales for replenishment underestimate simulated recovery times since heterogeneous rewetting fronts and low conductivities postpone the replenishment of dry regions.
- Under periodic conditions, a critical frequency above which dry regions do not form can be estimated for layers which are close to the surface (section 6.1.2). In deeper layers, rewetting occurs later and is therefore superimposed with root water uptake cycles such that drying and rewetting phases cannot be clearly separated.
- In section 6.2.1, the variability of pressure head is shown to increase during drying. By lowering high pressure head regions, root water uptake may decrease the variance of pressure head compared to equally dry states in scenarios without root water uptake. If drying is continued, the variance increases again since pressure head values become very low in lenses of coarse material. In the extreme case, wilted patches form which lead to very large values of the variance of pressure head.
- During drying, the variance of saturation increases and decreases during further, corresponding to a parabolic shape of the variance as function of the mean value. In the analyzed test cases, root water uptake increases the variance in comparison to equally dry states with the same mean saturation, where root water uptake is not considered.
- The variance of pressure head and saturation peak during rewetting with heterogeneous fronts since the variance increases at the arrival of tips until the mean front has passed. Under consideration of root water uptake, the peak value of the variances may be larger (section 6.2.2).
- The time lag between minimum of mean and maximum of variance of pressure head or saturation can be taken as a measure for the width of the pressure or saturation front. It depends on the local net infiltration rate q_l at one layer where q_l is the infiltration

rate at the top boundary subtracted by the extracted volume of water up to this layer. Since root water uptake continuously extracts water such that the net infiltration rate decreases with increasing depth, the time lag increases with increasing depth. Without root water uptake, the time lag between the extremes of mean and variance of pressure head or saturation is rather constant and depends on the infiltration rate at the top boundary.

- In section 6.3 it is shown that root water uptake strategy 2 influences the variance of pressure head and saturation. By extracting less at dry locations and more at wet locations, root water uptake model R_2 leads to distributions which are similar to cases without root water uptake. Thus, knowledge about the root water uptake strategy is crucial information when modeling unsaturated flow problems.

7 Final remarks

7.1 Summary and Conclusion

The joint influence of root water uptake and soil structure on unsaturated flow is studied. Soil hydraulic parameters are described as autocorrelated random fields. Root water uptake at the macroscopic scale is modeled as a function of atmospheric demand, root density, and stress-response function. This approach is referred to as 'standard model' for root water uptake in this work. An extension of the standard model for root water uptake is also considered, which accounts for locally occurring stress by preferential extraction of water at wet or easily accessible locations. Analytical first-order second-moment solutions for steady state flow in a layered medium are derived. In addition, two-dimensional numerical simulations of steady state and transient flow in autocorrelated Gaussian and non-Gaussian random fields with different patterns of extreme values are analyzed.

The present study shows that, with the parameters chosen, the analytical solutions in layered media can be used for predictions of the mean and variance of pressure head only under very wet conditions with the drawback that variances of the pressure head are overestimated if the variance of the loghydraulic saturated conductivity becomes large.

Under drier conditions, the combined investigation of both root water uptake and soil structure allows for the simulation of unsaturated flow phenomena that are not exhibited in either unvegetated (no roots) or homogeneous (no soil structure) soil and which cannot be predicted by first-order second-moment solutions. These phenomena concern (i) local wilting (ii) solute transport and (iii) the variability of pressure head and saturation, and are summarized below.

Local wilting

Large patches of coarse material can dry out due to limited replenishment of rainwater into their inner parts. If locally more water is extracted than can be replenished, root water uptake will lead to a gradual change of pressure heads in coarse lenses located in the root zone, which attain the wilting point pressure head, where root water uptake becomes zero. The patches are surrounded by relatively wet material. These regions lower the mean pressure head and lead to extremely large variances of the pressure head. The effect of local wilting is not observed under neglection of root water uptake or soil structure and can thus not be captured by first-order second-moment effective models. The feature of soil structure which is sensitive to the occurrence of local wilting is the existence of patches of coarse material with length scales that exceed the typical length, over which water can be drawn by root

water uptake. This structure property is not necessarily described by the correlation length of the heterogeneous parameter field, as coarse and fine material can have different patch sizes. In contrast, the bivariate spatial copula of the parameter field (Bárdossy, 2006) reflects the length scales of structures with different parameter ranges. The formation of dry regions could, thus, be eventually predicted with the help of two-point bivariate spatial copulas of the hydraulic parameter fields.

Timescales for the formation of dry spots during drying phases can be roughly estimated with the help of characteristic timescales for root water uptake and gravity flow. If periodic rewetting and drying cycles with equal frequencies are applied, a critical frequency below which dry spots form can be quantified. Since at deeper layers, drying and rewetting phases cannot be clearly separated due to later arrival of the rewetting front, this estimate holds only for locations close to the surface.

In the case that locally wilted areas occur, the standard root water uptake model would predict that the global root water uptake rate is decreased and the atmospheric demand is not met anymore. The local actual uptake rate is shown to be periodically reduced at layers close to the surface during drying phases if root water uptake is modeled according to the standard approach. The global actual uptake (integrated over the domain) is related to crop yield. In the test cases carried out in this study, crop yield is hardly affected, but a reduction occurs in principle. Based on this, one can imagine scenarios where the annual yield is immensely decreased, e.g. if parameter fields have very large patches of coarse material, plants with deeper root systems are modeled, or extended drying phases are considered.

Experimental studies suggest that plants can compensate for decreased uptake due to stress at layers close to the surface by enhanced uptake at deeper layers such that the global actual uptake is not reduced. Assuming that plants also compensate for localized stress, different uptake strategies which include compensation mechanisms are considered. The standard model for root water uptake (Strategy 1) is compared to three alternative models with a compensation strategy for local stress depending on the saturation (Strategy 2) or the relative permeability (Strategy 3) and a model where the deficit of uptake is equally distributed to unstressed parts of the soil (Strategy 4). Although with these compensation mechanisms the potential transpiration is met in total, the alternative root water uptake strategies can also lead to local stress and wilting in large lenses of coarse material. The formation of such dry regions is attenuated for Strategy 2 and 3, where the uptake rate is decreased in stressed parts and increased at favorable locations.

In general, the results obtained with the considered model concepts is debatable. A reduction of crop yield, obtained with the standard model, does not seem realistic, especially at steady state conditions, considering that the dry spots are local and the global amount of water in the medium is not below a critical value. Thus, in heterogeneous soils, it becomes more important to use strategies which include compensation mechanisms in the root water uptake model in order to maintain the global transpiration at the potential value although this may lead to an overestimation of crop yield if full compensation does not take place. Moreover, local spots with pressure head values at the wilting point, which occur with the standard and the alternative root water uptake strategies, do also not seem realistic as the wilted regions are surrounded by wet material. In fact, the main problem is that much infor-

mation to call such observations unrealistic or realistic is apparently not available. Hence, those macro-scale models for root water uptake which are based on a water reduction function under stressed conditions, may work well for homogeneous domains, but as soon as heterogeneity of soil hydraulic properties is considered, phenomena such as dry spots occur, that raise questions regarding to the general validity of the conceptual model.

If the observed effect of local wilting in certain soil structures finally is a model artifact and to what extent compensation takes place cannot be determined with large-scale approaches for root water uptake which are based on a water reduction function. Therefor soil physical and plant physiological aspects need to be taken into account.

Solute transport

The steady state water flux fields in G1-, T1- and IT1-fields are used to perform a numerical tracer experiment. A pulse of solute is released at the surface and monitored below the root-zone and above the groundwater table. Flux-averaged breakthrough curves (the temporal derivative of the total normalized concentration in the domain) are analyzed with emphasis on the influence of root water uptake and non-Gaussian soil structures. In the considered test cases, both factors are found to influence solute transport. Solute propagates through T1-fields, which have, under the conditions applied, connected pathways of high conductive material and large patches of low conductive material, the fastest, and IT1-fields, which have the opposite pattern, the slowest. In general, the travel time is controlled by the infiltration rate of rainwater at the top boundary. Differences between the structures increase with decreasing infiltration rate. In scenarios where root water uptake (standard approach) is included, the arrival time of bulk solute as well as differences between the considered structures, are in between the values of the two bounding scenarios without root water uptake (with an infiltration rate of q and $q-\tau$). Comparing two scenarios in vegetated and bare soil with the same groundwater recharge rate, root water uptake leads to faster flow paths through the root-zone in all considered structures. The concentration held back in stagnant zones (which is here called residual concentration) is in IT1-fields higher than in G1- and T1-fields. As root water uptake lowers the conductivity of coarse lenses such that less solute is transported into such regions, root water uptake may decrease the residual concentration in T1- and G1-fields.

This study shows, that differences of the transport behavior exist between the considered structures. Thus, the assumption of multi-Gaussian heterogeneity, which is often made in studies dealing with solute transport, might lead to over- or underestimation of arrival times of solute. The differences in propagation of solute between Gaussian and non-Gaussian fields are relevant for reactions that a solute undergoes on its way through the unsaturated zone. The lower the travel velocity is, the longer is the available reaction time such that more reactions and degradation can take place. In this sense, consideration of structure is important. Since, at equal groundwater recharge rate, a scenario with root water uptake leads to different travel times of the solute, which in turn affect the degradation process, it is not sufficient to model the entry of solute into groundwater resources based only on recharge rates. Thus, root water uptake and soil structure should be included in environmental modeling studies which aim at problems related to contaminant transport.

Variability of pressure head and saturation

It is analyzed in which way mean and variance of pressure head and saturation are influenced by root water uptake and heterogeneity of soil properties.

Steady state simulations in 2D fields yield that the variance of pressure head is high under very wet and very dry conditions and low close to the cross-over where the conductivity of coarse material and fine material in the considered fields are similar. Beyond the crossover (at lower water pressure heads), drier states are generally associated with a higher variability.

Under transient conditions, the variability of pressure head and saturation increases during drying phases. During rewetting, drier states are not necessarily associated with a higher variability, since in multi-dimensional structured media, a heterogeneous infiltration front develops which increases the variance of pressure head and saturation at a distinct soil layer as soon as rainwater arrives at this layer. When the infiltration front has passed this layer, the variances of pressure head and saturation decrease again and finally reach a steady state value. Depending on the uptake strategy of roots, variances of pressure head and saturation can be slightly smaller or larger during drying and rewetting, compared to the case without root water uptake. The pattern of the considered structures influences the mean and the variance of pressure head and saturation only slightly. Since root water uptake affects the variance of saturation in comparison to equally dry states without root water uptake, root water uptake also changes the relationship between variance and mean of saturation.

The point where the pressure head starts to increase at a distinct layer (minimum of pressure head) corresponds to the first arrival of water at this layer. The maximum of the variance can be taken as a measure for the arrival of the mean front. The observed time lag between the minimum of the mean and the maximum of the variance of pressure head or saturation can be taken as a measure for the width of the front. The front width increases with decreasing net infiltration rate. Thus, as the infiltration front travels through the domain, the width of the front is constant in scenarios without root water uptake while it increases with increasing depth if root water uptake is taken into account. Since the front widens with depth under consideration of root water uptake, predictions of arrival times of the infiltration front based on standard effective parameters for soil properties become more difficult and inaccurate with depth under consideration of root water uptake.

The coefficient of variation of pressure head is, in the analyzed test cases, dominated by the variance of pressure head such that it peaks temporally shifted to the mean. The coefficient of variation of saturation is dominated by the mean value and peaks only with a very small time lag compared to the minimum of the mean saturation.

In summary, this study demonstrates that root water uptake and heterogeneity of soil properties jointly affect unsaturated flow and cannot be safely ignored, as it is often the case in large scale applications. The actual impact of root water uptake depends on the considered strategy according to which plants extract water. Differences between the sensitivity to local wilting of Gaussian and non-Gaussian structures and the increase of variance of saturation, observed with the standard approach for root water uptake, are weakened if a more complex root water uptake strategy is taken into account. Using macroscopic approaches for root water uptake, it is generally not possible to evaluate which strategy is more realistic. However, the critical features of structure which are sensitive to the influence of root water uptake may be identified. According to the results of this study, one of these features is the existence of large patches of coarse material.

To make reliable predictions on flow processes on large scales, prequisite knowledge about uptake mechanisms is necessary when upscaled models are used. This knowledge is currently not available in complex structured soils. To come up with a reasonable approach for root water uptake on the macroscopic scale, we must learn from microscopic insights. This work points out that it is inappropriate to assume a homogeneous distribution of soil parameters, which is often done by plant scientists and hydrologists, and questions an equal uptake ability of plant roots in heterogeneous soils, especially under stressed conditions. We emphasize the need for biological studies to include the variation of soil hydraulic properties with a focus on growth and uptake in coarse material under dry conditions.

Until these major lacks in our understanding of root - soil interactions are overcome and the gained knowledge is transferred to effective models, it is important to be aware of the limitations of using large scale-standard models for root water uptake in structured soils.

7.2 Outlook

The hydological community would essentially benefit from an improved conceptional understanding of the uptake mechanism according to which a given plant species extracts water. Microscopic models of root networks, such as, e.g., the approach by Javaux et al. (2008) or Schneider et al. (2010), where the extraction rate is determined by the radial flow due to potential gradients, would be suitable. Approaches, which treat root water uptake as a energy optimizing problem (e.g. Adiku et al., 2000), might be promising as well, however implementation in two and three dimensions might be extremely difficult.

Following the results of this study, the analysis should concentrate on the behavior of a root network in the surrounding of lenses of coarse material at water shortage. Furthermore, the influence of root water uptake on the relationship between variance and mean of saturation in differently structured soils is an interesting question for future work. The results of this study indicate, that root water uptake and eventually the considered structures plays a role for the $\sigma_S(< S >)$-curve. Since the variance of saturation depends on the applied uptake strategy, a microscopic model for root water uptake should be used for this analysis as well.

Alternatively, achievements on the response of plants to heterogeneous structures in order to derive extraction pattern as well as compensation mechanisms on larger scales, may be obtained by carefully monitoring flow in vegetated, heterogeneous soils. Experimental work on root water uptake in heterogeneous media is scarce and further studies at all scales will surely contribute to fill the gap in our understanding.

Another open aspect is the dependence of critical pressure heads and wilting point in the Feddes-function on soil hydraulic properties. Theoretically, a variation of critical values can be reasoned with the model of de Jong van Lier et al. (2006). If a variation of critical values can be experimentally confirmed and the range of possible values quantified, critical pressure heads in the Feddes-function should be treated as a random space function depending on the soil hydraulic properties in future work. Depending on the actual values of critical pressure heads, this approach may prevent extremely low pressure head values and large variances, but will drastically reduce the actual transpiration rate, unless compensation methods are included. Resulting uptake pattern should be compared with field data to evaluate the model.

Bibliography

Adiku, S. G. K., Rose, C. W., Braddock, R. D., and Ozier-Lafontaine, H. (2000). On the simulation of root water extraction: examination of a minimum energy hypothesis. *Soil Sci.*, 165 (3):226–236.

Albertson, J. D. and Montaldo, N. (2003). Temporal dynamics of soil moisture variability: 1. Theoretical basis. *Water Resour. Res.*, 39:SWC 2 1–14.

Anderson, J. and Shapiro, A. M. (1983). Stochastic analysis of one-dimensional steady state unsaturated flow: A comparison of Monte Carlo and perturbation methods. *Water Resour. Res.*, 19(1):121–133.

Augé, R. M. and Moore, J. L. (2002). Stomatal response to nonhydraulic root-to-shoot communication of partial soil drying in relation to foliar dehydration tolerance. *Environ. Exp. Bot.*, 47:217 229.

Bárdossy, A. (2006). Copula-based geostatistical models for groundwater quality parameters. *Water Resour. Res.*, 42:W11416.

Basha, H. A. (1999). One-dimensional nonlinear steady infiltration. *Water Resour. Res.*, 35:1697–1704.

Bear, J. (1972). *Dynamics of Fluids in Porous Media*. New York, American Elsevier Pub. Co.

Bell, K. R., Blanchard, B. J., Schmugge, T. J., and Witzak, M. W. (1980). Analysis of surface moisture variations within large-field sites. *Water Resour. Res.*, 16 (4):796–810.

Birkholzer, J. and Tsang, C.-F. (1997). Solute channeling in unsaturated heterogeneous porous media. *Water Resour. Res.*, 33(10):2221 – 2238.

Bosma, W. J. P., Bellin, A., van der Zee, S. E. A. T. M., and Rinaldo, A. (1993). Linear equilibrium adsorbing solute transport in physically and chemically heterogeneous porous formation 2. Numerical results. *Water Resour. Res.*, 29:4031–4043.

Bouten, W. (1995). Soil water dynamics of the solling spruce stand, calculated with the FORHYD simulation package. *Ecol. Model.*, 83:67–75.

Braddock, R. D. and Parlange, J.-Y. (2000). Comment on 'One dimensional nonlinear steady infiltration'. *Water Resour. Res.*, 36(10):3111–3113.

Braddock, R. D. and Parlange, J.-Y. (2003). One-dimensional steady infiltration with water extraction. *Transport Porous Med.*, 51:113–121.

Brooks, R. H. and Corey, A. T. (1966). Properties of porous media affecting fluid flow. *J. Irrigation and Drainage Div., Proc. Am. Soc. Civil Eng. (IR2)*, 92:61–88.

Cardon, G. E. and Letey, J. (1992). Plant water uptake terms evaluated for soil water and solute movement models. *Soil Sci. Soc Am. J.*, 32:1876–1880.

Carsel, R. F. and Parrish, R. S. (1988). Developing joint probability distributions of soil water retention characteristics. *Water Resour. Res.*, 24 (5):755–769.

Choi, M. and Jacobs, J. M. (2007). Soil moisture variabililty of root zone profiles within SMEX02 remote sensing footprints. *Adv. Water Res.*, 30(4):883–896.

Choi, M., Jacobs, J. M., and Cosh, M. H. (2007). Scaled spatial variability of soil moisture fields. *Geophy. Res. Lett.*, 34:L01401.

Cirpka, O. A. (2007). *Ausbreitungs - und Transportvorgänge in Strömungen I: Strömungen in natürlichen Hydrosystemen*. Lecture notes.

Clausnitzer, V. and Hopmans, J. W. (1994). Simultaneous modeling of transient 3-dimensional root-growth and soil-water flow. *Plant Soil*, 164:299 – 314.

Coelho, F. E. and Or, D. (1996). A parametric model for two-dimensional water uptake intensity by corn roots under drip irrigation. *Soil Sci. Soc Am. J.*, 60:1039–1049.

Cornish, P. S. (1993). Soil macrostructure and root growth of establishing seedlings. *Plant Soil*, 151:119–126.

Dagan, G. (1989). *Flow and Transport in Porous Formations*. Springer-Verlag, New York.

Dagan, G. and Bresler, E. (1979). Solute dispersion in unsaturated heterogeneous soil at field scale: Theory. *Soil Sci. Soc. Am. J.*, 43:461 – 467.

Dalton, F. N., Raats, P. A. C., and Gardner, W. R. (1975). Simultaneous uptake of water and solutes by plant roots. *Agron. J.*, 67:334–339.

de Jong van Lier, Q., Metselaar, K., and van Dam, J. C. (2006). Root water extraction and limiting soil hydraulic conditions estimated by numerical simulation. *Vadose Zone J.*, 5:1264–1277.

Doussan, C., Pierret, A., Garrigues, E., and Pages, L. (2006). Water uptake by plant roots II - Modelling of water transfer in the soil root-system with explicit account of flow within the root system - Comparison with experiments. *Plant and Soil*, 183:99 – 117.

English, M. and Raja, S. N. (1996). Perspectives on deficit irrigation. *Agric. Water Manage.*, 32:1–14.

Famiglietti, J. S., Devereaux, J. A., Laymon, C. A., Tsegaye, T., Houser, P. R., Jackson, T. J., Graham, S. T., Rodell, M., and van Oevelen, P. J. (1999). Ground-based investigation of soil moisture variability within remote sensing footprints during the Southern Great Plains (SGP97) hydrology experiment. *Water Resour. Res.*, 35(6):1839–1851.

Famiglietti, J. S., Rudnicki, J. W., and Rodell, M. (1998). Variability in surface moisutre content along a hillslope transect: Rattlesnake Hill, Texas. *J. Hydrol.*, 210(1-4):259–281.

Feddes, R. A., Kowalik, P. J., Malinka, K. K., and Zaradny, H. (1976). Simulation of field water uptake by plants using a soil water dependent root extraction function. *J. Hydol.*, 31:13–26.

Feddes, R. A., Kowalik, P. J., and Zaradny, H. (1978). Simulation of field water use and crop yield. Simulation Monographs. *Pudoc. Wageningen*, 189pp.

Feyen, J., Jacques, D., Timmerman, A., and Vanderborght, J. (1998). Modelling water flow and solute transport in heterogeneous soils: A review of recent approaches. *J. Agr. Eng. Res.*, 70:231–256.

Flury, M., Leuenberger, J., Studer, B., and Flühler, H. (1995). Transport of anions and herbicides in a loamy and a sandy field soil. *Water Resour. Res.*, 31:823–835.

Fricke, T. (2004). The Hoshen-Kopelman Algorithm. *University of Berkeley, http://www.ocf.berkeley.edu/ fricke/projects/hoshenkopelman/hoshenkopelman.html*.

Gardner, W. R. (1960). Dynamic aspects of water availability to plants. *Soil Sci.*, 89:63–73.

Gelhar, L. W. (1993). *Stochastic subsurface hydrology*. Prentice-Hall.

Gray, W. G. and Hassanizadeh, S. M. (1998). Macroscale continuum mechanics for multiphase porous-media flow including phases, interfaces, common lines and common points. *Adv. Water Res.*, 21 (4):261–281.

Green, S. R., Kirkham, M. B., and Clothier, B. E. (2006). Root uptake and transpiration: From measurements and models to sustainable irrigation. *Agric. Water Manage.*, 86:165–176.

Guswa, A. J. (2005). Soil-moisture limits on plant uptake: An upscaled relationship for water -limited ecosystems. *Adv. Water Resour.*, 28:543–552.

Guswa, A. J., Celia, M. A., and Rodriguez-Iturbe, I. (2002). Models of soil moisture dynamics in ecohydrology: A comparative study. *Water Resour. Res.*, 38(9):1166.

Harter, T. and Yeh, T. C. J. (1998). Flow in unsaturated random porous media, nonlinear numerical analysis and comparison to analytical stochastic models. *Adv. Water Resour.*, 22(3):257–272.

Harter, T. and Zhang, D. X. (1999). Water flow and solute spreading in heterogeneous soil with spatially variable water content. *Water Resour. Res.*, 35(2):415–426.

Hasegawa, S. and Yoshida, S. (1982). Water uptake by dryland rice root system during soil drying cycle. *Soil Sci. Plant Nutr.*, 38:191–208.

Hatano, R., Iwanaga, K., Okajima, H., and Sakuma, T. (1988). Relationship between the distribution of soil macropores and root elongation. *Soil Sci. Plant Nutr.*, 34:535–546.

Hatano, R. and Sakuma, T. (1990). The role of macropores on rooting pattern and movement of water and solutes in various field soils. *Transaction of the 14th Congress of International Society of Soil Science (Kyoto)*, II:130–135.

Helmig, R. (1997). *Multiphase Flow and Transport Processes in the Subsurface*. Springer.

Helmig, R., Bastian, P., Class, H., Ewing, J., Hinkelmann, R., Huber, R. U., Jakobs, H., and Sheta, H. (1998). Architecture of the modular program system MUFTE-UG for simulating multiphase flow and transport processes in heterogeneous porous media. *Math. Geol.*, 2:123–131.

Herkelrath, W. N., Miller, E. E., and Gardner, W. R. (1977a). Water uptake by plants: I. Divided root experiments. *Soil Sci. Soc Am. J.*, 41:1033–1038.

Herkelrath, W. N., Miller, E. E., and Gardner, W. R. (1977b). Water uptake by plants: II. The root contact model. *Soil Sci. Soc Am. J.*, 41:1039–1043.

Hilfer, R. (2006). Macroscopic capillarity without a constitutive capillary pressure function. *Physica A: Statistical and Theoretical Physics*, 371(2):209–225.

Hoffman, G. and Genuchten, M. T. V. (1983). *Soil properties and efficient water use: Water management of salinity control.* ASA, Inc. 677 South Segoe Road, Madison, WI 53711 USA.

Hoogland, J. C., Feddes, R. A., and Belmans, C. (1981). Root water uptake model depending on soil water pressure head and maximum extraction rate. *Acta Hort*, 119:123.136.

Hopmans, J. W. (1987). A comparison of various methods to scale soil hydraulic properties. *J. Hydrol.*, 93:241–256.

Hopmans, J. W. and Bristow, K. L. (2002). Current capabilities and future needs of root water and nutrient uptake modeling. *Adv. in Agronomy*, 77:103–183.

Hopmans, J. W., Schukking, H., and Torfs, P. J. J. F. (1988). Two-dimensional steady state unsaturated water flow in heterogeneous soils with autocorrelated soil hydraulic properties. *Water Resour. Res.*, 24(12):2005–2017.

Hoshen, J. and Kopelman, R. (1976). Percolation and cluster distribution. I. Cluster multiple labeling technique and critical concentration algorithm. *Phys. Rev. B.*, 1(14):3438–3445.

Hu, Z. L. and Islam, S. (1998). Effects of subgrid-scale heterogeneity of soil wetness and temperature on grid-scale evaporation and its parametrization. *Int. J. Climatol.*, 18(1):49–63.

IPCC (2007). Fourth assessment report: Climate change 2007 (AR4).

Ivanov, V. Y., Fatichi, S., Jenerette, G. D., Espeleta, J. F., Troch, P. A., and Huxman, T. E. (2010). Hysteresis of soil moisture spatial heterogeneity and the 'homogenizing' effect of vegetation. *Water Resour. Res.*, 46:W09521.

Jarvis, N. J. (1989). A simple empirical model of root water uptake. *J. Hydrol.*, 107:57–72.

Jarvis, N. J. (1994). The MACRO model (Version 3.1), technical description and sample simulations. *Reports and Dissertations 19. Dept. Soil Sci., Swedish Univ. Agric. Sci., Uppsala, Sweden*, page 51pp.

Javaux, M., Schröder, T., Vanderborght, J., and Vereecken, H. (2008). Use of a 3-dimensional detailed modeling approach for predicting root water uptake. *Vadose Zone J.*, 7(3):1079 – 1088.

Katul, G., Todd, P., Pataki, D., Kabala, Z. J., and Oren, R. (1997). Soil water depletion by oak trees and the influence of root water uptake on the moisture content spatial statistics. *Water Resour. Res.*, 33(4):611–623.

Kim, C. P., Stricker, J. N. M., and Feddes, R. A. (1996). Influence of spatially variable soil hydraulic properties and rainfall intensity on the water budget. *Water Resour. Res.*, 32(6):1699–1712.

Kim, C. P., Stricker, J. N. M., and Feddes, R. A. (1997). Impact of soil heterogeneity on the water budget of the unsaturated zone. *Water Resour. Res.*, 33:991–999.

Laio, F., Porporato, A., Ridolfi, R., and Rodriguez-Iturbe, I. (2001). Plants in water-controlled ecosystems: Active role in hydrologic processes and response to water stress II. Probabilistic soil moisture dynamics. *Adv. Water Resour.*, 24(7):707 – 724.

Leib, B. G., Caspari, H. W., Redulla, C. A., Andrews, P. K., and Jabro, J. J. (2006). Partial rootzone drying and deficit irrigation of 'Fuji' apples in a semi-arid climate. *Irrig. Sci.*, 24:85–99.

Li, J. (2010). *Application of copulas as a new geostatistical tool.* PhD thesis, Institut für Wasserbau, Universität Stuttgart.

Li, K. Y., de Jong, R., and Boisvert, J. B. (2001). An exponential root-water-uptake model with water stress compensation. *J. Hydrol.*, 252:189–171.

Lu, Z. and Zhang, D. (2004). Analytical solutions to steady state unsaturated flow in layered, randomly heterogenous soils via Kirchhoff transformation. *Adv. Water Resour.*, 27:775–784.

Lu, Z., Zhang, D., and Robinson, B. A. (2007). Explicit analytical solutions for one-dimensional steady state flow in layered, heterogeneous unsaturated soils under random boundary conditions. *Water Resour. Res.*, 43:W09413.

Manthey, S., Hassanizadeh, M. S., and Helmig, R. (2005). Macro-scale dynamic effects in homogeneous and heterogeneous porous media. *Transp. Porous Med.*, 58:121–145.

Mantoglou, A. and Gelhar, L. W. (1987a). Capillary tension head variance, mean soil moisture capacity of transient unsaturated flow in stratified soils. *Water Resour. Res.*, 23:47–56.

Mantoglou, A. and Gelhar, L. W. (1987b). Effective hydraulic conductivities of transient unsaturated flow in stratified soils. *Water Resour. Res.*, 23:57–67.

Mantoglou, A. and Gelhar, L. W. (1987c). Stochastic modeling of large-scale transient unsaturated flow systems. *Water Resour. Res.*, 23:37–46.

Markar, M. S. and Mein, R. (1987). Modeling evapotranspiration from homogeneous soils. *Water Resour. Res.*, 23:2001–2007.

Miller, E. E. and Miller, R. D. (1956). Physical theory for capillary flow phenomena. *J. Appl. Phys.*, 27:324–332.

Molz, F. J. (1981). Models of water transport in the soil-plant system: A review. *Water Resour. Res.*, 17:245–260.

Molz, F. J. and Remson, I. (1970). Extraction term models of soil moisture use by transpiring plants. *Water Resour. Res.*, 6:1346–1356.

Neuweiler, I. (2005). *Upscaling methods for flow and transport problems in the subsurface*. Lecture notes.

Neuweiler, I. and Cirpka, O. A. (2005). Homogenization of Richards equation in permeability fields with different connectivities. *Water Resour. Res.*, 41:1–14.

Neuweiler, I. and Vogel, H. J. (2007). Upscaling for unsaturated flow for non-Gaussian heterogeneous porous media. *Water Resour. Res.*, 43:W03443.

Nimah, M. N. and Hanks, R. J. (1973). Model for estimating soil water, plant and atmospheric interrelations: I. Description and sensitivity. *Soil Sci. Soc. Amer. Proc.*, 37:522–527.

Oladhyshkin, S. and Novak, W. (2010). Polynomial chaos expansion for probability measures with arbitrary finite moments. *SIAM J. Sci. Comput.*, submitted.

Oldak, A., Jackson, T. J., and Pachepsky, Y. (2002). Using GIS in passive microwave soil moisture mapping and geostatistical analysis. *Int. J. Geogr. Inf. Sci.*, 16(7):681–698.

Pang, X. P. and Letey, J. (1998). Development and evaluation of ENVIRO-GRO, an integrated water, salinity, and nitrogen model. *Soil Sci. Soc.*, 5:1418–1427.

Passioura, J. B. (1988). Water transport in and to root. *Annu. Rev. Plant Phys.*, 39:245–265.

Passioura, J. B. (2002). Soil conditions and plant growth. *Plant, Cell and Environment*, 25:311–318.

Peck, A. J., Luxmoore, R. J., and Stolzy, J. L. (1977). Effects of spatial variability of soil hydraulic properties in water budget modeling. *Water Resour. Res.*, 13:348–354.

Philip, J. R. (1966). Plant water relations: Some physical aspects. *Annu. Rev. Plant Phys.*, 17:245–268.

Polmann, D. J., McLaughlin, D., Luis, S., Gelhar, L. W., and Ababou, R. (1991). Stochastic modeling of large-scale flow in heterogeneous unsaturated soils. *Water Resour. Res.*, 27(7):1447–1458.

Porporato, A., Daly, E., and Rodriguez-Iturbe, I. (2004). Soil water balance and ecosystem response to climate change. *Am. Nat.*, 164(5):625–633.

Porporato, A., Laio, F., Ridolfi, L., and Rodriguez-Iturbe, I. (2001). Plants in water-controlled ecosystems: Active role in hydrological processes and response to water stress. III. Vegetation water stress. *Adv. Water Res.*, 24:725–744.

Raats, P. A. C. (1974). Steady flows of water and salt in uniform soil profiles with plant roots. *Soil Sci. Soc. Am. Proc.*, 38:717–722.

Raats, P. A. C. (2007). Uptake of water from soils from plant roots. *Transp. Porous Med.*, 68:5–28.

Ritsema, C. J., Dekker, L. W., Dekker, J. M., and Hamminga, W. (1993). Preferential flow mechanism in a water repellent sandy soil. *Water Resour. Res.*, 29:2183–2193.

Rodriguez-Iturbe, I., Isham, V., Cox, D. R., Manfreda, S., and Porporato, A. (2006). Space-time modeling of soil moisture: Stochastic rainfall forcing with heterogeneous vegetation. *Water Resour. Res.*, 42:W06D05.

Rodriguez-Iturbe, I., Porporato, A., Ridolfi, L., Isham, V., and Cox, D. R. (1999). Probabilistic modelling of water balance at a point: The role of climate, soil and vegetation. *Proc. R. Soc. London, Ser. A*, 455:3789 – 3805.

Roose, T. and Fowler, A. (2004). A mathematical model for water and nutrient uptake by roots. *J. Theor. Biol.*, 228:173–184.

Roose, T. and Schnepf, A. (2008). Mathematical models of plant-soil interaction. *Philos. T. Roy. Soc. A*, 366:4597–4611.

Roth, K. (1995). Steady state flow in an unsaturated, two-dimensional macroscopically homogeneous Miller-similar medium. *Water Resour. Res.*, 31:2121–2140.

Roth, K. (2007). *Soil Physics*. Lecture notes.

Rubin, Y. and Or, D. (1993). Stochastic modeling of unsaturated flow in heterogeneous soils with water uptake by plant roots: The parallel columns model. *Water Resour. Res.*, 29(3):619 – 631.

Russo, D. (1988). Determining soil hydraulic properties by parameter estimation: On the selection of a model for the hydraulic properties. *Water Resour. Res.*, 24:453–459.

Ryu, D. and Famiglietti, J. S. (2005). Characterization of footprint-scale surface soil moisture variability using Gaussian and beta distribution functions during the Southern Great Plains (SGP97) hydrology experiment. *Water Resour. Res.*, 41:W12433.

Schneider, C. L., Attinger, S., Delfs, J. O., and Hildebrandt, A. (2010). Implementing small scale processes at the soil-plant interface - the role of root architectures for calculating root water uptake profiles. *Hydrol. Earth Syst Sci*, 14 (2):279–289.

Schulin, R., van Genuchten, M. T., Flühler, H., and Ferlin, P. (1987). An experimental study of solute transport in a stony field soil. *Water Resour. Res.*, 23:1785–1794.

Simunek, J. and Hopmans, J. W. (2009). Modeling compensated root water and nutrient uptake. *Ecol. Mod.*, 220:505–521.

Skaggs, T. H., van Genuchten, M. T., Shouse, P. J., and Poss, J. A. (2006). Macroscopic approaches to root water uptake as a function of water and salinity stress. *Agric. Water Manage.*, 86:140–149.

Stikic, R., Popovic, S., Srdic, M., Savic, D., Jovanovic, Z., Prokic, L., and Zdravkovic, J. (2003). Partial root drying (PRD): A new technique for growing plants that saves water and improves the quality of fruit. *Bulg. J. Plant Physiol.*, pages 164–171 (Special Issue).

Taylor, H. M. (1974). *Root behaviour as affected by soil structure and strength*. The plant root and its environment (University Press of Virginia: Charlottesville, VA) pp..271-291.

Taylor, H. M. and Kleppner, B. (1978). The role of rooting characteristics in the supply of water to plants. *Adv. Agron.*, 30:99–128.

Taylor, S. A. and Ashcroft, G. M. (1972). *Physical Edaphology*. Freeman and Co., San Francisco, California, p. 434-435.

Teuling, A. J. and Troch, P. A. (2005). Improved understanding of soil moisture variability dynamics. *Geophys. Res. Lett.*, 32.

Tillotson, P. M. and Nielsen, D. R. (1984). Scale factors in soil science. *Soil Sci. Soc. of Am.J.*, 48:953–959.

Tipler, P. A. (1999). *Physik*. Spektrum.

Tompkins, J. A., Gan, K. C., Wheater, H. S., and Hirano, F. (1994). Prediction of solute dispersion in heterogeneous porous media: Effects of ergodicity and hydraulic conductivity discretisation. *J. Hydrol.*, 159:105–123.

van Genuchten, M. T. (1980). A closed- form equation for predicting the hydraulic conductivity in unsaturated soils. *Soil Sci. Soc. Am. J.*, 44:892–898.

van Genuchten, M. T. (1987). A numerical model for water and solute movement in and below the root zone. Technical report, Unpublished Research Report, U.S. Salinity Laboratory, USDA, ARS, Riverside, CA.

Varney, G. T. and Canny, M. J. (1993). Rates of water uptake into the mature root system of maize plants. *New Phytol.*, 123:775–786.

Verburg, K., Ross, P. J., and Bristow, K. L. (1996). *SWIMv2.1 User Manual. Divisional report No. 130*. Division of Soils, CSIRO, Australia.

Vereecken, H., Kamai, T., Harter, T., Kasteel, R., Hopmans, J., and Vanderborght, J. (2007a). Explaining soil moisture variability as a function of mean soil moisture: A stochastic unsaturated flow perspective. *Geophys. Res. Lett.*, 34:1–6.

Vereecken, H., Kasteel, R., Vanderborght, J., and Harter, T. (2007b). Upscaling hydraulic properties and soil water flow processes in heterogeneous soils: A review. *Vadose Zone J.*, 6:1–28.

Vrugt, J. A., Hopmans, J. W., and Simunek, J. (2001a). Two dimensional root water uptake model for a sprinkler-irrigated almond tree. *Soil Sci.Soc. Am.*, 65:1027–1037.

Vrugt, J. A., van Wijk, M. T., Hopmans, J. W., and Simunek, J. (2001b). Comparison of one, two, and three-dimensional root water uptake functions for transient water flow modeling. *Water Resour. Res.*, 37:2457–2470.

Wang, E. and Smith, C. J. (2004). Modelling the growth and water uptake function of plant root systems: A review. *Aust. J. Agr. Eng.*, 55:501–523.

Warrick, A. W. (1974). Solution of the one-dimensional linear moisture flow equation with water extraction. *Soil Sci. Soc Am.*, 38:573–576.

Warrick, A. W. and Amoozegar-Fard, A. (1979). Infiltration and drainage calculations using spatially scaled hydraulic properties. *Water Resour. Res.*, 15(5):1116–1120.

Warrick, A. W., Mullen, G. J., and Nielsen, D. R. (1977). Scaling field-measured soil hydraulic properties using a similar media concept. *Water Resour. Res.*, 13:355–362.

Whisler, F. D., Klute, A., and Millington, R. J. (1968). Analysis of steady state evapotranspiration from a soil column. *Soil Sci. Soc. Am.Proc.*, 32:167–174.

Yeh, T. C. J., Gelhar, L. W., and Gutjahr, A. L. (1985a). Stochastic analysis of unsaturated flow in heterogeneous soils. 1. Statistically isotropic media. *Water Resour. Res.*, 21:447–456.

Yeh, T. C. J., Gelhar, L. W., and Gutjahr, A. L. (1985b). Stochastic analysis of unsaturated flow in heterogeneous soils. 2. Statistically anisotropic media with variable α. *Water Resour. Res.*, 21:457–464.

Yeh, T. C. J., Gelhar, L. W., and Gutjahr, A. L. (1985c). Stochastic analysis of unsaturated flow in heterogeneous soils 3. Observations and applications. *Water Resour. Res.*, 21:465–471.

Yuan, F. and Lu, Z. (2005). Analytical solutions for vertical flow in unsaturated, rooted soils with variable surface fluxes. *Soil Sci. Soc. Am. J.*, 4:1210–1218.

Zhang, D. (2002). *Stochastic Methods for Flow in Prorous Media*. Academic Press.

Zinn, B. and Harvey, C. F. (2003). When good statistical models of aquifer heterogeneity go bad: A comparison of flow, dispersion, and mass transfer in connected and multivariate Gaussian hydraulic conductivity fields. *Water Resour. Res.*, 39(3):WR001146.

Institut für Wasserbau
Universität Stuttgart

Pfaffenwaldring 61
70569 Stuttgart (Vaihingen)
Telefon (0711) 685 - 64717/64749/64752/64679
Telefax (0711) 685 - 67020 o. 64746 o. 64681
E-Mail: iws@iws.uni-stuttgart.de
http://www.iws.uni-stuttgart.de

Verzeichnis der Mitteilungshefte

5 Plate, Erich: *Beitrag zur Bestimmung der Windgeschwindigkeitsverteilung in der durch eine Wand gestörten bodennahen Luftschicht*,
und
Röhnisch, Arthur; Marotz, Günter: *Neue Baustoffe und Bauausführungen für den Schutz der Böschungen und der Sohle von Kanälen, Flüssen und Häfen; Gestehungskosten und jeweilige Vorteile*, sowie Unny, T.E.: *Schwingungsuntersuchungen am Kegelstrahlschieber*, 1967

6 Seiler, Erich: *Die Ermittlung des Anlagenwertes der bundeseigenen Binnenschiffahrtsstraßen und Talsperren und des Anteils der Binnenschiffahrt an diesem Wert*, 1967

7 *Sonderheft anläßlich des 65. Geburtstages von Prof. Arthur Röhnisch mit Beiträgen von* Benk, Dieter; Breitling, J.; Gurr, Siegfried; Haberhauer, Robert; Honekamp, Hermann; Kuz, Klaus Dieter; Marotz, Günter; Mayer-Vorfelder, Hans-Jörg; Miller, Rudolf; Plate, Erich J.; Radomski, Helge; Schwarz, Helmut; Vollmer, Ernst; Wildenhahn, Eberhard; 1967

8 Jumikis, Alfred: *Beitrag zur experimentellen Untersuchung des Wassernachschubs in einem gefrierenden Boden und die Beurteilung der Ergebnisse*, 1968

9 Marotz, Günter: *Technische Grundlagen einer Wasserspeicherung im natürlichen Untergrund*, 1968

10 Radomski, Helge: *Untersuchungen über den Einfluß der Querschnittsform wellenförmiger Spundwände auf die statischen und rammtechnischen Eigenschaften*, 1968

11 Schwarz, Helmut: *Die Grenztragfähigkeit des Baugrundes bei Einwirkung vertikal gezogener Ankerplatten als zweidimensionales Bruchproblem*, 1969

12 Erbel, Klaus: *Ein Beitrag zur Untersuchung der Metamorphose von Mittelgebirgsschneedecken unter besonderer Berücksichtigung eines Verfahrens zur Bestimmung der thermischen Schneequalität*, 1969

13 Westhaus, Karl-Heinz: *Der Strukturwandel in der Binnenschiffahrt und sein Einfluß auf den Ausbau der Binnenschiffskanäle*, 1969

14 Mayer-Vorfelder, Hans-Jörg: *Ein Beitrag zur Berechnung des Erdwiderstandes unter Ansatz der logarithmischen Spirale als Gleitflächenfunktion*, 1970

15 Schulz, Manfred: *Berechnung des räumlichen Erddruckes auf die Wandung kreiszylindrischer Körper*, 1970

16 Mobasseri, Manoutschehr: *Die Rippenstützmauer. Konstruktion und Grenzen ihrer Standsicherheit*, 1970

17 Benk, Dieter: *Ein Beitrag zum Betrieb und zur Bemessung von Hochwasserrückhaltebecken*, 1970

18 Gàl, Attila: *Bestimmung der mitschwingenden Wassermasse bei überströmten Fischbauchklappen mit kreiszylindrischem Staublech*, 1971, vergriffen

19 Kuz, Klaus Dieter: *Ein Beitrag zur Frage des Einsetzens von Kavitationserscheinungen in einer Düsenströmung bei Berücksichtigung der im Wasser gelösten Gase*, 1971, vergriffen

20 Schaak, Hartmut: *Verteilleitungen von Wasserkraftanlagen*, 1971

21 *Sonderheft zur Eröffnung der neuen Versuchsanstalt des Instituts für Wasserbau der Universität Stuttgart mit Beiträgen von* Brombach, Hansjörg; Dirksen, Wolfram; Gàl, Attila; Gerlach, Reinhard; Giesecke, Jürgen; Holthoff, Franz-Josef; Kuz, Klaus Dieter; Marotz, Günter; Minor, Hans-Erwin; Petrikat, Kurt; Röhnisch, Arthur; Rueff, Helge; Schwarz, Helmut; Vollmer, Ernst; Wildenhahn, Eberhard; 1972

22 Wang, Chung-su: *Ein Beitrag zur Berechnung der Schwingungen an Kegelstrahlschiebern*, 1972

23 Mayer-Vorfelder, Hans-Jörg: *Erdwiderstandsbeiwerte nach dem Ohde-Variationsverfahren*, 1972

24 Minor, Hans-Erwin: *Beitrag zur Bestimmung der Schwingungsanfachungsfunktionen überströmter Stauklappen*, 1972, vergriffen

25 Brombach, Hansjörg: *Untersuchung strömungsmechanischer Elemente (Fluidik) und die Möglichkeit der Anwendung von Wirbelkammerelementen im Wasserbau*, 1972, vergriffen

26 Wildenhahn, Eberhard: *Beitrag zur Berechnung von Horizontalfilterbrunnen*, 1972

27 Steinlein, Helmut: *Die Eliminierung der Schwebstoffe aus Flußwasser zum Zweck der unterirdischen Wasserspeicherung, gezeigt am Beispiel der Iller*, 1972

28 Holthoff, Franz Josef: *Die Überwindung großer Hubhöhen in der Binnenschiffahrt durch Schwimmerhebewerke*, 1973

29 Röder, Karl: *Einwirkungen aus Baugrundbewegungen auf trog- und kastenförmige Konstruktionen des Wasser- und Tunnelbaues*, 1973

30 Kretschmer, Heinz: *Die Bemessung von Bogenstaumauern in Abhängigkeit von der Talform*, 1973

31 Honekamp, Hermann: *Beitrag zur Berechnung der Montage von Unterwasserpipelines*, 1973

32 Giesecke, Jürgen: *Die Wirbelkammertriode als neuartiges Steuerorgan im Wasserbau*, und Brombach, Hansjörg: *Entwicklung, Bauformen, Wirkungsweise und Steuereigenschaften von Wirbelkammerverstärkern*, 1974

33 Rueff, Helge: *Untersuchung der schwingungserregenden Kräfte an zwei hintereinander angeordneten Tiefschützen unter besonderer Berücksichtigung von Kavitation*, 1974

34 Röhnisch, Arthur: *Einpreßversuche mit Zementmörtel für Spannbeton - Vergleich der Ergebnisse von Modellversuchen mit Ausführungen in Hüllwellrohren*, 1975

35 *Sonderheft anläßlich des 65. Geburtstages von Prof. Dr.-Ing. Kurt Petrikat mit Beiträgen von*: Brombach, Hansjörg; Erbel, Klaus; Flinspach, Dieter; Fischer jr., Richard; Gàl, Attila; Gerlach, Reinhard; Giesecke, Jürgen; Haberhauer, Robert; Hafner Edzard; Hausenblas, Bernhard; Horlacher, Hans-Burkhard; Hutarew, Andreas; Knoll, Manfred; Krummet, Ralph; Marotz, Günter; Merkle, Theodor; Miller, Christoph; Minor, Hans-Erwin; Neumayer, Hans; Rao, Syamala; Rath, Paul; Rueff, Helge; Ruppert, Jürgen; Schwarz, Wolfgang; Topal-Gökceli, Mehmet; Vollmer, Ernst; Wang, Chung-su; Weber, Hans-Georg; 1975

36 Berger, Jochum: *Beitrag zur Berechnung des Spannungszustandes in rotationssymmetrisch belasteten Kugelschalen veränderlicher Wandstärke unter Gas- und Flüssigkeitsdruck durch Integration schwach singulärer Differentialgleichungen*, 1975

37 Dirksen, Wolfram: *Berechnung instationärer Abflußvorgänge in gestauten Gerinnen mittels Differenzenverfahren und die Anwendung auf Hochwasserrückhaltebecken*, 1976

38 Horlacher, Hans-Burkhard: *Berechnung instationärer Temperatur- und Wärmespannungsfelder in langen mehrschichtigen Hohlzylindern*, 1976

39 Hafner, Edzard: *Untersuchung der hydrodynamischen Kräfte auf Baukörper im Tiefwasserbereich des Meeres*, 1977, ISBN 3-921694-39-6

40 Ruppert, Jürgen: *Über den Axialwirbelkammerverstärker für den Einsatz im Wasserbau*, 1977, ISBN 3-921694-40-X

41 Hutarew, Andreas: *Beitrag zur Beeinflußbarkeit des Sauerstoffgehalts in Fließgewässern an Abstürzen und Wehren*, 1977, ISBN 3-921694-41-8, vergriffen

42 Miller, Christoph: *Ein Beitrag zur Bestimmung der schwingungserregenden Kräfte an unterströmten Wehren*, 1977, ISBN 3-921694-42-6

43 Schwarz, Wolfgang: *Druckstoßberechnung unter Berücksichtigung der Radial- und Längsverschiebungen der Rohrwandung*, 1978, ISBN 3-921694-43-4

44 Kinzelbach, Wolfgang: *Numerische Untersuchungen über den optimalen Einsatz variabler Kühlsysteme einer Kraftwerkskette am Beispiel Oberrhein*, 1978, ISBN 3-921694-44-2

45 Barczewski, Baldur: *Neue Meßmethoden für Wasser-Luftgemische und deren Anwendung auf zweiphasige Auftriebsstrahlen*, 1979, ISBN 3-921694-45-0

46 Neumayer, Hans: *Untersuchung der Strömungsvorgänge in radialen Wirbelkammerverstärkern*, 1979, ISBN 3-921694-46-9

47 Elalfy, Youssef-Elhassan: *Untersuchung der Strömungsvorgänge in Wirbelkammerdioden und -drosseln*, 1979, ISBN 3-921694-47-7

48 Brombach, Hansjörg: *Automatisierung der Bewirtschaftung von Wasserspeichern*, 1981, ISBN 3-921694-48-5

49 Geldner, Peter: *Deterministische und stochastische Methoden zur Bestimmung der Selbstdichtung von Gewässern*, 1981, ISBN 3-921694-49-3, vergriffen

50 Mehlhorn, Hans: *Temperaturveränderungen im Grundwasser durch Brauchwassereinleitungen*, 1982, ISBN 3-921694-50-7, vergriffen

51 Hafner, Edzard: *Rohrleitungen und Behälter im Meer*, 1983, ISBN 3-921694-51-5

52 Rinnert, Bernd: *Hydrodynamische Dispersion in porösen Medien: Einfluß von Dichteunterschieden auf die Vertikalvermischung in horizontaler Strömung*, 1983, ISBN 3-921694-52-3, vergriffen

53 Lindner, Wulf: *Steuerung von Grundwasserentnahmen unter Einhaltung ökologischer Kriterien*, 1983, ISBN 3-921694-53-1, vergriffen

54 Herr, Michael; Herzer, Jörg; Kinzelbach, Wolfgang; Kobus, Helmut; Rinnert, Bernd: *Methoden zur rechnerischen Erfassung und hydraulischen Sanierung von Grundwasserkontaminationen*, 1983, ISBN 3-921694-54-X

55 Schmitt, Paul: *Wege zur Automatisierung der Niederschlagsermittlung*, 1984, ISBN 3-921694-55-8, vergriffen

56 Müller, Peter: *Transport und selektive Sedimentation von Schwebstoffen bei gestautem Abfluß*, 1985, ISBN 3-921694-56-6

57 El-Qawasmeh, Fuad: *Möglichkeiten und Grenzen der Tropfbewässerung unter besonderer Berücksichtigung der Verstopfungsanfälligkeit der Tropfelemente*, 1985, ISBN 3-921694-57-4, vergriffen

58 Kirchenbaur, Klaus: *Mikroprozessorgesteuerte Erfassung instationärer Druckfelder am Beispiel seegangsbelasteter Baukörper*, 1985, ISBN 3-921694-58-2

59 Kobus, Helmut (Hrsg.): *Modellierung des großräumigen Wärme- und Schadstofftransports im Grundwasser*, Tätigkeitsbericht 1984/85 (DFG-Forschergruppe an den Universitäten Hohenheim, Karlsruhe und Stuttgart), 1985, ISBN 3-921694-59-0, vergriffen

60 Spitz, Karlheinz: *Dispersion in porösen Medien: Einfluß von Inhomogenitäten und Dichteunterschieden*, 1985, ISBN 3-921694-60-4, vergriffen

61 Kobus, Helmut: *An Introduction to Air-Water Flows in Hydraulics*, 1985, ISBN 3-921694-61-2

62 Kaleris, Vassilios: *Erfassung des Austausches von Oberflächen- und Grundwasser in horizontalebenen Grundwassermodellen*, 1986, ISBN 3-921694-62-0

63 Herr, Michael: *Grundlagen der hydraulischen Sanierung verunreinigter Porengrundwasserleiter*, 1987, ISBN 3-921694-63-9

64 Marx, Walter: *Berechnung von Temperatur und Spannung in Massenbeton infolge Hydratation*, 1987, ISBN 3-921694-64-7

65 Koschitzky, Hans-Peter: *Dimensionierungskonzept für Sohlbelüfter in Schußrinnen zur Vermeidung von Kavitationsschäden*, 1987, ISBN 3-921694-65-5

66 Kobus, Helmut (Hrsg.): *Modellierung des großräumigen Wärme- und Schadstofftransports im Grundwasser*, Tätigkeitsbericht 1986/87 (DFG-Forschergruppe an den Universitäten Hohenheim, Karlsruhe und Stuttgart) 1987, ISBN 3-921694-66-3

67 Söll, Thomas: *Berechnungsverfahren zur Abschätzung anthropogener Temperaturanomalien im Grundwasser*, 1988, ISBN 3-921694-67-1

68 Dittrich, Andreas; Westrich, Bernd: *Bodenseeufererosion, Bestandsaufnahme und Bewertung*, 1988, ISBN 3-921694-68-X, vergriffen

69 Huwe, Bernd; van der Ploeg, Rienk R.: *Modelle zur Simulation des Stickstoffhaushaltes von Standorten mit unterschiedlicher landwirtschaftlicher Nutzung*, 1988, ISBN 3-921694-69-8, vergriffen

70 Stephan, Karl: *Integration elliptischer Funktionen*, 1988, ISBN 3-921694-70-1

71 Kobus, Helmut; Zilliox, Lothaire (Hrsg.): *Nitratbelastung des Grundwassers, Auswirkungen der Landwirtschaft auf die Grundwasser- und Rohwasserbeschaffenheit und Maßnahmen zum Schutz des Grundwassers*. Vorträge des deutsch-französischen Kolloquiums am 6. Oktober 1988, Universitäten Stuttgart und Louis Pasteur Strasbourg (Vorträge in deutsch oder französisch, Kurzfassungen zweisprachig), 1988, ISBN 3-921694-71-X

72 Soyeaux, Renald: *Unterströmung von Stauanlagen auf klüftigem Untergrund unter Berücksichtigung laminarer und turbulenter Fließzustände*,1991, ISBN 3-921694-72-8

73 Kohane, Roberto: *Berechnungsmethoden für Hochwasserabfluß in Fließgewässern mit überströmten Vorländern*, 1991, ISBN 3-921694-73-6

74 Hassinger, Reinhard: *Beitrag zur Hydraulik und Bemessung von Blocksteinrampen in flexibler Bauweise*, 1991, ISBN 3-921694-74-4, vergriffen

75 Schäfer, Gerhard: *Einfluß von Schichtenstrukturen und lokalen Einlagerungen auf die Längsdispersion in Porengrundwasserleitern*, 1991, ISBN 3-921694-75-2

76 Giesecke, Jürgen: *Vorträge, Wasserwirtschaft in stark besiedelten Regionen; Umweltforschung mit Schwerpunkt Wasserwirtschaft*, 1991, ISBN 3-921694-76-0

77 Huwe, Bernd: *Deterministische und stochastische Ansätze zur Modellierung des Stickstoffhaushalts landwirtschaftlich genutzter Flächen auf unterschiedlichem Skalenniveau*, 1992, ISBN 3-921694-77-9, vergriffen

78 Rommel, Michael: *Verwendung von Kluftdaten zur realitätsnahen Generierung von Kluftnetzen mit anschließender laminar-turbulenter Strömungsberechnung*, 1993, ISBN 3-92 1694-78-7

79 Marschall, Paul: *Die Ermittlung lokaler Stofffrachten im Grundwasser mit Hilfe von Einbohrloch-Meßverfahren*, 1993, ISBN 3-921694-79-5, vergriffen

80 Ptak, Thomas: *Stofftransport in heterogenen Porenaquiferen: Felduntersuchungen und stochastische Modellierung*, 1993, ISBN 3-921694-80-9, vergriffen

81 Haakh, Frieder: *Transientes Strömungsverhalten in Wirbelkammern,* 1993, ISBN 3-921694-81-7

82 Kobus, Helmut; Cirpka, Olaf; Barczewski, Baldur; Koschitzky, Hans-Peter: *Versucheinrichtung zur Grundwasser und Altlastensanierung VEGAS, Konzeption und Programmrahmen*, 1993, ISBN 3-921694-82-5

83 Zang, Weidong: *Optimaler Echtzeit-Betrieb eines Speichers mit aktueller Abflußregenerierung*, 1994, ISBN 3-921694-83-3, vergriffen

84 Franke, Hans-Jörg: *Stochastische Modellierung eines flächenhaften Stoffeintrages und Transports in Grundwasser am Beispiel der Pflanzenschutzmittelproblematik*, 1995, ISBN 3-921694-84-1

85 Lang, Ulrich: *Simulation regionaler Strömungs- und Transportvorgänge in Karstaquiferen mit Hilfe des Doppelkontinuum-Ansatzes: Methodenentwicklung und Parameteridentifikation*, 1995, ISBN 3-921694-85-X, vergriffen

86 Helmig, Rainer: *Einführung in die Numerischen Methoden der Hydromechanik*, 1996, ISBN 3-921694-86-8, vergriffen

87 Cirpka, Olaf: *CONTRACT: A Numerical Tool for Contaminant Transport and Chemical Transformations - Theory and Program Documentation* -, 1996, ISBN 3-921694-87-6

88 Haberlandt, Uwe: *Stochastische Synthese und Regionalisierung des Niederschlages für Schmutzfrachtberechnungen*, 1996, ISBN 3-921694-88-4

89 Croisé, Jean: *Extraktion von flüchtigen Chemikalien aus natürlichen Lockergesteinen mittels erzwungener Luftströmung*, 1996, ISBN 3-921694-89-2, vergriffen

90 Jorde, Klaus: *Ökologisch begründete, dynamische Mindestwasserregelungen bei Ausleitungskraftwerken*, 1997, ISBN 3-921694-90-6, vergriffen

91 Helmig, Rainer: *Gekoppelte Strömungs- und Transportprozesse im Untergrund - Ein Beitrag zur Hydrosystemmodellierung*-, 1998, ISBN 3-921694-91-4, vergriffen

92 Emmert, Martin: *Numerische Modellierung nichtisothermer Gas-Wasser Systeme in porösen Medien,* 1997, ISBN 3-921694-92-2

93 Kern, Ulrich: *Transport von Schweb- und Schadstoffen in staugeregelten Fließgewässern am Beispiel des Neckars*, 1997, ISBN 3-921694-93-0, vergriffen

94 Förster, Georg: *Druckstoßdämpfung durch große Luftblasen in Hochpunkten von Rohrleitungen 1997*, ISBN 3-921694-94-9

95 Cirpka, Olaf: *Numerische Methoden zur Simulation des reaktiven Mehrkomponententransports im Grundwasser*, 1997, ISBN 3-921694-95-7, vergriffen

96 Färber, Arne: *Wärmetransport in der ungesättigten Bodenzone: Entwicklung einer thermischen In-situ-Sanierungstechnologie*, 1997, ISBN 3-921694-96-5

97 Betz, Christoph: *Wasserdampfdestillation von Schadstoffen im porösen Medium: Entwicklung einer thermischen In-situ-Sanierungstechnologie*, 1998, ISBN 3-921694-97-3

98 Xu, Yichun: *Numerical Modeling of Suspended Sediment Transport in Rivers*, 1998, ISBN 3-921694-98-1, vergriffen

99 Wüst, Wolfgang: *Geochemische Untersuchungen zur Sanierung CKW-kontaminierter Aquifere mit Fe(0)-Reaktionswänden,* 2000, ISBN 3-933761-02-2

100 Sheta, Hussam: *Simulation von Mehrphasenvorgängen in porösen Medien unter Einbeziehung von Hysterese-Effekten*, 2000, ISBN 3-933761-03-4

101 Ayros, Edwin: *Regionalisierung extremer Abflüsse auf der Grundlage statistischer Verfahren*, 2000, ISBN 3-933761-04-2, vergriffen

102 Huber, Ralf: *Compositional Multiphase Flow and Transport in Heterogeneous Porous Media*, 2000, ISBN 3-933761-05-0

103 Braun, Christopherus: *Ein Upscaling-Verfahren für Mehrphasenströmungen in porösen Medien*, 2000, ISBN 3-933761-06-9

104 Hofmann, Bernd: *Entwicklung eines rechnergestützten Managementsystems zur Beurteilung von Grundwasserschadensfällen*, 2000, ISBN 3-933761-07-7

105 Class, Holger: *Theorie und numerische Modellierung nichtisothermer Mehrphasenprozesse in NAPL-kontaminierten porösen Medien,* 2001, ISBN 3-933761-08-5

106 Schmidt, Reinhard: *Wasserdampf- und Heißluftinjektion zur thermischen Sanierung kontaminierter Standorte*, 2001, ISBN 3-933761-09-3

107 Josef, Reinhold:, *Schadstoffextraktion mit hydraulischen Sanierungsverfahren unter Anwendung von grenzflächenaktiven Stoffen*, 2001, ISBN 3-933761-10-7

108 Schneider, Matthias: *Habitat- und Abflussmodellierung für Fließgewässer mit unscharfen Berechnungsansätzen*, 2001, ISBN 3-933761-11-5

109 Rathgeb, Andreas: *Hydrodynamische Bemessungsgrundlagen für Lockerdeckwerke an überströmbaren Erddämmen*, 2001, ISBN 3-933761-12-3

110 Lang, Stefan: *Parallele numerische Simulation instätionärer Probleme mit adaptiven Methoden auf unstrukturierten Gittern*, 2001, ISBN 3-933761-13-1

111 Appt, Jochen; Stumpp Simone: *Die Bodensee-Messkampagne 2001, IWS/CWR Lake Constance Measurement Program 2001*, 2002, ISBN 3-933761-14-X

112 Heimerl, Stephan: *Systematische Beurteilung von Wasserkraftprojekten,* 2002, ISBN 3-933761-15-8, vergriffen

113 Iqbal, Amin: *On the Management and Salinity Control of Drip Irrigation,* 2002, ISBN 3-933761-16-6

114 Silberhorn-Hemminger, Annette: *Modellierung von Kluftaquifersystemen: Geostatistische Analyse und deterministisch-stochastische Kluftgenerierung,* 2002, ISBN 3-933761-17-4

115 Winkler, Angela: *Prozesse des Wärme- und Stofftransports bei der In-situ-Sanierung mit festen Wärmequellen,* 2003, ISBN 3-933761-18-2

116 Marx, Walter: *Wasserkraft, Bewässerung, Umwelt - Planungs- und Bewertungsschwerpunkte der Wasserbewirtschaftung,* 2003, ISBN 3-933761-19-0

117 Hinkelmann, Reinhard: *Efficient Numerical Methods and Information-Processing Techniques in Environment Water,* 2003, ISBN 3-933761-20-4

118 Samaniego-Eguiguren, Luis Eduardo: *Hydrological Consequences of Land Use / Land Cover and Climatic Changes in Mesoscale Catchments*, 2003, ISBN 3-933761-21-2

119 Neunhäuserer, Lina: *Diskretisierungsansätze zur Modellierung von Strömungs- und Transportprozessen in geklüftet-porösen Medien*, 2003, ISBN 3-933761-22-0

120 Paul, Maren: *Simulation of Two-Phase Flow in Heterogeneous Poros Media with Adaptive Methods*, 2003, ISBN 3-933761-23-9

121 Ehret, Uwe: *Rainfall and Flood Nowcasting in Small Catchments using Weather Radar*, 2003, ISBN 3-933761-24-7

122 Haag, Ingo: *Der Sauerstoffhaushalt staugeregelter Flüsse am Beispiel des Neckars - Analysen, Experimente, Simulationen -,* 2003, ISBN 3-933761-25-5

123 Appt, Jochen: *Analysis of Basin-Scale Internal Waves in Upper Lake Constance,* 2003, ISBN 3-933761-26-3

124 Hrsg.: Schrenk, Volker; Batereau, Katrin; Barczewski, Baldur; Weber, Karolin und Koschitzky, Hans-Peter: *Symposium Ressource Fläche und VEGAS - Statuskolloquium 2003, 30. September und 1. Oktober 2003,* 2003, ISBN 3-933761-27-1

125 Omar Khalil Ouda: *Optimisation of Agricultural Water Use: A Decision Support System for the Gaza Strip,* 2003, ISBN 3-933761-28-0

126 Batereau, Katrin: *Sensorbasierte Bodenluftmessung zur Vor-Ort-Erkundung von Schadensherden im Untergrund*, 2004, ISBN 3-933761-29-8

127 Witt, Oliver: *Erosionsstabilität von Gewässersedimenten mit Auswirkung auf den Stofftransport bei Hochwasser am Beispiel ausgewählter Stauhaltungen des Oberrheins*, 2004, ISBN 3-933761-30-1

128 Jakobs, Hartmut: *Simulation nicht-isothermer Gas-Wasser-Prozesse in komplexen Kluft-Matrix-Systemen*, 2004, ISBN 3-933761-31-X

129 Li, Chen-Chien: *Deterministisch-stochastisches Berechnungskonzept zur Beurteilung der Auswirkungen erosiver Hochwasserereignisse in Flussstauhaltungen,* 2004, ISBN 3-933761-32-8

130 Reichenberger, Volker; Helmig, Rainer; Jakobs, Hartmut; Bastian, Peter; Niessner, Jennifer: *Complex Gas-Water Processes in Discrete Fracture-Matrix Systems: Upscaling, Mass-Conservative Discretization and Efficient Multilevel Solution,* 2004, ISBN 3-933761-33-6

131 Hrsg.: Barczewski, Baldur; Koschitzky, Hans-Peter; Weber, Karolin; Wege, Ralf: *VEGAS - Statuskolloquium 2004,* Tagungsband zur Veranstaltung am 05. Oktober 2004 an der Universität Stuttgart, Campus Stuttgart-Vaihingen, 2004, ISBN 3-933761-34-4

132 Asie, Kemal Jabir: *Finite Volume Models for Multiphase Multicomponent Flow through Porous Media*. 2005, ISBN 3-933761-35-2

133 Jacoub, George: *Development of a 2-D Numerical Module for Particulate Contaminant Transport in Flood Retention Reservoirs and Impounded Rivers,* 2004, ISBN 3-933761-36-0

134 Nowak, Wolfgang: *Geostatistical Methods for the Identification of Flow and Transport Parameters in the Subsurface,* 2005, ISBN 3-933761-37-9

135 Süß, Mia: *Analysis of the influence of structures and boundaries on flow and transport processes in fractured porous media*, 2005, ISBN 3-933761-38-7

136 Jose, Surabhin Chackiath: *Experimental Investigations on Longitudinal Dispersive Mixing in Heterogeneous Aquifers,* 2005, ISBN: 3-933761-39-5

137 Filiz, Fulya: *Linking Large-Scale Meteorological Conditions to Floods in Mesoscale Catchments,* 2005, ISBN 3-933761-40-9

138 Qin, Minghao: *Wirklichkeitsnahe und recheneffiziente Ermittlung von Temperatur und Spannungen bei großen RCC-Staumauern*, 2005, ISBN 3-933761-41-7

139 Kobayashi, Kenichiro: *Optimization Methods for Multiphase Systems in the Subsurface - Application to Methane Migration in Coal Mining Areas*, 2005, ISBN 3-933761-42-5

140 Rahman, Md. Arifur: *Experimental Investigations on Transverse Dispersive Mixing in Heterogeneous Porous Media,* 2005, ISBN 3-933761-43-3

141 Schrenk, Volker: *Ökobilanzen zur Bewertung von Altlastensanierungsmaßnahmen,* 2005, ISBN 3-933761-44-1

142 Hundecha, Hirpa Yeshewatesfa: *Regionalization of Parameters of a Conceptual Rainfall-Runoff Model*, 2005, ISBN: 3-933761-45-X

143 Wege, Ralf: *Untersuchungs- und Überwachungsmethoden für die Beurteilung natürlicher Selbstreinigungsprozesse im Grundwasser,* 2005, ISBN 3-933761-46-8

144 Breiting, Thomas: *Techniken und Methoden der Hydroinformatik - Modellierung von komplexen Hydrosystemen im Untergrund*, 2006, 3-933761-47-6

145 Hrsg.: Braun, Jürgen; Koschitzky, Hans-Peter; Müller, Martin: *Ressource Untergrund: 10 Jahre VEGAS: Forschung und Technologieentwicklung zum Schutz von Grundwasser und Boden,* Tagungsband zur Veranstaltung am 28. und 29. September 2005 an der Universität Stuttgart, Campus Stuttgart-Vaihingen, 2005, ISBN 3-933761-48-4

146 Rojanschi, Vlad: *Abflusskonzentration in mesoskaligen Einzugsgebieten unter Berücksichtigung des Sickerraumes,* 2006, ISBN 3-933761-49-2

147 Winkler, Nina Simone: *Optimierung der Steuerung von Hochwasserrückhaltebecken-systemen,* 2006, ISBN 3-933761-50-6

148 Wolf, Jens: *Räumlich differenzierte Modellierung der Grundwasserströmung alluvialer Aquifere für mesoskalige Einzugsgebiete*, 2006, ISBN: 3-933761-51-4

149 Kohler, Beate: *Externe Effekte der Laufwasserkraftnutzung*, 2006, ISBN 3-933761-52-2

150 Hrsg.: Braun, Jürgen; Koschitzky, Hans-Peter; Stuhrmann, Matthias: *VEGAS-Statuskolloquium 2006,* Tagungsband zur Veranstaltung am 28. September 2006 an der Universität Stuttgart, Campus Stuttgart-Vaihingen, 2006, ISBN 3-933761-53-0

151 Niessner, Jennifer: *Multi-Scale Modeling of Multi-Phase - Multi-Component Processes in Heterogeneous Porous Media*, 2006, ISBN 3-933761-54-9

152 Fischer, Markus: *Beanspruchung eingeerdeter Rohrleitungen infolge Austrocknung bindiger Böden,* 2006, ISBN 3-933761-55-7

153 Schneck, Alexander: *Optimierung der Grundwasserbewirtschaftung unter Berücksichtigung der Belange der Wasserversorgung, der Landwirtschaft und des Naturschutzes*, 2006, ISBN 3-933761-56-5

154 Das, Tapash: *The Impact of Spatial Variability of Precipitation on the Predictive Uncertainty of Hydrological Models,* 2006, ISBN 3-933761-57-3

155 Bielinski, Andreas: *Numerical Simulation of CO_2 sequestration in geological formations*, 2007, ISBN 3-933761-58-1

156 Mödinger, Jens: *Entwicklung eines Bewertungs- und Entscheidungsunterstützungssystems für eine nachhaltige regionale Grundwasserbewirtschaftung*, 2006, ISBN 3-933761-60-3

157 Manthey, Sabine: *Two-phase flow processes with dynamic effects in porous media - parameter estimation and simulation,* 2007, ISBN 3-933761-61-1

158 Pozos Estrada, Oscar: *Investigation on the Effects of Entrained Air in Pipelines,* 2007, ISBN 3-933761-62-X

159 Ochs, Steffen Oliver: *Steam injection into saturated porous media – process analysis including experimental and numerical investigations*, 2007, ISBN 3-933761-63-8

160 Marx, Andreas: *Einsatz gekoppelter Modelle und Wetterradar zur Abschätzung von Niederschlagsintensitäten und zur Abflussvorhersage, 2007,* ISBN 3-933761-64-6

161 Hartmann, Gabriele Maria: *Investigation of Evapotranspiration Concepts in Hydrological Modelling for Climate Change Impact Assessment*, 2007, ISBN 3-933761-65-4

162 Kebede Gurmessa, Tesfaye: *Numerical Investigation on Flow and Transport Characteristics to Improve Long-Term Simulation of Reservoir Sedimentation*, 2007, ISBN 3-933761-66-2

163 Trifković, Aleksandar: *Multi-objective and Risk-based Modelling Methodology for Planning, Design and Operation of Water Supply Systems*, 2007, ISBN 3-933761-67-0

164 Götzinger, Jens: *Distributed Conceptual Hydrological Modelling - Simulation of Climate, Land Use Change Impact and Uncertainty Analysis*, 2007, ISBN 3-933761-68-9

165 Hrsg.: Braun, Jürgen; Koschitzky, Hans-Peter; Stuhrmann, Matthias: *VEGAS – Kolloquium 2007,* Tagungsband zur Veranstaltung am 26. September 2007 an der Universität Stuttgart, Campus Stuttgart-Vaihingen, 2007, ISBN 3-933761-69-7

166 Freeman, Beau: *Modernization Criteria Assessment for Water Resources Planning; Klamath Irrigation Project, U.S.*, 2008, ISBN 3-933761-70-0

167 Dreher, Thomas: *Selektive Sedimentation von Feinstschwebstoffen in Wechselwirkung mit wandnahen turbulenten Strömungsbedingungen*, 2008, ISBN 3-933761-71-9

168 Yang, Wei: *Discrete-Continuous Downscaling Model for Generating Daily Precipitation Time Series*, 2008, ISBN 3-933761-72-7

169 Kopecki, Ianina: *Calculational Approach to FST-Hemispheres for Multiparametrical Benthos Habitat Modelling,* 2008*,* ISBN 3-933761-73-5

170 Brommundt, Jürgen: *Stochastische Generierung räumlich zusammenhängender Niederschlagszeitreihen*, 2008, ISBN 3-933761-74-3

171 Papafotiou, *Alexandros: Numerical Investigations of the Role of Hysteresis in Heterogeneous Two-Phase Flow Systems*, 2008, ISBN 3-933761-75-1

172 He, Yi: *Application of a Non-Parametric Classification Scheme to Catchment Hydrology*, 2008, ISBN 978-3-933761-76-7

173 Wagner, Sven: *Water Balance in a Poorly Gauged Basin in West Africa Using Atmospheric Modelling and Remote Sensing Information*, 2008, ISBN 978-3-933761-77-4

174 Hrsg.: Braun, Jürgen; Koschitzky, Hans-Peter; Stuhrmann, Matthias; Schrenk, Volker: *VEGAS-Kolloquium 2008 Ressource Fläche III*, Tagungsband zur Veranstaltung am 01. Oktober 2008 an der Universität Stuttgart, Campus Stuttgart-Vaihingen, 2008, ISBN 978-3-933761-78-1

175 Patil, Sachin: *Regionalization of an Event Based Nash Cascade Model for Flood Predictions in Ungauged Basins*, 2008, ISBN 978-3-933761-79-8

176 Assteerawatt, Anongnart: *Flow and Transport Modelling of Fractured Aquifers based on a Geostatistical Approach,* 2008, ISBN 978-3-933761-80-4

177 Karnahl, Joachim Alexander: *2D numerische Modellierung von multifraktionalem Schwebstoff- und Schadstofftransport in Flüssen*, 2008, ISBN 978-3-933761-81-1

178 Hiester, Uwe: *Technologieentwicklung zur In-situ-Sanierung der ungesättigten Bodenzone mit festen Wärmequellen,* 2009, ISBN 978-3-933761-82-8

179 Laux, Patrick: *Statistical Modeling of Precipitation for Agricultural Planning in the Volta Basin of West Africa,* 2009, ISBN 978-3-933761-83-5

180 Ehsan, Saqib: *Evaluation of Life Safety Risks Related to Severe Flooding,* 2009, ISBN 978-3-933761-84-2

181 Prohaska, Sandra: *Development and Application of a 1D Multi-Strip Fine Sediment Transport Model for Regulated Rivers,* 2009, ISBN 978-3-933761-85-9

182 Kopp, Andreas: *Evaluation of CO_2 Injection Processes in Geological Formations for Site Screening,* 2009, ISBN 978-3-933761-86-6

183 Ebigbo, Anozie: *Modelling of biofilm growth and its influence on CO_2 and water (two-phase) flow in porous media,* 2009, ISBN 978-3-933761-87-3

184 Freiboth, Sandra: *A phenomenological model for the numerical simulation of multiphase multicomponent processes considering structural alterations of porous media*, 2009, ISBN 978-3-933761-88-0

185 Zöllner, Frank: *Implementierung und Anwendung netzfreier Methoden im Konstruktiven Wasserbau und in der Hydromechanik*, 2009, ISBN 978-3-933761-89-7

186 Vasin, Milos: *Influence of the soil structure and property contrast on flow and transport in the unsaturated zone*, 2010, ISBN 978-3-933761-90-3

187 Li, Jing: *Application of Copulas as a New Geostatistical Tool*, 2010, ISBN 978-3-933761-91-0

188 AghaKouchak, Amir: *Simulation of Remotely Sensed Rainfall Fields Using Copulas*, 2010, ISBN 978-3-933761-92-7

189 Thapa, Pawan Kumar: *Physically-based spatially distributed rainfall runoff modelling for soil erosion estimation*, 2010, ISBN 978-3-933761-93-4

190 Wurms, Sven: *Numerische Modellierung der Sedimentationsprozesse in Retentionsanlagen zur Steuerung von Stoffströmen bei extremen Hochwasserabflussereignissen*, 2011, ISBN 978-3-933761-94-1

191 Merkel, Uwe: *Unsicherheitsanalyse hydraulischer Einwirkungen auf Hochwasserschutzdeiche und Steigerung der Leistungsfähigkeit durch adaptive Strömungsmodellierung*, 2011, ISBN 978-3-933761-95-8

192 Fritz, Jochen: *A Decoupled Model for Compositional Non-Isothermal Multiphase Flow in Porous Media and Multiphysics Approaches for Two-Phase Flow*, 2010, ISBN 978-3-933761-96-5

193 Weber, Karolin (Hrsg.): *12. Treffen junger WissenschaftlerInnen an Wasserbauinstituten*, 2010, ISBN 978-3-933761-97-2

194 Bliefernicht, Jan-Geert: *Probability Forecasts of Daily Areal Precipitation for Small River Basins,* 2011, ISBN 978-3-933761-98-9

195 Hrsg.: Koschitzky, Hans-Peter; Braun, Jürgen: *VEGAS-Kolloquium 2010 In-situ-Sanierung - Stand und Entwicklung Nano und ISCO -,* Tagungsband zur Veranstaltung am 07. Oktober 2010 an der Universität Stuttgart, Campus Stuttgart-Vaihingen, 2010, ISBN 978-3-933761-99-6

196 Gafurov, Abror: *Water Balance Modeling Using Remote Sensing Information - Focus on Central Asia,* 2010, ISBN 978-3-942036-00-9

197 Mackenberg, Sylvia: *Die Quellstärke in der Sickerwasserprognose: Möglichkeiten und Grenzen von Labor- und Freilanduntersuchungen,* 2010, ISBN 978-3-942036-01-6

198 Singh, Shailesh Kumar: *Robust Parameter Estimation in Gauged and Ungauged Basins,* 2010, ISBN 978-3-942036-02-3

199 Doğan, Mehmet Onur: *Coupling of porous media flow with pipe flow,* 2011, ISBN 978-3-942036-03-0

200 Liu, Min: *Study of Topographic Effects on Hydrological Patterns and the Implication on Hydrological Modeling and Data Interpolation,* 2011, ISBN 978-3-942036-04-7

201 Geleta, Habtamu Itefa: *Watershed Sediment Yield Modeling for Data Scarce Areas,* 2011, ISBN 978-3-942036-05-4

202 Franke, Jörg: *Einfluss der Überwachung auf die Versagenswahrscheinlichkeit von Staustufen,* 2011, ISBN 978-3-942036-06-1

203 Bakimchandra, Oinam: *Integrated Fuzzy-GIS approach for assessing regional soil erosion risks,* 2011, ISBN 978-3-942036-07-8

204 Alam, Muhammad Mahboob: *Statistical Downscaling of Extremes of Precipitation in Mesoscale Catchments from Different RCMs and Their Effects on Local Hydrology,* 2011, ISBN 978-3-942036-08-5

205 Hrsg.: Koschitzky, Hans-Peter; Braun, Jürgen: *VEGAS-Kolloquium 2011 Flache Geothermie - Perspektiven und Risiken,* Tagungsband zur Veranstaltung am 06. Oktober 2011 an der Universität Stuttgart, Campus Stuttgart-Vaihingen, 2011, ISBN 978-3-933761-09-2

206 Haslauer, Claus: *Analysis of Real-World Spatial Dependence of Subsurface Hydraulic Properties Using Copulas with a Focus on Solute Transport Behaviour,* 2011, ISBN 978-3-942036-10-8

207 Dung, Nguyen Viet: *Multi-objective automatic calibration of hydrodynamic models – development of the concept and an application in the Mekong Delta,* 2011, ISBN 978-3-942036-11-5

208 Hung, Nguyen Nghia: *Sediment dynamics in the floodplain of the Mekong Delta, Vietnam,* 2011, ISBN 978-3-942036-12-2

209 Kuhlmann, Anna: *Influence of soil structure and root water uptake on flow in the unsaturated zone,* 2012, ISBN 978-3-942036-13-9

Die Mitteilungshefte ab der Nr. 134 (Jg. 2005) stehen als pdf-Datei über die Homepage des Instituts: www.iws.uni-stuttgart.de zur Verfügung.